Knockout of A-kinase anchoring protein GSKIP in mice causes perinatal lethality

DISSERTATION

zur Erlangung des akademischen Grades des
Doktors der Naturwissenschaften
(Dr. rer. nat.)

eingereicht im Fachbereich Biologie, Chemie, Pharmazie
der Freien Universität Berlin

vorgelegt von

Veronika Anita Deák
aus Sopron

Berlin 2015

Diese Arbeit wurde von Februar 2012 bis Juli 2015 am Max-Delbrück-Centrum für Molekulare Medizin in der Helmholtz-Gemeinschaft (MDC) in Berlin unter der Leitung von PD Dr. Enno Klußmann angefertigt.

Dissertation eingereicht am: 30.07.2015

1. Gutachter: PD Dr. Enno Klußmann
2. Gutachter: Prof. Dr. Markus Wahl

Disputation am: 23.11.2015

SELBSTÄNDIGKEITSERKLÄRUNG

Hiermit erkläre ich, dass ich die vorliegende Arbeit selbständig und nur unter Verwendung der angegebenen Literatur und Hilfsmittel angefertigt habe. Des Weiteren versichere ich, dass die vorliegende Arbeit nie Gegenstand eines früheren Promotionsverfahrens war. Die dem Verfahren zugrunde liegende Promotionsordnung ist mir bekannt.

_____

Veronika Deák

Berlin, den 30.07.2015

DANKSAGUNG

Table of content

Abbreviations

*	Significant; $p \leq 0.05$
**	Very significant; $p \leq 0.01$
***	Highly significant; $p \leq 0.001$
°C	Degree celsius
µ	Micro
3´/5´UTR	3 prime/ 5 prime untranslated region
A	Ampere
aa	Amino acid
Abca3	ATP-binding cassette sub-family A member 3
AC	Adenylyl cyclase
Actn2	Actinin alpha 2
AEC	Alveolar epithelial cell
AKAP-Lbc	AKAP Lymphoid blast crisis
AKAPs	A-kinase anchoring proteins
AKB	A-kinase binding domains
Akt	Protein kinase B
Aldh4a1	Delta-1-pyrroline-5-carboxylate dehydrogenase
AMF	Autocrine motility factor
Ankrd1	Ankyrin repeat protein 1
ANOVA	Analysis of variance
APC	Adenomatous polyposis coli
AQP	Aquaporin
ASMC	Airway smooth muscle cell
ATP	Adenosine triphosphate
Atpif1	ATPase inhibitor
Axud1	Axin 1-upregulated 1
Bag1	BCL2-associated athanogene 1
β-Cat	β-catenin
BCAA	Branched chain amino acid
BMP	Bone morphogenetic protein
bp	Base pair
BSA	Bovine serum albumin
C	C-terminus
C (PKA C)	Catalytic subunitof PKA: isoforms Cα, Cβ, Cγ
cAMP	Cyclic adenosine monophosphate
Cdh2	Cadherin 2
Cdh4	Cadherin 4
cDNA	Copy DNA
cGMP	Cyclic GMP
CK1	Casein kinase 1
CL	Cardiolipin
c-Myc	Oncogene coding for a transcription factor
CNG	Cyclic-nucleotide-gated ion channels
CNS	Central nervous system
Col1a1	Collagen 1a1
COPD	Chronic obstructive pulmonary disease
COS	Fibroblast-like cell line derived from monkey kidney tissue
COX4	Cytochrome c oxidase
Cps1	Carbamoyl-phosphate synthase
Cre/loxP	Site-specific recombinase technology
CREB	cAMP response element-binding protein
CREB	cAMP responsive element binding
CreERT2	Inducible Cre recombinase
C-section	Caesarean sectioning
CTGF	Connective tissue growth factor
CytC	Cytochrome C
D/D	Dimerization and docking domains
D-AKAP	Dual-specific AKAP
Drp1	Dynamin related protein 1
DSHB	Developmental Studies Hybridoma Bank
Dvl	Dishevelled

E	Embryonic day of development
e.g.	For example
EDTA	Ethylenediaminetetraacetic acid
eIF2Bε	Eukaryotic translation initiation factor 2Bε
EM	Electron microscopy
EMT	Epithelial-to-mesenchyme transition
Eno3	Enolase 3
Epacs	Exchange proteins directly activated by cAMP
ERK	Extracellular-signal-regulated kinase
ETC	Electron transport chain
FAK	Focal adhesion kinase
FCS	Fetal calf serum
FGF	Fibroblast growth factor
Fig.	Figure
FRAT	Frequently rearranged in T-cell lymphoma
FSH	Follicle-stimulating hormone
FSK	Forskolin
FW	Forward
Fzd	Frizzled
g	Gram
G6Paseβ	Glucose-6-phosphatase β
G6PD	Glucose-6-phosphate dehydrogenase
GAPDH	Glyceraldehyde 3-phosphate dehydrogenase
GATA4	GATA binding protein 4
GC-MS	Gas chromatography-coupled mass spectrometry
GEFs	Guanine exchange factors
GID	GSK3β binding domain
Glud1	Glutamate dehydrogenase
GO	Gene ontology
GOE	Gene ontology enrichment
GPCRs	G protein-coupled receptors
GPI	Glucose-6-phosphate Isomerase; Glukokinase
G_s	Heterotrimeric G protein
GS	Glycogen synthase
GSK3α/β	Glycogen synthase kinase 3α/β
Gskip, *Gskip*	Human or *mouse* gene encoding GSK3β interaction protein
GSKIP	GSK3β interaction protein
GSKIP-L130P	Mutant variant of GSKIP where Lysine 130 was substituted by Proline
GSKIPtide	Peptide corresponding to amino acid residues 115-139 of GSKIP
GTP	Guanosine-triphosphate
h	Hour
H89	PKA inhibitor compound
HE	Hematoxylin eosin
HEK293	Human embryonic kidney cell line 293
HeLa	Immortalized cell line derived from the cervical cancer of patient named Henrietta Lacks
HIF-1	Hypoxia induced factor 1
HK	Hexokinase
HSP60	Heatshock protein 60
HSP90	Heatshock protein 90
IF	Intermediate filament
IFN	Interferon
IgG	Immunoglobulin class G
Ihh	Indian hedgehog
IMM	Inner mitochondrial membrane
IRF7	Interferon response factor 7
ISH	*In situ* hybridization
JAK	Janus kinase
Jurkat	Immortalized line of human T lymphocyte cells
K_D	Dissociation constant
kDa	Kilodalton
KI	Knock-in
Klf2	Kruppel-like factor 2
KO	Knockout

l	Liter
LC3A/B-I/II	Microtubule-associated protein 1A/1B-light chain 3
LRP5/6	Low-density lipoprotein receptor 5/6
LTP and LDP	Long-term potentiation and depression
M	Molar
m	Mili
MAP2	Microtubule-associated protein 2
MAPK	Mitogen-activated protein kinase
Mbd3l1	methyl-CpG binding domain protein 3-like 1
MCM	α-MHC-MerCreMer
MEF	Murine embryonic fibroblasts
MI	Myocardial infarction
min	Minute
miR-26a	MicroRNA-26a
mRNA	Mature RNA
mROS	Mitochondrial reactive oxygen species
mTOR	Mammalian target of rapamycin
Myh6	Myosin heavy polypeptide 6
Myl 1, 2, 3	Myosin light polypeptide 1, 2, 3;
N	N-terminus
n	Nano
n	Sample number
n.d.	Not determined
n.v.	Not valid
NADPH	Nicotinamide adenine dinucleotide phosphate
NCAM	Neural cell adhesion molecule
NCBI	National center for biotechnology information
NFATc	Nuclear factor of activated T-cells
NFκB	Nuclear factor kappa-light-chain-enhancer of activated B cells
NIH	National institute of health
NLK	Neuroleukin
NMR	Nuclear magnetic resonance
NO	Nitric oxide
NPPA	Natriuretic Peptide A
ns	Not significant
OMM	Outer mitochondrial membrane
OPA1	Optic atrophy 1
p	Value used for statistic assessment
P0	Postnatal day 0 of development
p53	Cellular tumor antigen p53
PAGE	Polyacrylamide gel electrophoresis
PAS	Periodic-acid Schiff
PBS	Phosphate buffered saline
PBSMT	Phosphate-buffered saline + Milk + Triton
PBS-T	Phosphate buffered saline + Triton
PC	Phosphatidylcholine
PCR	Polymerase chain reaction
PDE	Phosphodiesterase
PDH	Pyruvate dehydrogenase
Pdpn	Podoplanin
Pecam	Platelet endothelial cell adhesion molecule-1
PFA	Paraformaldehyde
PG	Phosphatidylglycerol
PHB1	Prohibitin 1
Phf1	PHD finger protein 1
PI	Phosphatidylinositol
PI3K	Phosphatidylinositol-4,5-bisphosphate 3-kinase
PKA	Protein kinase A
PKB	Protein kinase B
PKD	Protein kinase D
PLCβ3	Phospholipase C β3
POD	Peroxidase
PP1	Protein phosphatase type 1

PP2B	Calcineurin
Ppp1r11	Protein phosphatase 1, regulatory (inhibitor) subunit 11
PTEN	Phosphatidylinositol-3,4,5-trisphosphate 3-phosphatase
PVDF	Polyvinylidene fluoride
p-X	Phospho-X
R (PKA R)	Regulatory subunit of PKA: isoforms RIα, RIβ, RIIα or RIIβ
Rab32	Ras-related protein 32
Rap1, Rap2	Ras-related protein 1,2; GTPase
RAPSN	Receptor-associated protein of the synapse
Rev	Reverse
RGS1	Regulator of G protein signalling 1
RhoA	GTPase
RhoGEF	Rho guanine nucleotide exchange factor
RIPA buffer	Radioimmunoprecipitation assay buffer
ROS	Reactive oxygen species
RTqPCR	Real Time quantitative PCR
SDH	Succinate dehydrogenase
sec	Second
SEM	Standard error of the mean
SerX	Serine residue at amino acid position x
Shh	Sonic hedgehog
shRNA	Short-hairpin RNA
SH-SY5Y	Human neuroblastoma cell line
SLB	Standard lysis buffer
SMYD2	SET And MYND Domain Containing 2
Sord	Sorbitol
Sp-B	Surfactant protein B
Sp-C	Surfactant protein C
SRY	Sex-determining region Y
Stat	Signal Transducer and Activator of Transcription
STRING	Search Tool for the Retrieval of Interacting Genes/Proteins
t Test	Statistical hypothesis test in which the test statistic follows a Student's t-distribution
Tab.	Table
tau	Protein
TCA	Tricarboxylic acid cycle
Tcap	Titin-cap assembly protein
TCF/LEF	Transcription factor
TEM	Transmission electron microscopy
THAHIT	the AKAP/amphipathic helix identification tool
ThrX	Threonine residue at amino acid position x
TNF	Tumour necrosis factor
TNKS	Tankyrase
Tnnc1/Tnnt3	Troponin C, Troponin T3
Tpm	Tropomyosin
TRIM32	Tripartite motif-containing protein 32
tRNA	Transfer RNA
Ttn	Titin
UBC	Ubiquitin C
V	Volt
VCAM-1	Vascular cell adhesion molecule
VDAC	Voltage-dependent anion channel
VEGF	Vascular endothelial growth factor
Wnt	Glycoprotein
WT	Wild type
x g	Times gravity
Yrdc	YrdC domain containing
Zfp710	Zinc finger protein 710
α-MHC	α-Myosin heavy chain
χ^2	Chi square test in statistics

List of figures

List of tables

1. Summary

A-kinase anchoring proteins (AKAPs) control the localization of cAMP-dependent protein kinase A (PKA) and tether PKA to distinct cellular compartments. In addition, AKAPs engage in protein-protein interactions with PKA substrates and other signalling proteins and form multi-protein complexes. Thus AKAPs control temporally and spatially the access of PKA to its substrates as well as the crosstalk of PKA with other signalling pathways. Glycogen synthase 3β (GSK3β) interaction protein (GSKIP) was identified as an AKAP by our group. GSKIP directly interacts with PKA and GSK3β and facilitates the inhibitory phosphorylation of GSK3β at Ser9 by PKA in cultured cells. In order to determine the physiological function of GSKIP, in particular its involvement in PKA and GSK3β signalling, a conditional knockout (KO) mouse model had been developed. In this thesis, these GSKIP KO mice were characterized.

Downregulation of GSK3β Ser9 phosphorylation upon GSKIP KO was observed in mice early in development in whole embryos, E12.5 primary MEFs and also in later stage E18.5 organs, in line with previous observations in cells and validating the KO mouse model. GSKIP-deficient mice die at birth, presumably because they are unable to initiate breathing properly. GSKIP KO mice at E18.5 appear cyanotic, show a decreased breathing frequency and die within a few minutes. 95 % of E18.5 GSKIP KO mouse lungs do not inflate upon exposure to air. Body and lung weights are unchanged compared to wild type mice. Exposed to respiratory distress at birth, GSKIP-deficient animals possess damaged lung mitochondria and show severely altered metabolite profiles (both in lung and liver) compared to wild type controls, likely accounting for their death. Proteomics revealed the muscle-specific intermediate filament desmin to be at least 50 % downregulated in GSKIP-depleted lungs at E18.5, allowing for a potential connection of mitochondrial aberrations with respiratory failure ultimately causing the perinatal lethality of GSKIP KO mice. The perinatal lethality of conditional GSKIP KO mice at E18.5 points out the essential role of GSKIP for extrauterine life.
A 100 % penetrant phenotype in GSKIP KO mice is the incomplete closure of the palatal shelves. Amongst others, GSK3β and Wnt signalling are involved in the developmental stages that lead to the closure. GSKIP depletion delays ossification along the fusion area of secondary palatal bones. These findings indicate a function for GSKIP in the coordination of GSK3β and Wnt signalling in palatal shelf fusion.
Large-scale microarrays and validation experiments defined the *Gskip*-responsive genes *Frat2*, *Rgs1* and *Klf2* as downregulated upon GSKIP KO.

To circumvent embryonic lethality of the conditional GSKIP KO mice, tissue-specific promoters combined with the Cre/loxP-system were used to generate two adult inducible GSKIP KO mouse models. Since PKA and GSK3β are involved in different physiological processes, amongst others in the control of cardiac myocyte contractility, the depletion of GSKIP in the adult heart and in general in the adult mouse will help to define further molecular pathways involving GSKIP.

2. Zusammenfassung

A-Kinase-Ankerproteine (AKAP) bilden durch direkte Protein-Protein-Interaktionen mit der cAMP-abhängigen Proteinkinase A (PKA), PKA-Substraten sowie weiteren Signalproteinen Multiproteinkomplexe und verankern diese an spezifischen intrazellulären Kompartimenten. Dadurch kontrollieren AKAP zeitlich und räumlich sowohl den Zugang der PKA zu ihren Substraten, als auch die Integration der PKA in verschiedene Signaltransduktionskaskaden. *Glycogen synthase 3β (GSK3β) interaction protein* (GSKIP) wurde von unserer Arbeitsgruppe als neues AKAP identifiziert. GSKIP bindet PKA und GSK3β direkt und ermöglicht in kultivierten Zellen die PKA-vermittelte, inhibierende Phosphorylierung der GSK3β. Um die physiologische Bedeutung von GSKIP, insbesondere seine Funktion in PKA- und GSK3β-koordinierten Signalwegen, aufzuklären, war ein konditionelles *knockout (KO)*-Mausmodell generiert worden. In der vorliegenden Arbeit wurden diese GSKIP-*KO*-Mäuse charakterisiert.

Als Validierung des KO Modells konnte die Abnahme der PKA-abhängigen inhibitorischen GSK3β-Phosphorylierung in Abwesenheit von GSKIP sowohl in frühen Embryonalstadien als auch in primären murinen embryonalen Fibroblasten und in E18.5 Mausgeweben festgestellt und somit zuvor erzielte Ergebnisse aus der Zellkultur *in vivo* bestätigt werden. GSKIP-defiziente Tiere sterben bei der Geburt, da sie nicht in der Lage sind ihre initial einsetzende Atmung aufrecht zu erhalten. GSKIP-*KO*-Mäuse erscheinen an Tag E18.5 zyanotisch, leiden unter respiratorischem Stress und sterben innerhalb weniger Minuten. 95 % der GSKIP-defizienten E18.5 Lungen entfalten sich nicht. Körper- und Lungengewicht der Mäuse sind unverändert gegenüber wildtypischen Kontrolltieren. GSKIP-*KO*-Mäuse, die nach Geburt respiratorischem Stress unterliegen, zeigen gegenüber Kontrollen stark geschädigte Lungenmitochondrien und sowohl ihre Lungen- als auch Lebergewebe besitzen ein auffällig verändertes metabolisches Profil, welches wahrscheinlich für ihren Tod verantwortlich ist. Proteomanalysen identifizierten eine 50 %-ige Abnahme des muskelspezifischen Intermediärfilaments Desmin in GSKIP-*KO*-Mäusen. Die Verbindung des mitochondrialen Phänotyps mit einer muskelbedingten Fehlfunktion der Atmung würde potentiell die perinatale Letalität GSKIP-defizienter Mäuse erklären. Die perinatale Letalität der Mäuse an Tag E18.5 der Embryonalentwicklung unterstreicht die essentielle Rolle von GSKIP für das extrauterine Leben.
Ein 100 % penetranter Phänotyp GSKIP-defizienter Mäuse an Tag E18.5 ist die Ausprägung einer Gaumenspalte. Sowohl GSK3β- als auch Wnt-vermittelte Signalwege liegen als molekulare Mechanismen der Fusion der paarigen Gaumenknochen zugrunde. Im untersuchten Mausmodell war die Verknöcherung der knorpeligen Gaumenknochen in Abwesenheit von GSKIP verzögert. Die erzielten Ergebnisse deuten auf eine koordinierende Rolle von GSKIP in GSK3β- und Wnt-involvierten Signalkaskaden der embryonalen Gaumenknochenbildung und -verknöcherung hin.
Ein genomweiter *microarray* und anschließende Validierungsexperimente identifizierten Gene, deren Expression sich aufgrund der Ausschaltung von *Gskip* verändert: die Expression von *Frat2*, *Rgs1* und *Klf2* waren herunterreguliert.

Um die Letalität der konditionellen GSKIP-*KO*-Mäuse zu umgehen, wurden mit Hilfe gewebsspezifischer Promotoren in Kombination mit dem Cre/loxP System zwei adulte, induzierbare GSKIP-*KO*-Mausmodelle generiert. Da PKA und GSK3β in diversen physiologischen Zusammenhängen mitwirken, u.a. in der Regulation der Kardiomyozytenkontraktion, soll die Ausschaltung von GSKIP in adulten Mäusen und gezielt im adulten Herz weitere Studien zur Aufklärung molekularer Mechanismen ermöglichen.

3. Introduction

Parts of the thesis introduction have been published recently in a review (Deak & Klussmann 2015), attached in the appendix.

3.1 cAMP signalling pathway

Second messengers such as cyclic adenosine monophosphate (cAMP) play pivotal roles in cellular signalling events. They enable cells to transform extracellular stimuli into cellular responses, hence to react to chemical cues they sense in their environment. Extracellular signals are amplified by intracellular signalling cascades leading to the accumulation of second messengers which in turn bind downstream target proteins (McCormick & Baillie 2014). Nitric oxide (NO), Ca^{2+} and cyclic guanosine monophosphate (cGMP) are further examples of second messenger molecules.
Stimulation of G protein-coupled receptors (GPCRs) on the cell surface and subsequent activation of the stimulatory heterotrimeric G protein G_s (comprising α, β and γ subunits) leads to activation of adenylyl cyclase (AC) which synthesizes cAMP. Cyclic nucleotide phosphodiesterases (PDEs) in turn degrade cAMP and thus terminate cAMP-mediated signalling. The strategic positioning of the constitutive activePDEs establishes gradients of cAMP inside cells, which are sensed by cAMP effectors such as exchange proteins directly activated by cAMP (Epacs), cyclic-nucleotide-gated (CNG) ion channels and protein kinase A (PKA) (Fig. 1). Effectors of cAMP can be tethered to defined cellular sites and transform local cAMP elevations into specific cellular responses to each of the external stimuli, given that the activation threshold of the effectors (in terms of cAMP concentration) is overcome (Walsh *et al.* 1968; Zaccolo *et al.* 2006; Conti & Beavo 2007; Baillie 2009; McCormick & Baillie 2014; Roberts & Dart 2014).

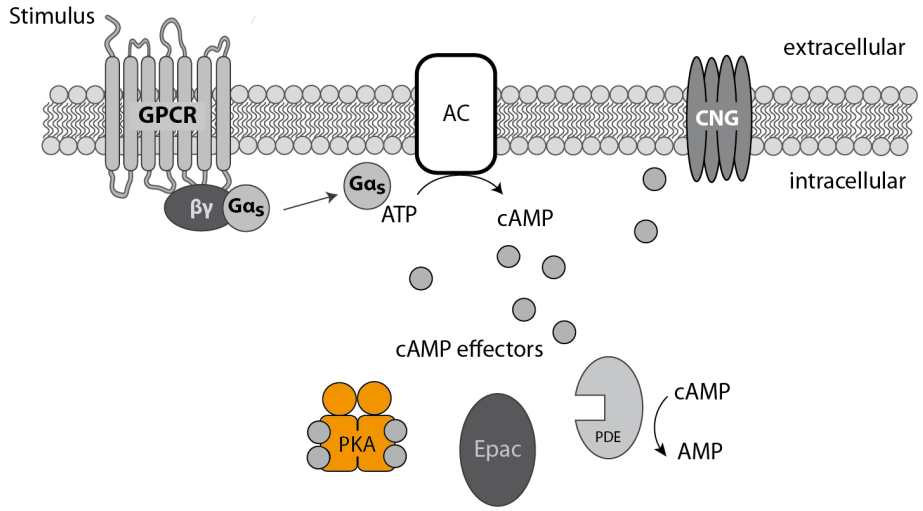

Fig. 1: **GPCR-dependent cAMP signalling cascade.** A plethora of stimuli (agonists) activate G protein-coupled receptors (GPCR), which in turn stimulate the heterotrimeric G protein G_s. $G\alpha_s$ dissociates from Gβ and Gγ subunits and activates adenylyl cyclase (AC) which converts ATP into cyclic AMP (gray). cAMP activates different cAMP effectors such as exchange proteins activated by cAMP (Epacs) and Protein kinase A (PKA; yellow). Constitutively active phosphodiesterases (PDEs) in turn degrade cAMP. In addition, cyclic nucleotide-gated channels (CNG) are cAMP-dependently activated. PDEs attenuate cAMP signalling by hydrolysis of cAMP to AMP.

ACs are a family of cAMP-generating enzymes, membrane-bound (AC1-AC9) or soluble (AC10), interacting with cytoskeletal structures, lipids and anchoring proteins (Cooper & Tabbasum 2014). All nine transmembrane ACs are activated by $G\alpha_s$ while the soluble AC10 is insensitive to it. The conversion of adenosine triphosphate (ATP) to cAMP is mediated in a single step reaction upon interaction of $G\alpha_s$ with AC: the oxygen on the 3' hydroxyl group of ATP attacks nucleophilically the α-phosphate, forms a phosphodiester bond and cleaves the pyrophosphate (Hurley 1999). ACs are widely expressed.
PDEs catalyze the hydrolysis of cAMP or cGMP to AMP or GMP, respectively (Rall & Sutherland 1958). 11 PDE families are known. They are structurally related (conserved C-terminal catalytic domain) but

functionally distinct and the majority of PDEs is encoded by more than one gene, accounting in total for more than 100 isozymes. While the isoforms PDE4, 7 and 8 are specific for cAMP conversion, PDE5, 6 and 9 are cGMP-activated and PDE1, 2, 3, 10 and 11 hydrolyze both cAMP and cGMP. The N-terminal regulatory region targets PDEs to different subcellular compartments and also enables isoform-specific protein-protein-interactions and signal transduction (Francis *et al.* 2011; Maurice *et al.* 2014).
CNG channels play an indispensable role in signal transduction pathways as they transduce changes of intracellular cyclic nucleotides into membrane potential and $[Ca^{2+}]_i$ changes. Activated by binding of cAMP or cGMP, these voltage-gated ion channels are non-selective for cations. CNG channels are expressed in rod and cone photoreceptors and olfactory receptor neurons (Biel & Michalakis 2009; Podda & Grassi 2014).
Epacs as cAMP-dependent guanine exchange factors (GEFs) induce the exchange of GTP for GDP on the small GTPases Ras-related protein 1 (Rap1) and Rap2 (de Rooij *et al.* 1999; Kraemer *et al.* 2001; Rehmann *et al.* 2006). There are two Epac isoforms, Epac1 and Epac2, with structural similarity in their C-terminal catalytic region, which activates RapGTPases. While Epac1 possesses only one binding domain for cyclic nucleotides, Epac2 contains two. Both are expressed during development as well as in mature tissue (Chen *et al.* 2014; Roberts & Dart 2014); Epac1 is ubiquitously expressed but predominantly found in kidney and heart, whereas Epac2 is mainly restricted to the brain, kidney and pancreas (Kawasaki *et al.* 1998; de Rooij *et al.* 2000).

3.1.1 Protein Kinase A and its anchoring by A-kinase anchoring proteins

Protein kinase A (PKA) is a serine/threonine kinase and the major cAMP effector, reflected also by its original name as cAMP-dependent protein kinase. It has been discovered in 1968 (Walsh *et al.* 1968) and brought into context with cAMP regulation (Gill & Garren 1970; Tao *et al.* 1970; Corbin *et al.* 1973). PKA is a ubiquitous kinase expressed in all mammalian cells and is involved in a plethora of biological processes, e.g. cell differentiation, proliferation and metabolism (Taylor *et al.* 2012; Taylor *et al.* 2013). In its inactive state the PKA holoenzyme consists of two catalytic (C) and two regulatory (R) subunits. Upon binding of two molecules of cAMP to each R subunit of PKA conformational changes occur and PKA is activated: the C subunits are released and in this active form phosphorylate nearby targets. Four different R subunits (RIα, RIβ, RIIα and RIIβ) and three different C subunit isoforms (Cα, Cβ, Cγ) are expressed in mammalian cells, and various splice variants have been reported. The C and R subunits can assemble in several combinations and give rise to a variety of PKA holoenzymes (Kim *et al.* 2007; Wu *et al.* 2007; Taylor *et al.* 2012; Taylor *et al.* 2013; Bruystens *et al.* 2014). According to the type of R subunit the holoenzyme is classified as type I or type II PKA. Type I PKA is activated at lower cAMP concentrations, while type II PKA requires higher cAMP concentrations and seems to have a more organized subcellular localization (Taylor *et al.* 2012).
The compartmentalization of PDEs and cAMP effectors is achieved by anchoring proteins, amongst them a family of proteins termed A-kinase anchoring proteins (AKAPs); they tether multi-protein complexes to defined cellular locations and spatially and temporally coordinate cellular signalling processes (Fig. 2). Hence, finetuning of very different tasks is enabled by restricting signalling to distinct microdomains.
AKAPs represent a family of more than 50 scaffolding proteins (including splice variants) whose common denominator is the ability to directly bind PKA. AKAPs commonly bind R subunits of PKA. Based on their R subunit selectivity, AKAPs are categorized as RI-, RII- or dual-specific (D-)AKAPs if they bind both RI and RII (Miki & Eddy 1999; Jarnaess *et al.* 2008; Skroblin *et al.* 2010).

3.1.2 AKAP-PKA interactions [taken from Deak and Klussmann, 2015]

AKAP-PKA interactions are mediated by highly conserved A-kinase binding domains (AKB) of AKAPs and the dimerization and docking (D/D) domains of the N-termini of R subunits of PKA. The D/D domains of R subunits dimerize and form a hydrophobic groove as a docking site for the AKAP. D/D domains are X-type four helix bundle structures (Newlon *et al.* 1999; Newlon *et al.* 2001; Gold *et al.* 2006; Kinderman *et al.* 2006; Taylor *et al.* 2008; Taylor *et al.* 2012; Taylor *et al.* 2013).

AKBs of the AKAP family are structurally conserved amphipathic α-helices of 14-18 amino acids in length (Carr *et al.* 1991). NMR and X-ray crystallographic analyses of AKB-derived peptides of several AKAPs confirmed the α-helical structure and showed that the hydrophobic phase of the helix docks into the hydrophobic groove formed by the D/D domain. The hydrophilic face of the helix can interact with hydrophilic amino acids at the rim of the D/D domain. Such interactions apparently increase the binding affinity (Gold *et al.* 2006; Hundsrucker *et al.* 2006; Kinderman *et al.* 2006; Sarma *et al.* 2010; Schafer *et al.* 2013).

A consensus sequence of polar and hydrophobic amino acids in conserved positions defines an AKAP signature motif: [AVLISE]-X-X-[AVLIF]-[AVLI]-X-X-[AVLI]-[AVLIF]-X-X-[AVLISE] (X = any amino acid, amino acids in [] represent alternatives at this position) (Vijayaraghavan *et al.* 1999; Hundsrucker *et al.* 2010). This AKAP signature motif was used to screen protein databases for new AKAPs. This approach identified GSK3β (Glycogen synthase kinase 3β) interaction protein (GSKIP) as an AKAP (Hundsrucker *et al.* 2010). Recently, another bioinformatics tool for the mapping of PKA binding domains and the prediction of novel AKAPs, THAHIT (the AKAP/amphipathic helix identification tool), was introduced and a list of new RIα and RIIα binding domains for existing AKAPs was published suggesting that various AKAPs are D-AKAPs (Burgers *et al.* 2014). This new tool not only uses sequence information from the PKA binding domains of known AKAPs but also includes the available structural information. THAHIT identified novel AKAPs, including a so far unknown AKAP of 330 kDa that is expressed in heart.

3.1.3 AKAP-mediated signalling processes [taken from Deak and Klussmann, 2015]

A plethora of extracellular cues leads to activation of the G_s/AC/PKA system of which all components are ubiquitously expressed. Through unique anchoring domains AKAPs tether PKA to defined cellular compartments (e.g. to the cytoskeleton, plasma membrane, the Golgi, vesicles, nucleus or mitochondria), and thereby regulate PKA signalling spatially and temporally (Fig. 2) (Wong & Scott 2004; Skroblin *et al.* 2010; Troger *et al.* 2012; Scott *et al.* 2013). The interaction of AKAPs with PKA increases the specificity of PKA signalling and facilitates specific cellular responses to each of the extracellular cues. AKAPs are engaged in further direct protein-protein interactions. Interactions with PKA substrates enable PKA to phosphorylate its local protein substrates and thereby to modulate their activities. In addition, AKAPs bind GPCRs (Appert-Collin *et al.* 2006), ACs (Dessauer 2009; Cooper & Tabbasum 2014), Epac (Nijholt *et al.* 2008), PDEs (Houslay 2010; Maurice *et al.* 2014), protein kinases (e.g. protein kinases C, D and N) (Perez Lopez *et al.* 2013), protein phosphatases such as PP1 (Schillace *et al.* 2001) and PP2B (calcineurin) (Oliveria *et al.* 2007; Flynn *et al.* 2008) and ion channels and pumps (e.g. L-type Ca^{2+} channels, Na^{+}-Ca^{2+} exchangers (Soni *et al.* 2014)). A few AKAPs additionally possess catalytic activity, e.g. the Rho guanine nucleotide exchange factor (RhoGEF) activity of AKAP-Lbc (Lymphoid blast crisis) that activates the small GTPase RhoA (Diviani *et al.* 2001) and the GTPase activity of Rab32 hydrolyzing GTP (Alto *et al.* 2002); as activities of some of the interacting proteins are modulated by second messengers other than cAMP, e.g. Ca^{2+}, AKAPs are not simple scaffolds but rather coordinate the crosstalk of cellular signalling processes. Aberrations in compartmentalized cAMP signalling and AKAP-mediated processes are associated with a range of diseases, including cancer, cardiovascular, neurological and inflammatory diseases (3.1.4).

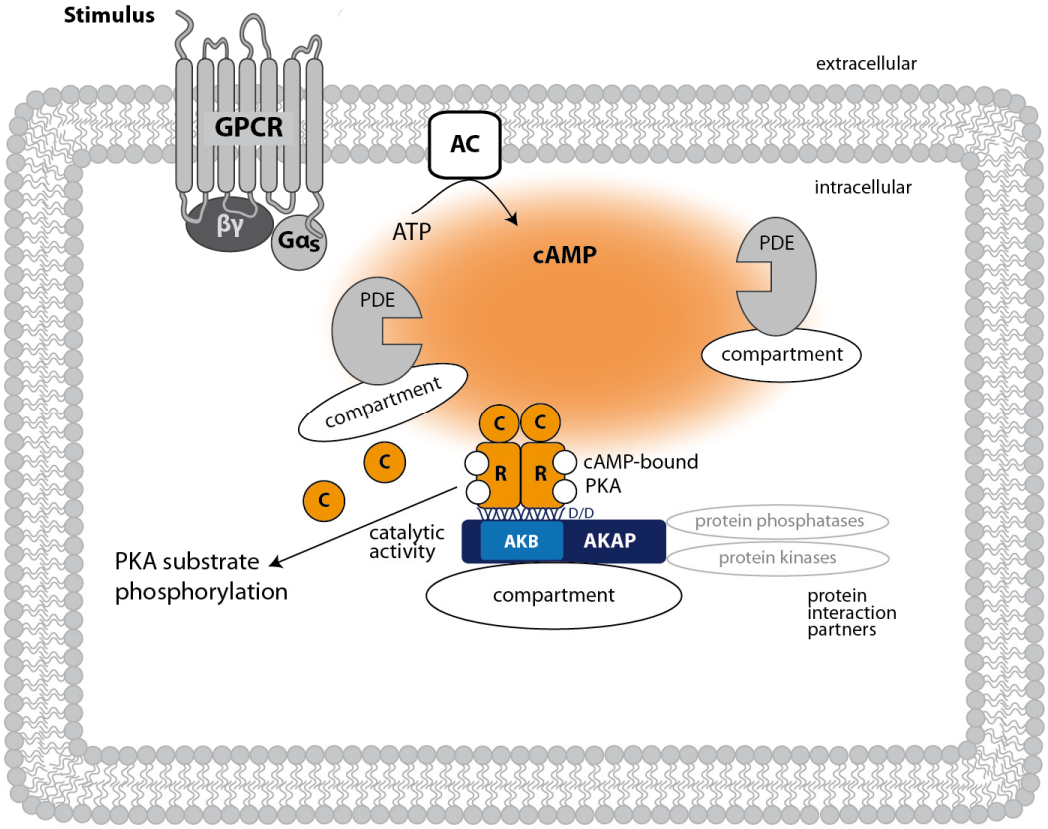

Fig. 2: **AKAPs as scaffolds in compartmentalized cAMP signalling.** GPCR-mediated activation of AC leads to an accumulation of the second messenger cAMP. PDEs are responsible for the establishment of local cAMP pools within subcompartments of cells. PKA activity is restricted to specific cellular compartments by the anchoring of PKA by AKAPs, enabling spatial and temporal control of PKA substrate phosphorylation. Upon binding of two molecules of cAMP to each R subunit of PKA the C subunits are released and available to phosphorylate nearby targets. The interaction of PKA R subunits with an AKAP is established between the R subunit D/D domain (helix bundle) and the AKB of the AKAP (α-helix). AKAPs function as signalling hubs, as they integrate further signalling pathways by binding further protein phosphatases and kinases. R and C, regulatory and catalytic subunits of PKA; D/D: dimerization and docking domain; AKB: A-kinase binding domain. Adapted from Deak and Klussmann, 2015 (Deak & Klussmann 2015).

3.1.4 Physiological function of AKAPs and their implication in disease [in part from Deak and Klussmann, 2015]

In vitro, cell-based and *in vivo* studies including knockdown approaches and gene targeting are shedding light on physiological functions and the pathophysiology of AKAPs. From the variety of studies it is clear that many cellular processes such as the regulation of cell cycle and cell migration (Gelman 2002), cardiac contractility (Carnegie *et al.* 2008; Hundsrucker & Klussmann 2008; Mauban *et al.* 2009; Diviani *et al.* 2013; Soni *et al.* 2014), sperm motility (Vijayaraghavan *et al.* 1997; Carr & Newell 2007; Luconi *et al.* 2011), insulin secretion (Lester *et al.* 1997) and T cell immune responses (Torgersen *et al.* 2008) are dependent on AKAPs.

The physiology and pathophysiology of AKAPs have been recently reviewed in detail, refer to publication attached to this thesis (Deak & Klussmann 2015). AKAPs are not only involved in heart, kidney, pancreas and brain function but are also relevant for glucose homoeostatis and red blood cell adhesion. Moreover, AKAPs are misregulated, amongst others, in cancer, chronic obstructive pulmonary disease (COPD) as well as schizophrenia.

3.1.5 The AKAP GSKIP [in part from Deak and Klussmann, 2015]

GSK3β interaction protein (GSKIP) was identified in our group by a bioinformatics consensus motif and peptide array screen (see 3.1.2) as a novel AKAP, directly interacting with PKA and GSK3β and thereby

facilitating the inhibitory phosphorylation of GSK3β on Serine 9 (Ser9) by PKA *in vivo* in cells (Hundsrucker *et al.* 2010). Further analysis has been conducted using an overexpression system *in vivo* in cells. The physiological function of the GSKIP/PKA/GSK3β complex is not known yet. GSKIP is detected in a wide range of rat tissues, pointing to a ubiquitous expression on protein level. Within cells GSKIP localizes mainly to the cytosol. GSKIP is evolutionary conserved among vertebrates and invertebrates with a conserved GSK3β binding domain (GID) while its interaction with RII subunits was observed in vertebrates only, ensuring its role as an AKAP in vertebrates (Hundsrucker *et al.* 2010).
GSKIP is so far the only AKAP with a nearly fully resolved 3D structure (Protein Data Bank code 1sgo; Fig. 3); of its 139 amino acids only the N-terminal 32 amino acids appeared unstructured in NMR analyses. The AKB resides between amino acids 28 and 52. The hydrophobic face of the helix lies on the surface of the protein; the hydrophilic face is buried by a β-sheet that follows the AKB in the primary structure (amino acids 49-115). The β-sheet, in turn, is followed by an α-helix that binds GSK3β (amino acids 116-139). GSKIP is an RII-specific AKAP as Biacore measurements showed nanomolar affinities for RII subunit binding of GSKIP, with a ten times higher affinity for RIIα compared to RIIβ (K_D = 5 nM vs. K_D = 43 nM).

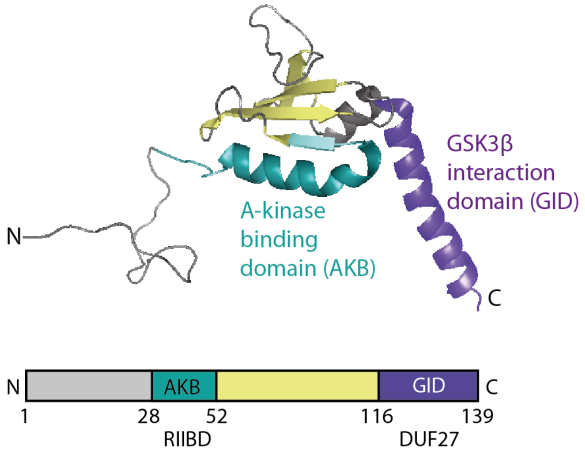

Fig. 3: **Human GSKIP protein tertiary and domain structure.** The NMR-based protein structure of human GSKIP (PDB ID: 1sgo) and its functional domains are shown (as obtained 2004 by the Northeast Structural Genomics Consortium). While the N-terminus (grey) is flexible and appears unstructured in NMR, the rest of the protein is built up by two α-helices (aa 33-48 and aa 116-139) and a β-sheet region (aa 49-115). Functionally assigned regions are highlighted in petrol (RII binding domain, also termed A-kinase binding domain (AKB)) and the GSK3β interaction domain (GID) in purple. Refer to text for details. N: N-terminus; C: C-terminus.

The work of our group as well as others demonstrated that GSKIP contains a C-terminal GID, namely a 25 amino acid region, which is similar to the GID of Axin. Both GSKIP and GSKIPtide (peptide corresponding to amino acid residues 115-139 of GSKIP) act as inhibitors of GSK3β and negatively regulate the GSK3β-Axin-β-catenin complex in Wnt signalling (Chou *et al.* 2006). The authors suggest that GSKIP may function similar to the Axin-GSK3β-interacting Wnt protein Frequently rearranged in advanced T-cell lymphomas (FRAT) and may substitute for FRAT participating in the GSK3β-Axin-β-catenin assembly; For Wnt signalling cascade see 3.2.
Moreover, GSKIP overexpression prevents neurite outgrowth of human neuroblastoma SH-SY5Y cells, more precisely retinoic acid-stimulated cell differentiation and GSK3β-mediated tau phosphorylation on Ser396 (Lin *et al.* 2009), known to be pathological in Alzheimer's disease. GSKIP increased β-catenin in the nucleus and CyclinD1 levels as well, promoting cell cycle progression in SH-SY5Y cells. In GSKIP overexpressing SH-SY5Y cells, N-Cadherin was down-regulated and N-Cadherin-associated β-catenin protein levels decreased in the cytosol. In turn, siRNA-mediated knockdown of GSKIP blocked neurite outgrowth. Thus, GSKIP might promote the translocation of β-catenin to the nucleus. Data from Chou *et al.* previously indicated that overexpression of GSKIP induced β-catenin accumulation in the cytoplasm and nucleus of HeLa cells, while the GSK3β binding-deficient mutant GSKIP-L130P did not cause changes (Chou *et al.* 2006).

Additionally, for the human Gskip gene (alias C14orf129 or HSPC120) alternatively spliced transcript variants have been observed. Currently, four variants are listed in the NCBI RefSeq database (Feb. 2015). While splice variant 1 is the longest, the other three differ in their 5' UTR compared to transcript 1. For the mouse *Gskip* gene (alias 4933433P14Rik) it is unknown whether different transcripts exist.

3.1.6 Glycogen synthase kinase 3β

GSK3 is a highly conserved pleiotropic serine/threonine kinase which is found in the cytosol, nucleus and mitochondria of all eukaryotic cells (Bijur & Jope 2003). There are two highly homologous genes encoding for two isoforms of GSK3, namely GSK3α and GSK3β. GSK3α is 51 kDa in size while GSK3β is slightly smaller with 47 kDa. They have structural similarities but are not redundant; the loss of one cannot be compensated by the other (see 3.3.2). GSK3 is a constitutively active enzyme and both isoforms phosphorylate primed substrates, i.e. which have been pre-phosphorylated by other kinases such as CK1, MAPK, or ERK (reviewed recently in (Beurel *et al.* 2014)).
Although GSK3β is the key enzyme of glycogen synthesis, originally identified as a regulator of glycogen synthase (GS), it is involved in various other cellular processes, including Wnt, NFκB, Hedgehog, Notch, Hippo, NFAT, PI3K and insulin signalling (Liu *et al.* 2007). GSK3β is regulated by a combination of phosphorylation, localization and sequestration by GSK3β-binding proteins (different GSK3 pools), not yet understood in detail (Kaidanovich-Beilin & Woodgett 2011). GSK3 regulates more than 50 substrates by phosphorylation allowing for modulation of diverse biological functions (Jope & Johnson 2004; Kockeritz *et al.* 2006). GSK3β is a converging point for multiple signalling pathways and is involved in multiple diseases, including diabetes, cancer, bipolar disorder, ischemia/reperfusion injury and in particular neurological neurodegenerative disorders such as Parkinson´s and Alzheimer´s disease (Li *et al.* 2014).
GSK3β activity is inhibited by Ser9 phosphorylation while the enzyme is activated by Tyr216 phosphorylation (Dajani *et al.* 2001). In mitochondria, especially in neuronal cells, GSK3β is regulated in the mitochondrial complex I and by ROS formation and has a regulatory function in mitochondrial cell death pathway. Kaidanovich-Beilin *et al.* published a list of numerous GSK3 substrates comprising metabolic enzymes (e.g. Glycogen synthase, Pyruvate dehydrogenase, Phosphocholine, ATP-citrate lyase), signalling proteins (e.g. Axin, APC, PKA RII, Cyclin D1, PTEN), structural proteins (e.g. tau, MAP2C, Dynamin1, NCAM, Neurofilament proteins, FAK, Dystrophin) and transcription factors (e.g. β-catenin, CREB, GATA4, c-Myc, NFATc, HIF-1, NFkB, p53) (Kaidanovich-Beilin & Woodgett 2011).
Of note, two AKAP family members other than GSKIP interact with GSK3 and facilitate GSK3β phosphorylation by PKA, namely Microtubule-associated protein 2 (MAP2) and AKAP220 (Tanji *et al.* 2002; Flynn *et al.* 2008).
The interaction for AKAP220 with GSK3β, PKA and protein phosphatase type 1 (PP1) in a quaternary complex was shown in COS cells (Tanji *et al.* 2002).
The expression of the MAP2D, a low-molecular weight splice variant of the MAP2 protein family, is induced by follicle-stimulating hormone (FSH) in rat granulosa cells and co-immunoprecipitates with PKA RII subunits. Additionally, an interaction of MAP2D and GSK3β and the GSK3β-mediated phosphorylation of MAP2D residues were shown. In a physiological context, increased PKA-induced Ser9 phosphorylation was observed in granulosa cells upon gonadotropin stimulation. Thus, it is postulated that MAP2 phosphorylation is PKA-dependently modulated by LH receptor-induced signalling cascades, involving GSK3β and opposing PP2A kinase activities (Salvador *et al.* 2004; Flynn *et al.* 2008).

3.2 GSK3 and the canonical Wnt pathway

The canonical β-catenin-dependent Wnt pathway involves GSK3β (Fig. 4). As GSKIP is postulated to be a negative regulator of GSK3β in Wnt signalling, this pathway is of relevance when studying GSKIP

functions. In addition, Wnt signalling is crucial for fate decisions during embryonic development and its dysregulation connected to various human diseases (Clevers & Nusse 2012).
In the absence of Wnt, β-catenin levels in the cell are low through its continuous proteasomal degradation. The assembly of a Wnt destruction complex, consisting in its core of Ademotous polyposis coli (APC), Axin, GSK3β and Casein kinase 1α (CK1α) mediates the phosphorylation and thus destabilization of β-catenin on different amino acid residues by CK1α (on Ser45) and subsequently by GSK3β (on Ser33, 37 and Thr41). This targets β-catenin for the recognition by the U3 ubiquitin ligase subunit β-Trpc, ubiquitination and subsequent 26S proteasome-mediated degradation. Upon binding of Wnt to the GPCR Frizzled (Fzd) and the co-receptor LRP5/6, the Wnt destruction complex is inhibited by Dishevelled (Dvl) and recruited to the intracellular side of the coreceptor. Hence β-catenin degradation is prevented and stabilized β-catenin translocates to the nucleus where β-catenin forms a complex with TCF/LEF transcription factors in the promoter region of Wnt target genes (e.g. CyclinD1, Axin2, c-Myc) and activates transcription (Niehrs 2012; Kim *et al.* 2013; Cruciat 2014; Sherwood 2015).

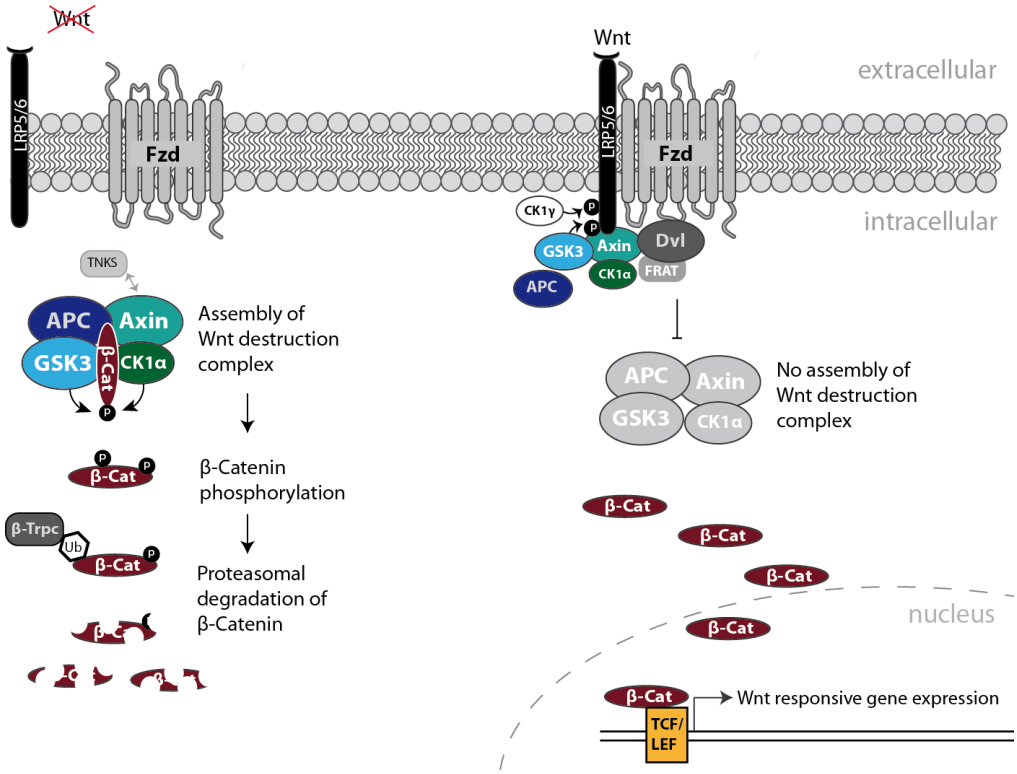

Fig. 4: **Canonical β-catenin-dependent Wnt signalling.** Without Wnt stimulation, no interaction between the coreceptors Frizzled (Fzd) and low-density lipoprotein receptor-related proteins 5/6 (LRP5/6) is observed. β-catenin (β-Cat) is captured by the so called Wnt destruction complex, comprising Ademotous polyposis coli (APC), Axin, GSK3β and Casein kinase 1α (CK1α). By phosphorylation β-Cat is destabilized, targeted for ubiquitinylation, recognized by the U3 ligase subunit β-Trpc and degraded by the 26S proteasome. Upon binding of Wnt to both co-receptors, Dishevelled (Dvl) together with Frequently rearranged in T-cell lymphoma (FRAT) is recruited to the intracellular side of LRP5/6 and further recruits Axin and GSK3. LRP5/6 is phosphorylated while the Wnt destruction complex cannot be assembled; hence, β-Cat is stabilized in the cytosol and translocates to the nucleus, where it induces the transcriptional activation of Wnt responsive genes. Tankyrases (TNKS) bind and destabilize Axin, thereby prolonging the half-life of β-Cat.

CK1-mediated phosphorylation occurs at different sites during Wnt signalling. β-Catenin and LRP6 are both targets of CK1. Upon Wnt stimulation, LRP6 is phosphorylated at Ser1490 by GSK3β while CK1γ phosphorylates the residues Thr1479, Thr1493 and Ser1496 (Cruciat 2014), resulting in the recruitment of Axin out of the destruction complex and stabilization of cytoplasmic β-catenin. Without Wnt, the assembly of the APC/Axin/GSK3/CK1α complex first mediates β-catenin phosphorylation by CK1α, followed by further GSK3-induced phosphorylation of pre-primed β-catenin.
Importantly, PKA has been shown to phosphorylate β-catenin on Ser675, but conversely leading to stabilization of β-catenin, inhibition of its ubiquitination and thus to activation of Wnt signalling (Hino *et al.* 2005).

3.3 PKA and GSK3 knockout mouse models – link to potential physiological roles of GSKIP in mice

The physiological functions of PKA and GSK3β have both been widely studied *in vivo* in mice. The following chapter summarizes the results showing phenotypes of conventional and conditional knockout (KO) mouse models and is meant to serve as a basis for the follow-up analysis of the GSKIP KO mouse model characterized during this thesis.

3.3.1 Mouse models targeting PKA regulatory R and catalytic C subunits

Animal models targeting PKA have been studied extensively (Kirschner *et al.* 2009). The catalytic subunit of PKA, as already described in 3.1.1, has three isoforms and conventional gene KO mouse models have targeted two of them, Cα and Cβ (Tab. 1). From the phenotypes listed in the upper part of Tab. 1 it becomes apparent that PKA C subunits are indispensable for normal spermatogenesis, cellular growth and normal neuronal development: the activation of specific PKA catalytic subunits is hence essential for proper molecular signalling. Early embryonic lethality was observed when both Cα subunits and Cβ1 were knocked out in mice completely; but, if one allele of either Cα or Cβ1 remained unaltered, lethality was postponed to later embryonic stages in *Prkaca*$^{-/-}$ *Prkacb[β1]*$^{+/-}$ animals while *Prkaca*$^{+/-}$ *Prkacb[β1]*$^{-/-}$ mice survived gestation with severe neuronal defects such as spina bifida (severe neural tube closure defect). Less frequently, cranial defects even caused exencephaly. Huang *et al.* showed *via* molecular analysis of diverse models that during neural tube formation neuronal cell patterning and differentiation is crucially dependent on PKA suppressing Sonic hedgehog (Shh) signalling (Huang *et al.* 2002). Cβ total KO mice exemplify that compensation by Cα is not sufficient to rescue neuronal signalling seen in these mice (Howe *et al.* 2002).
Several PKA R subunit KO mouse models were generated in the last two decades in order to define their physiological role (Tab. 1 *lower*). RI subunits are essential during development; biochemical characterization of early-stage *Prkar1a*$^{-/-}$ embryos revealed enhanced basal PKA activity (Amieux *et al.* 2002; Kirschner *et al.* 2005). Interestingly, the additional KO of *Prkaca* alleles improved substantially the phenotype but still resulted in embryonic lethality. This was widely interpreted to point out that the majority of developmental effects were caused by unregulated PKA activity (Kirschner *et al.* 2009). PKA RIα KO mice, especially heterozygous *Prkar1a*$^{+/-}$ animals, serve as genetic models for Carney Complex tumors; although early signs of tumorigenesis could not be determined in the animals (Amieux *et al.* 2002), long-term studies did indeed confirm a tumorigenic potential of this genetic alteration. The classification of the observed tumors differs strain-specifically, but tumors have been characterized independently by at least two groups (Veugelers *et al.* 2004; Kirschner *et al.* 2005). RIβ subunit deficiency in mice has been described to have no overt phenotype; brain PKA activity is unchanged compared to WT controls. When studying memory processes, *Prkar1b*$^{-/-}$ mice showed defective hippocampal function of synaptic long-term potentiation. Similar to *Prkar1b*$^{-/-}$ animals, *Prkar2a-/-* lack an obvious phenotype despite reduced total levels of PKA activity. Rao *et al.* studied more detailed long-term potentiation and depression (LTP and LDP) as well as visual cortex plasticity, unraveling decreased LTP despite unchanged LDP and an ocular dominance shift, implying a function of PKA RIIα in activity-dependent modification of synaptic connections (Rao *et al.* 2004).
Prkar2b $^{-/-}$ mice are apparently healthy and fertile but have diminished white adipose tissue despite normal food intake. Furthermore, this model displays a CNS phenotype with impaired ability to coordinate motor output, explained by drastic PKA activity reduction potentially leading to a perturbed subcellular localization of other PKA R subunits (Brandon *et al.* 1998).

Tissue-specific PKA subunit functions have been elucidated *via* generation of tissue-specific KO mouse models utilizing the Cre/loxP system (Tab. 1). Pituitary gland-specific KO of *Prkar1a (Prkar1a*-pitKO) causes pituitary tumorigenesis, neural crest-specific ablation of *Prkar1a* leads to Schwannomas (Schwann cell tumors) while heart-specific *Prkar1a* deletion is lethal at E11.5 with embryos exhibiting heart failure.

Tab. 1: **PKA-deficient mouse models and their phenotype.** Adapted & modified from Kirschner *et al.* (Kirschner *et al.* 2009).

Genotype		Phenotype (Ref.)
PKA C subunit		
	Prkaca-/- (both Cα1 and Cα2)	Growth retardation, Male infertility (sperm dysfunction due to *Cα2* KO); perinatal lethality (Skalhegg *et al.* 2002); decreased EGFR protein levels (Oksvold *et al.* 2008)
	Prkacb[β1]-/-	Phenotypically normal, deficiencies in neuronal signalling in hippocampus (Qi *et al.* 1996)
	Prkacb-/- (all 3 splice variants of Cβ)	Phenotypically normal, compensation by Cα but still cued (strain-specific) learning deficiencies (Howe *et al.* 2002)
	Prkaca-/-; Prkacb[β1]-/-	Early embryonic lethality (Huang *et al.* 2002)
	Prkaca+/-; Prkacb[β1]-/-	Severe spinal neural tube defects (Huang *et al.* 2002)
	Prkaca-/-; Prkacb[β1]+/-	Late embryonic lethality; (Huang *et al.* 2002) Spinal neural tube defects (75 %) Spinal neural tube defects + exencephaly (25 %)
PKA R subunit		
	Prkar1a-/-	Embryonic lethality (E10.5), inhibition of mesodermally-derived structures (heart and vasculature); increased basal PKA activity (Amieux *et al.* 2002; Kirschner *et al.* 2005)
	Prkar1a-/-; Prkaca-/-	Partial rescue of phenotype: restoration of mesodermal specification, heart formation; embryonic lethality later in development (Amieux *et al.* 2002)
	Prkar1a-/-; Prkaca+/-	Partial rescue of phenotype to an intermediate (Amieux *et al.* 2002)
	Prkar1b-/-	Viable, fertile, grossly normal appearance; deficient long-time memory (Brandon *et al.* 1995)
	Prkar2a-/-	No obvious phenotype (Burton *et al.* 1997); visual cortex plasticity changes, LTP decrease (Rao *et al.* 2004)
	Prkar2b-/-	Impaired motor coordination (Brandon *et al.* 1998); lean, resistant to diet-induced obesity (Cummings *et al.* 1996)
	Prkar2b-/-; Ucp1-/-	Lean phenotype retained by uncoupling protein 1 (Ucp1) (Nolan *et al.* 2004)
	Prkar2b-/-; Lep $^{ob/ob}$	Rescue of the obese Leptin phenotype of *Lep $^{ob/ob}$* mouse (Newhall *et al.* 2005)
	Prkar2b-/-; A^{y}	Rescue of obese phenotype of Agouti lethal yellow (A(y) mice (Czyzyk *et al.* 2008)
	Tissue-specific R subunit KOs	
	Pituitary-specific *Prkar1a*-pitKO	Late pituitary tumor development (after 18 months) (Yin *et al.* 2008b; Kirschner 2010)
	Heart-specific α-MHC-*Prkar1a*-KO	Embryonic lethality (E11.5); failure of heart development, myxomagenesis (Yin *et al.* 2008a)
	Neural crest-specific *Prkar1a*-TEC3KO	Schwann cell tumor development (50 % by 18 weeks, 80 % by 40 weeks) (Jones *et al.* 2008)

Taken together, *Prkacb, Prkar2a* and *Prkar2b* KO mice are viable and fertile while *Prkar1a* and *Prkac* KO animals are embryonically lethal. As GSKIP is predominantly binding PKA RIIα subunits (K_D = 5 nM), and with a lower affinity also RIIβ subunits (K_D = 43 nM) (Hundsrucker *et al.* 2010), a potential GSKIP KO phenotype could resemble the ones of *Prkar2a* and *Prkar2b* KO mice (GSKIP potentially displacing RII subunits of PKA).

3.3.2 GSK3 mouse models

GSK3-deficient animal models have been analysed with a distinct focus on brain as GSK3β is a key player in Alzheimer's disease. This chapter also reviews phenotypes studied unrelated to the CNS and brain (Tab. 2).
Conditional GSK3α KO mice are viable and fertile, born at expected Mendelian ratios and do not show a cardiac phenotype (Kerkela *et al.* 2008). In contrast, conditional GSK3β KO mice die early in development due to severe hepatic necrosis (Hoeflich *et al.* 2000) or cardiac patterning defects (Kerkela *et al.* 2008). First, GSK3β deletion leads to hypertrophic cardiomyopathy secondary to cardiomyoblast hyperproliferation associated with increased expression and nuclear localization of GATA4, cyclinD1 and c-Myc, three regulators of proliferation (Kerkela *et al.* 2008). GSK3β$^{-/-}$ embryos have ventricular septal defects. The phenotype of GSK3β KO mice is additionally characterized by an incomplete closure of the secondary palate, indicating that GSK3β is essential for normal mammalian craniofacial development (Liu *et al.* 2007). The interplay of Wnt and Shh signalling has been repeatedly studied in mice deficient for GSK3β. The precise regulation of both pathways, namely increased Wnt and decreased Shh signalling in the developing palate of GSK3β KO mice, is linked to palatal bone ossification: both higher levels of Wnt and lower levels of Shh have been described to inhibit osteogenic differentiation of mesenchymal cells (Nelson *et al.* 2011).

Furthermore, the disruption of GSK3β is accompanied by severe liver degeneration during mid-gestation, a phenotype consistent with the phenotype of mice lacking genes involved in the activation of the transcription factor activation NFκB with excessive tumor necrosis factor (TNF) toxicity (Hoeflich *et al.* 2000). GSK3β-deficient embryos were rescued by injection of TNF-α antibody inhibiting TNF. Embryonic fibroblasts isolated from GSK3β KO embryos were hypersensitive to TNF-α and showed diminished function of NFκB. In contrast, the heterozygous KO of GSK3β displays a remarkably milder phenotype (Beaulieu *et al.* 2004; O'Brien *et al.* 2004; Beaulieu *et al.* 2008; Bersudsky *et al.* 2008; Urs *et al.* 2011), described in Tab. 2.
Transgenic knock-in (KI) mice overexpressing GSK3β are embryonically lethal (Brownlees *et al.* 1997) while KI mice with constitutively active GSK3 show mainly impaired neuronal development (Tab. 2). With a focus on GSK3β, the tissue-specific KO mouse models helped to some degree to define neuronal phenotypes while tissue-specific KO in other organs displayed no consistent physiological changes. The kidney cortical tubule-specific, postnatal KO of GSK3β barely affects kidney morphology or function but increases glycogen accumulation in the tubules (Ge *et al.* 2011). The physiological effects of muscle-specific (Pansters *et al.* 2015) or postnatal forebrain neuron-specific GSK3β KO (Latapy *et al.* 2012) results only in minor changes. In contrast, neuronal progenitor-specific GSK3α and β KO led to very dramatic cell polarity loss in line with dysregulated β-catenin, Hedgehog, FGF and Notch pathways and perinatal lethality (Kim *et al.* 2009).

Tab. 2: **Phenotypes of mouse models targeting GSK3.** Adapted & modified from Kaidanovich-Beilin (Kaidanovich-Beilin & Woodgett 2011).

Genotype		Neuronal phenotype (Ref.)	Additional phenotype (Ref.)
Conventional KO			
	Gsk3α (Exon 2)	Viable; abnormal behavioural features; decreased number of Purkinje cells in cerebellum; decreased dendrite length and surface (Kaidanovich-Beilin *et al.* 2009)	Improved insulin sensitivity, hepatic glycogen accumulation (strain-specific, ICR background only) (MacAulay *et al.* 2007); Male infertility (Maurin *et al.* 2013); Lower sperm ATP levels, low amplitude of flagellar beat, Protein phosphatase PP1ɣ2 catalytic activity (Bhattacharjee *et al.* 2015); Progressive cardiomyocyte and cardiac hypertrophy, contractile dysfunction (Zhou *et al.* 2010); accentuated post-MI remodeling (Lal *et al.* 2012); Shortened life-span, accelerated age-dependent pathologies (Zhou *et al.* 2013)
	Gsk3β-/- (Exon 2)		Late embryonic lethality due to severe hepatic necrosis (E12.5) (Hoeflich *et al.* 2000) or cardiac patterning defects (Kerkela *et al.* 2008); cleft palate (Liu *et al.* 2007; He *et al.* 2010)
	Gsk3β+/- (Exon 2)	Viable, morphologically normal; lithium-mimetic, anti-depressant-like state (Beaulieu *et al.* 2004); reduced exploratory behaviour (O'Brien *et al.* 2004); increased anxiety (Bersudsky *et al.* 2008), reduced aggressive behaviour (Beaulieu *et al.* 2008), reduced responsiveness to amphetamine treatment (Beaulieu *et al.* 2004), increased morphine-induced locomotion (Urs *et al.* 2011)	
Conditional KO			
	GSK3β shRNA injection into hippocampus	Decreased immobility time in forced swim test; unchanged locomotor activity (Omata *et al.* 2011)	
	Transgenic forebrain-specific dominant-negative expression of GSK3β(Lys85A)	Increased apoptosis in the brain; behavioural deficits in motor coordination (Dominguez *et al.* 1995; Gomez-Sintes *et al.* 2007)	Normal growth; no tumors
Overexpression (KI)			
	GSK3β	Embryonic lethality (Brownlees *et al.* 1997)	
	Forebrain-specific Tet-GSK3β	Increased neuronal cell death, increased tau phosphorylation; decreased levels of nuclear β-catenin (Lucas *et al.* 2001); Reduced LTP induction (Hooper *et al.* 2007)	
	GSK3β-S9A: const. active GSK3β	Microcephaly; increased neuronal density (Spittaels *et al.* 2002),	Upregulated Akt1, downregulated PPP2R3A and GSK3α in striatum; reduced water consumption,

		decreased MAP2 levels; Hyperactivity (Prickaerts *et al.* 2006);	disturbed eating pattern (Prickaerts *et al.* 2006)
	Postnatal GSK3β-S9A: const. active GSK3β	Altered postnatal neuronal maturation and differentiation, reduced brain size but only subtle changes in psychomototric ability of adult and aging mice (Spittaels *et al.* 2002)	
	GSK3α-S21A,β-S9A: const. active GSK3α,β	Drastic impairment in neurogenesis due to reduced VEGF expression (Eom & Jope 2009); Increased susceptibility to hyperactivity, altered immobility time and mild anxiety (Polter *et al.* 2010)	Normal development and growth, no metabolic abnormalities (McManus *et al.* 2005); βKI mice attenuate hypertrophy and heart failure, while αKI mice promote hypertrophy and HF during pressure overload (Matsuda *et al.* 2008)
	Osteoclast-specific constitutively active GSK3β-S9A		Impaired osteoclast differentiation (Jang *et al.* 2011)
Tissue-specific KO			
	Cardiomyocyte-specific GSK3α		Limits ventricular remodeling; post-myocardial infarction cardiac function preserved (Ahmad *et al.* 2014)
	Hepatic or skeletal muscle-specific GSK3α		No differences in glucose tolerance or insulin sensitivity
	Kidney cortical tubule -specific GSK3β		Increased glycogen accumulation in kidney tubules (Ge *et al.* 2011), barely affecting kidney function
	Muscle-specific GSK3β		Early muscle mass recovery accelerated, post-natal myogenesis promoted (Pansters *et al.* 2015)
	Postnatal forebrain pyramidal neuron-specific GSK3β	Increased anxiety, pro-social phenotype (Latapy *et al.* 2012)	
	Palatal mesenchyme-specific GSK3β		Survived birth and no cleft palate (He *et al.* 2010)
	Palatal epithelium-specific GSK3β		Secondary cleft palate, failure of palate elevation after E14.5 (He *et al.* 2010)
	Neuronal progenitor-specific GSK3α,β	Lethality at P0; Dramatic hyperproliferation of neuronal progenitors, dysregulation of β-catenin, Hedgehog, FGF and Notch signalling, loss of cell division polarity (Kim *et al.* 2009)	

Dysregulation of GSK3β has been implicated in a large number of human disorders like inflammatory diseases, diabetes, stroke and Alzheimer's disease (Martinez *et al.* 2002). Due to the indispensable role of both GSK3β and GSKIP in mouse development the gene KO of GSKIP might exhibit a GSK3β-related phenotype and expected to be associated amongst others with major physiological brain dysfunction and disease.

To sum up the final introductory chapter, many of the total KO mouse models described above showed embryonic lethality but were still of value for initial analyses when assessing the function of their *in vivo* target in a complex physiological context of a model organism. It is difficult to predict the physiological function of GSKIP, but the absence of viable KO animals at 4 weeks of age [PhD thesis P. Skroblin] certainly indicates an indispensable role of GSKIP in development. Hence the phenotypes presented (Tab. 1, Tab. 2) at least offer a glimpse into potential roles of GSKIP *in vivo* in mice.

3.4 Aim of thesis

The aim of this work is to define the physiological function of GSKIP *in vivo* in a conditional KO mouse model targeting the AKAP GSKIP. When mating heterozygous GSKIP KO mice, there are no viable homozygous GSKIP KO progeny. By defining cause and time point of death of the conditional GSKIP KO mice it is intended to define critical processes responsible for the lethality. GSKIP is a ubiquitously expressed protein. Both GSK3β and PKA have been extensively studied in KO mice as well as the involvement of PKA and GSK3 signalling in embryonic development. How these proteins, both interacting with GSKIP, are involved in the molecular mechanisms underlying development and which role GSKIP plays in these processes will be elucidated by morphological and molecular analysis of the observed GSKIP KO phenotype. The overall aim is to confirm and broaden previous data from cell studies.

Additionally, altered mRNA and protein expressions upon GSKIP KO are studied for determination of physiological processes and signalling cascades involving GSKIP, both on a small scale and by large-scale gene expression and metabolomics approaches.

To overcome the lethality of the constitutive GSKIP KO, different adult inducible KO mouse models are planned to be generated. Several AKAPs as well as GSKβ are important signalling molecules amongst others in cardiomyocytes. Inducible heart-specific and inducible tissue-non-specific KOs will be established to serve as new tools in order to determine the function of GSKIP independent of its role in development in the adult organism.

4. Material and Methods

4.1 Material

4.1.1 Equipment and software

Tab. 3: **Equipment**

Equipment	Description	Supplier
Agilent 2100 Bioanalyzer	RNA on-chip gel electrophoresis running and documentation device	Agilent Technologies (Santa Clara, US)
Applied Biosystems ViiA™ 7 Real-Time PCR Cycler	RTqPCR cycler	Life Technologies GmbH (Darmstadt, D)
BioRad iQ5 Cycler	RTqPCR cycler	Bio-Rad Laboratories GmbH (München, D)
Centrifuge 5415 D	Benchtop centrifuge	Eppendorf (Hamburg, D)
Centrifuge Universal 320 R	Centrifuge	Hettich (Tuttlingen, D)
Cryo-container 5100-0001	Freezing container	Thermo Fisher Scientific/NALGENE (Bonn, D)
Dissection tools	Forceps, scissors for mouse dissection	FST (Heidelberg, D)
Duomax 1030	Rocker switch	Heidolph Instruments (Schwabach, D)
Enspire® 2300	Microplate reader	PerkinElmer (Rodgau, D)
GelDoc 2000	Gel documentation system	Bio-Rad Laboratories GmbH (München, D)
IKA® MS 3 basic	Small shaker	IKA (Wilmington, US)
IKA® RCT Standard	Heating plate	IKA (Wilmington, US)
Incubator CB210	Cell incubator	Binder (Tuttlingen, D)
Keyence BZ-8100E	Digital microscope	Keyence (Osaka, Japan)
Leica MZ16 stereomicroscope + DFC 495 camera	Dissection microscope	Leica Microsystems (Houston, US)
MicroCentrifuge 2	Micro-scale centrifuge	NeoLab (Heidelberg, D)
Microwave AEG Micromat_Duo	Heating device for agarose gel casting	AEG (Berlin, D)
Mini Star Galaxy	Mini-scale centrifuge	VWR (Randor, US)
MiniProtean®	Polyacrylamide gel electrophoresis cell	Bio-Rad Laboratories GmbH (München, D)
Mortar and pestle	Tissue homogenisation on dry ice	KPM (Berlin, D)
NanoDrop ND-1000	Spectrophotometer	PeqLab Biotechnologie GmbH (Erlangen, D)
Odyssey Imager	Western Blot detection system	LI-COR Biosciences (Bad Homburg, D)
PerfectBlue mini L	Agarose gel electrophoresis chamber	PeqLab Biotechnologie GmbH (Erlangen, D)
PipetBoy acu IBS	Pipettor	Integra Biosciences/ Ibs (Fernwald, D)
Pipettes 2,5/ 10/ 20/ 200/ 1000/ 5000 µl	Pipetting	Eppendorf (Hamburg, D)
Power Pac 1000/ 3000	Power supply	Bio-Rad Laboratories GmbH (München, D)
RS-TR05	Falcon rotor	Phoenix Intruments (Garbsen, D)
Sonopuls HD 2070	Ultrasound homogenizer	Bandelin electronic GmbH& Co. KG (Berlin, D)
Tecnai G^2 20 LaB6	Transmission electron microscope	Fei (Hillsboro, US)
Thermomixer Compact	Shaking heater	Eppendorf (Hamburg, D)
Tissue Grind Tube & Pestle	Tissue Grinding (soft lysis)	Wheaton Scientific (Millville, US)
Titramax 100	Plate shaking device	Heidolph Instruments (Schwabach, D)
TProfessional TRIO	Thermocycler	Biometra (Göttingen, D)
TransBlot	Semi-Dry Western Blot module	Bio-Rad Laboratories GmbH (München, D)

Tab. 4: **Disposable material**

Material	Description	Supplier
6 /12 /24 /96 well plates	Cell culture plate	TPP (Trasadingen, CH)
Cell culture dish (60 mm)	Cell culture dish	TPP (Trasadingen, CH)
Cryo-vials E309.1	Cryoconservation of cells	Carl Roth GmbH & Co KG (Karlsruhe, D)
Reaction tubes	Laboratory essential	Sarstedt (Nümbrecht, D)
Filter tips	Pipette tips for cell culture, PCR and RNA processing	StarLab (Hamburg, D)
Glass vials and caps	Container for glutaraldehyde fixation	TPP (Trasadingen, CH)
MicroAmp Optical 96-/ 384-well Reaction Plate with Barcode	RTqPCR plates	Life Technologies GmbH (Darmstadt, D)
Mini Protean® TGX™ 4-20 % Precast Gel	Commercial gradient gels for SDS-PAGE (surfactant protein analysis)	Bio-Rad Laboratories GmbH (München, D)
Optical Adhesive Film	RTqPCR seal	Life Technologies GmbH (Darmstadt, D)
PCR tubes, coloured	Tubes for PCR applications	Biozym Scientific (Oldendorf, D)
Pipette tips	Laboratory essential	StarLab (Hamburg, D)
PVDF membranes T830.1	Western Blotting membranes	Carl Roth GmbH & Co KG (Karlsruhe, D)
Rotbart® extra dünn	Rasor blades	Gillette (Berlin, D)
Scalpels	Dissection, Primary cell culture	B Braun (Melsungen, D)
T75 cell culture flask	Cell culture flask	TPP (Trasadingen, CH)

Tab. 5: **Commercial kits**

Kits	Description	Supplier
Agilent RNA 6000 Nano Chips	RNA quality control	Agilent Technologies (Santa Clara, US)
Coomassie PlusTM Protein Assay Reagent + Albumin (BSA) Standart Ampules	Determination of total protein amount	Thermo Fisher Scientific (Bonn, D)
GeneMATRIX Tissue DNA Purification Kit	Kit for isolation of total DNA from human and animal tissues	Roboklon (Berlin, D)
Illumina® TotalPrep™-96 RNA Amplification Kit	RNA amplication and labeling for Illumina Microarray	Illumina (San Diego, US)
PepTaq® Assay	non-radioactive detection of cAMP-dependent protein kinase	Promega (Madison, US)
QiaShredder Columns	Tissue disruption prior to RNA isolation	Qiagen (Venlo, NL)
RNeasy Mini Kit	Total RNA purification	Qiagen (Venlo, NL)
SuperScript ® III First-Strand Synthesis SuperMix	cDNA synthesis	Life Technologies GmbH (Darmstadt, D)

Tab. 6: **Software**

Software	Purpose	Supplier/URL
DAVID Bioinformatics Resources 6.7	Functional annotations and gene conversion, Gene Ontology enrichment	National Institute of Allergy and Infectious Diseases (NIAID), NIH; david.abcc.ncifcrf.gov/
EndNote X7	Reference manager	Thomson Reuters (Toronto, CA)
Excel 2010	Spreadsheet	Microsoft (Redmond, US)
GOEAST Ver 1.30	Gene ontology analysis	Institute of Genetics and Developmental Biology, Chinese Academy of Sciences; http://omicslab.genetics.ac.cn/GOEAST/
GraphPad Prism 5.01	Statistical analysis	GraphPad Software, Inc. (La Jolla, US)
Illustrator CS5	Graphics, drawings	Adobe Systems, Inc. (San Jose, US)
Image Studio Ver 2.0	Western Blot analysis	LI-COR Biosciences (Bad Homburg, DE)
ImageJ 1.47v	Image processing	NIH; http://rsb.info.nih.gov/ij/
Keyence BZ Application Ver 1.1 + Analyzer Ver 3.6	Image observation and processing	Keyence (Osaka, Japan)
Perseus	Proteomics analysis and visualization tool	MPI Munich; http://www.perseus-framework.org/ (München, DE)
Photoshop CS5	Image processing	Adobe Systems, Inc. (San Jose, US)
Power Point 2010	Presentations	Microsoft (Redmond, US)
PyMol Molecular Graphics	Molecular visualization tool	Schrödinger, Inc. (New York, US)
PyRAT (Python Based Relational Animal Tracking) Ver v3.2-315-g9224591	Animal organization and husbandry tool	Scionics Computer Innovation (Dresden, D)
SerialCloner Ver 2.5	Sequence analysis	serialbasics.free.fr/Serial_Cloner.html
STRING Ver 9.1	Functional protein annotation network	http://string-db.org/
Word 2010	Word processing	Microsoft (Redmond, US)

4.1.2 Antibodies

Tab. 7: **Antibodies used for Western Blotting or Immunostaining**

Primary antibody	Origin	Company; Order Number
2H3 neurofilament	Mouse	DSHB (University of Iova, US); #2H3
Akt (pan)	Rabbit	Cell Signalling Technology (Danvers, US); #4060
Aldh4a1	Rabbit	Santa Cruz Biotechnology (Dallas, US); #sc-367309
AQP5	Rabbit	Alomone Labs (Israel); #AQP-005
Atpif1	Rabbit	Cell Signalling Technology (Danvers, US); #8528
Axin1	Rabbit	Cell Signalling Technology (Danvers, US); #3323S
Axud1	Goat	Santa Cruz Biotechnology (Dallas, US); #sc-49281
β-catenin (6B3)	Rabbit	Cell Signalling Technology (Danvers, US); #9582S
Col1a1	Rabbit	Santa Cruz Biotechnology (Dallas, US); #sc-8784
Cox4	Rabbit	Cell Signalling Technology (Danvers, US); #4844
Cps1	Mouse	Santa Cruz Biotechnology (Dallas, US); #sc-376190
CTGF	Rabbit	Santa Cruz Biotechnology (Dallas, US); #sc-25440
CyclinD1 (SP4)	Rabbit	Abcam (Cambridge, UK); #ab1663
Cytochrome C	Rabbit	Cell Signalling Technology (Danvers, US); #4280
Desmin	Rabbit	Cell Signalling Technology (Danvers, US); #5332
Drp1	Rabbit	Cell Signalling Technology (Danvers, US); #8570
E-Cadherin	Rat	Abcam (Cambridge, UK); #ab11512
Eno3	Rabbit	Biorbyt (Cambridge, UK); orb5157
FRAT2 MaxPab polyclonal (B01)	Rabbit	Abnova (Taipei, Taiwan); #H00023401-B01

G6Paseβ	Rabbit	Santa Cruz Biotechnology (Dallas, US); #sc-134714
G6PD	Rabbit	Cell Signalling Technology (Danvers, US); #12263
GAPDH	Rabbit	Cell Signalling Technology (Danvers, US); #2118S
GAPDH	Mouse	Santa Cruz Biotechnology (Dallas, US); #sc-166574
Glud1	Rabbit	Cell Signalling Technology (Danvers, US); #12793
GPI	Mouse	Santa Cruz Biotechnology (Dallas, US); #sc-365066
GSK3β	Rabbit	Cell Signalling Technology (Danvers, US); #9315
GSKIP	Rabbit	custom-made (Hundsrucker *et al.* 2010) by Biogenes (Berlin; D)
Hexokinase pan	Mouse	Abcam (Cambridge, UK); #ab58979
Hexokinase-2 (C6G5)	Rabbit	Cell Signalling Technology (Danvers, US); #2867
Hsp60	Rabbit	Cell Signalling Technology (Danvers, US); #4870
Hsp90	Mouse	Stressgen (Victoria, CAN); SPA-830
IRF7	Rabbit	Santa Cruz Biotechnology (Dallas, US); #sc-9083
LRP5/6	Rabbit	Cell Signalling Technology (Danvers, US); #3395
mTOR	Rabbit	Cell Signalling Technology (Danvers, US); #2983
N-Cadherin	Rabbit	Cell Signalling Technology (Danvers, US); #13116P
NPPA	Rabbit	Abcam (Cambridge, UK); #ab14348
NPPA	Rabbit	Thermo Fisher Scientific (Bonn, D); PA5-29559
PDH	Rabbit	Cell Signalling Technology (Danvers, US); #3205
PHB1	Rabbit	Cell Signalling Technology (Danvers, US); #2426
phospho-Akt Ser473	Rabbit	Cell Signalling Technology (Danvers, US); #4060
phospho-Akt Thr308	Rabbit	Cell Signalling Technology (Danvers, US); #2965
Phospho-Drp1 Ser637	Rabbit	Cell Signalling Technology (Danvers, US); #6319
phospho-Glycogen Synthase Ser641	Rabbit	Cell Signalling Technology (Danvers, US); #3891
phospho-GSK3β Ser9	Rabbit	Cell Signalling Technology (Danvers, US); #9323S
phospho-LRP5/6 Ser1490	Rabbit	Cell Signalling Technology (Danvers, US); #2568
phospho-mTOR Ser2448	Rabbit	Cell Signalling Technology (Danvers, US); #2971
Phospho-PKA substrate (RRXS*/T*)	Rabbit	Cell Signalling Technology (Danvers, US); #9624
Phospho-PKA substrate (RRXS*/T*)	Rabbit	Cell Signalling Technology (Danvers, US); #9621
phospho-tau Ser396	Mouse	Cell Signalling Technology (Danvers, US); #9632
phospho-β-catenin Ser33/37,Thr41	Rabbit	Cell Signalling Technology (Danvers, US); #9561S
phospho-β-catenin Ser675	Rabbit	Cell Signalling Technology (Danvers, US); #9567
PKA-RIIα	Mouse	BD Biosciences (Heidelberg, D); #612243
PKA-C	Mouse	BD Biosciences (Heidelberg, D); #61098
PLCβ3	Rabbit	Novis Biologicals (Littleton, US); NBP1-19442
RGS1 (H-70)	Rabbit	Santa Cruz Biotechnology (Dallas, US); #sc-20758
SDHA	Rabbit	Cell Signalling Technology (Danvers, US); #5839
SMYD2 (D14H7)	Rabbit	Cell Signalling Technology (Danvers, US); #9734S
Sord	Rabbit	Santa Cruz Biotechnology (Dallas, US); #sc-366370
Sp-B	Rabbit	Santa Cruz Biotechnology (Dallas, US); #sc-13978
Sp-C	Rabbit	Santa Cruz Biotechnology (Dallas, US); #sc-13979
Talin-2	Rabbit	Genetex (Irvine, US); GTX63116
Tau	Mouse	Cell Signalling Technology (Danvers, US); #4019
VCAM-1/CD106	Goat	R&D Systems (Minneapolis, US); AF643
VDAC	Rabbit	Cell Signalling Technology (Danvers, US); #4661
Secondary antibody		
Peroxidase (POD)-anti-goat IgG	Donkey	Jackson ImmunoResearch Laboratories; #705-035-147
POD-anti-mouse IgG	Donkey	Jackson ImmunoResearch Laboratories; #715-035-151
POD-anti-rat IgG	Donkey	Jackson ImmunoResearch Laboratories; #712-035-153
POD-F(ab')$_2$-anti-rabbit IgG	Donkey	Jackson ImmunoResearch Laboratories; #711-036-152

4.1.3 Oligonucleotides

Tab. 8: **DNA oligonucleotides for genotyping PCR or cloning steps**

Name	Use (ref. to 4.2.1.3; 4.2.3.2.1)	DNA sequence 5´- 3´
Amp Neo2-Rev	Genotyping: PCR del	TAG TGT TGC TTT TAA GAC AGG GTT T
CN129-5‘-PCR-loxP-FW	Genotyping: PCR del and PCR loxP	AAA AGT TTA AAA AGG TCT GGA AAG C
CN129-5‘-PCR-loxP-Rev	Genotyping: PCR loxP	TCT GCA AGA AAG GAG TAA CAG ATT T
Cre-fw	Genotyping: PCR Cre	GAC CAG GTT CGT TCA CTC ATG G
Cre-rev	Genotyping: PCR Cre	AGG CTA AGT GCC TTC TCT ACA C
MerCreMer-fw	Genotyping: PCR MerCreMer	GTC TGA CTA GGT GTC CTT CT
MerCreMer-rev	Genotyping: PCR MerCreMer	CGT CCT CCT GCT GGT ATA G

RAPSN-fw	Genotyping: PCR RAPSN	AGG ACT GGG TGG CTT CCA ACT CCC AGA CAG
RAPSN-rev	Genotyping: PCR RAPSN	AGC TTC TCA TTG CTG CGC GCC AGG TTC AGG
SRY-fw	Genotyping: PCR SRY	TGA CTG GGA TGC AGT AGT TC
SRY-rev	Genotyping: PCR SRY	TGT GCT AGA GAG AAA CCC TG

Oligonucleotides were purchased from BioTeZ Berlin Buch GmbH (Berlin, D), synthesized in 10 nmol scale, dissolved in *A. dest*. and stored as 100 mM stock solutions at -20 °C.

Tab. 9: **RTqPCR mouse primers for TaqMan® Gene Expression Assays**
FAM, VIC: reporter dye type; NFQ-MGB: non-fluorescent quencher-minor groove binder

Gene	**Gene symbol**	**ASSAY ID**	**Label type (Reporter/ Quencher)**
Frat2	Frat2	Mm00844593_s1	FAM/NFQ-MGB
Klf2	Klf2	Mm01244979_g1	FAM/NFQ-MGB
Gapdh	Gapdh	Mm99999915_g1	VIC/NFQ-MGB
Gpi1	Gpi1	Mm01962484_u1	FAM/NFQ-MGB
Gskip	4933433p14Rik	Mm00618119_m1	FAM/NFQ-MGB
Rgs1	Rgs1	Mm00450170_m1	FAM/NFQ-MGB
Lung marker genes			
Abca3	Abca3	Mm00550501_m1	FAM/NFQ-MGB
Aqp5	Aqp5	Mm00437579_m1	FAM/NFQ-MGB
Pdpn	Pdpn	Mm01348912_g1	FAM/NFQ-MGB
Pecam1	Pecam-1	Mm01242584_m1	FAM/NFQ-MGB
Scgb3a2	Ugrp1	Mm00504412_m1	FAM/NFQ-MGB
Sftpb	Sftpb	Mm00455678_m1	FAM/NFQ-MGB
Sftpc	Sftpc	Mm00488144_m1	FAM/NFQ-MGB

All TaqMan® Primers including probes were designed by and purchased from Life Technologies (Darmstadt, D) and stored at -20 °C.

4.1.4 Chemicals and buffers

All chemicals used for preparing buffers and solutions (Tab. 10) were obtained from Sigma-Aldrich (Taufkirchen, D) or Carl Roth GmbH & Co. KG (Karlsruhe, D), unless indicated otherwise. All buffers were prepared with *A. dest.*

Tab. 10: **Buffers and solutions**

Buffer/ Solution	**Composition**
Alcian Blue Alizarin Red staining solution	1 volume 0.3 % Alcian Blue in 70 % EtOH, 1 volume 0.1 % Alizarin Red in 70 % EtOH, 1 volume acetic acid (100 %), 17 volumes 70 % EtOH
Blocking buffer (Western Blot)	1x TBS-T; 1 % bovine serum albumin (BSA)
DNA Digestion Buffer	1 M Tris pH 8.0; 3 M KCl; 0.5 M EDTA pH 8.0; 0.005 % NP_40; 0.45 % Tween 20
Mitochondria Analysis Buffer	120 mM KCl, 10 mM Tris pH 7.4; 5 mM KH_2PO_4
Mitochondria Isolation Buffer	250 mM sucrose, 10 mM Tris pH 7.4; directly before procedure 1mM EDTA added
Paraformaldehyde (PFA) 4 %	1x PBS; 4 % PFA; pH 7.5, heat to 60 °C to dissolve, store in aliquots at -20 °C
Phosphate-buffered saline (PBS)	137 mM NaCl; 2.7 mM KCl; 1.5 mM KH_2PO_4; 8.1 mM Na_2HPO_4; pH 7.4
Phosphate-buffered saline + Milk + Triton (PBSMT)	1x PBS; 2 % instant skim milk powder; 0.1 % Triton X-100
Phosphate-buffered saline + Triton (PBT)	1x PBS; 0.2 % BSA; 0.1 % Triton X-100
Phosphate-buffered saline + Tween (PBS-T)	1x PBS; 0.05 % Tween-20
PKA extraction buffer	25mM Tris-HCl (pH 7.4); 0.5 mM EDTA; 0.5 mM EGTA; 10 mM β-mercaptoethanol; 1 µg/ml leupeptin; 1 µg/ml aprotinin; Protease inhibitor Complete mini EDTA-free (1 tablet for 10 mL)
Ponceau Red	0.25 % Ponceau-S in 3 % (v/v) acetic acid
RIPA lysis buffer 1 x	50 mM Tris HCl pH 7.4; 150 mM NaCl; 1 mM EDTA; 0.5 % Na-Desoxycholate; PhosSTOP EASY (1 tablet for 10mL), Complete mini EDTA-free (1 tablet for 10mL)
Sample buffer 4 x	40 (v/v) % glycerine; 8 % (w/v) SDS; 250 mM Tris-HCl; 30 mM DTT; 0.04 % bromophenol blue; pH 6.8
SDS-polyacrylamide gel electrophoresis (PAGE) running buffer	25 mM Tris; 192 mM glycine; 0.1 % SDS
Semi-dry transfer buffer (Western Blot)	48 mM Tris; 39 mM glycine; 1.3 mM SDS; 20 % (v/v) methanol

Separating gel buffer (SDS-PAGE)	0.625 M Tris-HCl; pH 6.8
Stacking gel buffer (SDS-PAGE)	0.75 M Tris-HCl; pH 8.8
Standard lysis buffer (SLB)	10 mM K_2HPO_4; 150 mM NaCl; 5 mM EDTA; 5 mM EGTA; 0.5 % Triton X-100; pH 7.4; PhosSTOP EASY (1 tablet for 10mL), Complete mini EDTA-free (1 tablet for 10mL)
Stripping buffer	100mM NaOH; 0.5 % DTT; 2 % SDS
Tank Blot Transfer Buffer	20 mM Tris; 150 mM glycine; 0.052 mM SDS; 20 % (v/v) methanol
Tris-acetate-EDTA (TAE) buffer	40 mM Tris; 1 mM EDTA; 1.14 % (v/v) glacial acetic acid
Tris-buffered saline (TBS)	10 mM Tris-HCl; 150 mM NaCl; pH 7.4
Tris-buffered saline + Tween (TBS-T)	1x TBS; 0.05 % Tween-20

Tab. 11: **Chemicals and substances**

Substance	Company; article number (#)
Agarose LE	Biozym Scientific (Oldendorf, D); #840004
Complete mini EDTA-free	Roche Diagnostics (Mannheim, D); #REF0693159001
Coomassie Plus™ Protein Assay Reagent + Albumin (BSA) Standart Ampules	Thermo Fisher Scientific (Bonn, D); #23236
DAB Peroxidase Substrate Kit	Vector Laboratories (Burlingame, US); #SK-4100
DMEM-GlutaMAX™	Life Technologies GmbH (Darmstadt, D); #21885108
DNase I	Qiagen (Venlo, NL)
dNTPs Set 5mM	Roboklon (Berlin, D), #E2800-04
Spectra™ Multicolor High Range Protein Ladder	Thermo Fisher Scientific (Bonn, D); #26625
Spectra™ Multicolor Low Range Protein Ladder	Thermo Fisher Scientific (Bonn, D); #26628
Fetal calf serum (FCS) Superior	Biochrom/ Merck Millipore (Schwalbach, D), lot S 0615
HyperLadder™ 1 kb (formerly HyperLadder I)	BioLine GmbH (Luckenwalde, D); #BIO33025
HyperLadder™ 50 bp (formerly HyperLadder II)	BioLine GmbH (Luckenwalde, D); #BIO33054
Immobilon™ Western Chemiluminescent HRP substrate	Merck Millipore (Schwalbach, D); #WBKLS0500
Lumi-Light Western Blotting Substrate	Roche Diagnostics (Mannheim, D); #12015200001
OptiTaq DNA Polymerase 5 U/ µl	Roboklon (Berlin, D), #E2600-04
Pappenheim Stain (May Grünwald & Giemsa) Blood smear staining kit	Morphisto (Frankfurt, D); #11103
PhosSTOP *EASY* pack	Roche Diagnostics (Mannheim, D); #REF04906837001
Precision Plus Protein Standard Dual Color	Bio-Rad Laboratories GmbH (München, D), #161-0374
Prestained Pol Buffer C 10 x	Roboklon (Berlin, D), #E2600-04
Proteinase K	Carl Roth (Karlsruhe, D); 10 mg/ ml
Redsafe	Intron Biotechnology (Seongnam, KR); #21141
RNase AWAY	Molecular Bio Products (D); #7000
Skim milk powder	Fluka Analytical/ Sigma (Taufkirchen, D); #70166
TaqMan Gene Expression Master Mix	Life Technologies GmbH (Darmstadt, D); #4369016
Trypsin-EDTA	Biochrom AG (Berlin, DE); #L2153

4.1.5 Large-scale gene expression array

Tab. 12: **Illumina Microarray specification**

Array	Sample size	Sample distribution
Mouse WG-6 Vers 2.0 Illumina BeadChip Kit	6 beadchips with 6 samples each	36 samples distributed on the 6 beadchips in a defined pattern avoiding batch and edge effects

4.1.6 Cells

Tab. 13: **Cell culture and conditions**

Primary cells	Description	Culture medium	Origin
MEF	Mouse embryonic fibroblasts	DMEM-GlutaMAX™; 10 % fetal calf serum (FCS); 1 % penicillin/streptomycin (100 U/ ml)	generated in house; ref. to Methods 4.2.7

4.1.7 Mouse strains

Tab. 14: **Mouse strains generated and maintained for experiments**

Mouse strain	Origin	Details	Remarks
C57BL/6	Jackson Lab; bred in house	Widely used inbred strain	used for control purposes and for backcrossing
GSKIP flox	generated at MPI Dresden	B6.129P2-Gskip$^{tm1.1}$Mdcb; loxP flanked GSKIP sequence	used for generation of conditional and inducible GSKIP KO models
GSKIP del	generated at MPI Dresden	B6.129P2-Gskip$^{tm1.2}$Mdcb; Exon 2 of GSKIP deleted	*Gskip* $^{-/-}$ not viable
UBC Cre	Jackson Lab; Cat. No 008085	B6.Cg-Tg(UBC-cre/ESR1) 1Ejb/J; Tamoxifen-inducible tissue-non-specific UBC Cre	UBC Cre $^{+/+}$ not viable; Mice hemizygous for this Cre-ERT2 transgene are viable and fertile. Mice from this founder line have strong tamoxifen-inducible *cre* activity in all reported tissue types (http://www.informatics.jax.org). Breeding scheme: hemizygote x non-carrier (C57BL/6)
MerCreMer	Jackson Lab; Cat. No 005657	B6.FVB(129)-Tg(Myh6-cre/Esr1*)1Jmk/J; Tamoxifen-inducible heart muscle-specific MerCreMer	Mice homozygous for the αMHC-MerCreMer transgene are viable and fertile prior to tamoxifen administration. Cre recombinase expression in heart tissue has been confirmed; heart cell-specificity compared to brain, kidney, lung, liver and skeletal muscle confirmed (http://www.informatics.jax.org). Breeding scheme: homozygote x homozygote
UBC GSKIP	generated in house	B6.129P2-Gskip(UBC-cre/ESR1)tm1.1Mdcb/J; Tamoxifen-inducible GSKIP KO mouse with tissue-non-specific UBC Cre and floxed GSKIP allele	Breeding scheme: hemizygote x non-carrier (*Gskip*$^{flx/flx}$)
MerCreMer GSKIP	generated in house	B6.129P2-Gskip(Myh6-cre/Esr1*)tm1.1Mdcb/J; Tamoxifen-inducible GSKIP KO mouse with heart muscle-specific MerCreMer and floxed GSKIP allele	Breeding scheme: homozygote x homozygote

4.2 Methods

4.2.1 Animal experimental work

4.2.1.1 Mouse husbandry

All mice were housed and maintained in a specific pathogen-free environment in the animal facilities of the Max-Delbrück-Zentrum für Molekulare Medizin (MDC) in Berlin-Buch according to the recommendations of FELASA, with chow and water ad libitum in air-conditioned rooms at 22-23 °C with a standard 12 h light/dark cycle. 4 weeks after birth, mice were routinely weaned, ear-punched for numbering and young female and male mice separated. After genotyping, routinely one or two females were placed in a cage with one appropriate male mouse for standard breeding events. All procedures were carried out in accordance with ethical guidelines of the Landesamt für Gesundheit und Soziales (LaGeSo), Berlin. Embryo analysis as well as generation of various mouse strains was conducted as approved by license G 0361/13. PyRat software was used for animal organization and documentation; strains were named in the software as listed in Tab. 14 and generations specified and abbreviated according to their generation type (with N1/ 2/ 3 etc. for backcrossed generations while filial generations where assigned F1/ 2/ 3 etc.).

4.2.1.2 Breeding and generation of mouse strains

4.2.1.2.1 Generation of conditional *Gskip* knockout mice

Heterozygous *Gskip*$^{+/-}$ KO mice were generated by P. Skroblin *via* targeting Exon 2 of *Gskip* for loxP-mediated excision upon Cre recombination, resulting in the deletion of 86 out of a total of 119 amino acids of GSKIP (PhD thesis P. Skroblin). The start codon for GSKIP is located in Exon 2 and thus upon excision of Exon 2 no functional GSKIP is expected. A mouse embryonic stem cell clone (donor strain 129SvEv) with the targeting vector was expanded and injected into recipient blastocysts harvested from C57BL/6 mice (receiver strain). Offspring chimeric mice (arising from both donor and receiver cells) were bred with wild type (WT) C57BL/6 to establish germline transmission of the targeted GSKIP allele (Friedel *et al.* 2011).
Heterozygous *Gskip*$^{+/-}$ mice were generated by breeding *Gskip*$^{flx/wt}$ mice with a Cre deleter strain expressing a ubiquitous and constitutively active Cre recombinase. The above-mentioned steps were performed as part of the PhD project of P. Skroblin. *Gskip*$^{+/-}$ mice are viable and fertile. At least 5 backcrosses have been carried out before any experiments on phenotype and genotype were initiated (termed N5 animals), resulting already in 97 % identity of genetic backgrounds among the offspring with approx. 97 % of the donor genome eliminated (Rogner & Avner 2003). *Gskip*$^{-/-}$ mice were generated by intercrossing two *Gskip*$^{+/-}$ animals. *Gskip*$^{+/-}$ as well as *Gskip*$^{flx/wt}$ mice were backcrossed to C57BL/6 animals at least 10 times (until the end of this PhD project) in order to entirely eliminate donor-strain genome material other than the targeted *Gskip* allele.

4.2.1.2.2 Generation of inducible adult *Gskip* knockout mice

To circumvent the embryonic lethality of conditional *Gskip* KO mice tamoxifen-inducible mice were generated (Friedel *et al.* 2011).

Two different Cre recombinases were integrated into the genome of *Gskip*$^{flx/flx}$ animals.
On the one hand, alpha-MHC-MerCreMer mice were chosen, possessing a cardiac myocyte-specific Myh6 (Myosin, heavy polypeptide 6, also called alpha-MHC) promoter controlling the expression of tamoxifen-inducible Cre recombinase allowing the KO of a gene in an adult organism (Sohal *et al.* 2001). The MerCreMer double fusion protein consists of a Cre recombinase cDNA, flanked at both ends by a mutated estrogen receptor binding domain; under physiological conditions this mutated domain does not bind its natural ligand 17ß-estradiol but its synthetic ligand 4-hydroxytamoxifen and tamoxifen. MerCreMer is present in the cytoplasm but activated only after binding of tamoxifen, inducing the translocation of MerCreMer to the nucleus followed by homologous recombination. Breeding of these mice to floxed GSKIP mice results in offspring in which GSKIP can be specifically knocked out in cardiomyocytes after tamoxifen administration within 4-8 weeks. The α-MHC-MerCreMer model is widely used and has been established in the cardiovascular research field (Lisewski *et al.* 2008; Di *et al.* 2010; Hall *et al.* 2011). On the other hand, the UBC-Cre-ERT2 mouse model was used for generating adult tissue-non-specific inducible GSKIP KO mice (Gruber *et al.* 2010; Bauler *et al.* 2011). This model is a tamoxifen inducible UBC-Cre-ERT2 strain with a human Ubiquitin C (UBC) promoter sequence *upstream* of the Cre-ERT2 fusion gene (Ruzankina *et al.* 2007). Cre-ERT2 encodes a fusion protein consisting of a Cre recombinase with a triple-mutated estrogen ligand binding domain. The chosen promoter is expressed in almost all tissues. The fusion protein functions as described earlier for the MerCreMer fusion protein and is only activated upon binding of its synthetic ligand tamoxifen. Upon breeding with loxP flanked mice homologous recombination is induced after intraperitoneal application of tamoxifen within 4-8 weeks in all tissues.

Establishment of heart-specific inducible Gskip knockout mice

MerCreMer$^{+/wt}$ and MerCreMer$^{+/+}$ mice, received from Jackson Immunoresearch, were bred with GSKIP$^{flx/flx}$ mice in order to obtain MerCreMer$^{wt/+}$ *Gskip*$^{wt/flx}$ mice. By intercrossing two MerCreMer$^{+/+}$ *Gskip*$^{wt/flx}$ mice MerCreMer$^{+/+}$ *Gskip*$^{flx/flx}$ mice were generated. Afterwards the new mouse strain "MerCreMer GSKIP" was maintained routinely by intercrossing males and females of the same MerCreMer$^{+/+}$ *Gskip*$^{flx/flx}$ genotype.

Establishment of tissue-non-specific inducible Gskip knockout mice

UBC Cre$^{wt/+}$ *Gskip*$^{flx/flx}$ mice were generated *via* the same breeding scheme. Their maintenance breeding of UBC Cre$^{wt/+}$ *Gskip*$^{flx/flx}$ intercrosses yielded less offspring as 25 % of the progeny carried two alleles with UBC-Cre-ERT2 insertion, which has been confirmed to be lethal (http://www.informatics.jax.org). Thus this strain was maintained by consistently crossing hemizygotes (UBC$^{wt/+}$ *Gskip*$^{flx/flx}$) with non-carriers (UBC Cre$^{wt/wt}$ *Gskip*$^{flx/flx}$).

Notably, even though it has been shown that a hemizygous MerCreMer allele is sufficient for the induction of cardiomyocyte-specific excision of floxed sequences upon tamoxifen administration, MerCreMer$^{+/wt}$ and MerCreMer$^{+/+}$ mice had to be distinguished for breeding purposes by backcrossing with C57BL/6 followed by MerCreMer PCR in order to define whether the mice are homozygous or hemizygous carriers of the MerCreMer allele; the MerCreMer$^{+/+}$ *Gskip*$^{flx/flx}$ and MerCreMer$^{+/wt}$ *Gskip*$^{flx/flx}$ mice were distinguished accordingly. For mice carrying the UBC Cre allele, no distinction between UBC$^{+/wt}$ and UBC$^{+/+}$ genotypes was necessary as UBC$^{+/+}$ mice are not viable.

Tab. 15: **Mouse genotypes and their definition.**
MCM: MerCreMer, UBC: UBC-CreERT2.

Genotype	Definition	Alternative name
Gskip$^{+/+}$	Carrier of two *Gskip* WT alleles	WT GSKIP
Gskip$^{flx/+}$	Carrier of one *Gskip* WT allele and one *Gskip* allele flanked by loxP sequences	Single-floxed GSKIP
Gskip$^{flx/flx}$	Homozygous carrier of two copies of *Gskip* allele flanked with loxP sequences	Double-floxed GSKIP
Gskip$^{+/-}$	Carrier of one *Gskip* WT allele and one *Gskip* allele with deleted Exon 2 (one KO allele)	Heterozygous GSKIP KO
Gskip$^{-/-}$	Homozygous carrier of two copies of *Gskip* allele with deleted Exon 2 (two KO alleles)	Homozygous GSKIP KO
MCM$^{wt/wt}$	Carrier of two WT alleles, corresponding to no MerCreMer insertion	MCM negative
MCM$^{+/wt}$	Carrier of one WT allele without MerCreMer insertion and one allele with MerCreMer insertion (published to be efficient enough for heart-specific KO upon Tamoxifen administration (Lisewski *et al.* 2008; Di *et al.* 2010; Hall *et al.* 2011))	MCM positive
MCM$^{+/+}$	Homozygous carrier of two alleles with MerCreMer insertion	MCM double-positive
UBC$^{wt/wt}$	Carrier of two WT alleles, corresponding to no UBC-Cre-ERT2 insertion	UBC-Cre negative
UBC$^{wt/+}$	Carrier of one WT allele without MerCreMer insertion and one allele with UBC-Cre-ERT2 insertion	UBC-Cre positive
UBC$^{+/+}$	Homozygous carrier of two alleles with UBC-Cre-ERT2 insertion; not viable	---

4.2.1.3 Animal genotyping

For mouse genotyping the following PCR protocols were routinely used (Tab. 18) with the established standard reaction setup shown in Tab. 17. DNA was isolated prior to PCR (4.2.3.1.1). Usually the combination of two PCRs allowed the distinct assignment of a specific genotype as illustrated in Tab. 16. For sex determination of E18.5 mice SRY was amplified with primers specific for the Y chromosome gene *Sry* (sex-determining region Y) and the same samples were run for a control RAPSN PCR in parallel. Animals carrying the *Rapsn* gene (receptor-associated gene of synapse; housekeeping gene; used as internal control), which were at the same time genotyped as non-carriers for the *Sry* gene, were considered to be female while mice being positive for both *Rapsn* and *Sry* were regarded as male. Genotyping primers are listed in Tab. 8 and detailed PCR protocols in Tab. 18.

Tab. 16: **PCR combinations for routine genotyping**

Mouse strain	Genotypes to be distinguished	Combination of genotyping PCRs
C57BL/6	corresponds to *Gskip*$^{wt/wt}$	Routinely not genotyped
GSKIP flox	*Gskip*$^{wt/wt}$; *Gskip*$^{flx/wt}$; *Gskip*$^{flx/flx}$	PCR loxP + PCR del
GSKIP del	*Gskip*$^{wt/wt}$; *Gskip*$^{+/-}$; *Gskip*$^{-/-}$	PCR loxP + PCR del
UBC Cre	UBC$^{wt/+}$; UBC$^{wt/wt}$	PCR Cre
UBC GSKIP	UBC$^{wt/+}$ *Gskip*$^{wt/wt}$; UBC$^{wt/wt}$ *Gskip*$^{wt/wt}$; UBC$^{wt/+}$ *Gskip*$^{flx/wt}$; UBC$^{wt/wt}$ *Gskip*$^{flx/wt}$; UBC$^{wt/+}$ *Gskip*$^{flx/flx}$; UBC$^{wt/wt}$ *Gskip*$^{flx/flx}$	PCR Cre + PCR loxP
MerCreMer	MCM$^{wt/wt}$; MCM$^{wt/+}$; MCM$^{+/+}$	PCR MerCreMer
MerCreMer GSKIP	MCM$^{wt/+}$ *Gskip*$^{wt/wt}$; MCM$^{wt/wt}$ *Gskip*$^{wt/wt}$; MCM$^{+/+}$ *Gskip*$^{wt/wt}$; MCM$^{wt/+}$ *Gskip*$^{flx/wt}$; MCM$^{wt/wt}$ *Gskip*$^{flx/wt}$; MCM$^{+/+}$ *Gskip*$^{flx/wt}$; MCM$^{wt/+}$ *Gskip*$^{flx/flx}$; MCM$^{wt/wt}$ *Gskip*$^{flx/flx}$; MCM$^{+/+}$ *Gskip*$^{flx/flx}$	PCR MerCreMer + PCR loxP

4.2.1.4 Embryo analysis

Timed matings were set up between two *Gskip*$^{+/-}$ animals for the generation of homozygous GSKIP KO mice and for embryo analysis. For timed pregnancies, routinely one or two females were placed in a cage with one appropriate male for one night and the presence of a vaginal plug was determined on the following morning. Mice were separated again and the day of positive plug considered as day 0.5.
Genotype ratios were calculated at various embryonic stages (genotyping of biopsies) and compared with expected Mendelian ratios in order to determine the time point of death of GSKIP KO mice. E18.5 (abdominally delivered *via* Caesarean sectioning) and P0 (naturally delivered) embryos were weighted. Organ dissections were carried out at different embryonic stages. Lungs were removed and weighted and their ability to float on PBS surface was tested. Observations were documented with a digital camera where indicated. For protein and RNA analysis embryos and tissues were cleaned in ice cold PBS and kept on ice until they were quickly snap-frozen in liquid nitrogen and stored at -80 °C until further processing. For determination of gross morphological abnormalities embryos as well as isolated tissues were rinsed briefly in PBS, fixed in 4 % PFA and stored at 4 °C until further procedures after successful genotyping.

4.2.2 Histologic methods

4.2.2.1 Preparation of Paraffin-embedded sections and HE staining

For histologic analysis freshly dissected tissues and/or whole embryos were fixed in 4 % PFA for 24 hours up to several days at 4 °C. Species were dehydrated at room temperature by an ascending alcohol series and afterwards embedded in paraffin. Hematoxylin-Eosin stain according to standard protocols was used on sections of paraffin-embedded lungs as well as ethylenediaminetetraacetic acid (EDTA)-decalcified embryonic heads. In addition, mechanically inflated E18.5 lung tissues were stained for glycogen-rich structures using Periodic-acid Schiff (PAS) according to standard protocols. E18.5 whole embryo morphological studies were conducted in collaboration with S. Bachmann (by C. Dittmayer; Vegetative Anatomie Berlin) based on optimized laboratory protocols with prolonged incubation steps due to the large specimen size and high bone content of E18.5 embryos (Fixed specimen were decalcified with the chelating agent EDTA). Paraffin sections of 2-4 µm thickness were generated and stained with Hematoxylin-Eosin and Azan dye. For microscopic evaluation a digital bright-field microscope (Keyence) was used.

4.2.2.2 Preparation of sections for transmission electron microscopy

For transmission electron microscopy of lung ultrastructures freshly dissected lungs of E18.5 embryos were cut into 1-2 mm pieces using extra-thin razor blades and immediately fixed in 2.5 % glutaraldehyde (EM grade) in 0.2 M sodium cacodylate buffer (pH 7.4) for 24 hours to several days at 4 °C. In parallel, fixation

with a different buffer system using 2.5 % glutaraldehyde (EM grade) in 0.1 M phosphate buffer (pH 7.0) was initiated as a potential unspecific precipitation of surfactant components upon using phosphate buffer instead of cacodylate buffer can occur (O'Hare K & Braunschweig 1975). The tissue samples were post-fixed with 1 % osmium tetroxide (OsO_4) and 0.08 % potassium ferrocyanide (II) in 0.1 M sodium cacodylate buffer (pH 7.4) for 1.5 hours. Tissues were dehydrated at room temperature by an increasing alcohol series and afterwards embedded in Epon (synthetic resin). Post-fixation, embedding and sectioning was performed at the electron microscopy multiuser facility in collaboration with S. Bachmann. Semithin sections of 0.5 µm were used for orientation and ultrathin sections of 50-60 nm cut for imaging. Imaging and analysis of the ultrathin sections was performed on a FEI Transmission electron microscope in collaboration with C. Dittmayer.

4.2.2.3 Histologic blood stain

E 18.5 embryonic blood films were prepared for gross analysis of blood composition and blood cells. May Grünwald & Giemsa Pappenheim staining of blood smears were performed according to the manufacturer´s protocol (Morphisto, Frankfurt, D). Briefly, blood smears were fixed with methanol, air-dried, May Grünwald Eosin stained, washed repeatedly, Giemsa stained, washed again and mounted in aqueous mounting solution (Carl Roth, Karlsruhe, D). The principle of this stain is based on electrostatic interactions between the dye and the target molecule. The Giemsa Stain is an acidic dye (eosin) while May Grünwald stain is composed of methylene blue and azure B, two basic dyes, allowing the distinction of eosinophil granulocytes (stained dark red), erythrocytes (red), basophil granulocytes (blue, purple), neutrophil granulocytes (light purple) and nuclei of leucocytes (blue as well). The blood smears were documented on a digital microscope.

4.2.2.4 Alizarin Red / Alcian Blue whole-mount stain of cartilage and bone

For whole-mount staining of skulls E18.5 or P0 embryos were dissected and decapitated. The lower jaw of the skull including the tongue was carefully removed, the remaining upper part of the skull eviscerated and fixed in 99 % ethanol at RT for several days (in a total volume of 15 ml per skull). The material was processed by 24 hour incubation in acetone at RT for fat removal. Samples were rinsed once in H_2O dest. Each skull was moved to a new tube with 15 ml freshly prepared Alizarin Red / Alcian Blue double staining solution (0.3 % Alcian Blue, 0.1 % Alizarin Red, see Material for details) optimized according to Erdogan (Erdogan 1995). Staining was performed at 40 °C for 4 days under rotation in an incubator. Skulls were briefly washed and transferred into 1.5 % aqueous KOH for 4 days (moving the specimen from time to time) for clearing purposes. The skulls were transferred into an aqueous solution of 20 % glycerin containing 1 % KOH until the skeletal skulls were clearly visible through the surrounding tissue. Cleared specimens were placed successively into 50 %, 80 % and 100 % glycerin for long-term storage and imaging. Stained skulls were viewed under a stereomicroscope connected to a Leica DFC 495 camera (Leica Microsystems, US) using the PlanApo 0.63 objective.

4.2.3 Molecular biology methods

4.2.3.1 DNA processing

4.2.3.1.1 Isolation of genomic DNA from mouse biopsies

For routine genotyping, mouse tissue, tailcut or earpinch material was used for genomic DNA isolation. For material from the mouse strain GSKIP del DNA was isolated and purified using the GeneMATRIX Tissue DNA Purification Kit (Roboklon) according to the manufacturer's protocol, DNA eluted with pre-heated

elution buffer and stored at 4 °C. For all other mouse strains (GSKIP flox, MerCreMer, UBC Cre, MerCreMer GSKIP, UBC GSKIP) DNA was isolated with a simplified DNA isolation protocol. For this, mouse biopsies were Proteinase K digested overnight at 56 °C and 650 rpm shaking in 300 µl DNA digestion buffer and 5 µl Proteinase K (10 mg/ml) each. The next day, Proteinase K was heat-inactivated at 90 °C and 650 rpm shaking for 30 minutes, followed by thorough mixing. The samples were cooled down to room temperature and spun down at 14,700 x g and stored at 4 °C. 0.5-1.5 µl of the supernatant (corresponding to unpurified eluted genomic DNA) or of the eluted purified DNA (GSKIP del material) was routinely used for genotyping.

4.2.3.2 Analysis and modification of DNA

4.2.3.2.1 Polymerase chain reaction

In vitro amplification of DNA sequences was carried out by polymerase chain reaction (PCR). For routine genotyping isolated genomic mouse DNA was amplified. The PCR setup used for all genotyping PCRs is listed in Tab. 17, while details for each specific PCR protocol are given in Tab. 18.

Tab. 17: **PCR reaction setup used for all genotyping PCRs**

Components	Volume per reaction
OptiTaq DNA Polymerase 5 U/ µl	0.1 µl
10 x Polymerisation Buffer C (prestained)	1.5 µl
dNTPs 5 mM	0.6 µl
Forward Primer 10 µM	0.67 µl
Reverse Primer 10 µM	0.67 µl
DNA	0.5-1.5 µl
H_2O (d.d.)	ad 15 µl

Tab. 18: **PCR protocols used for routine genotyping**

PCR type	Del PCR	loxP PCR	MerCreMer PCR	Cre PCR	SRY PCR + RAPSN PCR
Initial denaturation	3 min 94 °C	5 min 94 °C	4 min 95 °C	5 min 95 °C	5 min 95 °C
Denaturation	15 sec 94 °C	25 sec 94 °C	30 sec 94 °C	30 sec 95 °C	30 sec 95 °C
Annealing	30 sec 55 °C	40 sec 55 °C	30 sec 55 °C	30 sec 60 °C	30 sec 63 °C
Extension	2 min 72 °C	40 sec 72 °C	2 min 72 °C	30 sec 72 °C	45 sec 72 °C
Cycle number (Denaturation, Annealing, Extension)	35	35	35	35	40
Final extension	10 min 72 °C	7 min 72 °C	5 min 72 °C	5 min 72 °C	5 min 72 °C
Primers used (Ref. to Tab. 8)	CN129-5'-PCR-loxP-FW & Amp Neo2-Rev	CN129-5'-PCR-loxP-FW & CN129-5'-PCR-loxP-Rev	MerCreMer-fw & MerCreMer-rev	Cre-fw & Cre-rev	SRY-fw & SRY-rev / RAPSN-fw & RAPSN-rev
Predicted size of PCR products	*Gskip* +: 1921 bp *Gskip* -: 434 bp (*Gskip* flx: 2063 bp)	*Gskip* flx: 371 bp *Gskip* +: 325 bp *Gskip* -: no product	MCM+: 400 bp MCM-: no product	Cre+: 400 bp Cre-: no product	Sry+: 230 bp Sry-: no product Rapsn+: 590 bp Rapsn-: no product

4.2.3.2.2 Agarose gel electrophoresis

Agarose gel electrophoresis was used to separate DNA molecules according to their size. All genotyping PCRs were carried out using 2 % agarose gels (diluted in TAE). DNA staining was carried out using RedSafe (1:20,000). Samples were run at 100-120 V for 45-60 minutes in TAE buffer filled running chambers using the PerfectBlue mini system (PeqLab). The separated DNA fragments were visualized under UV light using the Gel Doc2000 gel documentation device.

4.2.4 Biochemical methods

4.2.4.1 Preparation of affinity purified anti-GSKIP antibody from rabbit serum

A rabbit polyclonal antiserum (8877) was raised against recombinant full-length GSKIP (amino acids 1-139) (Biogenes, Berlin, Germany). Specific antibodies were isolated by affinity chromatography of the antisera using GSKIP immobilized on thiopropyl-Sepharose 6B (GE Healthcare) as previously described (Henn *et al.* 2004; Hundsrucker *et al.* 2010). The purified antibody was stored in glycerol at -20 °C.

4.2.4.2 Protein expression analysis

4.2.4.2.1 Homogenisation and lysis of tissue and cells

Organs and whole embryos were grinded to powder using mortar and pestle on dry ice and resuspended in standard 1x RIPA buffer containing protease and phosphatase inhibitors (Roche) while MEFs were washed with PBS, scraped in RIPA buffer and lysed by pipetting up and down several times. All homogenates were sonicated (6 x, 60 % power) and centrifuged (15,000 x g; 4 °C; 15 min) to remove nuclei and debris. Total protein concentrations were quantified (ref. to 4.2.4.2.2) and lysates stored at -80 °C until utilized for the detection of proteins *via* SDS-PAGE.

4.2.4.2.2 Determination of total protein concentration using Bradford-Coomassie assay

Protein concentration in lysates was determined using Coomassie Plus Bradford protein assay (Thermo Scientific) according to the manufacturer`s protocol. This colorimetric method for total protein quantitation is based on the binding of proteins to Coomassie in an acidic system leading to a color change from brown to blue, measured as an absorption maximum shift from 465 nm to 595 nm. A standard curve was determined by measuring the absorbance of known concentrations of BSA after addition of Coomassie Reagent at a wavelength of 595 nm using the Enspire® 2300 microplate reader and the slope of the linearly fitted curve used for calculating the protein concentrations in the unknown samples. Lysates were adjusted to the desired concentrations by addition of RIPA lysis buffer and for SDS-PAGE an appropriate volume of 4 x Laemmli sample loading buffer was added.

4.2.4.2.3 SDS-Polyacrylamide gel electrophoresis

In order to separate protein lysates into individual proteins the method of SDS polyacrylamide gel electrophoresis (SDS-PAGE) was used. The principle of this technique is based on the different molecular weights for single proteins within a protein mixture enabling an electrophoretic separation by size on a SDS-polyacrylamide gel using a Tris-HCl buffered system (Burnette 1981). Total proteins (10-50 µg) were separated at 25 mA per gel by 12 % SDS-PAGE (4-20 % gradient gels used for surfactant proteins SP-B and SP-C) in SDS-PAGE running buffer using MiniProtean® electrophoresis chambers. Precision Plus Protein™ Dual Color Standard (Bio-Rad) was included as protein size marker or, in case of very small proteins, the Low Range Protein Ladder Spectra™ (Fermentas) was used. For proteins with a size above 150-200 kDa (e.g. LRP6) 8 % SDS-PAGE was carried out for better separation and the Multicolor High Range Protein Ladder Spectra™ (Fermentas) loaded as size marker. For Atpif1 separation (12 kDa), 15 % gels were loaded.

4.2.4.2.4 Immunoblotting: Transfer and detection of proteins

For the identification and quantitative analysis proteins separated by SDS-PAGE were transferred from the acrylamide gels to polyvinylidene fluoride (PVDF) membranes using the semi-dry Trans Blot system from BioRad (including Semi-dry Transfer Buffer) applying 20 V for 1.5 hours. Alternatively, for the transfer of

large proteins (size > 200 kDa) onto PVDF membranes the wet tank blotting system (filled with Tank Blot Transfer Buffer) was employed at 4 °C, 110 V for 2.5 hours.
Membranes were blocked one hour at room temperature with 1 % BSA in TBS-T and then incubated overnight at 4 °C with primary antibodies diluted in 1 % BSA in TBS-T (Tab. 19 *upper*). Membranes were washed three times 10 minutes with TBS-T, followed by an incubation of at least one hour with horseradish peroxidase-conjugated secondary antibodies (Jackson Immuno Research; Tab. 19 *lower*) and again three washing steps in TBS-T. A peroxidase substrate containing ECL substrate (Millipore or Roche) was added and proteins visualized using an Odyssey Imaging System (LI-COR Bioscience). Signal intensities were quantified using ImageJ1.47v software (NIH).
For redetection of proteins, membranes were washed three times in PBS-T after detection, incubated in stripping buffer gently shaking for 3 hours at room temperature and thoroughly washed again in TBS-T. Then membranes were blocked with 1 % BSA in TBS-T for one hour at room temperature and treated with primary as well as secondary antibodies as before and detected again.

Tab. 19: **Primary and secondary antibody dilutions used in Western Blotting**. If not stated otherwise, antibodies supplied by Cell Signaling or Abcam were diluted 1:1,000, antibodies from Santa Cruz 1:300 and BD antibodies 1:500.

Primary antibody	**Origin**	**Dilution**
Abcam antibodies	Rabbit, Mouse, Rat	1:1,000
Aqp5 (Alomone Labs)	Rabbit	1:500
BD Antibodies	Mouse	1:500
Cell Signalling Antibodies	Rabbit, Mouse	1:1,000
Eno3 (Biorbyt)	Rabbit	1:250
FRAT2 (Abnova)	Rabbit	1:250
GSKIP; custom-made	Rabbit	1:500
Hsp90 (Stressgen)	Mouse	1:1,000
NPPA (Thermo)	Rabbit	1:500
PLCβ3 (Novis)	Rabbit	1:1,000
Santa Cruz Antibodies	Rabbit, Mouse	1:300
Surfactant protein antibodies Sp-B, Sp-C	Rabbit	1:200
Talin-2 (Genetex)	Rabbit	1:1,000
VCAM-1 (R&D)	Goat	1:1,000
Secondary antibody		
Peroxidase (POD)-anti-goat IgG	Donkey	1:10,000
POD-anti-mouse IgG	Donkey	1:10,000
POD-anti-rat IgG	Donkey	1:10,000
POD-F(ab')$_2$-anti-rabbit IgG	Donkey	1:10,000

4.2.4.3 Whole-mount 2H3 neurofilament immunohistochemistry of early-stage embryos

E10.5 embryos were carefully removed from the uterus of plug-positive pregnant *Gskip*$^{+/-}$ females (mated previously with *Gskip*$^{+/-}$ males) and preferably their yolk sack (or embryonic material) preserved for genotyping. Embryos were placed in fresh 4 % PFA in PBS for overnight fixation. After three washing steps in PBS-T on a rocket switch, embryos were subjected to ascending concentrations of methanol at room temperature (incubation in 25 %, 50 %, 75 % and 100 % methanol for one hour each) and stored at -20 °C. Embryos of defined genotypes were bleached for one hour in H_2O_2 / methanol (1:5) at -20 °C to quench endogenous peroxidase activity and afterwards transferred back to 100 % methanol. *Gskip*$^{+/+}$ and *Gskip*$^{-/-}$ embryos were rehydrated in decreasing concentration of methanol (75 %, 50 %, 25 % methanol; PBS) at 4 °C for 30 minutes each. Holes were pinched with a fine needle along the spinal cord of the embryos to increase penetration of the antibody. Throughout the subsequent procedure specimen were gently agitated to improve tissue penetration and processed in an optimized working volume of 1 ml each (ideally in 24-well plates). Embryos were incubated twice for one hour each in PBSMT (1x PBS; 2 % instant skim milk powder; 0.1 % Triton X-100), followed by an overnight incubation in anti-neurofilament antibody diluted in PBSMT at 4 °C on a plate shaker. The next day, embryos were washed twice in PBSMT at 4 °C and three times in PBSMT at room temperature for one hour each before they were incubated overnight in diluted peroxidase

(POD)-coupled secondary antibody. Next, embryos were cleared by washing twice in PBSMT at 4 °C and three times in PBSMT at room temperature for one hour each. The subsequent final washing was carried out for 20 minutes in PBT (1x PBS; 0.2 % BSA; 0.1 % Triton X-100) at room temperature. For detection of POD-derived signal, embryos were incubated for a few minutes in diaminobenzidine (DAB) / nickel substrate working solution (Vector Laboratories) according to the manufacturer's protocol under visual investigation until a gray-black reaction product of appropriate intensity was observed. The reaction was stopped by quickly placing stained specimen in water. The whole-mount neurofilament stain was documented with a Leica MZ16 stereomicroscope connected to a DFC 495 camera (Leica Microsystems, US) using the PlanApo 0.63 objective at 2 x and 3 x magnification.

Tab. 20: **Antibody dilutions for whole-mount embryo stain**

Primary antibody	**Origin**	**Dilution**
2H3 neurofilament	Mouse	1:25 in PBMST
Secondary antibody		
POD-F(ab')$_2$-anti-mouse IgG	Donkey	1:500 in PBMST

4.2.4.4 PepTaq® cAMP-dependent protein kinase assay

A non-radioactive assay was conducted in order to define PKA activity in unstimulated as well as forskolin-stimulated MEFs. Cells were lysed in an appropriate volume of PKA extraction buffer and equal amounts of total protein were used for the PepTaq PKA activity assay (Promega). The protocol was run according to the manufacturer's protocol. Briefly, freshly lysed cells containing kinase were incubated with a defined amount of positively charged PepTaq Peptide for 30 minutes at room temperature and the reaction stopped by heating the samples to 95 °C followed by electrophoretic separation of the samples on a 0.8 % agarose gel (without RedSafe). The assay makes use of a colored fluorescent peptide (PepTaq A1 peptide) substrate, serving as a specific substrate for PKA. Phosphorylated substrates' net charge changes from +1 to -1, allowing a rapid separation of positively (unphosphorylated) and negatively charged (phosphorylated) substrates on an agarose gel.
In order to semi-quantitatively assess PKA activity in the samples, the agarose gels were examined under UV light. Signal intensities were quantified using ImageJ1.47v software (NIH).

4.2.5 Gene expression analysis

4.2.5.1 RNA isolation

Total RNA was isolated from homogenized mouse tissue using Trizol (Sigma) and chloroform according to the manufacturer's protocol. For analysis of lung differentiation marker gene expression as well as for the Illumina microarray approach, the RNeasy Kit (Qiagen) including QiaShredder tissue disruptor columns were used according to the manufacturer's protocol for total RNA isolation from homogenized tissue. DNase digestion was included. The eluted, purified RNA was measured in a NanoDrop spectrophotometer and its extinction at 260 nm and 280 nm as well as its concentration determined. The ratio of 260 to 280 assesses the purity of nucleid acid sample; for RNA a ratio around 2 is considered as pure.

4.2.5.2 Real-Time Reverse Transcription-PCR

RNA (500-1,000 ng) was reverse transcribed to cDNA according to the SuperScript III First-Strand Synthesis Kit protocol (Invitrogen) using random hexamer primers. Duplex-Real-time RT-PCR was performed using the TaqMan system on a BioRad iQ5 cycler or for lung differentiation gene analysis on an Applied Biosystems ViiA™ 7 Real-Time PCR cycler. TaqMan chemistry is based on fluorescently labeled

probes (target-specific oligonucleotide harboring a fluorescent reporter dye at the 5' end and a non-fluorescent quencher at the 3' end of each probe), first annealing and hybridizing to the complementary cDNA target of interest and, if target is present, followed by an AmpliTaq Polymerase-mediated cleavage between reporter and quencher, resulting in an increase of fluorescence intensity of the reporter. Intact probes suppress the energy transfer between reporter (FAM or VIC) and quencher and thus reporter fluorescence. Displacement of the fragments enables further polymerization of the specific target after binding of a new probe, leading to exponential accumulation. Amplification of PCR products is directly measured by monitoring the increase of reporter fluorescence. Duplex-PCR was carried out by combining FAM-labeled probes complementary to the target of interest and VIC-labeled probes for mouse *Gapdh* as an internal control in the same wells. The comparative $2^{-\Delta\Delta C_T}$ method (Livak & Schmittgen 2001) was chosen for relative gene expression analysis relating target transcript expression in GSKIP KO mouse tissue to that of WT (untreated control). The housekeeping gene *Gapdh* was included as a control to normalize PCRs for the amount of RNA added to the reverse transcription reaction. Reactions were carried out in a total volume of 20 µl on microtiter plates.

4.2.5.3 RNA quality control and Illumina Gene expression microarray

Quality of the RNA was examined using the Bioanalyzer2100 using Agilent RNA 6000 Nano Chips. For this, on-chip-gel electrophoresis of isolated mouse tissue total RNA was conducted on a nano- scale using a microfabricated chip: RNA samples were electrophoretically separated and RNA fragments detected *via* laser-induced fluorescence. The ratio of 18S to 28S rRNA was calculated based on an algorithm taking the entire electrophoretic trace into account (presence or absence of degradation products) and expressed as RNA integrity number (RIN). The RIN represents a numerical assessment of RNA integrity and based on a numbering system from 1 to 10, with 1 being the most degraded profile and 10 being the most intact and does not depend on RNA sample concentration. This system is widely used as a quality control and microarrays require a minimum RIN value of 8 (Imbeaud *et al.* 2005; Schroeder *et al.* 2006).
RNA with RIN ≥ 9 was amplified and biotin-labeled using Illumina® TotalPrep™-96 RNA Amplification Kit according to the manufacturer's protocol. Briefly, cDNA was synthesized, purified, *in vitro* transcribed to yield cRNA followed by a cRNA purification step. 1.5µg labeled cRNA (in a total volume of 10 µl) from 4 or 5 E18.5 embryonic tissues of each genotype and each tissue was hybridized to Mouse WG-6 Vers 2.0 Illumina Chips. Loading, hybridization, washing and scanning of microchips and data analyses were performed in collaboration with N. Hübner. The experiment included the analysis of lung (n = 4), brain (n = 4), heart (n = 5) and kidney (n = 5) gene expression changes and aimed to compare the gene expression of GSKIP KO tissues with the expression of WT control tissues (N5 mice used). Bioinformatic analysis of microarray data was performed by H. Schulz: the Illumina Mouse WG-6 Version 2.0 arrays have been normalized using the BeadStudio Gene Expression Module v3.3.7 and quantile normalization without background correction. The quality of arrays and the general expression profile has been checked by principal component analysis (PCA) using Partek Genomic Suite (6.3 beta), correlation as a dispersion matrix and normalized Eigenvector scaling (Suppl. Fig. 3 A - D). Sample 9253003003_b had a high number of probes not expressed: n = 11,910 vs. an average of 13 230 at a BeadStudio detection p-value threshold of 0.05. Additionally is the kidney WT sample 9253003003_b essentially responsible for the development of principal component (PC) #4 which describes 8.16 % of the dataset variance (Suppl. Fig. 3 B, Y-axis). After quantile normalization and exclusion of the outlier sample and the exclusion of low or not expressed genes (maximum Illumina detection p-value > 0.05) a parametric two way ANOVA was performed controlling the conditions "tissue" (brain, heart, kidney, lung), "modification" (WT and GSKIP-KO) and interaction (tissue*modification). Resulting p-values were Benjamini Hochberg false discovery rate (FDR)-corrected and probes undergo 5 % FDR in "modification" or "interaction" (n = 498) were average linkage and K-Mean clustered (Suppl. Fig. 3 F and H respectively) using standardized signal values and the Euclidean distance function. K-Mean clustering was performed with K = 7 according to local minimum of the Davies Bouldin K estimation procedure (Suppl. Fig. 3 G) and with or without removal of the tissue effect (Suppl. Fig. 3 H left

and right respectively). Residual and fitted values, QQs and leverage effects of probes undergo 5 % FDR in "modification" or "interaction" were plotted (Suppl. Fig. 3 provided by H. Schulz).

4.2.6 Large-scale metabolomics and proteomics analysis

Lung, liver and blood of E18.5 embryos were collected on ice, snap-frozen and kept at - 80 °C. Analysis, statistical evaluation and comparison of the metabolite profile of GSKIP KO and WT lung, liver and blood (4 samples of each genotype; N5/6 mice) was carried out in collaboration with S. Kempa, based on a combination of separation and detection using two-dimensional gas chromatography-coupled mass spectrometry (GC-MS). E18.5 lung and liver were also processed for proteomics analysis including trypsin digestion, GC-MS and protein identification using database comparison by G. Mastrobuoni (n = 2 for KO tissues, n = 3 for WT tissues). Data preprocessing was performed in collaboration with S. Kempa and further analyzed and visualized using Perseus Software. Due to the small sample size (n < 3), statistical evaluation could not be performed on proteomics data.

4.2.7 Generation of primary mouse embryonic fibroblasts

Timed breedings were set up between two *Gskip*$^{+/-}$ animals for the generation of primary MEFs from *Gskip*$^{+/+}$ as well as *Gskip*$^{-/-}$ embryos. Embryos were removed from the uterus at stage E12.5, followed by further sterile dissection steps to remove the head and all organs. Each embryo was treated separately and material was taken for routine genotyping. Trypsin/EDTA (0.05 %) was added and incubated for 5 minutes at 37 °C 5 % CO_2. Embryos were cut into small pieces and pipetted up and down repeatedly, followed by 5 minutes incubation at 37 °C 5 % CO_2. Trypsin digestion was stopped by addition of DMEM and the cell suspension centrifuged at 700 x g for 5 minutes. Cells were seeded on 60 mm cell culture dishes in DMEM + 10 % FCS + Penicillin / Streptomycin and passaged on the following day after genotype confirmation. During protocol establishment, cells were resuspended and cryopreserved in freezing medium (90 % FCS + 10 % DMSO) using cryoconservation vials placed in an isopropyl alcohol-filled polycarbonate freezing container (Mr. Frosty™, Nalgene) allowing the cells to slowly cool down to -80 °C with a constant temperature decline of 1 °C per minute, ensuring successful recovery after thawing. MEFs are growing fast in the first five passages and slow down their proliferation rate to switch to a senescent state afterwards (Jozefczuk *et al.* 2012). Despite their most common use as a feeder layer for embryonic stem cells, MEFs served during this project as primary GSKIP KO cell system for initial biochemical experiments. Our observations did confirm that cells taken into culture after being frozen show much slower proliferation and change their behaviour and shape compared to freshly isolated MEFs. Thus, only freshly isolated MEFs with a passage number below P4 were used for experiments. For PepTaq PKA activity assays (4.2.4.4) cells were stimulated with 40 µM Forskolin for 30 minutes and/or with 20 µM H89 30 minutes prior to FSK treatment before lysis.

4.2.8 Isolation of embryonic lung tissue mitochondria

Mitochondria were isolated out of WT E18.5 lung tissue using a sucrose buffer system. Fresh tissue was homogenized (in 400 µl of mitochondrial isolation buffer per E18.5 lung) with 10 strokes using a glass Dounce homogenizer (Wheaton, Millville, US). The homogenate was centrifuged for 10 minutes at 1,300 g at 4 °C to spin down nuclei and cell debris. The supernatant was collected and centrifuged for 30 minutes at 12,000 g at 4 °C to separate the cytosolic fraction from the mitochondria. The supernatant was used as a cytosolic control, while the pelleted mitochondria were washed two times with mitochondrial isolation buffer (without EDTA). The pellet was than dissolved in 40 µl of mitochondrial analysis buffer and both cytosolic and mitochondrial fractions analyzed by Western Blot.

4.2.9 Microscopic methods

4.2.9.1 Digital microscopy

HE-, Azan- and PAS-stained paraffin sections of tissue as well as Pappenheim-stained blood smears were documented using a Digital Keyence BZ-8100E Microscope. The settings chosen were the following:

Tab. 21: **Objectives and settings**

Objective type	Magnification	Channel
Plan Apo Na0.10 (Nikon)	2x	Bright field
Plan Apo Na0.20 (Nikon)	4x	Bright field
Plan Apo Na0.45 (Nikon)	10x	Bright field
Plan Apo Na0.75 (Nikon)	20x	Bright field
Plan Apo Na0.95 (Nikon)	40x	Bright field

4.2.9.2 Electron microscopy

Transmission electron microscopy (Tecnai G^2 20 LaB6; Fei) was used for the generation of high magnification bright field electron images from lung tissue sections with a significantly higher resolution compared to standard light microscopy. An image is formed from the electrons interacting with and passing through the tissue section and the emitting electron waves detected *via* a sensor such as a CDD camera. The thickness and composition of the material thus defines the occlusion and absorption of electrons in the sample; regions with more atoms (thicker regions) appear dark (electron dense) while regions which do not contain atoms appear bright.

4.2.10 Statistical analysis

Studies were performed with littermate controls to limit possible environmental influences. All values are presented as mean ± SEM. Data were analyzed with GraphPad Prism 5.01 software using paired or unpaired Students t-test (for comparison of 2 groups) or one-way ANOVA (for comparison of 3 groups). The Chi Square test was applied to genotype distributions and lung floating ability testing while two-sided Fisher´s exact test was done for analysis of sex distribution. A p value ≤ 0.05 was considered statistically significant.

5. Results

This doctoral thesis builds on previous studies. GSKIP was shown to directly interact with both PKA-RIIα subunits and GSK3β (Chou *et al.* 2006; Ewing *et al.* 2007; Hundsrucker *et al.* 2010). GSKIP is ubiquitously expressed in a broad range of rat tissues and has a predominant cytosolic localisation. In addition, GSKIP increased the PKA-mediated inhibitory phosphorylation of GSK3β on Ser9. A conditional GSKIP KO mouse model has been generated but not yet studied (PhD thesis P. Skroblin).

The present work expands previous knowledge on GSKIP by defining its *in vivo* physiological function in a KO mouse model; the ubiquitous expression of GSKIP was confirmed in adult mouse organs (chapter 5.1) and the successful generation of the conditional *Gskip* KO mouse model verified (5.2). Heterozygous adult *Gskip* KO mice were studied (5.3) and homozygous *Gskip* KO mice characterized: the time point of death of the embryonically lethal KO mouse model was determined (5.4) and its phenotype analysed in detail (5.4; 5.5; 5.7). Gene expression alterations upon *Gskip* KO were investigated on a large-scale and two altered genes successfully validated (5.6). Due to mitochondrial function abnormalities observed in cultured A549 lung cells upon *Gskip* knockdown (PhD thesis E. Perets), the metabolic phenotype of *Gskip* KO mice was assessed by metabolomics (5.8). In addition, biochemical studies of GSKIP-deficient embryonic tissues (5.9), early-stage whole embryos (5.9.1) as well as of primary mouse embryonic fibroblasts (5.9.3) were carried out: GSKIP-dependent GSK3β Ser9 phosphorylation changes were detected in early embryonic stages rather than in late gestation tissues. The chapter is concluded by proteomics analyses (5.9.2). To overcome the embryonic lethality of the conditional *Gskip* KO model, strategies were developed and two adult inducible *Gskip* KO mouse models generated allowing future evaluation of GSKIP's function independent of its role in development (7.4).

5.1 GSKIP is expressed ubiquitously in adult mouse tissue

Previous studies have shown that GSKIP is widely expressed in tissues of adult WT Wistar rats ((Hundsrucker *et al.* 2010); PhD thesis P. Skroblin). In WT C57Bl6 mice, GSKIP is as well ubiquitously expressed in all tested adult organs (Fig. 5). However, GSKIP protein expression levels vary between organs: while brain, colon, pancreas, spleen and testis tend to express high levels of GSKIP, heart and kidney medulla express less GSKIP. The same is the case for protein expression of GSKIP´s known interaction partners PKA RIIα and GSK3β with the exception of adult kidney cortex where no GSK3β was observed (Fig. 5). High levels of all three proteins (GSK3β, PKA RIIα, GSKIP) were detected in lung, brain, colon, pancreas, and testis.

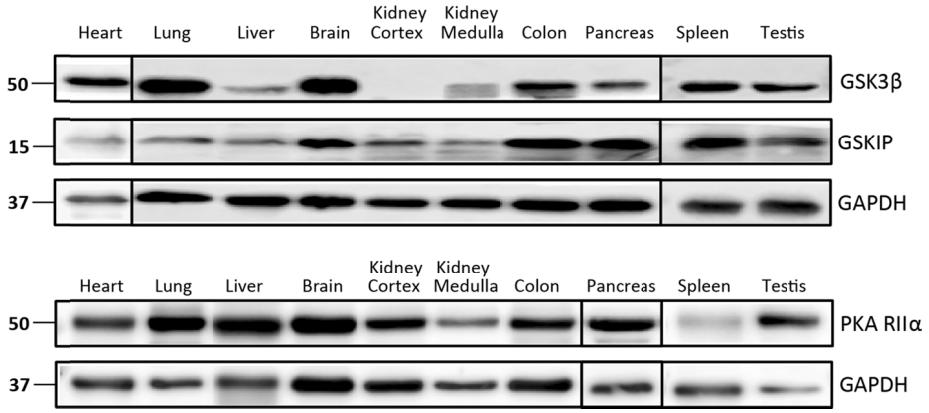

Fig. 5: **GSKIP, GSK3β and PKA protein expression in adult mouse organs.** GSKIP as well as PKA RIIα subunits are expressed in all mouse tissues tested. GSK3β protein was detectable in all tissues except kidney cortex. 25 µg protein lysates were loaded, separated by 12 % SDS-PAGE and detected *via* Western blot. Representative blots from three independent experiments are shown.

In line with the above shown mouse data, the human protein atlas (Ponten *et al.* 2008; Uhlen *et al.* 2015), recently updated for GSKIP expression revealed comparable ubiquitous cytosolic GSKIP protein expression in all human tissues with highest expression observed in the digestive tract (glandular cells). PKA-RIIα as well as GSK3β localization is described to be predominantly cytoplasmic and RIIα additionally partly membranous in human tissue (www.proteinatlas.org).

In order to define the physiological function of GSKIP *in vivo*, a KO mouse model was generated (PhD thesis P. Skroblin).

5.2 Conditional knockout of *Gskip* in mice

For the generation of a conditional GSKIP KO mouse the Cre/loxP system was used (Rajewsky *et al.* 1996). Exon 2 of the *Gskip* gene, containing the start codon and coding for 86 out of a total of 139 amino acids including the RII-binding domain, was flanked by loxP sites ("floxed") and thereby targeted for Cre-mediated deletion and inactivation of the *Gskip* gene (PhD thesis P. Skroblin; Fig. 6 A). The successful depletion of *Gskip* was confirmed at mRNA (Fig. 6 B) and protein level (Fig. 6 C) in tissue of newborn mice. As expected, there is no *Gskip* mRNA or protein detectable upon deletion of Exon 2. GSKIP is expressed at birth in all tested WT newborn (P0) mouse organs (Fig. 6 C).

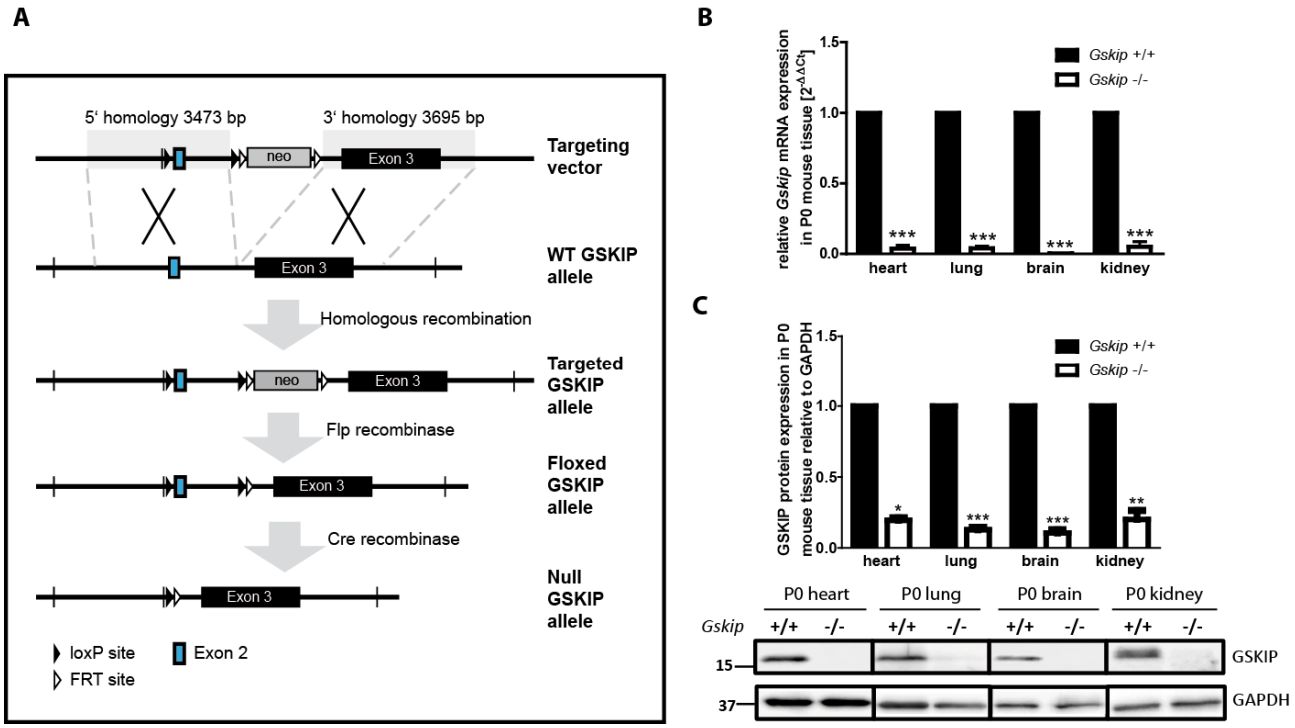

Fig. 6: **Generation of conditional *Gskip* knockout mice.** A) Strategy for the targeted generation of a conditional *Gskip* KO in mice. Exon 2 of GSKIP was targeted for loxP-mediated excision upon Cre recombination. B) *Gskip* mRNA expression in P0 mouse tissue, relative to *Gapdh* mRNA expression. GSKIP KO was normalized to WT. $n \geq 5$. C) GSKIP protein expression in P0 WT and GSKIP KO mice. *Upper panel:* Densitometric analysis of GSKIP protein expression relative to GAPDH. GSKIP KO was normalized to WT. $n \geq 11$. *Lower panel:* Representative Western blot of P0 tissue lysates. Protein lysates were separated by 12 % SDS-PAGE. GAPDH was used as a loading control. Mean ± SEM. Student`s t-test. $^{*}p \leq 0.05$.

5.3 Adult *Gskip*$^{+/-}$ and wild type mice express similar protein levels

Initially, adult *Gskip*$^{+/-}$ mice were analyzed biochemically and their breeding characteristics observed. *Gskip*$^{+/-}$ mice are viable, fertile and exhibit no overt phenotype. As GSKIP is a ubiquitous protein (Fig. 5), it is challenging to define which adult organ could be of particular interest for studying the heterozygous effect of *Gskip* KO. Thus, various tissues were analyzed (Fig. 7).

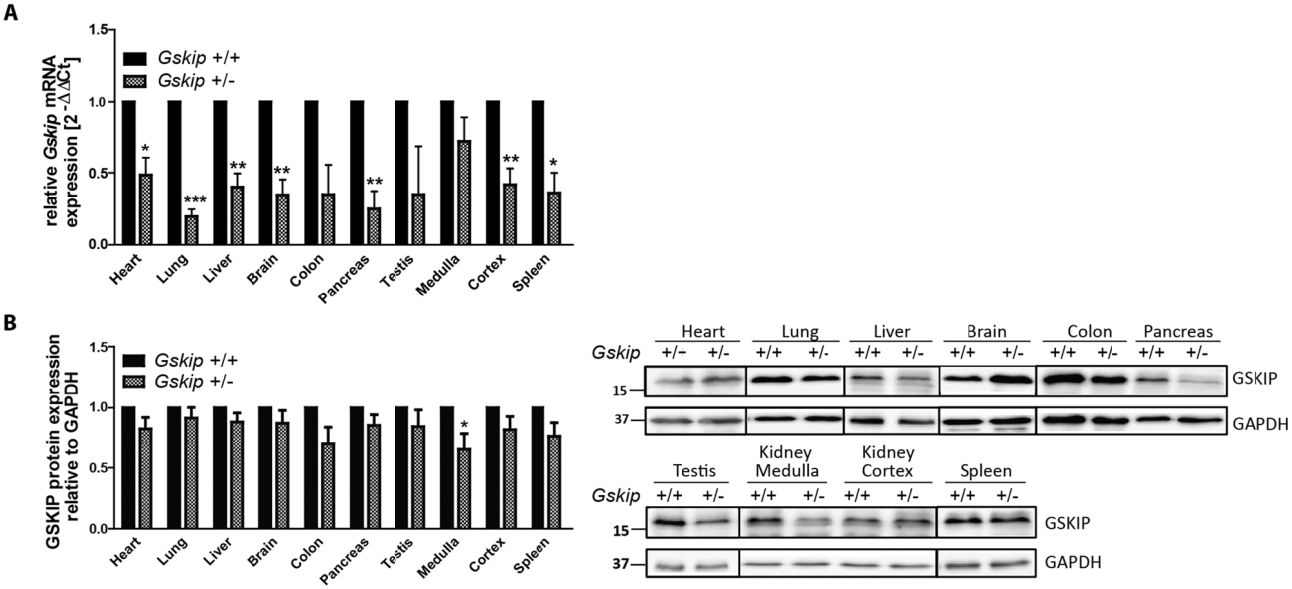

Fig. 7: **Loss of one allele of GSKIP reduces mRNA but not protein abundance.** A) *Gskip* mRNA expression in adult mouse tissues, relative to *Gapdh* mRNA expression. GSKIP KO (*Gskip*$^{-/-}$) was normalized to WT (*Gskip*$^{+/+}$). n ≥ 4. B) GSKIP protein expression in adult WT and heterozygous GSKIP KO mice. *upper panel:* Densitometric analysis of GSKIP protein expression relative to GAPDH. GSKIP KO was normalized to WT. n ≥ 8. n = 3 for testis. *lower panel:* Representative Western blot of adult mouse tissue lysates. Lysates were separated by 12 % SDS-PAGE. GAPDH was used as a loading control. Mean ± SEM. Student`s t-test. *p ≤ 0.05.

The *Gskip* mRNA level in adult *Gskip*$^{+/-}$ mice was significantly down-regulated in heart, lung, liver, brain, colon, pancreas, kidney cortex and spleen with the strongest reduction in heterozygous KO lung (Fig. 7 A). The GSKIP protein levels were not affected in any tissue upon haplotype insufficiency (Fig. 7 B; Fig. 8 A). Only in kidney medulla the level was significantly reduced. Hence, adult *Gskip*$^{+/-}$ animals compensate on protein level for the heterozygous loss of *Gskip*.

For all further experiments, GAPDH was included as a loading control and for normalization both for mRNA and protein expression studies. As there is a variation between animals of different litters, paired statistical analysis was carried out comparing always the expression levels between WT *Gskip*$^{+/+}$ and KO *Gskip*$^{+/-}$ (or later *Gskip*$^{-/-}$) animals within the same litter. These littermates naturally share a genetic background as equal as possible (arising from the same parents), are exposed to the same environmental influence and therefore variations observed between WTs of different litters can be minimized for relative comparison. The paired analysis was also used for normalization of obtained data: expression levels in WT controls were set one and the levels in heterozygous (and later homozygous) animals were determined as fold-changes compared to WT.

Several GSKIP-associated proteins were investigated in adult *Gskip*$^{+/-}$ mice (Fig. 8): the known GSKIP interaction partner GSK3β (Fig. 8 A, B) and its inhibitory Ser9 phosphorylation (Fig. 8 A, C), β-catenin as a potential GSKIP-controlled Wnt target gene (Fig. 8 A, D) and the inactivating GSK3β-mediated Ser641 phosphorylation of Glycogen Synthase (pGS Ser641) (Fig. 8 A, E). Glycogen Synthase (GS) is not only a key enzyme of glycogen metabolism but also directly regulated by both PKA (Ser8 phosphorylation) and GSK3β (Ser641/645/649/653 phosphorylation). Some small tendencies but no significant expression alterations were observed when analyzing the signal intensity quantification of up to 11 tissue pairs for

GSK3β and pGSK3β Ser9. For β-catenin protein expression a significant GSKIP-dependent reduction was noted solely in colon tissue. The levels of GS Ser641 phosphorylation did not change markedly; the significant increase of GS Ser641 phosphorylation in GSKIP-deficient pancreas is of less than 10 %.

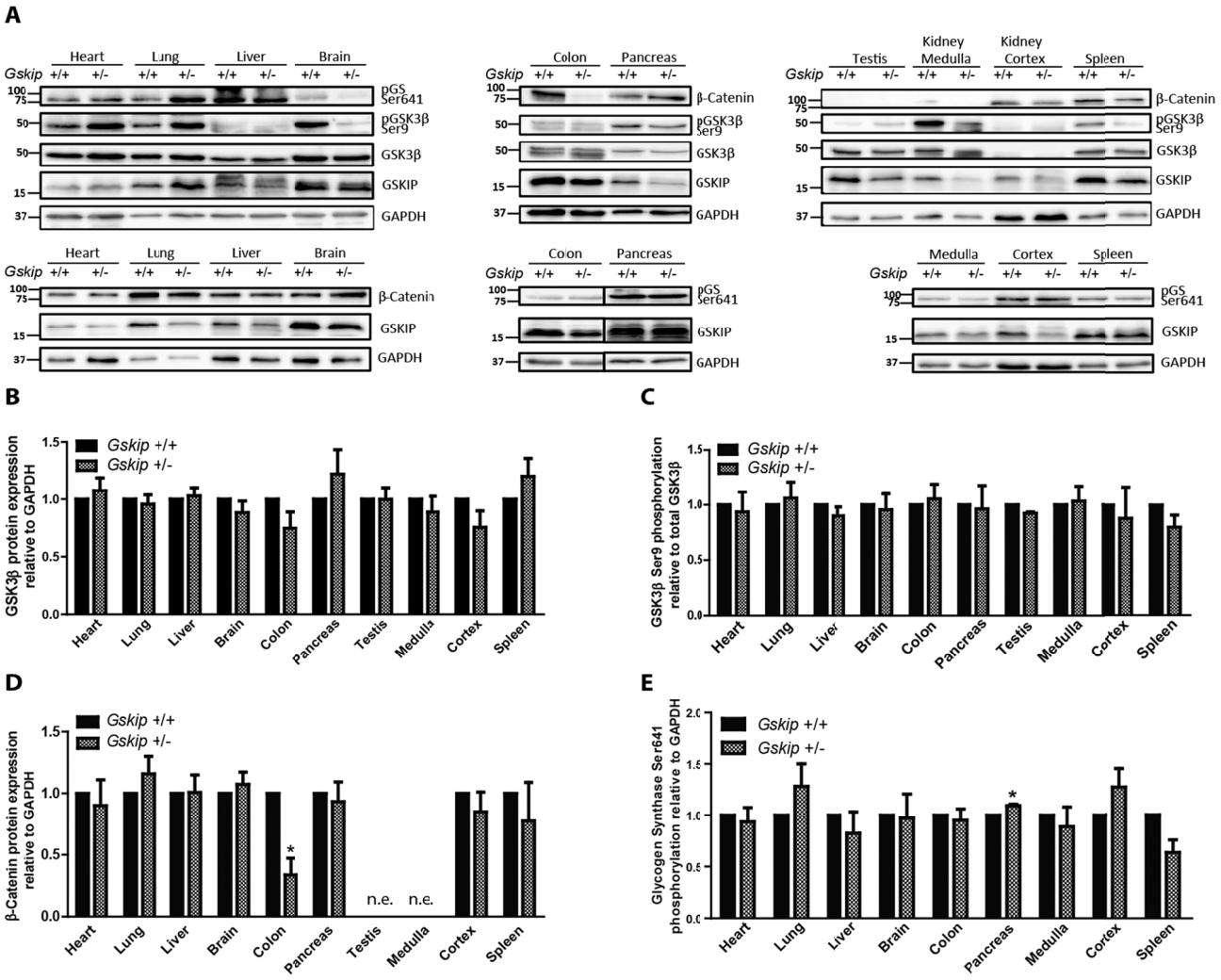

Fig. 8**: Heterozygous knockout of *Gskip* does not markedly influence protein expression of GSKIP-associated proteins**. Protein expression in adult WT and heterozygous GSKIP KO mice was tested. A) Representative Western blots of adult mouse tissue lysates are shown. Proteins (25 µg per lane) were separated by 12 % SDS-PAGE. GAPDH was used as a loading control. B) - E) Densitometry of protein expression relative to GAPDH. GSKIP KO was normalized to WT. $n \geq 8$ (B, C) and $n \geq 3$ (D, E). Mean ± SEM. Student`s t-test. *$p \leq 0.05$. n.e.: not expressed.

Next, neither for PKA RIIα subunits, nor for the GSKIP interaction protein SMYD2 (N-lysine methyltransferase; GSKIP co-immunoprecipitated with SMYD2 (Ewing *et al.* 2007)) or the Wnt pathway-associated protein Axin1 significant changes were detectable on the protein level upon heterozygous loss of *Gskip* in adult mice (Fig. 9).

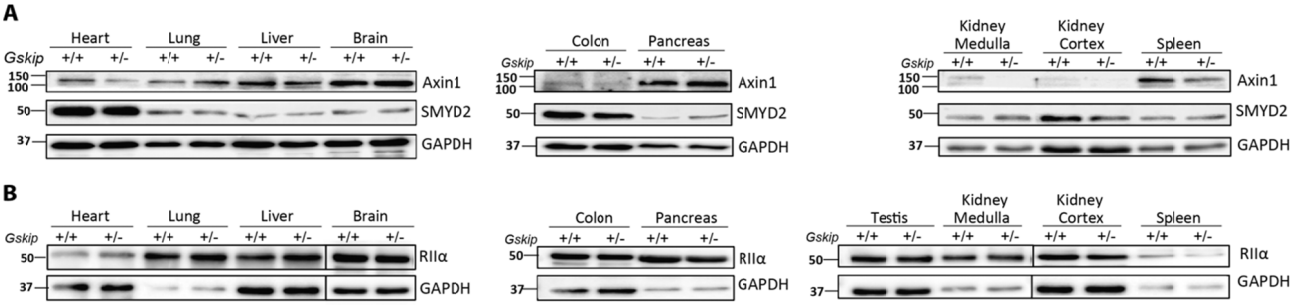

Fig. 9: **Axin1, SMYD2 and PKA RIIa protein expression is not markedly changed in adult heterozygous GSKIP KO mouse tissue.** Equal amounts of proteins were loaded and separated on 12 % SDS gels and blotted onto PVDF membranes. Representative Western blots are shown. GAPDH was included as a loading control. n = 3.

To sum up, the minor changes on protein level for GSKIP, its known interaction partners and some Wnt-related proteins did not point to major GSKIP-dependent biochemical modifications in adult heterozygous KO mice. In addition, behaviour and breeding properties of heterozygous KO mice were unremarkable compared to WT mice and did not hint at any severe physiological changes in adult *Gskip*$^{+/-}$ mice under normal unchallenged conditions. *Gskip*$^{+/-}$ mice did not show reduced fitness or survival. Thus, no further analysis was carried out with these animals.

5.4 GSKIP KO mice die at birth due to respiratory distress

When mating heterozygous *Gskip*$^{+/-}$ animals no viable homozygous progeny are born (PhD thesis P. Skroblin), pointing to an indispensable role of GSKIP during development.
Timed matings between two heterozygous GSKIP KO animals were set up for embryo analysis at different developmental stages. First, embryonic GSKIP protein expression was investigated in whole embryo lysates in WT and *Gskip*$^{-/-}$ and revealed expression starting at embryonic day (E) 10.5 (Fig. 10), thus making it feasible to study its function in development. For protein expression at later stages, refer to 5.9.1.

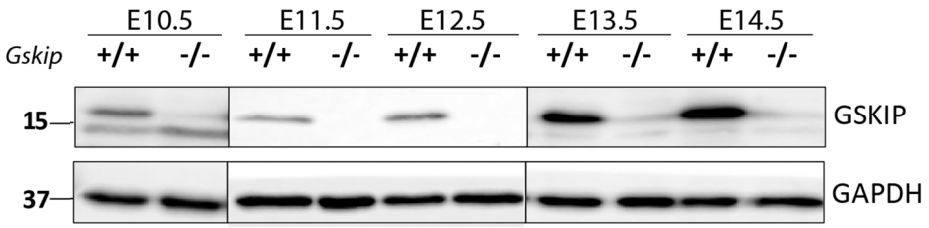

Fig. 10: **GSKIP is expressed during embryonic development starting at E10.5.** Representative Western blots of whole embryo lysates are shown. The lysates were separated by 12 % SDS-PAGE. Equal amounts of proteins (25 µg each) were loaded. GAPDH served as a loading control.

Next, genotype distributions of embryos derived from timed matings between two heterozygotes (*Gskip*$^{+/-}$) were calculated. The expected Mendelian ratio of WT to heterozygous to homozygous KO mice of 1:2:1 was observed up to stage E16.5 (Fig. 11).

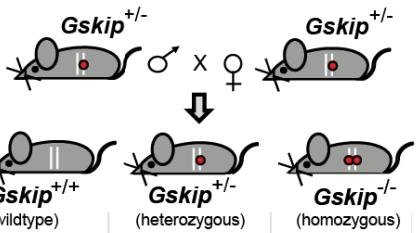

total embryo number	stage	(wildtype)	(heterozygous)	(homozygous)	Chi Square test [p]
66	E11.5	26 %	51 %	23 %	0.9114 ns
118	E12.5	32 %	42 %	26 %	0.4645 ns
71	E14.5	23 %	52 %	25 %	0.9170 ns
73	E16.5	28 %	45 %	27 %	0.8029 ns
425	E18.5	29 %	53 %	18 %#	0.0473 *
99	P0	22 %	66 %	12 %#	0.0301 *
373	P28-35	47 %	53 %	0 %	< 0.0001 ***
expected mendelian ratio		**25 % (1)**	**50 % (2)**	**25% (1)**	

died within few min or found dead

Fig. 11: **Embryo genotype analysis:** Genotype ratio distribution of offspring from *Gskip*$^{+/-}$ x *Gskip*$^{+/-}$ matings at different embryonic stages. Percentages were calculated for all three genotypes and compared to the expected Mendelian ratio. Embryos from at least 10 litters were included for each embryonic stage. $\chi 2$ test was used for statistical analysis, comparing absolute numbers of the observed distributions with the expected Mendelian distributions, see also Suppl. Fig. 1. *$p \leq 0.05$.

Even though *Gskip*$^{-/-}$ embryos were observed at E18.5 and postnatal day 0 (P0) (Fig. 11), none of the observed E18.5 GSKIP KO embryos was alive for more than 5-30 minutes and all P0 GSKIP KO embryos were found dead in the cage. At P0 maternal cannibalism could not be excluded and might thus have led to an underrepresentation of *Gskip*$^{-/-}$ embryos counted. Thus the number of GSKIP KO embryos considerably decreased after embryonic day E16.5 and were significantly below the expected Mendelian ratio of 25 % at

E18.5 (Caesarean sectioning; C-section) and P0 (birth). Therefore, parturition (P0) is the critical time point for survival of GSKIP KO mice. Even if they were delivered *via* C-section at E18.5, thus not exposed to the stress induced by the process of natural parturition, GSKIP KO mice died within less than 30 minutes, pointing to a perinatal lethality of the conditional GSKIP KO mice.

All GSKIP KO embryos appeared cyanotic, pale and tended to have a shortened neck compared to WT littermates (Fig. 12 A). External intestinal loops were observed occasionally (other observations such as protrusions of the head, less visible eyes and more spongy bodies have decreased in frequency with increasing number of backcrosses). Visual observations during dissections showed the presence of all organs in GSKIP KO mice at E18.5. Besides, no diaphragm defects or gross histological abnormalities were revealed by analysis of Azan-stained E18.5 whole-body sections at different planes (Fig. 12 B) performed in collaboration with C. Dittmayer. In accordance with ethical guidelines, animals were sacrificed by decapitation; hence whole-body sections lack the skull. No significant changes in body weight were noticed between WT, heterozygous and homozygous GSKIP KO embryos, neither at E18.5, nor at P0 (Fig. 12 C). In addition, E18.5 GSKIP KO mice exhibited distinct gasping movements and costal retraction, indicating a normal neuromuscular function and respiratory drive, but compared to WT littermates a reduced breathing frequency was observed. Despite extensive breathing effort, the death of GSKIP KO mice occurred within 30 minutes after delivery.

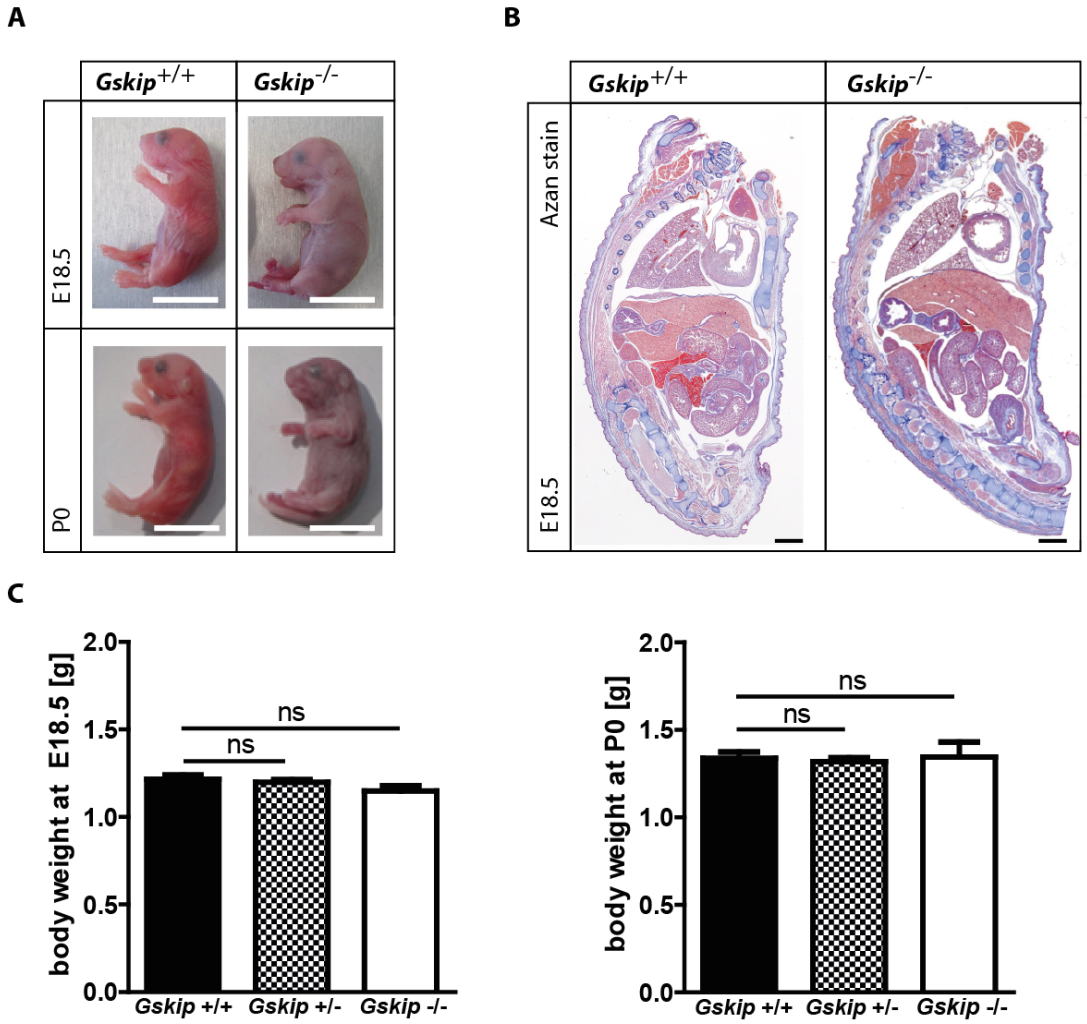

Fig. 12: **Embryo phenotype analysis.** A) Representative images of WT (*Gskip*$^{+/+}$) and KO (*Gskip*$^{-/-}$) embryos at embryonic stage E18.5 and P0. Scale bar: 1 cm. B) Representative images of Azan-stained whole-body paraffin sections of E18.5 specimen (by C. Dittmayer). Scale bar: 15 mm. D) Body weight comparison of *Gskip*$^{+/+}$, *Gskip*$^{+/-}$ and *Gskip*$^{-/-}$ littermates at E18.5 ($n \geq 16$ for each group) and P0 ($n \geq 6$ for each group). Mean ± SEM. One-Way ANOVA. ns: not significant.

From this time point on E18.5 embryonic material was utilized for all major studies, representing the latest possible developmental stage before the perinatal death makes analysis impractical. E18.5 embryos start respiration within seconds after their abdominal delivery and enable analysis on late-stage developmental changes avoiding the exposition of embryos to the stress of parturition itself. In contrast, P0 newborn mice struggle during natural delivery from the process of parturition (e.g. abdominal squeezing). Their survival is affected highly by the stress they encounter and especially weak newborns, such as homozygous GSKIP KOs, are thus not suitable for postnatal studies at all.

In order to exclude that the observed phenotypes are biased by their sex, 85 *Gskip*$^{+/+}$ and *Gskip*$^{-/-}$ E18.5 embryos were genotyped for the presence of the Y chromosome specific gene *Sry* (Fig. 13). Both male and female embryos were present among the tested groups in a similar distribution. Male (*Sry*-positive) embryos accounted for approx. 50 % of all GSKIP KO embryos. Thus, the phenotype of GSKIP KO mice is sex-independent and no correlation was detected between sex and the severity of the observed GSKIP KO phenotype.

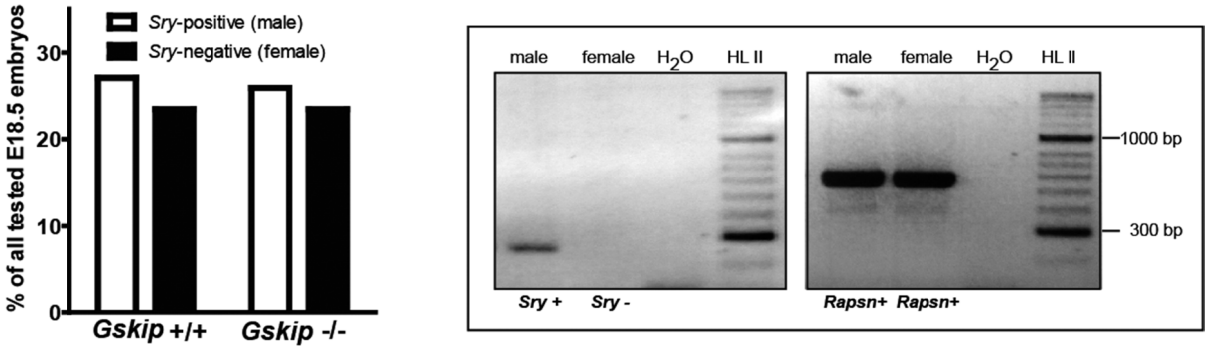

Fig. 13: **Distribution of sexes among E18.5 embryos.** The presence of the Y chromosome-specific gene *Sry* was tested in 43 WT (*Gskip*$^{+/+}$) and 42 KO (*Gskip*$^{-/-}$) E18.5 embryos (from 22 litters) by PCR. Sex distribution among all tested embryos was calculated in percent. *Rapsn* gene PCR (housekeeping gene) was included as a control. Embryos genotyped positive for both *Sry* and *Rapsn* were considered to be male, while females where only positive for *Rapsn* gene expression. HyperLadder II (HL II) was loaded as a DNA size marker. Fisher´s exact test was applied and no significant changes observed (see Appendix for statistics).

A hematopoietic defect in GSKIP KO mice would explain the rather pale appearance and breathing problems, even though no growth retardation or bleeding abnormalities were measured. As the limited blood volume of E18.5 embryos did not allow blood cell counts or haemoglobin measurements, initial blood analysis was performed *via* staining of histological blood smears. No obvious differences were observed concerning morphology and staining characteristics of blood cells (Fig. 14 A). First trials for the determination of bleeding time did not hint at a potential bleeding disorder. In addition, neither blood spots on the skin, nor internal bleedings were noticed for *Gskip*$^{-/-}$ mice. The gross oxygen saturation of the blood, determining blood colour, did not show GSKIP-dependent differences (Fig. 14 B): optical inspection shows that freshly collected blood from GSKIP-deficient E18.5 mice appears in the same red colour as GSKIP WT blood. Thus it seems unlikely that the inability to breathe relies on a profound blood oxygenation deficit.

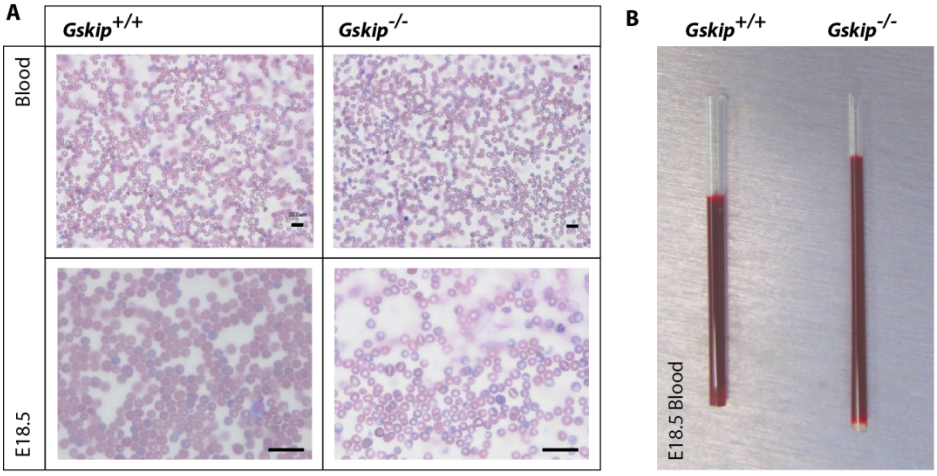

Fig. 14: **Blood analysis of GSKIP-deficient mice at E18.5.** A) Blood cell analysis of WT (*Gskip*$^{+/+}$) and Gskip-deficient (*Gskip*$^{-/-}$) animals stained with Pappenheim May Grünwald Giemsa (Morphisto). Scale bar: 20 µm. Magnification 20 x and 60 x respectively. B) Fresh blood of WT and GSKIP KO E18.5 mice in glass capillaries. Blood oxygen saturation is not strikingly changed, as visually no colour difference is observed.

The cause of the perinatal lethality observed seemed to be acute respiratory distress marked by cyanosis and severe dyspnea. Thus, *Gskip*$^{-/-}$ embryos were exposed to 100 % oxygen for several minutes in order to define if cyanosis was due to reduced oxygen diffusion *via* the blood, but cyanosis did not improve visually. To distinguish whether a newborn was born dead or alive, a lung-floating test was performed which is used as a standard autopsy technique for humans. As residual air remains in the lung even after death it causes the tissue to float on a liquid PBS surface. For the analysis of GSKIP KO embryos, the presence of air in the lung was used as an indicator for initiated breathing before death. Lungs were dissected, their weights determined and their ability to float on a liquid surface was tested (Fig. 15 A, B). No significant alterations were noticed in post mortem lung weight to body weight ratios at E18.5, excluding the pathologic condition of pulmonary hypoplasia in GSKIP KO mice (Fig. 15 A). Only 4.2 % out of 24 tested GSKIP KO lungs floated on a PBS surface (Fig. 15 B), pointing to lung atelectasis and a failure of GSKIP KO E18.5 embryos and P0 newborns to properly initiate breathing once exposed to air after Caesarean sectioning or natural parturition. The results obtained from lung floating measurements indicate that cyanosis resulted from a failure of lung inflation rather than reduced oxygen diffusion: thus, blood is likely passing the lung without gas exchange in GSKIP KO mice.

Moreover, gross morphological evaluations showed that both WT and GSKIP KO lungs were in the terminal saccular stage of lung development possessing normal lobation and orientation (Fig. 15 C, D). There were no obvious upper respiratory airway obstructions. Nonetheless, lungs of GSKIP KO mice had narrower airspaces and appeared slightly less expanded compared to WT controls (Fig. 15 D lower panels), but did not prove an inability to replace the embryonic lung liquid fluid during the first few breaths after birth by inhaled air.

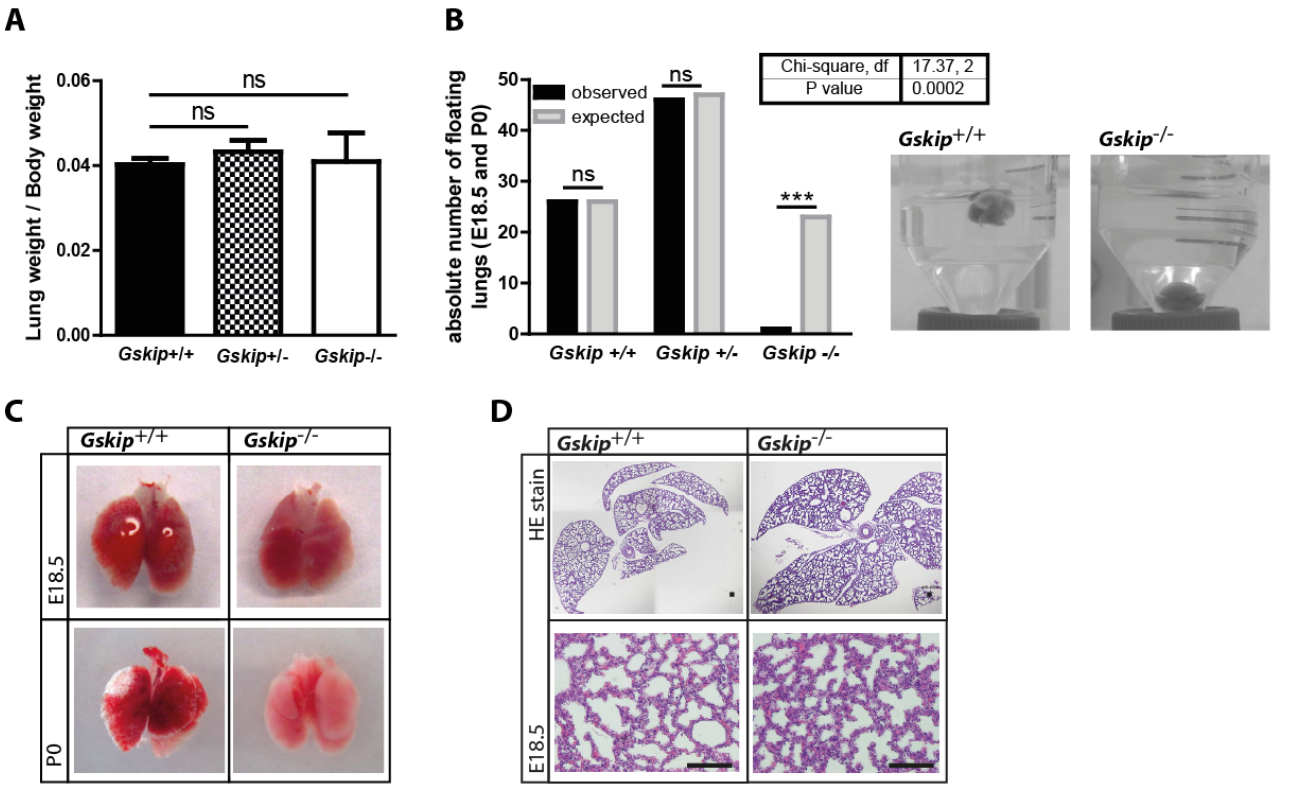

Fig. 15: **The lung of GSKIP KO mice.** A) Lung weight to body weight ratio. Wet lung weights and body weights were determined at E18.5 ($n \geq 6$ for each group) and ratios calculated. Mean ± SEM. One-Way ANOVA. B) *left:* Floating E18.5 and P0 lungs of WT (*Gskip*$^{+/+}$), heterozygous (*Gskip*$^{+/-}$) and KO *(Gskip*$^{-/-}$) mice. The lung´s ability to float on PBS surfaces was tested and the number of floating lungs compared with the expected number (100 % of all tested lungs) for each genotype (to allow for statistical assessment). $n \geq 24$ for each group. Fisher´s exact test. *$p \leq 0.05$. *right:* Representative images of dissected lungs in PBS. C) Representative images of GSKIP$^{+/+}$ and GSKIP$^{-/-}$ embryonic lungs at E18.5 and P0. D) HE-stained histological sections of E18.5 lungs. Scale bar: 100 µm. ns: not significant.

Albeit the presence of a thoracic diaphragm (as shown in Fig. 12 B) and the fact that a gross defect of the diaphragm could already be ruled out by the observed gasping movements of the GSKIP KO, the early embryonic neuronal innervation (taking place early in gestation) was analysed by studying cranial nerve branching in E10.5 embryos. Neuronal innervation analysis is of interest in order to define whether the respiratory distress is due to neuronal developmental defects of the hindbrain or brainstem.

The hindbrain is the area of the brain regulating, amongst others, essential autonomic functions such as breathing and blood circulation; it comprises the pons, the medulla oblongata and the cerebellum. The brainstem contributes to breathing control as it contains the respiratory pattern generators innervated by neuron clusters located in medulla oblongata, the so called retrotrapezoid nucleus (Guyenet *et al.* 2012). The mammalian respiratory tract harbours both intrinsic and extrinsic neurons; they form a complex neural network to control breathing, mucus secretion, smooth muscle tone and trigger reflexes such as coughing (Carr & Undem 2003; Canning 2006; Myers 2007). Respiratory neurogenesis is not fully understood in mice. It has been repeatedly described that intrinsic neurons do not contribute significantly to lung innervation but rather innervate the trachea. This indicates that the lung is predominantly innervated by extrinsic neurons with cell-bodies within the brainstem and axons traveling along the *nervus vagus* to the respiratory tract where they innervate neuroendocrine bodies of the lung epithelium and the airway smooth muscle (Aven & Ai 2013). In the developing hindbrain, sensory and motor neurons (cranial nerves) are formed, each having a specific target tissue and a unique appearance. Their anatomical organization reflects their embryonic origin as cranial nerves arise from sequentially occurring segments along the anteroposterior axis. Thus, cranial nerves can be used as markers for normal hindbrain formation (Cordes 2001), while the phrenic nerve, originating from the 4th cervical nerve in the neck, is the main innervator of the thoracic diaphragm. Nonetheless, the *vagus* nerve (X in Fig. 16 A) is the cranial nerve linked both to lung innervation and respiratory control and additionally passing by the diaphragm.

A neurofilament 2H3 staining at E10.5 (Fig. 16 A) allowed to count and compare cranial and sensory nerves between WT and GSKIP KO embryos and to define whether abnormal nerve development is the cause of the observed lung phenotype. In addition, neuronal abnormalities at this early gestational stage may serve as an indicator for the development of a brain phenotype at a later developmental stage.

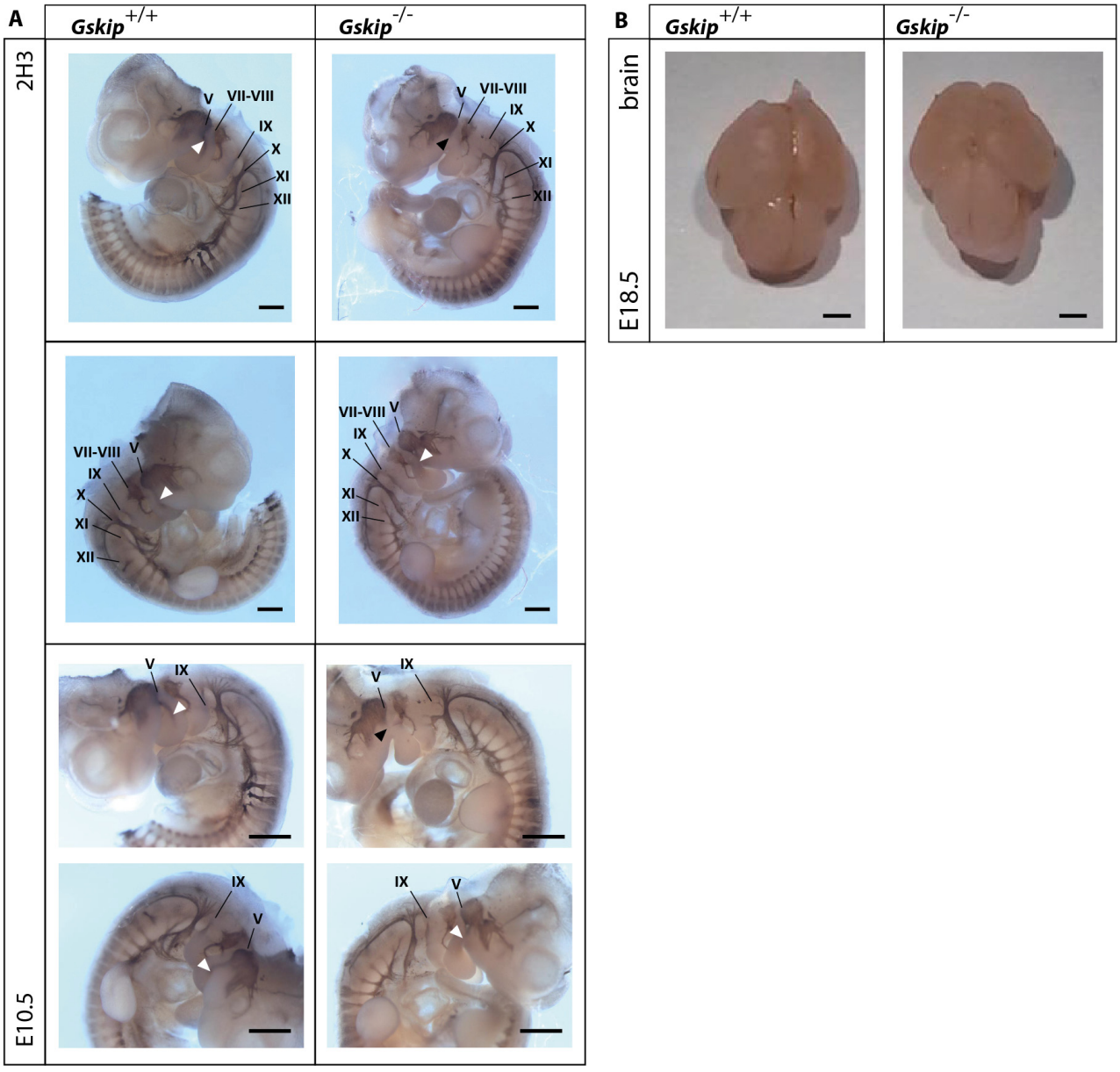

Fig. 16: **Analysis of cranial and sensory nerves in GSKIP knockout embryos.** A) Whole-mount immunostain of cranial nerves and ganglia in early-stage E10.5 embryos. Carefully dissected E10.5 embryos of appropriate genotypes were stained *en bloc* with primary neurofilament 2H3 (DSHB) and POD-coupled secondary antibodies. Representative images of DAB-detected E10.5 embryos are shown, pictured with a camera connected to a stereomicroscope. Arrows indicate the stained V (trigeminal) nerve, which did stain well on one body side (white arrows), but less good on the other body side (black arrows). Scale bar: 5 mm. B) Representative images of dissected, PFA-fixed brains of E18.5 mice do not display obvious size differences when comparing GSKIP WT and KO mice. Scale bar: 1 mm. V: trigeminal, VII: facial, VIII: acoustic, IX: glossopharyngeal, X: vagus, XI: spinal accessory, XII: hypoglossal nerves.

No differences were obtained: all cranial motor nerves (cranial ganglia) were visible in GSKIP KO embryos and their branching comparable to the neurofilaments of WT littermates stained with a 2H3 antibody (Fig. 16 A). The black arrows in the upper images (for both magnifications) indicate the absence or only faint appearance of cranial nerve pair V compared to the same nerve in WT (white arrow). However, looking at this nerve from the other body side, WT and KO E10.5 embryos showed nerve pair V in the same intensity, thus pointing to a staining artefact rather than a missing nerve. The *vagus* nerve (X) was visibly stained in both genotypes just as all other cranial nerves. This is in line with previous results and further confirms that

the respiratory distress is not caused by neuronal innervation defects as hindbrain formation is not affected by GSKIP KO. Additionally, E18.5 embryonic brains were visually compared for a quick assessment of brain size; there was no gross remarkable size difference noted (Fig. 16 B).

5.5 GSKIP KO mice display a secondary cleft palate

In addition to the lung phenotype, an anatomical dysfunction of the secondary palate was noted in GSKIP-deficient mice as an incomplete closure of the palatal bones at E18.5 and P0 (Fig. 17 A). Such a palatal cleft may contribute to the inability to breathe properly. Histological examination of HE-stained E16.5 and E18.5 mouse skull sections confirmed the pronounced palatal cleft (Fig. 17 B): upon GSKIP KO secondary palatal shelf formation is disturbed in the upper jaw and the two lateral hard palatal shelves do not fuse, resulting in no separation between nasal and oral cavity. In WT controls the two lateral maxillary palatal paired shelves were fused and the midline epithelial seam disappeared, as shown in Fig. 17 for *Gskip*$^{+/+}$ mice at E16.5, E18.5 and P0 developmental stages. Palatal shelf development is taking place between E12.5 and E15.5 (Ferguson 1988); by E16.5 the closure of the two lateral palatal bones is completed, as confirmed by histological analysis of *Gskip*$^{+/+}$ mice.

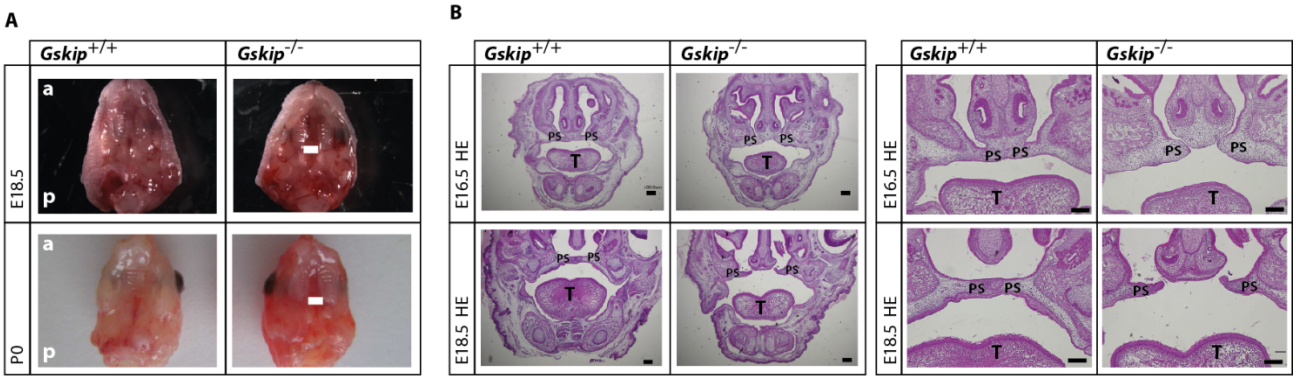

Fig. 17: **GSKIP knockout mice display a secondary palatal bone cleft.** A) Representative images of WT (*Gskip*$^{+/+}$) and KO (*Gskip*$^{-/-}$) upper jaws at embryonic stages E18.5 and P0. White bars indicate the observed cleft between the two palatal shelves of the upper jaw. a: anterior; p: posterior. B) Representative HE-stained coronal sections of paraffin-embedded E16.5 and E18.5 WT (*Gskip*$^{+/+}$) and KO (*Gskip*$^{-/-}$) skulls. Scale bar: 200 µm.
T: tongue, PS: palatal bone shelves.

GSK3β has been determined to be an intrinsic regulator of palatal shelf elevation (He *et al.* 2010) and the inactivation of GSK3β in the palatal epithelium of mice causes a cleft palate phenotype similar to the observed GSKIP phenotype (Liu *et al.* 2007). Lrp6 (Song *et al.* 2009), Wnt5a (He *et al.* 2008) and Wnt9b (Juriloff *et al.* 2006) KO mice as well show a secondary cleft palate. On the molecular level the developmental processes mediating elevation, rotation and fusion of the palatal shelves involve Shh/Ihh, TGFβ, BMP as well as Wnt signalling (Levi *et al.* 2011). Onset of palatal clefting is linked to disruptions in various Wnt genes (Juriloff *et al.* 1996; Juriloff *et al.* 2001; Juriloff *et al.* 2005; Levi *et al.* 2011). Increased Wnt and decreased Shh signalling were demonstrated to inhibit GSK3β-dependent palatal bone ossification (Nelson *et al.* 2011).
To study palatal ossification, a whole-mount Alcian blue/Alizarin red staining of the upper skull was performed with an emphasis on the secondary palatal bone and cartilage structures surrounding the cleft area. The properties of the dyes used account for the characteristic color pattern as seen in Fig. 18 for GSKIP WT specimen. Calcific deposition such as in bones appears purple (stained by Alizarin red), while cartilage is stained as glycan-rich structure in blue by the acidic dye Alcian blue. The purple border along the bones is less thick (black arrows in Fig. 18) and thus ossification delayed in the KO compared to WT. In addition, invagination-like elevated cartilage structures along the lateral hard palate fusion line in anterior direction (white arrows) are observable in GSKIP-deficient animals, which are not apparent in WT littermate skulls. When comparing WT and GSKIP KO, the reduced amount of purple structures, meaning less ossification in general within the secondary palatal shelf fusion area is strikingly evident, indicating impaired ossification

within the palatal arch. Thus GSKIP might be involved in GSK3β-dependent, Wnt- and Shh-mediated processes of secondary palate formation and ossification.

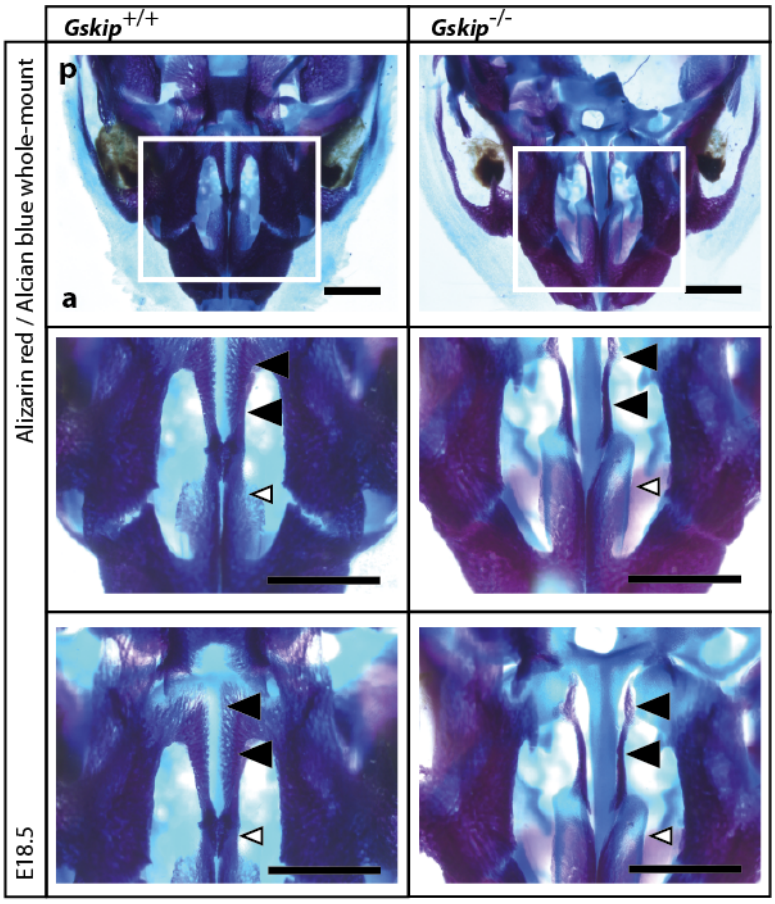

Fig. 18: **Loss of GSKIP causes delayed ossification along the secondary palate fusion site in the mouse upper jaw.** Whole-mount Alcian blue/ Alizarin red staining of dissected, eviscerated mouse skulls at E18.5. Representative images are shown. n = 5. *Top row*: overview, *upper rows:* magnification of white box. Black arrows: border of palatal bones; White arrows: anterior lateral hard palate fusion line; p: posterior; a: anterior. Scale bar: 1 mm.

Most likely the observed cleft palate alone does not explain the respiratory distress GSKIP KO mice suffer from and therefore are unlikely to be the primary cause of death; indeed, additional studies were initiated in order to define the morphological and molecular basis of lung dysfunction in GSKIP-deficient mice. In the following, details underlying the observed physiological changes were elucidated.

5.6 High-throughput gene expression profiling of GSKIP KO mice

A large-scale gene expression analysis was carried out using the Illumina Microarray approach, simultaneously measuring expression levels of thousands of genes within a particular mRNA sample. This high-throughput expression profiling revealed that 462 genes are significantly differently expressed in GSKIP KO mouse tissues compared to WT controls (Fig. 19 left; $n \geq 4$). Loading, hybridization, washing and scanning of microchips were performed in collaboration with N. Hübner. Data preprocessing including normalization, background correction and statistical evaluation (4.2.5.3) was done by H. Schulz (10.2.1; Suppl. Fig. 3). To narrow down the number of hits, only genes with at least 50 % up- or downregulation were considered. This threshold (in combination with a p value ≤ 0.05) is frequently chosen and feasible when evaluating microarray datasets (Jeffery *et al.* 2006; McCarthy & Smyth 2009) and resulted in 122 genes being altered upon GSKIP KO. Two genes encoding FRAT2, as a GSK3β binding protein, and RGS1, as a regulator of G protein signalling were both successfully validated and established as altered upon

GSKIP KO during this thesis work. Validation was conducted primarily on protein level as functional changes upon GSKIP KO were in the main focus; mRNA levels were checked in a second step.

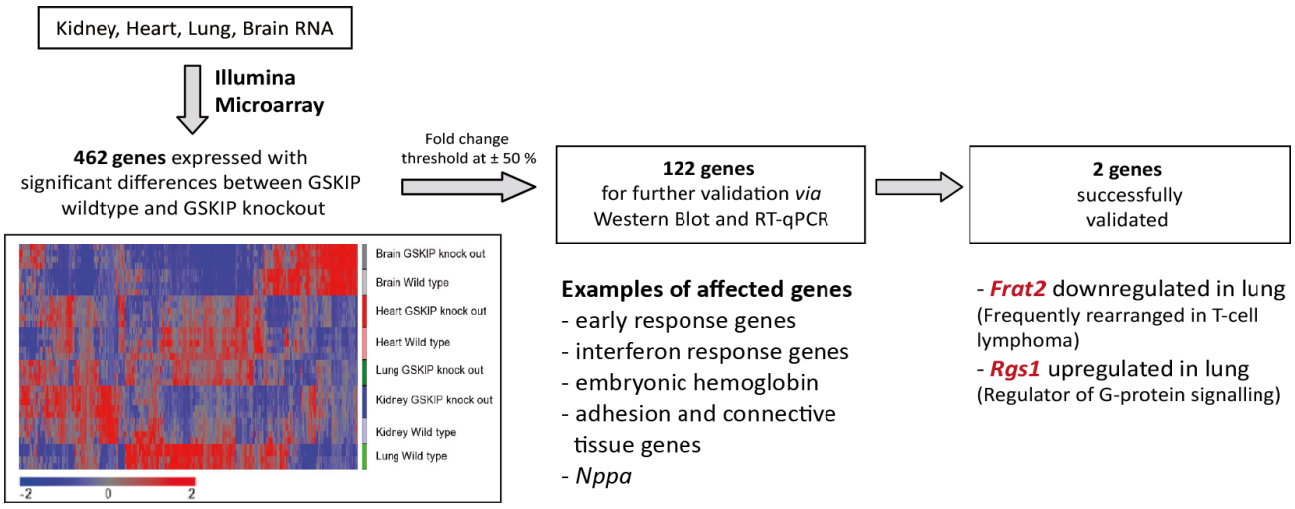

Fig. 19: **Summary of the experimental procedure of large-scale gene expression analysis of E18.5 GSKIP knockout mouse tissues.** Illumina Microarray workflow: cRNA from at least 4 different animals of each genotype derived from kidney, heart, lung and brain was loaded and hybridized to Mouse WG-6 Vers 2.0 Illumina Chips, revealing 462 genes expressed significantly different in GSKIP KO mouse tissues compared to WT control. A summarizing heatmap is shown as a summary. By setting a threshold at ≥ 50 % up- or downregulation (± 1.5), 122 genes were determined for potential further validation. The altered expression of genes was successfully validated for *Frat2* and *Rgs1*.

5.6.1 122 genes are differentially expressed upon knockout of GSKIP in mouse tissue

Initially, gene lists were analyzed in a "global" approach, trying to define those, which were changed in all tissues upon KO of GSKIP independent of the tissue type. 23 genes were initially identified (listed in Tab. 22). However, after setting the threshold of 50 % change only three genes remained, namely 4933433P14Rik (*Gskip;* positive control), *Fos* and *Hbb-y* (Tab. 23). *Hbb-y* could not be confirmed as a hit and *Fos* was excluded from validation as it is an early response gene. The rapid and transient activation of immediate early primary response genes and transcription factors such as *Fos* within few minutes is induced by a large variety of stimuli and does not require *de novo* protein synthesis (Herschman 1991). In this experiment *Fos* may be changed due to the lethality of the mouse rather than GSKIP deficiency.

Tab. 22: **Global assessment of significant gene expression changes comparing WT and GSKIP-deficient mouse tissues.** n ≥ 4.

Tissue	**Genes significantly changed between WT and GSKIP KO**	**Genes significantly changed by ≥ 50 % between WT and GSKIP KO**
Brain	183 (19 unique)	21 (11 unique)
Heart	266 (10 unique)	37 (6 unique)
Lung	362 (31 unique)	88 (47 unique)
Kidney	229 (9 unique)	39 (13 unique)
Total genes changed	**462**	**122**
Venn Diagrams	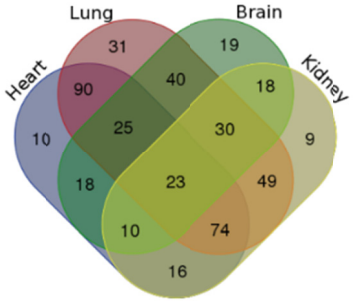	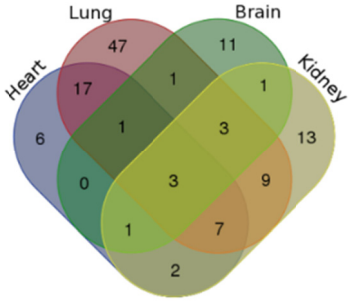
Genes changed in all tissue	**23**	**3**

Gene Symbols (RefSeq)	4933433P14Rik *(Gskip)* *Fos* *Hbb-y* C130027E04Rik 2310005L22Rik C230043E16Rik *Ccl4* *Klf9* *Zbtb46* 9430049I24Rik 2610019E17Rik *Lims2* *Hist1h1c* *Spata5l1* *Frat2* *Tdrd7* 1500005N04Rik *Frap1* *Hist2h2aa1* *Rbbp4* *Mycbp* E130302P19Rik E130118D18Rik	4933433P14Rik *(Gskip)* *Fos* *Hbb-y*

Tab. 23: **Gene expression alterations upon KO of GSKIP in mice, independent of tissue-type, shown as fold-change of gene expression compared to WT**. Fold-change < 1: downregulation; Fold-change > 1: upregulation. (Grey: positive control).

Symbol (RefSeq)	brain	heart	kidney	lung	Definition (Ensembl)
Fos	-1.60834	-3.39594	-1.99732	-4.40688	FBJ osteosarcoma oncogene (Fos)
Hbb-y	1.68075	2.85882	1.80612	1.58326	hemoglobin Y, beta-like embryonic chain (Hbb-y)
4933433P14Rik	-1.97299	-2.32426	-2.09949	-2.60787	Gsk3β interaction protein (Gskip)

As visualized by Venn Diagrams in Tab. 22, several tissues share diverse sets of significantly altered genes and therefore it was demanding to decide which candidate genes to choose for further validation. Gene lists were annotated using the web tool DAVID (Huang da *et al.* 2009). No known PKA or GSK3β substrates were among the altered gene candidates, and gene ontology enrichment analysis also did not reveal genes amongst the altered candidates coding for known proteins from any PKA- or GSK3β-mediated pathways. But even independent of PKA and GSK3β neither gene ontology, nor functionally related gene analysis yielded an over- or underrepresentation of genes for any pathways.
Next, total gene lists were screened, irrespective of whether they affect all organs or only individual organs, and single genes depicted which are involved e.g. in hematopoiesis (*Hbb-y*), cell adhesion (*Ctgf, Col1a1, Vcam1*) or different signalling pathways (*Irf7, Stat1*) for initial validations. NPPA (as the highest hit with a 22.6-fold increase in gene expression upon GSKIP KO), CTGF (-1.75-fold), COL1A1 (1.57-fold), VCAM1 (1.52-fold), IRF7 (-1.57fold), STAT1 (-1.54-fold), embryonic *Hbb-y* (average increase of 1.98-fold) and the Axin-related protein AXUD1 (-2.7-fold) were tested on protein level (or in case of lacking commercial antibodies on mRNA level) for GSKIP-dependent expression changes but were not confirmed to be altered (Suppl. Fig. 8) with the exception of the GSK3β interaction protein FRAT2.

RT-qPCR analysis revealed a 60 % downregulation of *Frat2* (Frequently rearranged in T-cell lymphoma 2) gene expression in GSKIP KO lungs compared to WT tissue (Fig. 20). This result was confirmed by Western blotting and showed significantly decreased FRAT2 protein expression in almost all tested GSKIP KO tissues. In GSKIP KO lungs the reduction on protein level was less pronounced: approx. 30% downregulation of FRAT2 was observed compared to 60 % downregulation on mRNA level. FRAT2 is a GSK3β-binding protein known to compete with Axin for binding of GSK3β and thereby disrupting the Wnt destruction complex and causing an accumulation of β-catenin in vertebrates (Dajani *et al.* 2003). Both FRAT1 and FRAT2 are post-translationally modified by phosphorylation (van Amerongen *et al.* 2004). Neither FRAT1 KO mice, nor FRAT2, FRAT3 or FRAT-triple-KO mice show any known abnormalities; they are viable, healthy and fertile. Hence, Wnt signalling in higher vertebrates does not seem to be critically dependent on FRAT (van Amerongen *et al.* 2005). Nevertheless, FRAT oncoproteins are discussed to be at the intersection of canonical and noncanonical Wnt signalling pathways, similar to the dual function of

Dishevelled in the Wnt/β-catenin and Frizzled/PCP pathways (van Amerongen *et al.* 2010). FRAT has been shown to interact with Dvl (Li *et al.* 1999). A connection between Dvl, GSKIP and FRAT2 is hypothesized. The KO of GSKIP in lung tissue is linked to reduced FRAT2 expression (Fig. 20 A), possibly due to a redundancy between GSKIP and FRAT2. e.g. if less GSKIP is present to bind and inhibit GSK3β, less FRAT2 is needed to compete for GSK3β binding. This hypothesis needs further analysis. Furthermore, FRAT2 protein showed ubiquitous expression in adult mouse organs (Fig. 21), excluding it from being only relevant during development. Unfortunately, the FRAT2 antibody used worked only in mouse tissue and there was no working commercially available FRAT2 antibody to this date for further cell studies.

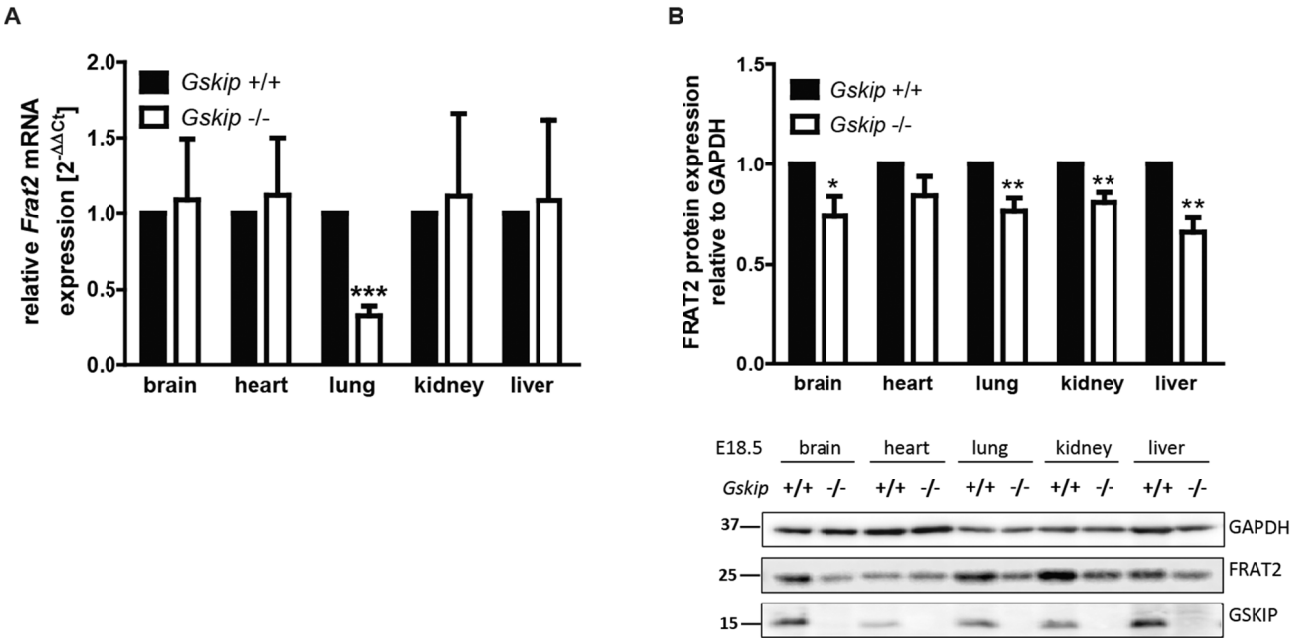

Fig. 20: **Validation of GSKIP-dependent *Frat2* gene and protein expression changes.** *Frat2* mRNA (A) and protein (B) expression in E18.5 GSKIP WT and KO tissue, relative to GAPDH. GSKIP KO was normalized to WT. mRNA expression in all tissues was determined by RTqPCR using the TaqMan system. A representative Western blot is shown, including densitometric evaluation of signal intensities. n ≥ 6. Mean ± SEM; paired Student´s t-test; *p ≤ 0.05.

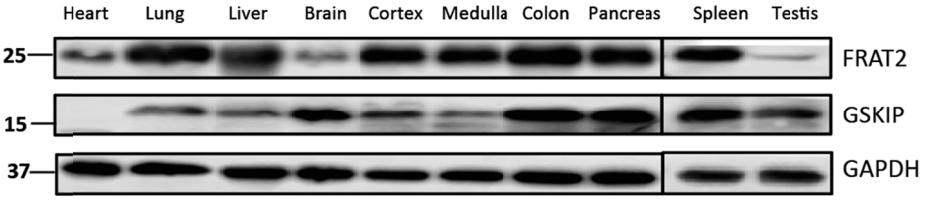

Fig. 21: **FRAT2 is expressed ubiquitously in adult C57Bl6 mice**. Adult mouse tissues were homogenized, lysed and 25 µg of proteins separated by 12 % SDS-PAGE. A representative Western blot of three independent experiments is shown.

5.6.2 88 genes are differentially expressed upon knockout of GSKIP in mouse lung

After the lung phenotype of GSKIP KO mice was confirmed, microarray data was re-analysed with a strong focus on lung-specific gene expression alterations. Of the 362 genes with significant differences in their expression 88 genes were above the threshold of 1.5, listed in Tab. 24. The 88 depicted genes were further processed and analysed using web-based bioinformatics tools.

Tab. 24: **88 significantly changed genes in the lung of GSKIP-deficient mice compared to WT exceeding threshold at 50 %.** Definition according to Ensembl, release 78 – December 2014; n.d.: not defined gene. Fold-change < 1: downregulation; Fold-change > 1: upregulation. grey: not confirmed by validation on protein level. Red: confirmed genes. n ≥ 4.

Symbol (RefSeq)	Fold-change compared to WT	Definition (Ensembl)
Fosb	-6.30119	FBJ osteosarcoma oncogene B (Fosb)
Atf3	-5.22085	activating transcription factor 3 (Atf3)
Fos	-4.40688	FBJ osteosarcoma oncogene (Fos)
Egr1	-3.77137	early growth response 1 (Egr1)
Cyr61	-3.29577	cysteine rich protein 61 (Cyr61)
Axud1	-2.76368	AXIN1 up-regulated 1 (Axud1)
Apold1	-2.67621	PREDICTED: apolipoprotein L domain containing 1 (Apold1)
Car4	-2.65521	carbonic anhydrase 4 (Car4)
Cyr61	-2.62133	cysteine rich protein 61 (Cyr61)
4933433P14Rik	-2.60787	Gsk3β interaction protein (Gskip)
Junb	-2.47836	Jun-B oncogene (Junb)
Myd116	-2.29983	myeloid differentiation primary response gene 116 (Myd116)
LOC100038882	-2.27786	PREDICTED: hypothetical protein LOC100038882 (LOC100038882)
8430403J19Rik	-2.21972	RIKEN cDNA 8430403J19 gene; n.d.
Klf4	-2.20217	Kruppel-like factor 4 (gut) (Klf4)
Tmem49	-2.19802	transmembrane protein 49 (Tmem49)
Dusp1	-2.19385	dual specificity phosphatase 1 (Dusp1)
Sgk1	-2.13533	serum/glucocorticoid regulated kinase 1 (Sgk1)
Rgs1	-2.09591	regulator of G-protein signalling 1 (Rgs1)
Igf2bp3	-2.05146	insulin-like growth factor 2 mRNA binding protein 3 (Igf2bp3)
Hist1h1c	-1.98321	histone cluster 1, H1c (Hist1h1c)
2810454F19Rik	-1.92958	RIKEN cDNA 2810454F19 gene; n.d.
Chst1	-1.89155	carbohydrate (keratan sulfate Gal-6) sulfotransferase 1 (Chst1)
4732473B16Rik	-1.87711	RIKEN cDNA 4732473B16 gene (4732473B16Rik)
Ifit3	-1.86564	interferon-induced protein with tetratricopeptide repeats 3 (Ifit3)
Idb2	-1.85529	n.d.
Ifi27	-1.84072	interferon, alpha-inducible protein 27 (Ifi27)
1500001E21Rik	-1.82555	Calmodulin 1/2/3
Tmem100	-1.82497	transmembrane protein 100 (Tmem100)
Klf2	-1.82453	Kruppel-like factor 2 (lung) (Klf2)
Jun	-1.80554	Jun oncogene (Jun)
Cirbp	-1.79042	cold inducible RNA binding protein (Cirbp)
Wfdc1	-1.76720	WAP four-disulfide core domain 1 (Wfdc1)
LOC380706	-1.76573	n.d.
Scel	-1.74476	sciellin (Scel)
9430049I24Rik	-1.74473	RIKEN cDNA 9430049I24 gene; n.d.
Lims2	-1.74321	LIM and senescent cell antigen like domains 2 (Lims2)
8430438E03Rik	-1.74299	RIKEN cDNA 8430438E03 gene; n.d.
Sfrs5	-1.72376	splicing factor, arginine/serine-rich 5 (SRp40, HRS) (Sfrs5), transcript variant 2
Frat2	-1.72276	frequently rearranged in advanced T-cell lymphomas 2 (Frat2)
A130095K04Rik	-1.71319	RIKEN cDNA A130095K04 gene; n.d.
Klf6	-1.69563	Kruppel-like factor 6 (Klf6)
Ccl4	-1.68336	chemokine (C-C motif) ligand 4 (Ccl4)
Gbp3	-1.67891	guanylate nucleotide binding protein 3 (Gbp3)
Trim30	-1.67885	tripartite motif-containing 30 (Trim30)
Per	-1.66273	Period circadian clock (Per)
1500041J02Rik	-1.65933	Coenzyme Q10 homolog B (S. cerevisiae)
Zfp36	-1.64072	zinc finger protein 36 (Zfp36)
Usp18	-1.63689	ubiquitin specific peptidase 18 (Usp18)
LOC100047427	-1.62778	PREDICTED: similar to thyroid hormone receptor (LOC100047427)
H2-Q5	-1.62274	histocompatibility 2, Q region locus 5 (H2-Q5)
Dtna	-1.60172	Dystrobrevin alpha (Dtna)
Lgals3bp	-1.60096	lectin, galactoside-binding, soluble, 3 binding protein (Lgals3bp)
Lamc2	-1.59561	Laminin, gamma 2 (Lamc2)
Slamf9	-1.58379	SLAM family member 9 (Slamf9)
Gpr146	-1.58029	G protein-coupled receptor 146 (Gpr146)
LOC638301	-1.57131	PREDICTED: similar to interferon activated gene 204 (LOC638301)
Ldlr	-1.56461	Low density lipoprotein receptor (Ldlr)
Ctgf	-1.56215	Connective tissue growth factor (Ctgf)
Gbp3	-1.55475	guanylate binding protein 3 (Gbp3)
Irf7	-1.55195	interferon regulatory factor 7 (Irf7)
Sh3rf2	-1.54512	SH3 domain containing ring finger 2 (Sh3rf2)
Spink2	-1.54213	serine peptidase inhibitor, Kazal type 2 (Spink2)
9530077A17Rik	-1.53979	RIKEN cDNA 9530077A17 gene; n.d.
Ifi35	-1.52938	interferon-induced protein 35 (Ifi35)
Amhr2	-1.52235	anti-Mullerian hormone type 2 receptor (Amhr2)
Gpr146	-1.51091	G protein-coupled receptor 146 (Gpr146), transcript variant 2 (Gpr146)
Sfrs5	-1.50699	splicing factor, arginine/serine-rich 5 (SRp40, HRS) (Sfrs5), transcript variant 1
D14Ertd668e	-1.50449	DNA segment, Chr 14, ERATO Doi 668, expressed (D14Ertd668e)
LOC100041797	1.50844	PREDICTED: hypothetical protein LOC100041797 (LOC100041797)
Vcam1	1.51758	vascular cell adhesion molecule 1 (Vcam1)

Snora65	1.52399	small nucleolar RNA, H/ACA box 65 (Snora65) on chromosome 2 (Snora65)
2610037P13Rik	1.53724	RIKEN cDNA 2610037P13 gene; n.d.
Rbm3	1.56655	RNA binding motif protein 3 (Rbm3)
Slc40a1	1.57312	solute carrier family 40 (iron-regulated transporter), member 1 (Slc40a1)
Hbb-y	1.59181	hemoglobin Y, beta-like embryonic chain (Hbb-y)
Ppp1r3c	1.59444	protein phosphatase 1, regulatory (inhibitor) subunit 3C (Ppp1r3c)
scl00238693.1_37	1.60096	n.d.
Zfp748	1.60276	zinc finger protein 748 (Zfp748), transcript variant 1
Igsf10	1.60402	Immunoglobulin superfamily, member 10 (Igsf10)
Zfp60	1.65004	zinc finger protein 60 (Zfp60), transcript variant 2
Cpa3	1.65035	carboxypeptidase A3, mast cell (Cpa3)
H13	1.67454	n.d.
6720463L11Rik	1.67565	RIKEN cDNA 6720463L11 gene; n.d.
2610019E17Rik	1.67543	Novel gene associated with 75614
Skp2	1.82766	S-phase kinase-associated protein 2 (p45) (Skp2), transcript variant 2
1110001A07Rik	1.83081	RIKEN cDNA 1110001A07 gene (1110001A07Rik); n.d.
Fbxo30	2.15396	F-box protein 30 (Fbxo30)
Lrrc29	2.20159	leucine rich repeat containing 29 (Lrrc29)
Angptl4	2.38172	angiopoietin-like 4 (Angptl4)
Nppa	22.2971	natriuretic peptide precursor type A (Nppa)

For functional profiling, lung gene ontology enrichment (GOE) (set of hierarchical controlled terms split into three categories: cellular component, molecular function and biological process) was tested. In addition to the initially used DAVID resource, a second web-based tool was utilized called GOEAST (Zheng & Wang 2008). GOE was conducted with the gene list dataset of Tab. 24 by entering the corresponding Illumina Probe IDs. With this approach a list of differentially expressed genes is taken and statistical analysis used to identify GO categories that are over- or under-represented in the GSKIP-deficient condition under study. Given a set of differentially expressed genes, this approach compares the number of differentially expressed genes found in each GO category of interest with the number of genes expected to be found in the same category just by chance.

No significantly enriched GO terms were observed regarding biological process or cellular component (Tab. 25; Suppl. Fig. 4). However, GOE analysis for molecular function revealed non-significant enrichments for nucleic acid as well as sequence-specific DNA binding transcription factor activity (10 out of 88 genes enriched; $p = 0.0951$) (Tab. 25; Suppl. Fig. 4). No functional category of gene expression was overrepresented for neither any metabolic, nor developmental processes.

Tab. 25: **GOE analysis for lung gene lists using the online enrichment analysis tool GOEAST** (Zheng & Wang 2008) **(2015.05.07)**. For graphical presentation, see 10.2.3. Grey: non-significant results; black: statistically significant results.

Genes used in GOEAST analysis	**GO enrichment for** Cellular component	**GO enrichment for** Molecular function	**GO enrichment for** Biological process
88 genes with at least 1,5-fold-changes	no enrichment	- nucleic acid binding transcription factor activity ($p = 0.0951$) - sequence-specific DNA binding transcription factor activity ($p = 0.0951$)	no enrichment
All 362 significantly changed genes	- nucleus ($p \leq 0.01$) - protein-DNA complex/ nucleosome ($p = 0.0575$) - nucleoplasm ($p = 0.0965$) -nucleosome ($p = 0.0575$)	- insulin-like growth factor binding ($p \leq 0.01$) - cation/ metal/ transition metal/ zinc ion binding ($p \leq 0.01$) - heterocyclic and organic cyclic compound/nucleic acid/ DNA binding ($p \leq 0.05$)	- regulation of metabolic process: regulation of DNA-dependent transcription ($p \leq 0.01$) - 6 ns enriched processes (Suppl. Fig. 7)

Due to the poor outcome, a second more comprehensive GOE analysis was run on the same tool including all 362 initially annotated, significantly changed genes upon GSKIP KO in E18.5 lungs, irrespective of their fold-change (Tab. 25; Suppl. Fig. 5; Suppl. Fig. 6; Suppl. Fig. 7). Results were different compared to the restricted list of genes (Suppl. Fig. 5-6; 10.2.3.2): Significant enrichments were discovered for the nucleus (cellular component GOE), in line with the observed term enrichment regarding regulation of DNA-dependent transcription (biological process GOE; 106 out of 362 entered genes). Investigating molecular function GOE, insulin-like growth factor binding (6 out of 362 genes), zinc ion binding (78 out of 362 genes) and DNA binding (47 out of 362 genes) were enriched significantly (Tab. 25). Some of these processes can

be categorized as metabolic process changes, no developmental processes showed an enhancement in terms of GO.

More precisely, lung differentiation or developmental pathways did not seem to be altered upon GSKIP KO on the large-scale gene expression microarray, even though the lung-specific gene *Klf2* was significantly decreased in GSKIP-deficient E18.5 lung tissue (Tab. 24). *Klf2* is a zinc-finger transcription factor, predominantly expressed in embryonic and adult lung (Wani *et al.* 1999a), spleen and vascular system and has been shown to be essential for normal lung development (Wani *et al.* 1999b). In mouse lung carcinoma MLE-12 cells overexpressing *Klf2* the expression of type 1 alveolar pneumocyte (epithelial cell) markers such as *Pdpn* (T1α) and *Aqp5* was induced in a dose-dependent manner, while *Klf2* did not alter type 2 pneumocyte marker gene expressions. In addition, chimeric $Klf2^{-/-}$ mouse lack mature type 1 pneumocytes and die shortly after birth. $Klf2^{-/-}$ lung analysis confirmed reduced type 1 pneumocyte marker gene expression and further proved *Klf2* to be a driver of type 1 pneumocyte cell differentiation and normal lung development (Pei *et al.* 2011). Nonetheless, the major function of *Klf2* is the regulation of T-cell migration and to promote T-cell quiescence rather than a lung-specific function, reviewed in (Richardson *et al.* 2012). For further studies on lung differentiation genes, refer to 5.7.1.

One additional candidate gene appeared interesting regarding its connection to GPCR signalling and was therefore further analyzed: *Rgs1*, encoding the protein regulator of G protein signalling 1 (RGS1), was successfully validated as significantly changed upon GSKIP KO (Fig. 22). While in the Illumina Array *Rgs1* gene expression was significantly decreased the decrease on mRNA level was confirmed using RT-qPCR (Fig. 22 A) but on protein level a 4-fold increase of RGS1 expression in GSKIP-deficient lungs was found (Fig. 22 B).

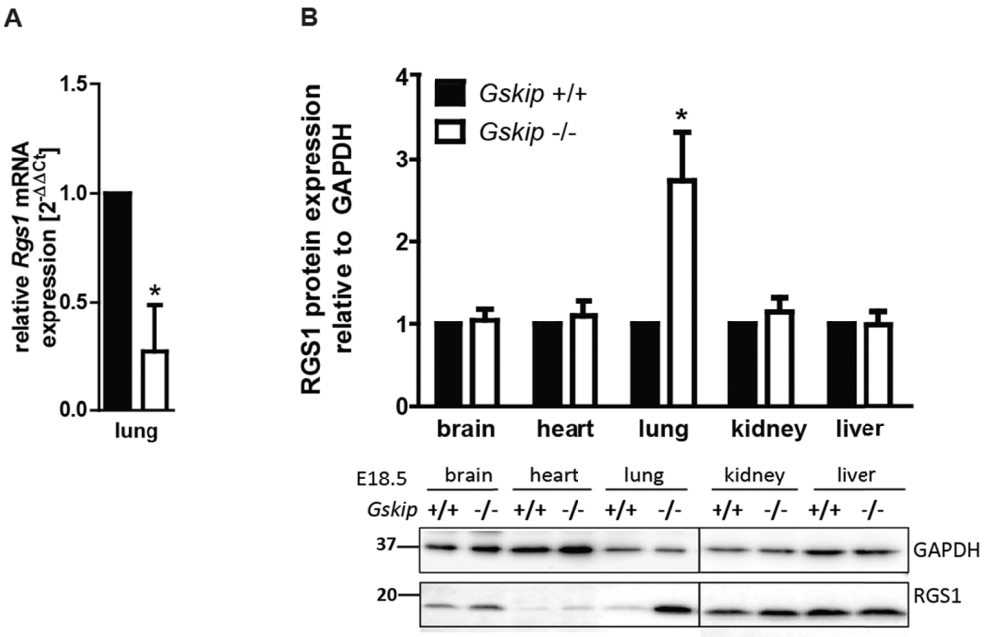

Fig. 22: **Validation of microarray reveals GSKIP-dependent *Rgs1* gene and RGS1 protein expression changes.** *Rgs1* mRNA (A) and protein (B) expression in E18.5 GSKIP WT and KO tissue, relative to GAPDH. GSKIP KO was normalized to WT. mRNA expression was tested in a lung-specific RTqPCR using the TaqMan system, while organ lysates were separated and proteins detected *via* Western blot. A representative blot is shown, including densitometric evaluation of signal intensities. $n \geq 6$. Mean ± SEM; paired Student´s t-test; $*p \leq 0.05$.

RGS proteins accelerate the GTPase activity of heterotrimeric G-protein Gα subunits, thereby inhibiting it (Hurst & Hooks 2009). Axin belongs to this protein family as well. RGS1 transcript expression is increased in several cancers (Hurst & Hooks 2009), but there is no link between RGS1 and lung so far. The signalling pathway that involves GSKIP and RGS1 is unknown. Whether there is a direct or indirect interaction between RGS1 and GSKIP remains to be studied. RGS1 KO mice show abnormal B-cell responses to chemokines and altered spleen architecture (Moratz *et al.* 2004). Interferon signalling in immune cells leads

to induction of RGS1 (Tran *et al.* 2010), so interferon response of GSKIP KO animals is currently being analyzed (PhD thesis A. Dema).

5.7 GSKIP´s function in lung development and physiology

5.7.1 Lung cell differentiation studies of GSKIP-deficient mice point towards AEC1 cell prematurity

Histologically, lung development is divided into four stages in mice starting at E9.5: pseudoglandular stage (E9.5-E16.6), canalicular stage (E16.6-17.4), terminal saccular stage (E17.4-P5) and alveolar stage (P5-30) (Warburton *et al.* 2000). Mouse pulmonary lobation differs from humans: the mouse right lung comprises 4 lobes while the left lung is unilobar (see Fig. 15 C, D) with the lobes being well established by E12 (Warburton *et al.* 2000).
In the airways epithelial cell lineages are arranged in a spatial pattern: squamous epithelium seams the larynx while the upper airways are lined with ciliated cells and mucus secreting cells surrounding pulmonary neuroendocrine cells. Clara cells are situated in the lower airways (proximal epithelium) and alveolar type 1 and 2 epithelial cells (AECs) cover the alveoli (distal epithelium). The primitive epithelium of early murine embryonic lung at E12-E14 co-expresses numerous cell lineage markers distinguishing later in development (by E18) distinct differentiated cell types, e.g. the surfactant associated protein encoding genes specifically expressed in type 2 AECs (AEC2). It is known that in late lung development cell proliferation declines and lung cell size is reduced as cells lose glycogen and undergo morphogenesis to differentiate into different cell types (O'Hare & Sheridan 1970; Adamson & Bowden 1975).

At E17.5 saccular stage begins and type 1 and 2 cell differentiation is initiated. Thus, mRNA expression at E18.5 was tested for type 1 and type 2 AEC differentiation marker genes as well as markers for lamellar bodies, endothelial cells and Clara cells (Fig. 23 A). While marker gene expression was unaltered for AEC2 differentiation (such as *Sftpc, Abca*) as well as for lung endothelial cells (*Pecam-1*), Clara cells (*Scgb3a2, Sftpb)* and lamellar bodies (*Abca3*), altered mRNA expression was observed for AEC1 cell markers such as *Aqp5* and *Pdpn*, pointing to a potential failure of type 1 cell differentiation in the developing lung of GSKIP KO mice (*Sftpb* expression change reached significance but was only of a minor extend). While loss of T1α, encoded by *Pdpn* gene, is associated with respiratory failure at birth and AEC type 1 differentiation defects in T1α KO mice, the physiological function of AQP5 in lung physiology is controversial. AQP5 KO mice do not have a lung phenotype under normal physiologic conditions. AQP5 deletion leads to a dramatic decrease in airspace-capillary osmotic water permeability, physiological consequences were not observed, even after maximal stimulation of active fluid absorption *via* β-agonist (Ma *et al.* 2000). But, *Aqp5* as well as *Pdpn* mRNA levels are highly elevated if newborn mice are exposed to hyperoxia and remain high in mice even after they are returned to room air (Yee *et al.* 2014). Furthermore, PKA-dependent AQP5 translocation has been shown for AQP5-expressing cornea and lens as well as for cells of the salivary gland and for lung bronchial epithelium. Here, the substantial upregulation of *Aqp5* gene expression upon GSKIP KO in mouse lungs was clearly compensated on protein level, showing a slight but significant downregulation (Fig. 23 B). Additionally, *Klf2* gene expression analysis was included as *Klf2* alterations were observed earlier (5.6.2) and *Klf2* as early-response transcription factor is described to be essential for normal lung development (Wani *et al.* 1999b). RTqPCR indeed confirmed the significant downregulation of *Klf2* in GSKIP-deficient E18.5 lungs on mRNA level.

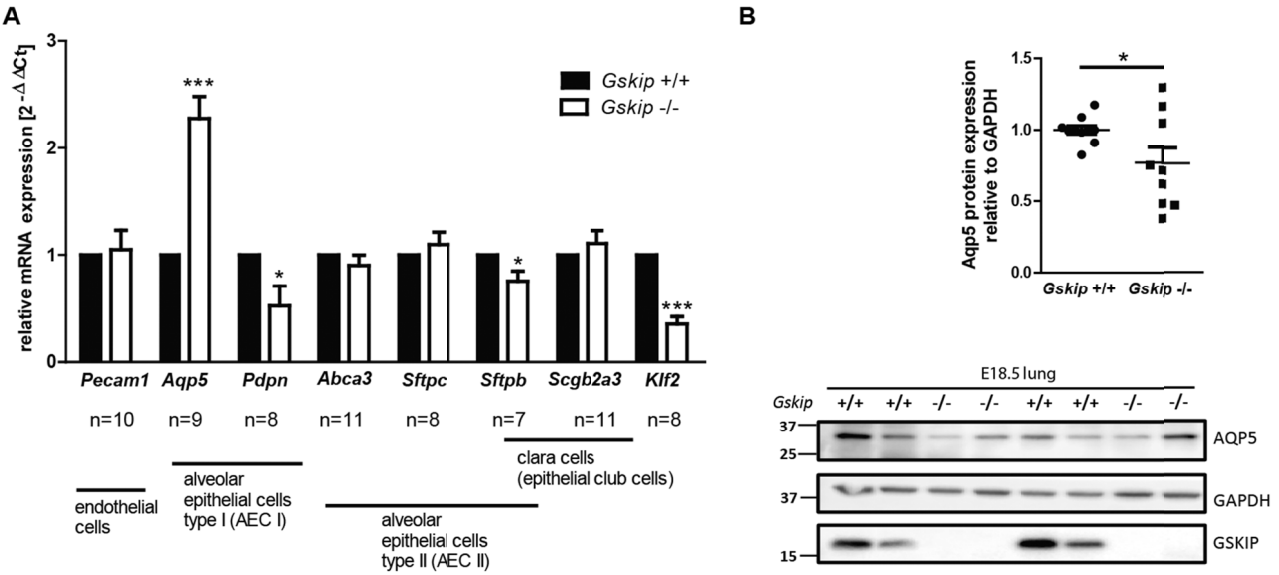

Fig. 23: **Lung cell differentiation analysis.** A) Cell differentiation marker gene expression at E18.5 in lung tissue. Lung mRNA was assayed for relative gene expression changes, comparing mRNA expression in GSKIP-deficient and WT tissue. n ≥ 7. B) Western blot analysis of AQP5, GSKIP and GAPDH in E18.5 lung tissue. WT compared to GSKIP KO. A representative Western blot is shown as well as the densitometric evaluation of signal intensities, relative to GAPDH and normalized to WT. n = 10. Mean ± SEM. unpaired Student´s t-test; *p ≤ 0.05.

The obtained results suggest that the differentiation of endothelial cells, Clara cells (ciliated epithelial cells in the proximal airways) as well as of AEC2 is not altered. Surfactant protein mRNA expression was unaffected by GSKIP KO concerning AEC2-specific surfactant protein C (SP-C) and the expression changes concerning the gene encoding surfactant protein SP-B only minor even though reaching significance (refer to 5.7.2 for SP-B and SP-C protein expression). However, *Aqp5* and *Pdpn* mRNA levels were dysregulated, hence indicating perturbed AEC1 cell proliferation, differentiation or maturation at E18.5 in GSKIP-deficient lungs. Unchanged wet lung weight (Fig. 15) in combination with unaltered lung size argues against abnormal cell numbers in GSKIP KO lungs. Noteworthy, if cell numbers were reduced and cell size increased at the same time (or the other way round), wet lung weight determination would not necessarily detect it. Type 1 alveolar epithelial cells are responsible for gas exchange and ion/fluid balance and discussed as potential contributors to chronic neonatal lung disease. For 40 years, the source of AEC1 has been believed to be AEC2; In 2014, several publications showed that AEC1 and AEC2 are likely arising directly from a bipolar progenitor cell expressing some of each class of AEC1 and 2 cell markers before further differentiation (Desai *et al.* 2014).

Likely due to the fact that type 1 and type 2 pneumocytes only represent a small percentage of total lung cells, no significant expression differences were observed for any type 1 or type 2 pneumocyte marker genes when comparing WT and GSKIP KO lung tissue on the microarray. Nonetheless, not yet determined genes encoding proteins potentially mediating type 1 or 2 pneumocyte differentiation other than *Klf2* might be among the obtained differentially expressed gene candidates. KLF2 is a major driver in the maturation of gas-permeable AEC1 and activates a genetic program consistent with AEC1 development such as the gene expression of *Aqp5* and *Pdpn* through the direct interaction of KLF2 with AEC1 marker gene promoters (Pei *et al.* 2011). This does not explain the observed upregulation of *Aqp5,* but possibly the reduced *Pdpn* gene expression upon GSKIP KO, thus linking differentiation marker gene analysis results with *Klf2* downregulation.

5.7.2 Histological assessment of GSKIP-dependent lung phenotype

Airway surface liquid is forming a barrier between the cells covering the respiratory tract and the air (Akella & Deshpande 2013). The composition of this liquid differs along the respiratory tract dependent on the population of cells in different regions: the upper respiratory tract airway lining fluid contains more mucus

and immune-protective proteins while the liquid lining the alveoli is rich in surfactant and phospholipids. The volume of alveolar lining fluid is controlled by ion and water channels (Hollenhorst *et al.* 2011). Decreased surfactant with decreased volume of lining fluid results in lung collapse (Akella & Deshpande 2013).

The functional alveolar surface is formed mainly by two types of epithelial pneumocytes, the alveolar cell types I (flattened shape) and II (cuboidal shape). Macrophages are also present in alveoli, removing microorganisms and particles, which enter the alveoli with the air (Crapo *et al.* 1982; Dobbs *et al.* 1998; Maina 2000; Ridge *et al.* 2003). While type 1 AEC are involved in gas exchange and ion/fluid balance, type 2 cells are the major cells involved in surfactant production and secretion.

Morphological analysis of HE-stained paraffin section indicates the presence of both flattened type I and cuboidal type II alveolar epithelial cells (AEC) at E18.5 in WT as well as GSKIP KO lungs lining the peripheral alveolar saccules (Fig. 24 B) and no morphological alterations were observed regarding lung development: pulmonary lobation and alveolar structure appear normal; GSKIP deletion did not affect lung morphology at the light-microscopic level. In Fig. 24 A the alveolar walls of saccules, so called primary septae, appear only slightly thickened in KO lungs compared to WT; the KO seems less inflated but the absence of air as indicated previously by negative lung floating test (Fig. 15) was not confirmed at this point.

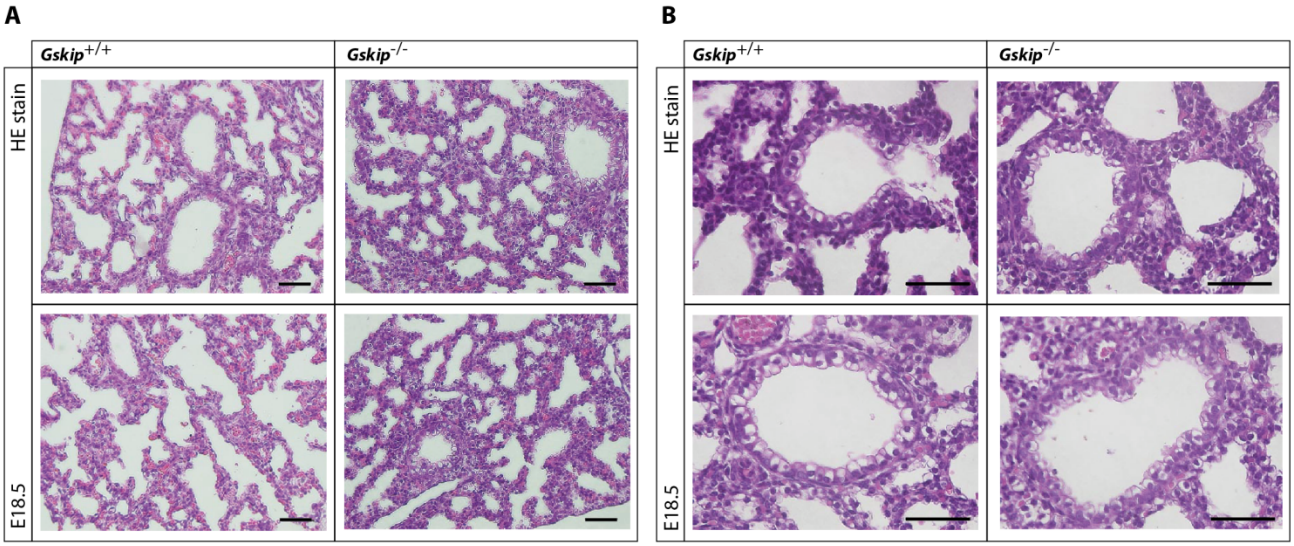

Fig. 24: **GSKIP KO does not cause gross morphological changes in E18.5 lung.** Representative images of PFA-fixed, paraffin-embedded and HE-stained histological lung sections are shown, imaged with a digital bright-field microscope using a magnification of A) 20 x and B) 40 x. Scale bar: 50 µm.

During expiration the surface pressure in the alveoli increases and is lowered by the presence of surfactant, protecting the alveoli against rupture. Lung surfactant forms a lipid monolayer at the liquid-air-interface of alveoli and reduces the surface tension along the lung epithelium, thereby enabling gas exchange (Andreeva *et al.* 2007). Lung surfactant synthesis and secretion are of crucial importance during lung maturation and known to be regulated by hormones and numerous other factors. The synthesis itself takes place in multivesicular and lamellar bodies of AEC2 (TEM analysis in 5.7.3).

Fetal type II cells accumulate glycogen in a notably high amount. It has been discussed for long but not yet proven that these accumulations serve as a carbon source for lipid synthesis (Maniscalco *et al.* 1978; Ridsdale & Post 2004). With the first breath at birth a considerable secretion of surfactant occurs requiring a prior *de novo* synthesis of surfactant components by AEC2 cells. Later, surfactant is not produced in huge amounts but rather recycled continuously. Periodic acid Schiff (PAS) staining is routinely used to study the enrichment of glycogen by which immature secretory AEC2 cells that are secreting surfactant are characterized. PAS-stained lung sections were analysed but did not show any alterations concerning glycogen content of AEC2 cells (Fig. 25 A).

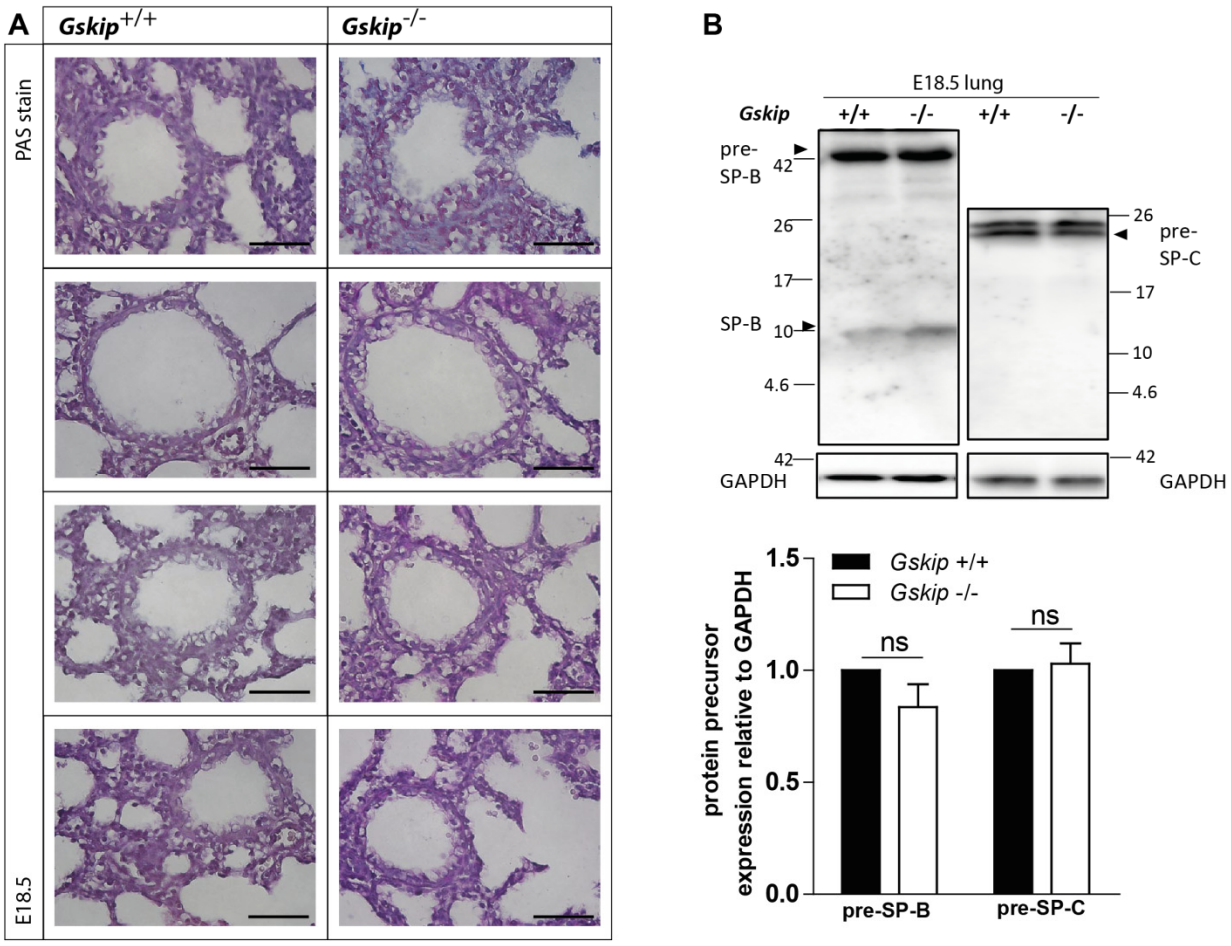

Fig. 25: **GSKIP-deficient lung alveolar epithelial cells (AECs) do not differ in their glycogen content and show the same surfactant proteins compared to E18.5 wild type lungs.** A) Morphological analysis of glycogen in GSKIP-deficient (*Gskip*$^{-/-}$) E18.5 lung AEC2 compared to WT (*Gskip*$^{+/+}$) tissue. Periodic-acid Schiff (PAS)-stained sections of PFA-fixed, paraffin-embedded E18.5 lungs were pictured using bright-field microscopy on a digital Keyence microscope with 40 x magnification. Scale bar: 50 µm. B) Protein expression of AEC surfactant proteins. Precursor surfactant B (pre-SP-B; 42 kDa) and surfactant C (pre-SP-C; 21 kDa) proteins from E18.5 lung lysates separated on 15 % SDS gels and detected *via* Western blot, WT compared to GSKIP KO lung tissue. Representative blots are shown. Densitometric evaluation of signal intensities, relative to GAPDH signal, normalized to WT. n ≥ 11. Mean ± SEM.

In a next step, the presence of surfactant, a phospholipid-rich lipoprotein secreted mainly by AEC2, was analyzed on protein level, as maturation of surfactant synthesis and secretion are key in determining if a newborn lung can sustain gas exchange without collapsing. However, proteins only count for about 10 % of surfactant. Surfactant consists mainly of glycerophospholipids (80 %), amongst others phosphatidylcholine, and the remaining 10 % are cholesterol (Goerke 1998). The predominant proteins in surfactant are the surfactant proteins (SP)-A, SP-B, SP-C and SP-D. SP-A and SP-D are hydrophilic glycoproteins and play a role in protection against infection while SP-B and SP-C are hydrophobic. SP-C is only expressed in AEC2 cells while SP-B is expressed in AEC2 as well as proximal lung epithelial (Clara) cells (Andreeva *et al.* 2007; Akella & Deshpande 2013).

Notably, SP-B deficiency is linked to surfactant deficiency and respiratory failure both in humans and mice. SP-B-deficient mice show vesiculated lamellar bodies with few or no bilayer membranes: trafficking, storage and function of surfactant proteins and phospholipids is impaired resulting in fatal respiratory distress syndrome (along with respiratory failure at birth) (Tokieda *et al.* 1997). Rescue experiments with targeted expression of SP-B in AEC2 but not in Clara cells of *Sftpb*$^{-/-}$ mice did rescue the perinatal lethal phenotype (Akinbi *et al.* 1997). Surprisingly, SP-C KO mice survive with essentially normal gas exchange as SP-B apparently is sufficient for *in vivo* surfactant function. Nonetheless, SP-C KO mice display minor instability of surfactant film and develop chronic progressive respiratory disease (Glasser *et al.* 2003).

Mature SP-B of 9 kDa is generated from pro-SP-B (43 kDa) by several steps including processing intermediates of a size of 23 kDa within the secretory compartments of AEC2. SP-C is processed from a

21 kDa preprotein to an intermediate of 15 kDa in size and a final mature 4 - 11 kDa protein (Andreeva *et al.* 2007). Despite several trials with different gel types and different lung tissue samples (from different developmental stages), the used antibodies did not reproducibly recognize mature surfactant proteins (rarely bands occured around 9 kDa for SP-B), but the precursor proteins of SP-B and SP-C, respectively (Fig. 25 B). Neither pre-SP-B, nor pre-SP-C showed any GSKIP-dependent expression changes upon GSKIP KO in E18.5 lungs, excluding these two proteins being in charge for lung collapse or a potential surfactant synthesis defect in the analyzed KO mouse model. (The mature proteins should however be present at this stage at least in the WT lung, as in the next chapter the secreted surfactant could be visualized by tramsmission electron microscopy).

The combination of lung cell differentiation gene analysis, PAS staining, higher magnification HE staining and surfactant protein presence allows so far to conclude that vasculogenesis, alveolar structure and AEC2 cells are unaltered upon GSKIP KO. To identify whether AEC1 cells are indeed immature, further clarifying experiments with higher resolution were necessary.

5.7.3 TEM reveals mitochondrial damage in E18.5 GSKIP KO lung cells

Transmission electron microscopy (TEM) was used to study subcellular compartments within the lung. TEM was carried out with ultra-thin 50 nm Epon sections of E18.5 lungs derived from C sections (lungs being exposed to air prior fixation). Microscopic analysis confirmed the presence of all types of respiratory cells in the bronchi of GSKIP KO mice when compared to WT, thus supporting previous results obtained from gene expression analysis and light microscopy. Both type 1 (longitudinal flattened) and 2 (cuboidal) AECs were present lining the air-exposed bronchial structures. Fibroblasts were seen as well (Fig. 26 A; white arrows). Lamellar bodies were present in AEC2 both in WT and KO conditions (Fig. 26 B; white stars), confirming previous mRNA data showing unaltered lamellar body marker *Abca3* expression (Fig. 23 A). Surfactant itself cannot be visualized under TEM, but a tubular myelin-rich structure including secreted lamellar bodies (supposed to be the non-functional surfactant which is shortly recycled), shown as typical intraluminal agglomerates, were observed in huge amounts predominantly in WT lungs (Fig. 26 B). In contrast, considerably fewer aggregates were found in KO lungs, underlining the absence of breathing in the KO mice and hence the missing physical (mechanical stretch) and chemical stimuli inducing surfactant secretion. Large amounts of glycogen (small black “dots” e.g. in Fig. 26 C) were noticed in the cytosol of both WT and KO alveolar epithelial cells, being a hallmark of AECs at this transition state between intrauterine and extrauterine life. No signs of glycogen overload were noted (in line with unchanged PAS stain, Fig. 25). Ciliated cells enabling lung liquid clearance were existent in both WT and KO lungs and cilia structure (9+2) unaltered. AEC1 cells appeared structurally unaltered.
From TEM analysis alone it is speculative to conclude whether AEC1 cells are immature and underrepresented within the lung epithelium of GSKIP KO mice. The relative number of AEC1 within a section is difficult to assess in an objective, unbiased way. Comparison with published AEC1 prematurity phenotypes such as in T1α, Glycocorticoid or Thyroid hormone receptor KO mice (Gong *et al.* 2001; Pei *et al.* 2011) demonstrates that prematurity of lung AEC1 was characterized by unaffected AEC1 appearance under TEM in combination with marker gene studies resulting in a profound downregulation of AEC1-specific differentiation genes. Hence, previously observed marker gene alterations (Fig. 23 A) pointing towards AEC1 immaturity might be the cause of respiratory insufficiency in GSKIP KO mice, likely due to AEC1 dysfunction.
Importantly, severely damaged mitochondria were detected irrespective of cell type in GSKIP KO lungs (Fig. 26 C). WT mitochondria were visible as grey longitudinal organelles with ordered membrane and cristae structure. Contrary, KO mitochondria look swollen, roundish and white with diffuse intra-mitochondrial membrane arrangements and fragmented cristae, and the majority of GSKIP KO mitochondria ruptured.

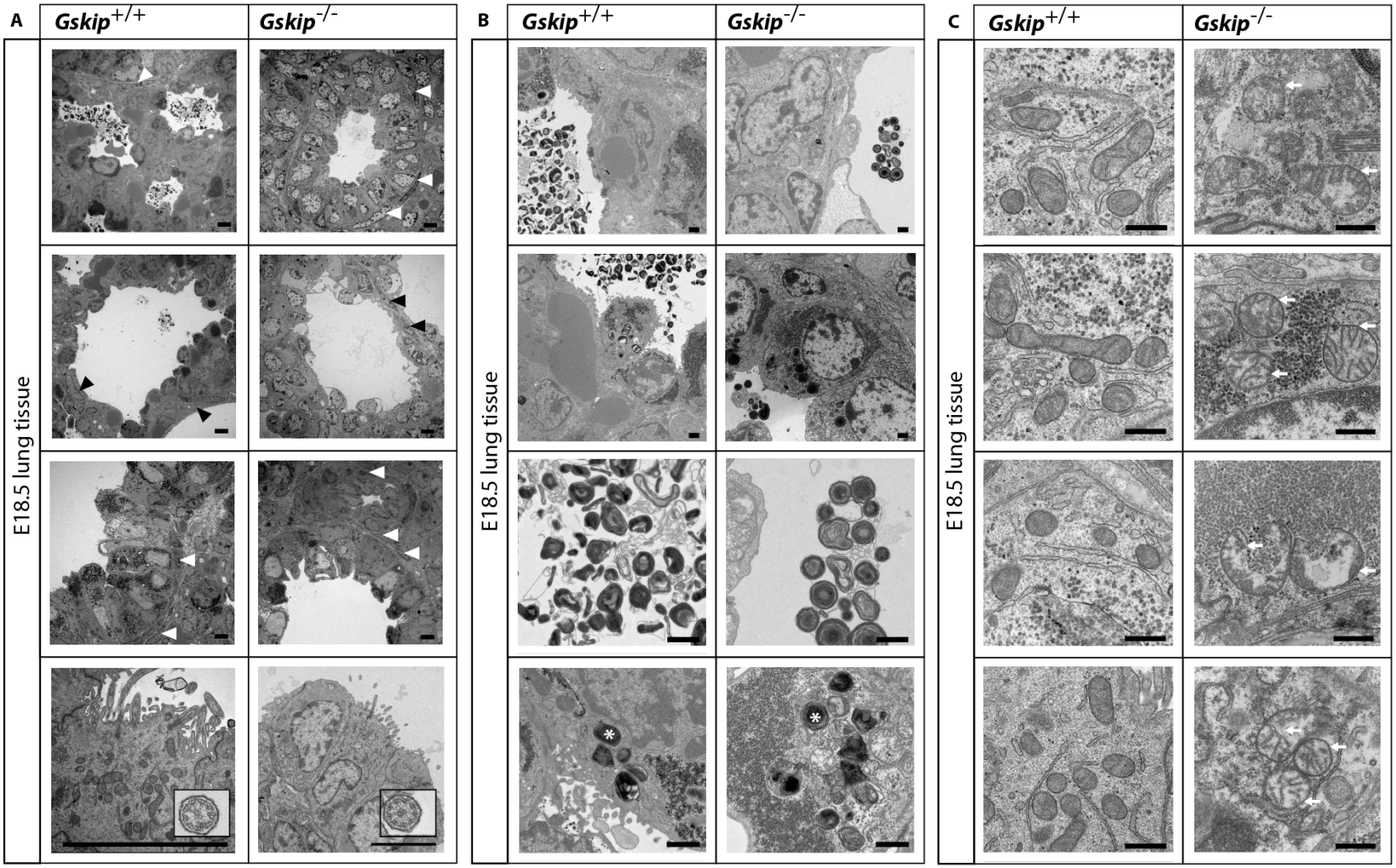

Fig. 26**: GSKIP knockout mouse lungs show reduced amount of secreted lamellar bodies in the bronchial lumen and display severe mitochondrial damage in airway epithelial cells.** Representative TEM images of ultra-thin WT (*Gskip*$^{+/+}$) and KO (*Gskip*$^{-/-}$) lung tissue sections at embryonic stage E18.5, dissected and fixed after embryo delivery *via* C-section and thus exposure to air. n = 3. A) All characteristic lung cell types lining the bronchus are present in WT and KO lung sections. AEC1 (black arrowheads) are flattened cells covering 90 % of the bronchial airway surface while cuboidal type 2 AEC and macrophages are the most abundant cells, seen both in WT and KO bronchi. Cilia can be observed on the outer membrane of AEC2. White arrowheads: fibroblasts. Scale bar: 5 µm. *Bottom panel* (right corners): 135 000 x magnification of lung cell cilia. B) Lamellar bodies (*lowest panel;* white stars) are present in WT and KO lung type 2 AEC and secreted into the bronchial lumen to produce surfactant, building up a surface-inactive network of phospholipids and tubular myelin constantly recycled by macrophages and AEC2. Surface-active surfactant cannot be visualized under TEM (layer above alveolar fluid lining cellular surface towards the bronchial lumen). Scale bar: 1 µm. C) Mitochondria of GSKIP-deficient cells show severely misarranged cristae and membrane structures (white arrows). Scale bar: 500 nm. Sample processing and images in collaboration with C. Dittmayer (Charité).

Of importance, other membranous cell compartments such as the ER and Golgi, which are more susceptible to TEM artefacts appear unremarkable, excluding the observed mitochondrial phenotype from being introduced by sample fixation and/or processing. Collectively, the data indicate that lung mitochondria of GSKIP-deficient mice likely acquired their damages within a few minutes after birth when embryos were exposed to the extrauterine environment with an increased oxygen concentration compared to hypoxic *in utero* conditions. The combination of mitochondrial damage in the lung and AEC1 immaturity should be ultimately lethal for GSKIP KO mice failing to adapt to extrauterine life.

5.8 Metabolic profiling of GSKIP-deficient mice by large-scale metabolomics

Metabolomics is used to characterize on a broad scale the set of metabolites (metabolic intermediates) in a biological system. Here, metabolomics was used to assess metabolic variations in different mouse organs (lung, liver, blood) resulting from GSKIP KO at developmental stage E18.5, the previously defined time point of death.

The metabolomics analysis (identifying 121 metabolites) was performed by S. Kempa (4.2.6), yielding a list of significantly changed metabolites for the tested tissues and blood comparing WT animals with GSKIP-deficient mice (Suppl. Tab. 3): 29 lung metabolites, 20 liver metabolites and 13 blood metabolites were detected being significantly altered upon GSKIP KO, pointing to a clear metabolic phenotype of the conditional GSKIP KO mouse.
First, the resulting metabolites were classified into groups according to their biological molecular classification. Next, a computational method was used for the bioinformatics analysis of the metabolite set in order to define affected metabolic pathways and metabolites of special interest, followed by a closer analysis of particular metabolic pathways, relevant enzymes and the evaluation of their expression at protein level by Western Blot. At a later stage, proteomics analysis was added (5.9.2).

5.8.1 Lung-specific metabolite analysis reveals GSKIP-dependent metabolic disturbances at E18.5 in mice

Initial analysis of metabolomics data was restricted towards the metabolite changes upon GSKIP KO in the mouse lung at E18.5. Chemical classification of 29 altered lung metabolites (Tab. 26) demonstrated an imbalanced amino acid homoeostasis (in total 9 essential and non-essential amino acids (aa) up- or downregulated), a perturbed tricarboxylic acid (TCA) cycle (4 intermediates highly altered) and reduced levels of amines such as putrescine and ethanolamine, the latter one representing a phospholipid head group. Sugar metabolism showed significant alterations compared to WT lung tissue, including the most highly upregulated metabolite detected in this screening, namely Glucose-6-phosphate. These severe perturbations might overall contribute to the severe mitochondrial phenotype of E18.5 GSKIP KO lungs observed in TEM (Fig. 26).

Tab. 26: **Lung metabolite set changes detected upon GSKIP KO in E18.5 mouse lung**. Fold-changes compared to WT are shown. n = 3. Red: significantly up-regulated; Blue: significantly down-regulated metabolite. Black: ≤ 20 % change. p ≤ 0.05. For detailed statistics, refer to Suppl. Tab. 3.

Classification	Detected metabolite	Significant fold-change (KO vs. WT)
Amino acid, essential	L-Lysine	**0.50**
	Leucine	**1.40**
	Valine	**2.01; 1.40**
	Phenylalanine	**1.39**
	Methionine	**1.21**
Amino acid, non-essential	Serine	**1.77; 1.45**
	Glutamic acid	**1.59**
	Proline	**0.66; 1.17**
	Aspartic acid	**0.64**
TCA intermediate	Succinic acid	**2.20**
	Fumaric acid	**0.74**
	Citric acid	**0.34**
	Pyruvic acid	**0.12**
Amine	Ethanolamine	**0.57**
	Putrescine	**0.48**
	Ethanolaminephosphate	**0.85**
Sugars and sugar acids	Glucose-6-phosphate	**2.64; 2.25; 2.09**
	Lactose	**1.58**
	Xylose	**0.76**
	Sucrose	**0.75**
	Gluconic acid	**0.73; 0.84**
	Threonic acid	**0.64; 0.63**
	Galacturonic acid	**0.60**
Others		
Antioxidant, Vitamin	Ascorbic acid	**1.85**
Purine derivative	Hypoxanthine	**1.84**
Vitamin (B5)	Pantothenic acid	**1.47**
Inorganic acid	Phosphoric acid	**1.28**
Creatine derivative	Creatinine	**1.27**
Dicarbonic acid (α-Hydroxy acid)	Glutaric acid, 2-oxo	**0.16**
Dicarbonic acid (α-Hydroxy acid)	Glutaric acid, 2-hydroxy	**0.86**
α-Hydroxy acid	Glycolic acid	**0.85**
Alcohol of cyclohexan	Inositol (Myo)	**0.84**

The next step was a functional interpretation of the lung metabolite data set. Several tools for visualization and functional interpretation of metabolomics experiments are available, the majority of them being web-based freeware (reviewed e.g. in (Gehlenborg *et al.* 2010; Chagoyen & Pazos 2013)). Here, MetaboAnalyst 3.0 (Xia *et al.* 2009; Xia *et al.* 2015) was chosen for this purpose as it represents a module combining species-specific metabolite enrichment analysis with pathway topology analysis (*Mus musculus* chosen as reference organism) and yielding a combined interpretation of the lung metabolites listed in Tab. 26 (compounds submitted for pathway analysis). Thus, the enormous amount of metabolic pathways being active in an organism or cell was narrowed down to the ones significantly enriched of changes. The results are shown in Tab. 27 and plotted in Fig. 27: Red circles represent significantly enriched metabolic pathways, implicating the pathways with the highest impacts in terms of significantly overrepresented amount of altered metabolites compared to total metabolites present in a metabolic pathway. The higher the impact and the higher the p value, the more relevant the pathway for the analysis of GSKIP-dependent changes, hence the most meaningful ones being on the top right corner. GSKIP KO in lungs accounts for significant changes in valine, leucine and isoleucine (amino acid) biosynthesis, aminoacyl-tRNA biosynthesis and TCA cycle, followed by the amino acid metabolisms for alanine, aspartate and glutamate as well as for cysteine and methionine.

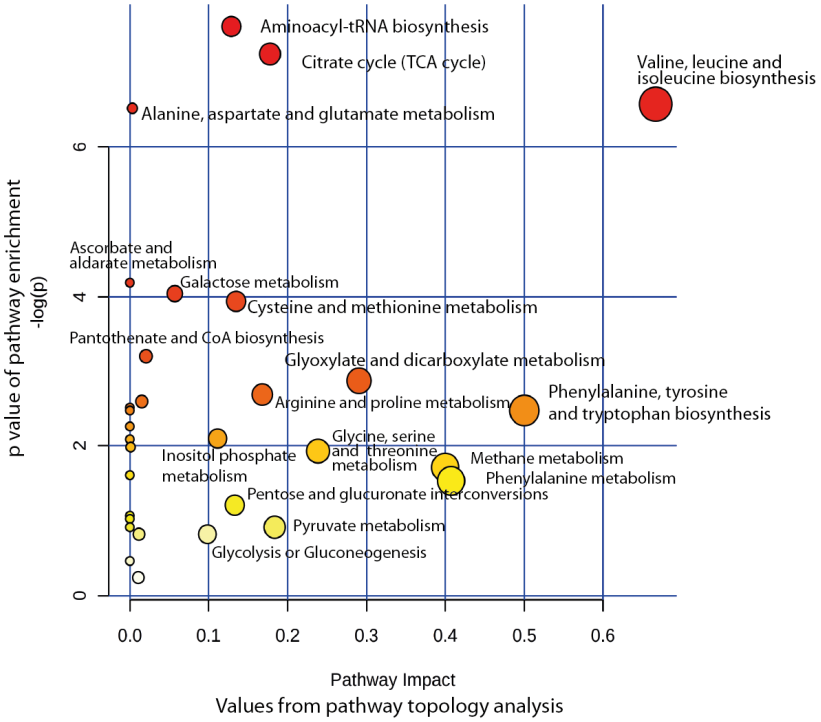

Fig. 27: **Functional interpretation of altered lung metabolites reveals GSKIP-dependent metabolic processes at E18.5.** MetaboAnalyst 3.0 pathway analysis showing all matched pathways according to p values from pathway enrichment analysis and pathway impact values from topology analysis for altered lung metabolites upon KO of GSKIP at developmental stage E18.5. The higher the impact and the p value, the more relevant is the indicated metabolic process for GSKIP-deficient metabolism in lung.

Tab. 27: **GSKIP KO accounts for relevant changes in lung metabolism.** Pathway analysis module results for GSKIP KO lung metabolites by MetaboAnalyst 3.0.
Red: significantly enriched pathways (with highest p and highest pathway impact values). Total: total number of metabolites within the pathway. Hits: altered metabolites submitted to the analysis within all metabolites of a metabolic process. FDR: False Discovery Rate-adjusted p value. Algorithms used for analysis: Hypergeometric test for overrepresentation analysis, relative-betweenness centrality for pathway topology analysis.

Pathway Name	Total	Hits	p	-log(p)	FDR	Pathway Impact
Aminoacyl-tRNA biosynthesis	**69**	**7**	**4.9369E-4**	**7.6136**	**0.029208**	**0.12903**
Citrate cycle (TCA cycle)	20	4	7.1238E-4	7.2469	0.029208	0.17794
Valine, leucine and isoleucine biosynthesis	**11**	**3**	**0.0013908**	**6.5779**	**0.030118**	**0.66666**
Alanine, aspartate and glutamate metabolism	24	4	0.0014692	6.5231	0.030118	0.00316
Ascorbate and aldarate metabolism	9	2	0.015159	4.1891	0.22774	0.0
Galactose metabolism	26	3	0.017539	4.0433	0.22774	0.05678
Cysteine and methionine metabolism	27	3	0.019442	3.9403	0.22774	0.1351
Pantothenate and CoA biosynthesis	15	2	0.040752	3.2003	0.41771	0.02041
Glyoxylate and dicarboxylate metabolism	18	2	0.057022	2.8643	0.49648	0.29032
Arginine and proline metabolism	44	3	0.068557	2.6801	0.49648	0.16804
Sphingolipid metabolism	21	2	0.075169	2.588	0.49648	0.01504
Butanoate metabolism	22	2	0.081584	2.5061	0.49648	0.0
Lysine biosynthesis	4	1	0.084766	2.4679	0.49648	0.0
Phenylalanine, tyrosine and tryptophan biosynthesis	4	1	0.084766	2.4679	0.49648	0.5
Biotin metabolism	5	1	0.10485	2.2553	0.57315	0.0
Inositol phosphate metabolism	28	2	0.12322	2.0938	0.60052	0.11163
Cyanoamino acid metabolism	6	1	0.1245	2.0835	0.60052	0.0
Glycerophospholipid metabolism	30	2	0.13809	1.9799	0.62867	9.3E-4
Glycine, serine and threonine metabolism	31	2	0.14567	1.9264	0.62867	0.23848
Methane metabolism	9	1	0.18098	1.7093	0.74203	0.4
Valine, leucine and isoleucine degradation	**38**	**2**	**0.20084**	**1.6053**	**0.78422**	**0.0**
Phenylalanine metabolism	11	1	0.21666	1.5294	0.80756	0.40741
Pentose and glucuronate interconversions	16	1	0.29941	1.2059	1.0	0.13333
Starch and sucrose metabolism	19	1	0.34492	1.0644	1.0	0.0
Propanoate metabolism	20	1	0.35945	1.0232	1.0	0.0
Lysine degradation	23	1	0.40118	0.91334	1.0	0.0
Pyruvate metabolism	23	1	0.40118	0.91334	1.0	0.18375
Glutathione metabolism	26	1	0.44028	0.82035	1.0	0.01145
Glycolysis or Gluconeogenesis	26	1	0.44028	0.82035	1.0	0.09891
Tyrosine metabolism	44	1	0.62788	0.46541	1.0	0.0
Purine metabolism	68	1	0.7859	0.24092	1.0	0.01064

Valine, leucine and isoleucine are branched-chain amino acids (BCAAs) and are essential. While isoleucine was not among the altered metabolites, leucine as well as valine show a significant accumulation of at least 40 % in GSKIP-deficient lung tissue at E18.5. Thus, BCAA accumulation in mice points towards a BCAA degradation/catabolism dysfunction as BCAA biosynthesis/anabolism is not occuring. One key enzyme of this process is the branched chain α-keto acid dehydrogenase complex (BCKDC) located at the inner mitochondrial membrane, catalyzing an oxidative decarboxylation step. Mutations of the BCKDC gene in humans are associated with severely decreased BCKDC activity and a subsequent build-up of BCAA and its harmful derivatives in the body, causing a sweet smell of body excretions such as urine, a pathologic condition named Maple Syrup Urine Disease (Chuang *et al.* 1982). However, gene ontology (GO) terms of BCAA degradation were not over-represented in GSKIP KO lungs.

Each amino acid is ligated to its cognate transfer RNA (tRNA) by a specific aminoacyl-tRNA synthetase. Aminoacyl-tRNA synthetases are known to form multiprotein complexes and to be not only responsible for the first step of protein biosynthesis but are also involved in numerous signalling processes (Park *et al.* 2008). In addition to cytosolic protein biosynthesis, mitochondria have their own way of synthesizing relevant proteins during mitochondrial protein biosynthesis. Two pools of aminoacyl-tRNA-synthetases exist, one cytosolic and one mitochondrial, both encoded by nuclear genes and afterwards imported into the mitochondrion, while all 22 mitochondrial tRNAs are encoded by the mitochondrial genome (Diodato *et al.* 2014). A large amount of mitochondrial protein synthesis deficiencies in humans is characterized by mutations in the nuclear gene encoding mitochondrial aminoacyl-tRNA-synthetases and most of them account for an early onset disease inherited in an autosomal recessive pattern with phenotypes ranging from CNS pathologies to cardiac hypertrophy and renal failure (Park *et al.* 2008; Yao & Fox 2013; Diodato *et al.* 2014). Functional studies showed that pathogenic mutations impair the binding between tRNAs and their cognate amino acids, thus probably accumulation of amino acids might result. The same might be the case in GSKIP-deficient organs: altered mitochondrial biosynthesis of aminoacyl-tRNAs could be explained by the fact that the majority of in total 9 changed amino acids showed an increase in concentration compared to WT situation (6 out of 9, see Tab. 26), potentially due to a reduced aminoacyl-tRNA-synthetase function and thus causing a mitochondrial phenotype in mice comparable to the mitochondrial phenotype of aminoacyl-tRNA-synthetase mutations in humans. How this might relate specifically to lung mitochondrial damage in the GSKIP KO needs further clarification.
Even though MetaboAnalyst discovered a significant over-representation of metabolites from the alanine, aspartate and glutamate metabolism, its relevance for the metabolome seems only minor (implicated by a pathway impact value ≤ 0.01 in Tab. 27). However, minor alanine, aspartate and glutamate metabolism alterations together with one additional amino acid metabolism affected (cysteine and methionine) indeed may account for several disturbed amino acid metabolic processes in E18.5 lungs upon GSKIP KO. Linking these perturbed pathways to earlier observations regarding the lung phenotype of GSKIP KO mice remains challenging.
Prior to dissection, embryos were exposed to air and thus the embryonic lungs initiated respiration, leading to respiratory distress in the KO lungs. Whether this short-term stress situation can be immediately reflected in metabolite changes or if the metabolic changes are based on *in utero* processes, remains uncertain. Unborn embryos are supplied with nutrients including amino acids by maternal blood across the placenta; perturbed amino acid homoeostasis might arise from disturbed amino acid uptake by embryonic tissue. If and how the reduced ability to metabolize BCAA or increased absorption of BCAA might refer to newborn lung problems, remains to be elucidated.

The visual interpretation using MetaboAnalyst did not take into account fold-changes of metabolites. This is exemplified by the two metabolites with the highest fold-changes, namely glucose 6-phosphate (key compound of glycolysis, the pentose phosphate pathway and gluconeogenesis) and pyruvate (important for both TCA cycle and glycolysis). Both metabolites were not accompanied by sufficient additional intermediates to result in glycolysis to be recognized as a highly relevant pathway. In contrast, TCA cycle

(with 20 metabolites in total) was predicted to be important for tissue metabolism due to the presence of four altered TCA compounds (out of 20 candidates) within the submitted metabolite list leading to its classification as “enriched”.

Thus, for further analysis of the most obvious metabolite changes and their degree of up/downregulation results were included in a scheme shown in Fig. 28. The scheme illustrates specific enzymes as possible candidates responsible for the observed metabolite alterations in GSKIP-deficient tissue (Fig. 28; marked in red and blue).

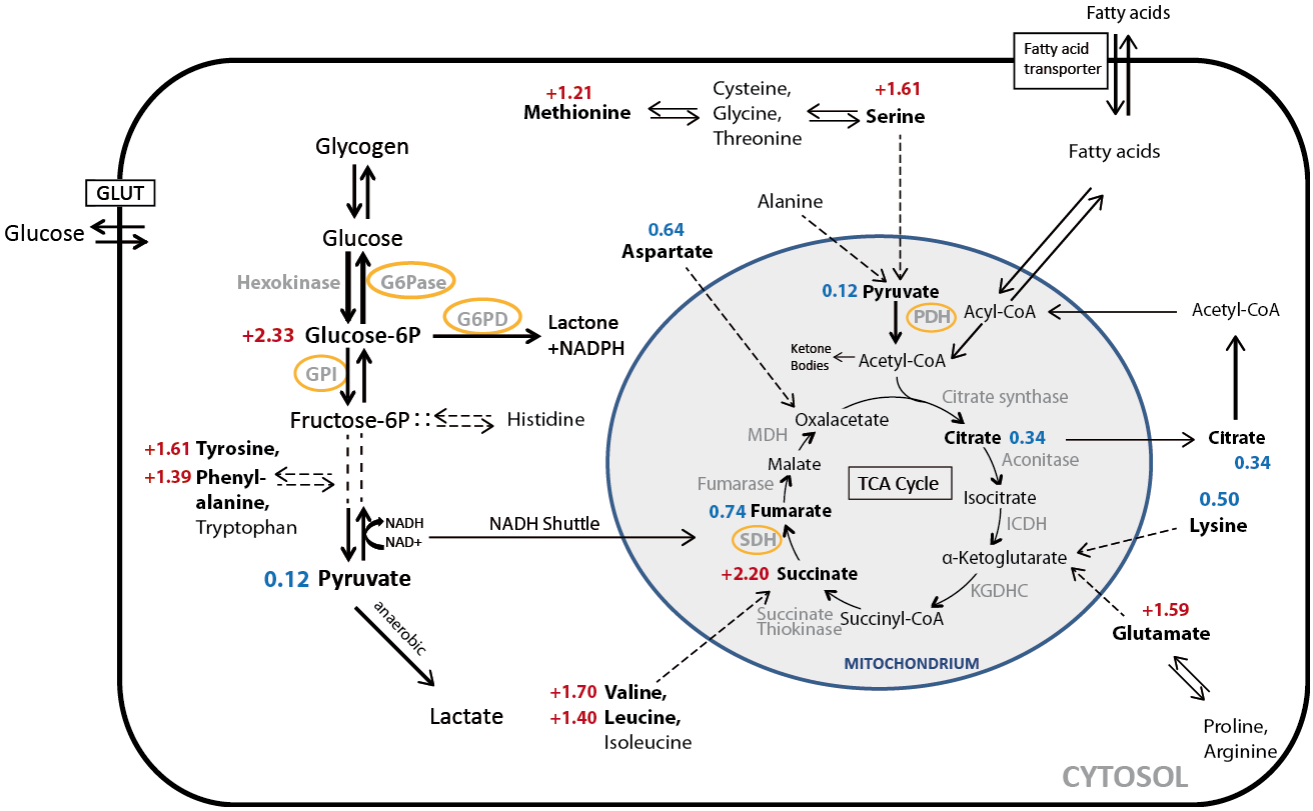

Fig. 28: **Major GSKIP-dependent fold-changes of lung metabolites affect cytosolic as well as mitochondrial metabolism.** Fold-changes are represented as values in front of metabolite names. Red: upregulation. Blue: downregulation. Candidate enzymes analysed by further methods (Fig. 29) are marked in yellow. Dashed lines show amino acid catabolism integration into metabolic processes. KGDHC: α-ketoglutarate dehydrogenase complex; ICDH: Isocitrate dehydrogenase; MDH: Malate dehydrogenase. CoA: Coenzyme A. For more abbreviations, see text.

The protein expressions of key enzymes were analysed (Fig. 29), amongst them three cytosolic enzymes and two enzymes of TCA cycle, namely succinate-dehydrogenase A (SDH, isoform A), pyruvate dehydrogenase C (PDH, isoform C), glucose-6-phosphatase β (G6Pase, isoform β), glucose-6-phosphate dehydrogenase (G6PD) and glucose-6-phosphate isomerase (GPI; also called Glucokinase). Only GPI displayed minor changes for lung upon GSKIP KO, most likely contributing to the metabolite perturbations in the cytosol rather than in mitochondria. GPI catalyses the second step of glycolysis, converting glucose-6-phosphate to fructose-6-phosphate in the cytosol. For mice, only one isoform has been reported. On mRNA level, however, no alterations were observed for *Gpi1*, neither in KO lung, nor in liver tissue. GPI is also referred to as neuroleukin (NLK) and autocrine motility factor (AMF) (Niinaka *et al.* 1998). GPI deficiency in humans is linked to a rare form of hemolytic anemia (Whitelaw *et al.* 1979).

In addition, in E18.5 liver G6PD showed a significant downregulation on protein level. G6PD catalyzes the rate-limiting step of the oxidative pentose-phosphate pathway, which represents a route for the dissimilation of carbohydrates besides glycolysis. The main function of this enzyme is to provide reducing equivalents (NADPH) and pentose phosphates for fatty acid and nucleic acid synthesis. Similar to GPI deficiency, patients with G6PD deficiency (due to inherited G6PD mutations) suffer from acute hemolytic attacks.

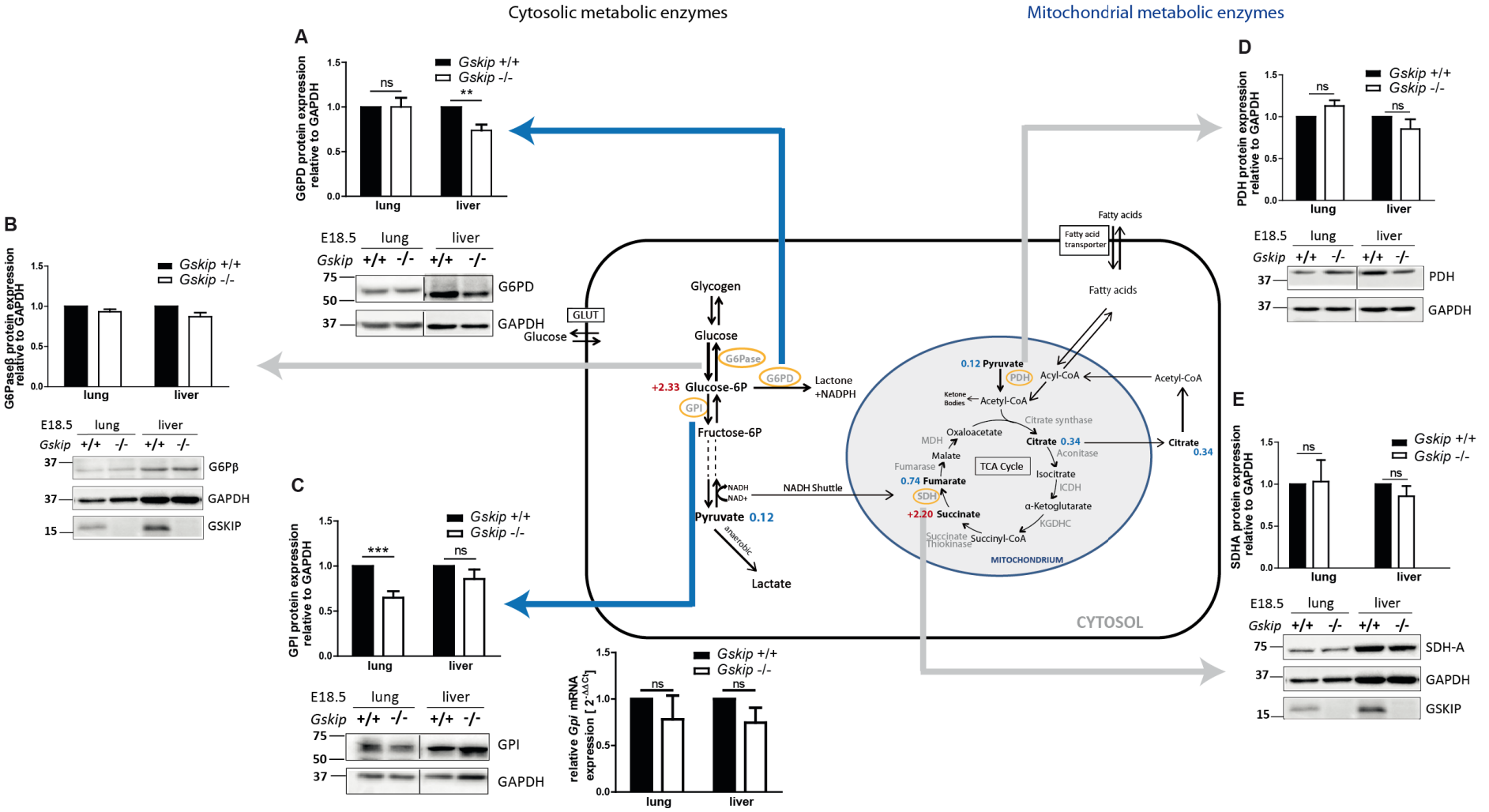

Fig. 29: **Enzyme expression analysis of GSKIP-deficient E18.5 mouse lung and liver confirms alterations of cytosolic metabolism.** Cytosolic as well as mitochondrial enzymes potentially responsible for the observed metabolite fold-changes (red and blue values next to metabolite name) were analysed on protein level *via* Western blot. Grey arrows point towards unchanged enzyme expression, while blue arrows highlight two cytosolic enzymes altered upon GSKIP KO either in lung or liver lysates at E18.5. Representative blots are shown. A) Protein expression of Glucose-6-phosphate dehydrogenase (G6PD) converting glucose-6-phosphate to lactone. B) Protein expression of Glucose-6-phosphatase (G6Pase) converting glucose-6-phosphate to glucose. C) Cytosolic glucose-6-phosphate isomerase (GPI) protein (left) and *Gpi1* mRNA (right) expression, an enzyme converting glucose-6-phosphate to fructose-6-Phosphate. D) Protein expression of the mitochondrial Pyruvate dehydrogenase (PDH) converting pyruvate to acetyl-CoA. E) Protein expression of the mitochondrial enzyme converting succinate to fumarate (E; Succinate dehydrogenase, SDH). Densitometry of protein expression relative to GAPDH is shown. GSKIP KO was normalized to WT. n ≥ 8 (A, C, D, E); n = 2 (B). n = 3 for mRNA expression. Mean ± SEM. Student`s t-test. *p ≤ 0.05.

However, the disease is usually asymptomatic throughout the life of the patients and solely triggered by exogenous agents such as drugs, food or infection causing a life-threatening sudden hemolytic anemia. Reduced G6PD enzyme activity causes red blood cell abnormalities as in red blood cells the pentose phosphate pathway is the only way to provide NADPH due to the general absence of mitochondria in erythrocytes (Luzzatto & Seneca 2014).
Therefore, reduced enzyme activities of both GPI and G6PD should affect erythrocytes of GSKIP KO mice and be linked to an anemic phenotype. Noteworthy, as shown in Fig. 14, the routine blood smear analysis did not support this hypothesis. For validation of the two altered enzymes detected, see 5.9.2.

5.8.2 Tissue type-independent metabolic phenotype of GSKIP KO mice

Investigating metabolic changes including E18.5 lung, liver and blood accounted for four commonly altered metabolites with significant differences between WT and GSKIP KO: pyruvate as the end product of glycolysis entering the TCA cycle, the essential BCAAs leucine and valine as well as pantothenic acid (also called Vitamin B5) (Tab. 28). Pantothenate is the precursor of Coenzyme A (CoA) and cannot be synthesized by mammals; they must obtain it from their diet. Mammals convert it (using amongst others cysteine and ATP) into CoA, the essential coenzyme in energy-yielding reactions such as fatty acid catabolism, oxidation and pyruvate oxidation in TCA cycle (Venner *et al.* 1990). Of note, the majority of metabolites showed up in one system only. Detailed liver and blood metabolite datasets are listed in the appendix (10.3.1; Suppl. Tab. 3).

Tab. 28**: Commonly altered metabolites determined by metabolomics in E18.5 mouse blood, lung and liver.** Significant fold-changes of metabolites in GSKIP KO are shown related to WT control. n = 3. Red: significantly up-regulated; Blue: significantly down-regulated metabolite. $p \leq 0.05$.

Detected metabolite	Significant fold-change (KO vs. WT)		
	Blood	Lung	Liver
Pyruvic acid	0.44	0.17	0.12
Leucine	1.71	1.39	1.40
Valine	1.31	1.44	2.01
Pantothenic acid (Vit B5)	1.27	1.32	1.47

For liver and blood metabolites a pathway analysis integrating metabolite enrichment analysis and pathway topology using MetaboAnalyst 3.0 was conducted analogous to the analysis of the lung. For pathway analysis details, see the appendix (Suppl. Tab. 4; Suppl. Tab. 5). The inquiry yielded several relevant pathways being of significance for the metabolic GSKIP KO liver phenotype (Fig. 30 A): the most significant alterations were determined for aminoacyl-tRNA biosynthesis, followed by valine, leucine and isoleucine biosynthesis, cystein and methionine metabolism, pantothenate and CoA biosynthesis and for TCA cycle. Moreover, in contrast to both analysed tissues, the metabolic set analysis of GSKIP-deficient blood, plotted in Fig. 30 B, demonstrated only one pathway to be crucial, namely valine, leucine and isoleucine (BCAA) biosynthesis, the most relevant one already described in detail for lung. Additionally, significant alterations were defined for pantothenate and CoA biosynthesis and TCA cycle, with p values comparable to those of the same pathways in liver. Of note, the highest changes observed for lung (5.8.1) were only partially recognized in liver and blood: while pyruvate was highly reduced in all three systems, the upregulation of glucose-6-phosphate was only present in liver and lung: red blood cells do not have mitochondria and thus depend solely on the pentose phosphate pathway to metabolize glucose-6-phosphate. This result suggests that the pentose phosphate pathway is functional and not responsible for overall glucose-6-phosphate elevation in lung and liver. This rather points towards gluconeogenesis and glycolysis to be impaired in converting glucose-6-phosphate into fructose-6-phosphate (by GPI) or dephosphorylating glucose-6-phosphate to glucose (by G6Pase). Blood analysis of enzyme expressions was limited as the lysis itself was not sufficient to obtain reproducibly signals for Western blotting. But due to the absence of

mitochondria blood cells should not have the characteristic mitochondrial phenotype observed for lung cells (and expected in further tissues) and hence the blood was not chosen for further investigations.

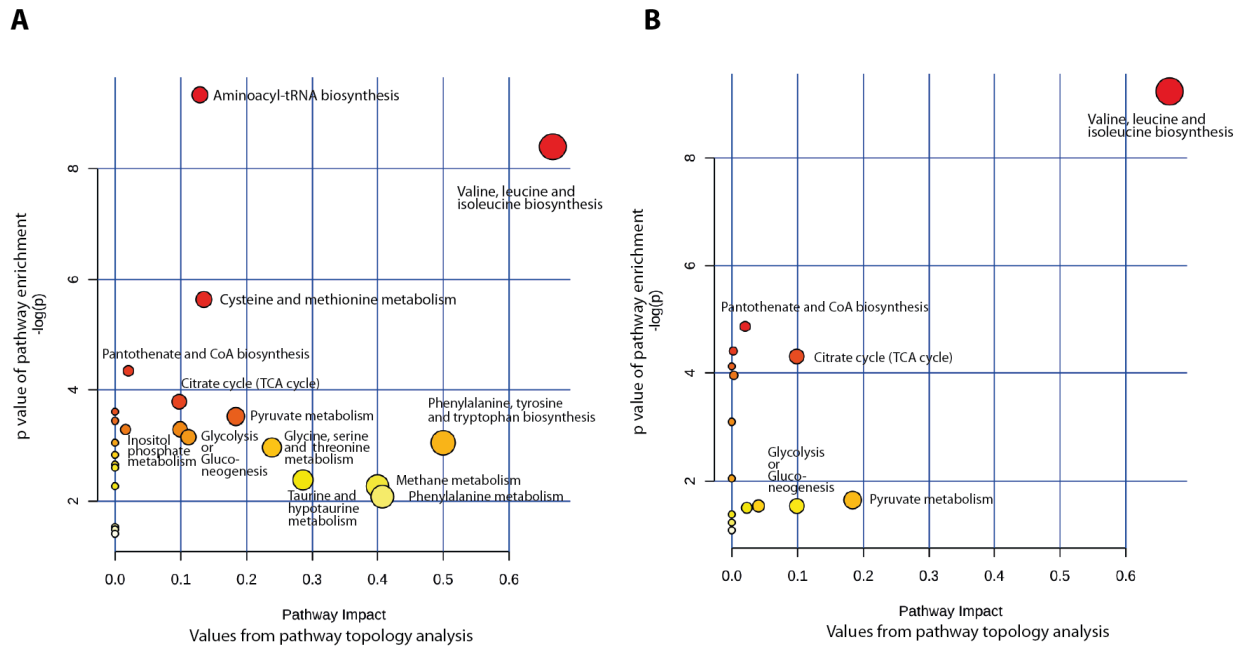

Fig. 30: **Functional interpretation of altered liver (A) and blood (B) metabolites reveals GSKIP-dependent, relevant metabolic processes at E18.5.** All matched pathways according to p values from pathway enrichment analysis and pathway impact values from topology analysis for altered metabolites upon KO of GSKIP at developmental stage E18.5 are shown (derived by MetaboAnalyst 3.0); The higher the impact and the p value, the more relevant is the indicated metabolic process for GSKIP-deficient metabolism in the liver (A) or blood (B).

Comparison of lung (Fig. 27), liver (Fig. 30 A) and blood (Fig. 30 B) plots revealed an obvious common significant enrichment of metabolite changes responsible for impaired valine, leucine and isoleucine biosynthesis in both tested organs and in blood, moving the metabolic pathway for BCAA synthesis into the focus. Succinate is enriched in lung and liver, probably triggered by an increased BCAA (valine, leucine, isoleucine) catabolism, but no succinate changes were measured in blood. However, it is not known how this might link to such an extreme decrease in pyruvate.

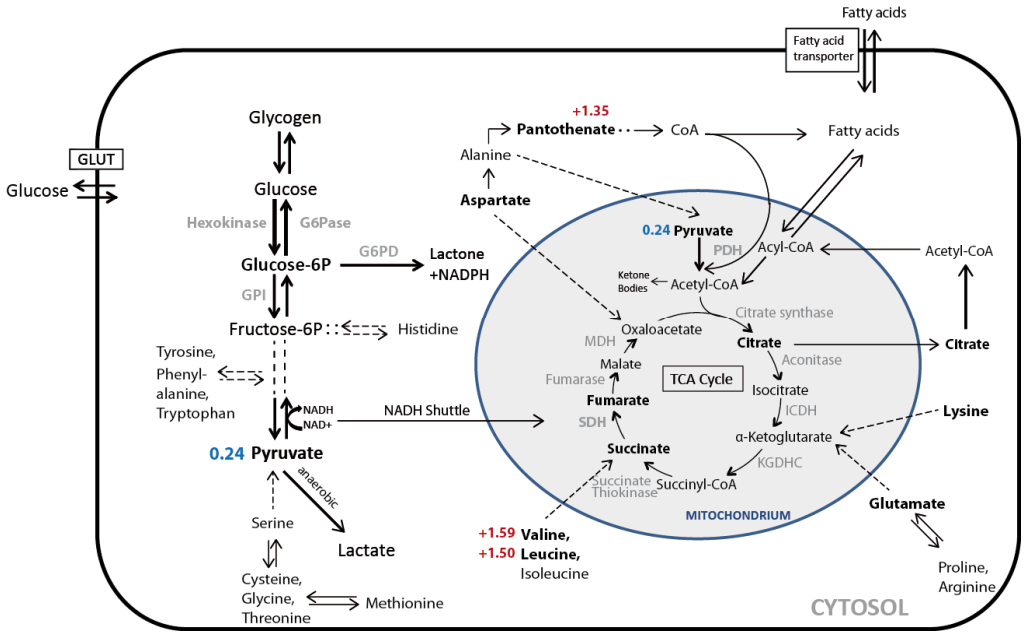

Fig. 31: **Common GSKIP-dependent changes in metabolites of lung, liver and blood at E18.5.** Relative fold-changes are indicated in front of metabolite names as average of lung, liver and blood values. Red: upregulation. Blue: downregulation. Dashed lines show amino acid catabolism product integration into metabolic processes at different positions. KGDHC: α-ketoglutarate dehydrogenase complex; ICDH: Isocitrate dehydrogenase; MDH: Malate dehydrogenase. CoA: Coenzyme A. For more abbreviations, see text.

5.9 Biochemical analysis of GSKIP knockout mice

5.9.1 Diminished GSK3β Ser9 phosphorylation confirmed *in vivo* in mice

Initially, protein expression was analysed upon GSKIP KO in whole tissues of E18.5 mice as this embryonic stage has been defined to be critical for survival of GSKIP KO mice (Fig. 32). In the absence of GSKIP, the inhibitory phosphorylation of GSK3β on Ser9 (related to GAPDH) is markedly reduced in brain and liver tissue to 60 % compared with expression in WT controls (Fig. 32 A, B); a slight but significant reduction of pGSK3β-Ser9 expression also occurs in GSKIP KO lung and kidney. Notably, total GSK3β protein levels are significantly decreased upon KO of GSKIP in the majority of tested E18.5 mouse tissues (Fig. 32 B), presumably due to transcriptional regulation or degradation. Hence, there is only a minor net effect on GSK3β inhibition in tissues where total GSK3β levels are unaffected but Ser9 phosphorylation decreased, showing an increase in constitutively active GSK3β, such as it is the case in GSKIP KO kidney. As published by our group, GSKIP forms a complex with regulatory RIIα subunits of PKA and GSK3β and thereby facilitates the inhibitory phosphorylation of GSK3β at Ser9 upon overexpression of GSKIP in cultured cells (Hundsrucker *et al.* 2010). Thus, the mouse model confirms the hypothesis as depletion of GSKIP diminishes GSK3β Ser9 phosphorylation in mouse tissues at E18.5. However, in most tissues there is a less pronounced effect on pGSK3β-Ser9 as expected, probably due to the fact that PKA is not the only kinase phosphorylating GSK3β on Ser9 and GSKIP is not responsible for all PKA-mediated GSK3β Ser9 phosphorylation.

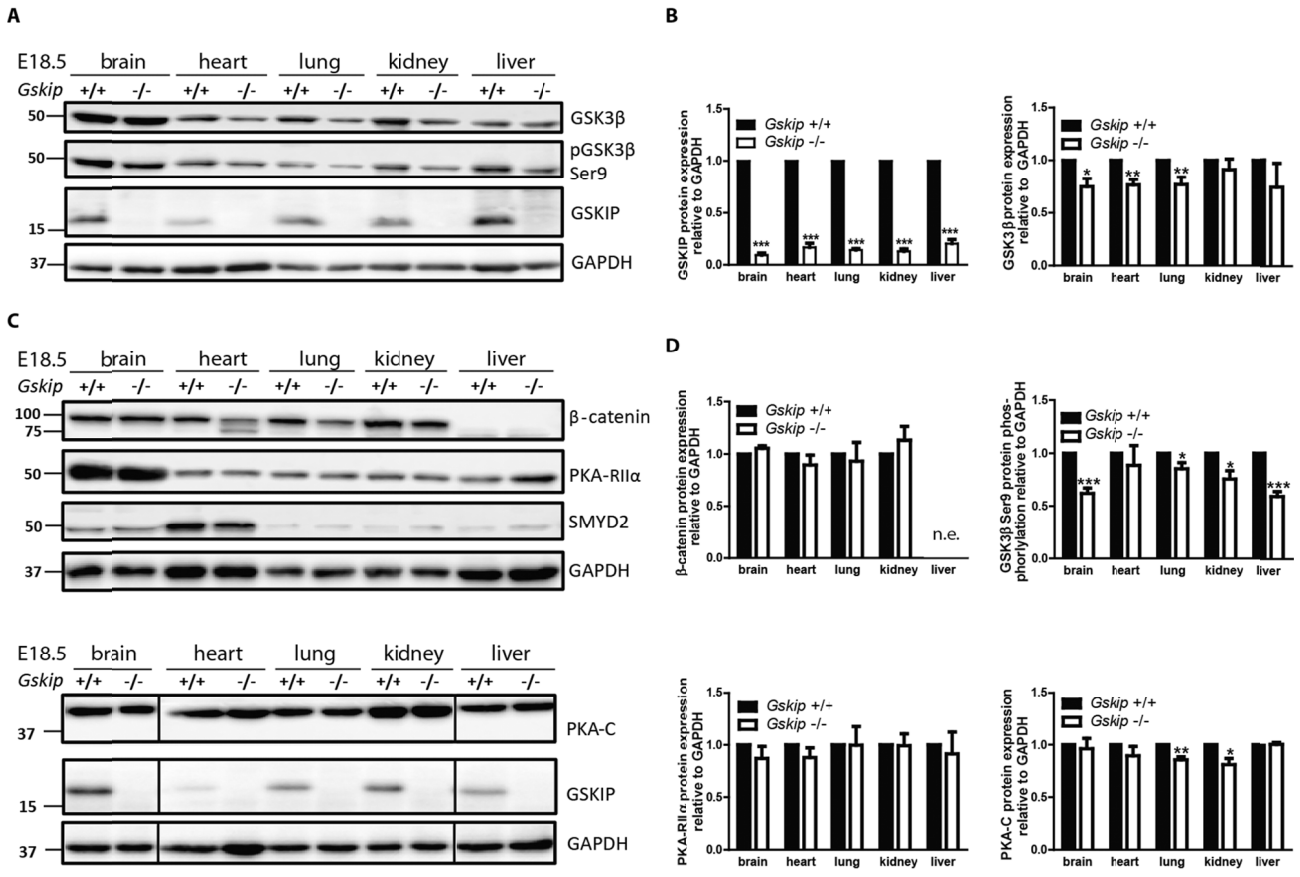

Fig. 32: **GSKIP-dependent protein expression in E18.5 mouse tissue confirms GSK3β Ser9 phosphorylation changes.** Western blot analysis of E18.5 tissue lysates from WT (*Gskip*$^{+/+}$) and KO (*Gskip*$^{-/-}$) mice. Proteins (15 µg) were separated by 12 % SDS-PAGE. GAPDH was included as a loading control. A) Shown are representative Western blots for GSK3β, pGSK3β Ser9 and GSKIP expression. B) Densitometric analyses of GSK3β Ser9 phosphorylation and total GSK3β protein expression, relative to GAPDH. GSKIP KO was normalized to WT. n ≥ 6. C) Representative blots for β-catenin, PKA-RIIα, SMYD2 and PKA-C. D) Densitometry of β-catenin, GSKIP and PKA-RIIa as well as C subunit protein expression, relative to GAPDH. GSKIP KO was normalized to WT. n.e.: not expressed. n ≥ 5. Mean ± SEM; paired Student´s t-test; *p ≤ 0.05.

No significant changes were detected upon KO of GSKIP for protein expression of PKA regulatory RIIα subunits or for SMYD2, a protein interaction partner of GSKIP (Fig. 32 C, D). Minor reductions were observed in KO lungs and kidneys for PKA catalytic C subunits.

β-catenin is regulated by the Wnt destruction complex comprising APC, β-catenin, GSK3β and Axin. Upon Wnt ligand binding to Frizzled receptor the canonical Wnt signalling pathway is activated, the destruction complex is disassembled and β-catenin translocates into the nucleus where it initiates Wnt target gene transcription (Cruciat 2014) (3.2). Hence, the expression of the Wnt signalling proteins β-catenin (Fig. 32 C, D), Axin 1 (Fig. 33 A) and GSK3β targets were studied exploring a potential involvement of GSKIP in developmental Wnt signalling.

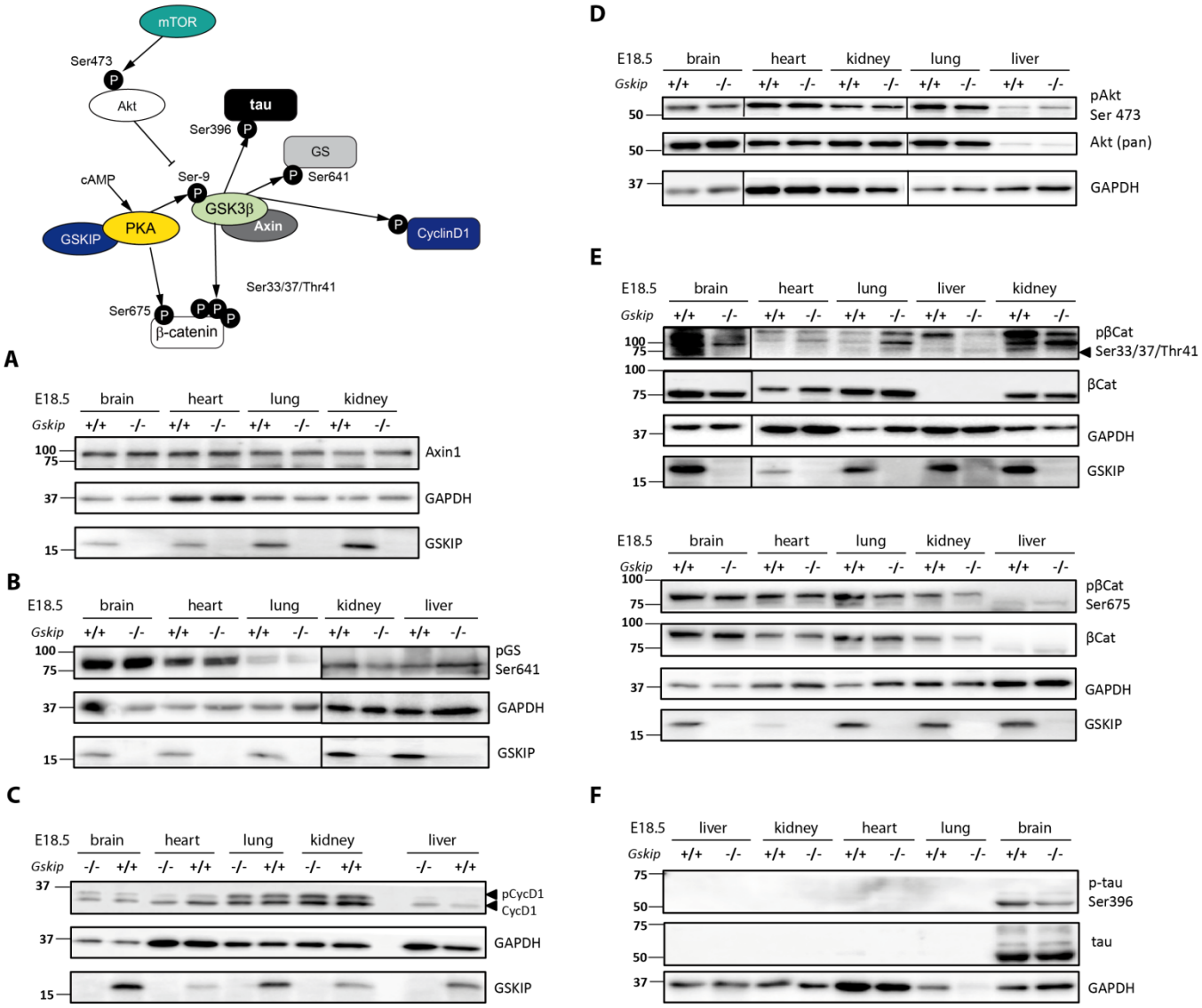

Fig. 33: **GSKIP does neither influence the expression and phosphorylation of proteins involved in the Wnt signalling pathway, nor GSK3β substrates at E18.5.** Western blot analysis of E18.5 tissue lysates from WT (*Gskip*$^{+/+}$) and KO (*Gskip*$^{-/-}$) mice. Proteins (15 µg) were separated by 12 % SDS-PAGE. GAPDH was detected as a loading control. Representative Western blots are shown for Axin1 (A), phospho-Glycogen synthase (GS) (B), (phospho-)CyclinD1 (C), (phospho-)Akt (D), (phospho-)β-catenin (E) and (phospho-)tau (F) in various tissue types. The interplay between tested proteins is shown in a scheme. Densitometric analysis of n ≥ 3 did not yield any significant changes (Suppl. Fig. 9).

So far, none of the tested GSK3β substrates (β-catenin, tau, CyclinD1, GS) revealed significant protein expression alterations in the absence of GSKIP in any tested mouse tissue at E18.5 (Fig. 33; Suppl. Fig. 9); in addition, phosphorylation of the above-mentioned targets was unaffected: the inhibitory Ser641 phosphorylation of Glycogen Synthase (GS) mediated by GSK3β showed no alteration upon GSKIP KO (Fig. 33 B), even though Glucose-6-phosphate, profoundly elevated upon GSKIP KO in E18.5 lungs, is an allosteric activator of GS (Skurat & Roach 1995). Both total and phosphorylated CyclinD1 protein levels did

not change GSKIP-dependently in mouse tissues (Fig. 33 C). β-catenin is phosphorylated by GSK3β on Ser33, 37 and Thr41 Fig. 33 E *upper*), targeting β-catenin for its ubiquitination and proteasomal degradation. While Ser33/37/Thr41 phosphorylation by GSK3β destabilizes β-catenin, phosphorylation of the Ser675 residue by PKA (Fig. 33 E *lower*) stabilizes β-catenin: however, neither GSK3β-, nor PKA-induced β-catenin phosphorylation events were impaired in the absence of GSKIP. The brain-specific protein tau showed a small tendency towards a GSKIP-dependent decline of tau Ser396 phosphorylation that is mediated by GSK3β (Fig. 33 F), but was not confirmed by further repetitions (work of M. Elkewedi). Besides, activated Ser473-phosphorylated Akt was studied as it is involved in GSK3β regulation by preventing GSK3β Ser9 phosphorylation (Sarbassov *et al.* 2005), but no GSKIP-dependent effect was observed on phospho-Akt Ser473 or total Akt protein expression (Fig. 33 D).
These observations are in line with microarray data, which on mRNA level also did not detect changes for Wnt signalling pathway genes or GSK3β targets in E18.5 mouse organs (5.6.1).

As GSKIP is ubiquitously expressed, it is challenging to determine the tissue where GSKIP might have the most prominent physiological role during development. Phenotype studies revealed that gross morphological changes regarding early mouse organ development do not occur upon KO of GSKIP. Nevertheless, the observed cleft palate and the fact that cleft palate formation starts as early as E12.5 made it reasonable to study protein expression in whole embryos at different embryonic stages.

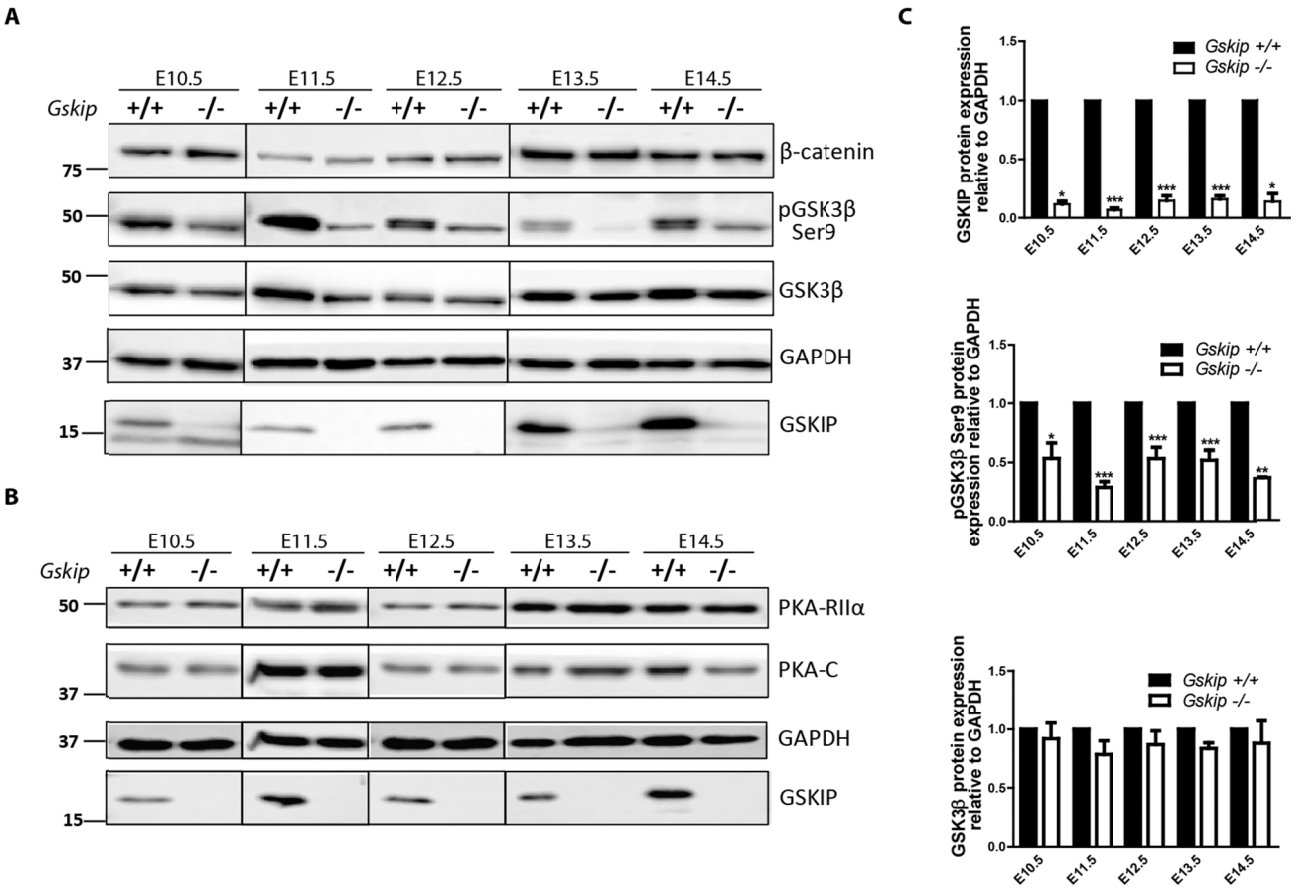

Fig. 34: **Protein expression analysis in whole embryos at different embryonic stages E10.5-E14.5 revealed reduced GSK3β Ser9 levels in absence of GSKIP.** Western blot analysis of whole embryo lysates from WT (*Gskip*$^{+/+}$) and KO (*Gskip*$^{-/-}$) mice. Proteins (15 µg) were separated by 12 % SDS-PAGE. GAPDH was detected as a loading control. A and B) Representative Western blots of whole embryo lysates for β-Catenin, pGSK3β Ser9, GSK3β, PKA RIIα, PKA C subunits and GSKIP. C) Densitometic analysis of GSKIP, GSK3β Ser9 phosphorylation and total GSK3β protein expression, relative to GAPDH. GSKIP KO was normalized to WT. $n \geq 4$. Mean ± SEM; paired Student´s t-test; $^{*}p \leq 0.05$.

GSKIP is present at all tested embryonic stages (starting from E10.5) and already at E10.5 a significant GSKIP-dependent reduction of GSK3β Ser9 phosphorylation by at least 50 % was detected, constantly present throughout development (Fig. 34 A, C *middle*). Protein expressions fluctuate during development

(e.g. β-catenin), but GSKIP-dependent expression changes were not observed in whole embryo lysates (Fig. 34): total β-catenin and PKA subunit protein levels were unaltered upon GSKIP KO.

Due to the mitochondrial phenotype observed, numerous mitochondrial proteins were aimed at for elucidation in GSKIP-deficient lungs. Mitochondria are regulating signalling processes *via* the release of cytochrome C (CytC), production of mitochondrial reactive oxygen species (mROS) and by anchoring proteins to the outer mitochondrial membrane (OMM) (Chandel 2014). The question arose whether the observed mitochondrial damage could be due to mROS, known to be associated with human mitochondrial disorders (Sarbassov *et al.* 2005).

The analysis was started by testing different proteins located in the mitochondrial inner membrane (IMM) and/or part of the electron transport chain (ETC) illustrated in Fig. 35 A. Succinate dehydrogenase, or complex II, couples the oxidation of succinate to fumarate (as a component of TCA cycle) to the reduction of ubiquinone to ubiquinol in the ETC (Da Cruz *et al.* 2008). CytC transfers electrons between the complexes III and IV and is involved in the initiation of apoptosis (Sarbassov *et al.* 2005). COX4 is one of the nuclear-coded polypeptide chains of CytC oxidase, the terminal oxidase in mitochondrial electron transport and crucial for stability of Complex IV (Osman *et al.* 2009). No significant changes were detected for the aforementioned proteins when comparing E18.5 GSKIP-deficient lungs with WT tissue (Fig. 35 B, D).
Opening of the mitochondrial permeability transition pore, a principle trigger of cell death and a non-specific mega channel in the IMM, is regulated amongst others by GSK3β (Miki *et al.* 2009; Miura & Tanno 2012). Recent findings show that following oxidative stress GSK3β translocates from the cytosol to the mitochondria in a kinase activity- and voltage-dependent anion channel 2 (VDAC2)-dependent manner as GSK3β translocation was abrogated in absence of VDAC2 (Tanno *et al.* 2014). Hence, VDAC expression was assessed but was not altered upon GSKIP KO in lung (Fig. 35 B *middle*).
As an additional integrator of cell survival and death, GSKIP-deficient lungs were assayed for heat shock protein HSP60. HSP60 is a mitochondrial member of stress-induced heat shock proteins and as a chaperone implicated in mitochondrial protein import and folding of proteins generated in the mitochondrial matrix (Venner *et al.* 1990). Upon KO of GSKIP, HSP60 levels stayed unaltered in E18.5 lung tissue Fig. 35 C, D).
Prohibitin 1 (PHB1) (Zhou & Qin 2013), a negative regulator of cell proliferation, is connected to cell cycle progression, senescence, apoptosis and mitochondrial structure. PHB1 forms a ring-like complex at the IMM, responsible for mitochondrial protein and mtDNA stability as well as respiratory chain assembly (Da Cruz *et al.* 2008; Osman *et al.* 2009). The absence of prohibitins induces the generation of ROS, disorganized mitochondrial nucleoids, abnormal cristae morphology and an increase in apoptosis upon stimulation (Osman *et al.* 2009). Furthermore, prohibitins (e.g. linked to optic atrophy protein 1 processing) are involved in mitochondrial fusion and cristae morphogenesis (Osman *et al.* 2009), the latter of which is perturbed upon GSKIP KO in E18.5 lungs. Lung lysates were analyzed for PHB1 protein changes but differences between wild-type and KO were not spotted (Fig. 35 C, D).
Mitophagy, the removal of damaged or excessive mitochondria by autophagy, is accompanied by the formation of autophagosomes and the sequestration of mitochondria. Autophagy is marked by the conversion of LC3A/B-I (16 kDa) into LC3A/B-II (14 kDa). In addition, upon autophagy mammalian target of rapamycin (mTOR), sensing cellular nutrition status, is inhibited. mTOR is regulated e.g. by the availability of amino acids, especially by BCAA (Jung *et al.* 2010), as well as by oxygen levels within the cell. mTOR phosphorylation of residue Ser2448 is mediated *via* the PI3K / Akt pathway and leads to the activation of mTOR, hence inhibition of mitophagy (Morita *et al.* 2015). However, upon GSKIP KO in E18.5 lungs, no change in the ratio of LC3A/B-I to LC3A/B-II was detected (Fig. 35 C, D). Furthermore, neither total mTOR protein expression, nor mTOR Ser2448 phosphorylation showed differences between WT and GSKIP-deficient tissue, presumably excluding a GSKIP-dependent induction of autophagy upon respiratory distress in E18.5 lungs (Fig. 35 C, D).

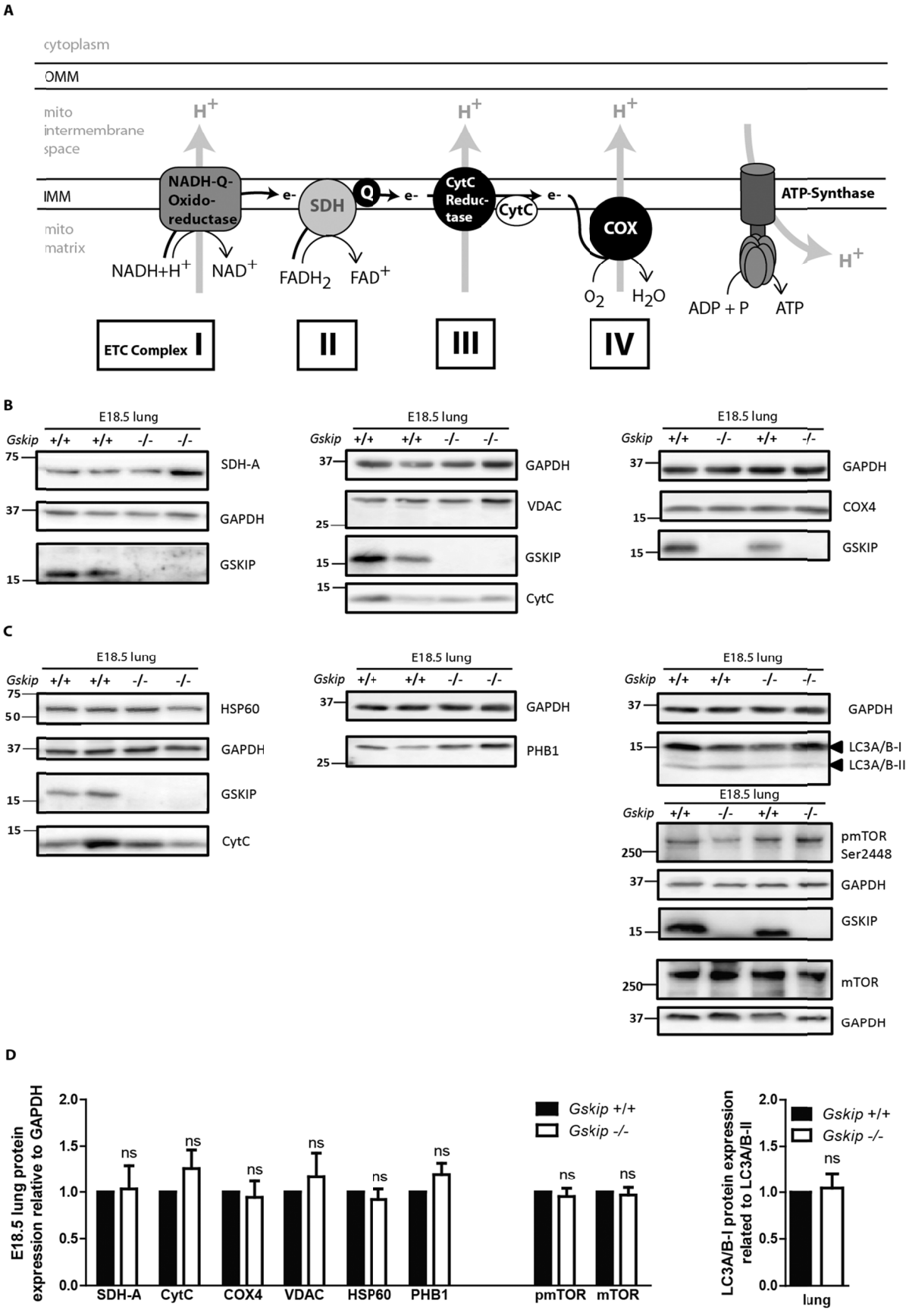

Fig. 35: **Expression of mitochondrial proteins including the electron transport chain was not altered GSKIP-dependently in E18.5 lung.** Western blot analysis of E18.5 lung lysates from WT (*Gskip*$^{+/+}$) and KO (*Gskip*$^{-/-}$) mice. Proteins (15 µg) were separated by 12 % SDS-PAGE. GAPDH was included as a loading control. A) The electron transport chain is depicted for illustration of the analysed complexes. OMM/IMM: inner/outer mitochondrial membrane. Q: Ubiquinone. See text for details. B) Representative Western blots are shown for one subunit of complex II, namely SDH-A (B *left*), Cytochrome C as a core player in Complex III (B *middle*) as well as for one chain of Complex IV termed COX4 (B *right*). VDAC expression was assayed as well. C) HSP60, PHB1, (p)mTOR as well as autophagy marker LC3A/B-I and -II expression on Western blots. See text for abbreviations. D) Densitometric evaluation of signal intensities, relative to GAPDH. The conversion of LC3A/B-I into -II is expressed as a ratio. GSKIP KO was normalized to WT. n ≥ 7. Mean ± SEM; paired Student´s t-test. ns: not significant.

To answer the question whether GSKIP is only cytosolic or also shows a mitochondrial expression in E18.5 lungs which may link to the mitochondrial phenotype observed in E18.5 lung sections, WT lungs of E18.5 mice were lysed and fractionated, separating the cytosol from a fraction enriched in mitochondria (Fig. 36). GSKIP expression, however, was only detectable in the cytosolic lung fractions, while in mitochondrial fractions GSKIP was absent. GAPDH is known to precipitate with the cytoskeleton, explaining the GAPDH signals in the mitochondrial preparations while Hsp90 proved to be a better suitable cytosolic marker. Hence, in E18.5 lung tissue GSKIP is expressed in the cytosol only and is not present in (or translocated to) mitochondria.

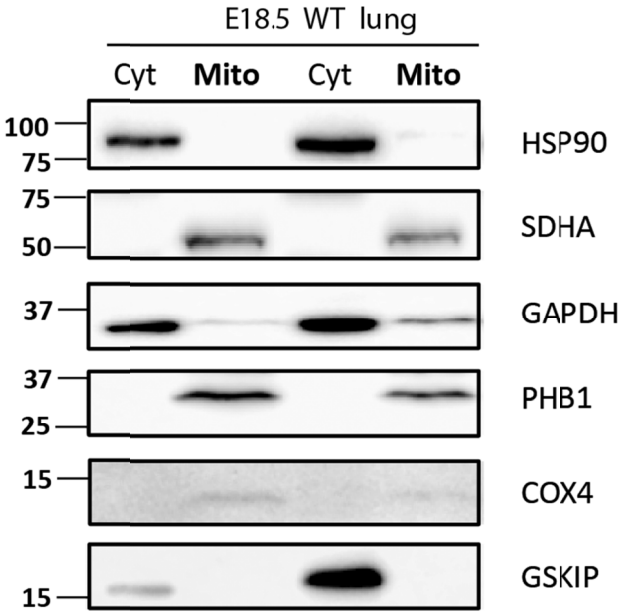

Fig. 36: **GSKIP is a cytosolic protein and does not localize to E18.5 lung mitochondria.** Representative blots from six independent fractionation experiments are shown, protein lysates separated by SDS-PAGE. Different cytosolic (HSP90, GAPDH) as well as mitochondrial markers (SDH-A, PHB1, COX4) were analysed to confirm fractionation purity to define GSKIP expression as cytosolic. Cyt: cytosolic fraction; Mito: mitochondrial fraction. n = 6.

Next, E18.5 lungs were tested for overall PKA activity by blotting for phospho-PKA substrates using an antibody recognizing peptides and proteins containing a PKA consensus site (a phospho-Ser/Thr residue with arginine at the -3 and -2 positions thought to be characteristic for PKA) but also other arginine-directed kinases (such as PKC, PKG, Akt). No consistent differences were detected upon GSKIP KO for PKA substrate phosphorylation (Fig. 37 A and D).
LRP5/6, the Wnt cell surface coreceptor implicated in the recruitment of the Wnt destruction complex, has been mainly characterized for its function in bone homoeostasis, especially as regulator of bone density and mineralization (Gong *et al.* 2001). Of note, LRP5 KO mice suffer from low bone mass (Fujino *et al.* 2003) while LRP6-deficient mice die at birth due to severe developmental abnormalities, including the truncation of the axial skeleton, limb defects and malformation of the urogenital system (Pinson *et al.* 2000). LRP5/6 phosphorylation at Ser1490 is mediated by GSK3β and CK1 and is a prerequisite for the subsequent binding of Axin (3.2). Therefore, GSKIP´s influence on LRP5/6 protein expression and phosphorylation was investigated but no consistent GSKIP-dependent LRP5/6 expression or Ser1640 LRP5/6 phosphorylation alterations were recognized in lung tissue (Fig. 37 B and D).

One additional connection that has been unraveled by E. Perets in our laboratory in parallel to this thesis is a GSKIP-dependent shift in epithelial-to-mesenchyme transition (EMT) in A549 lung carcinoma cells: GSKIP knockdown induced a significant upregulation of E-Cadherin and concurrent downregulation of N-Cadherin, both representing intercellular junction proteins. However, *in vivo* in E18.5 mouse lung tissue these observations were not confirmed (Fig. 37 C and D).

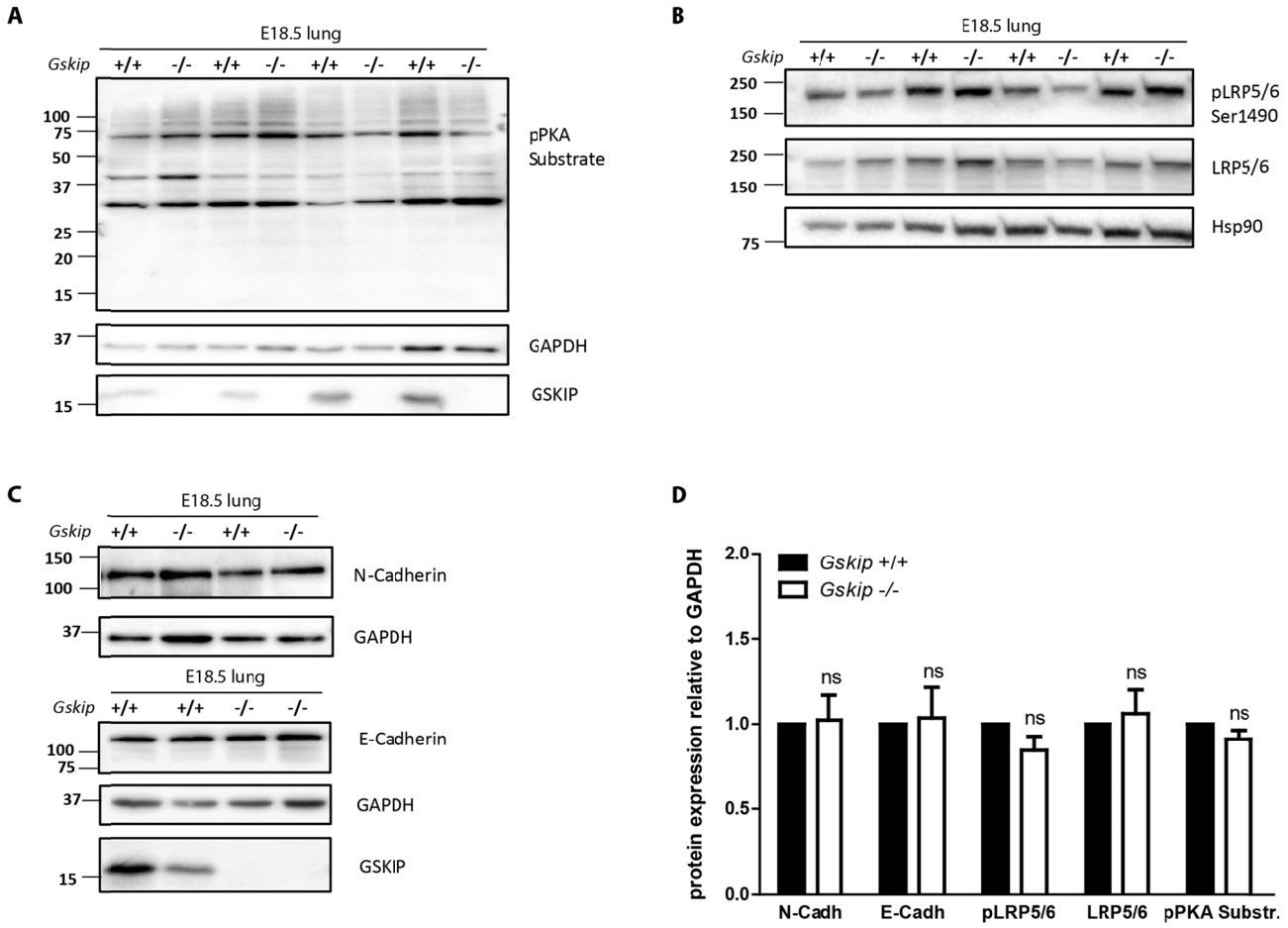

Fig. 37: **Protein expression analysis of E18.5 mouse lung did not reveal GSKIP-dependent modifications neither on EMT, nor on PKA or LRP5/6 phoshorylation.** Western blot analysis of E18.5 lung lysates from WT (*Gskip*$^{+/+}$) and KO (*Gskip*$^{-/-}$) mice. Equal amounts of proteins were loaded and lysates separated by 12 % SDS-PAGE (8 % in B). GAPDH (or Hsp90 in B) was used as a loading control. Representative Western blots are shown for phospho-PKA substrates (CS; #9624) (A), (phospho-)LRP5/6 (B) as well as N- and E-Cadherin (C). D) Densitometric evaluation of signal intensities, relative to GAPDH [in case of (p)LRP5/6 to Hsp90]. GSKIP KO was normalized to WT. n ≥ 4. Mean ± SEM; paired Student´s t-test. ns: not significant.

Summarizing the last section, diminished PKA-dependent GSK3β Ser9 phosphorylation upon GSKIP KO in mice was detected, confirming previous findings of our group underpinning a role of GSKIP in this phosphorylation event *in vivo*. However, in tissues and whole embryo for the waste number of tested proteins (excluding previously validated effects on FRAT2, RGS1, GPI and G6PD expression) no consistent protein expression changes were detected. Even for mitochondrial proteins none of the analysed proteins allowed so far to narrow down the observed phenotype to any mitochondrial process: neither abnormal LC3- or mTOR-mediated mitophagy, nor altered apoptosis induction (CytC release) were identified upon GSKIP deficiency. Moreover, the large-scale array did neither reveal significantly dysregulated expression for genes encoding any of the studied proteins, nor did it help to link enzyme expression to the observed metabolite shifts in GSKIP KO. It is possible that in the absence of GSKIP enzyme activities are changed rather than enzyme expression levels. Hence, a more appropriate analysis studying GSKIP´s influence on the proteome was initiated.

5.9.2 Large-scale proteome study points towards strong expression changes concerning mitochondrial as well as non-mitochondrial proteins in GSKIP-deficient lungs at E18.5

A large-scale study of the proteome was initiated in parallel to metabolomics in order to define GSKIP-dependent changes of protein abundance, with focus on E18.5 lung and liver, in collaboration with G. Mastrobuoni. In total, 6598 proteins were detected by proteomics analysis.

Proteins identified *via* proteomics were interpreted and expression levels compared. All proteins were included that were identified at least in one KO sample and at least in one WT sample by the presence of at least two unique peptides allowing for clear assignment. Results were visualized using Perseus software. The scatter plots for both E18.5 lung and liver are shown in Fig. 38 as average protein intensities, WT plotted against GSKIP mutant tissue.

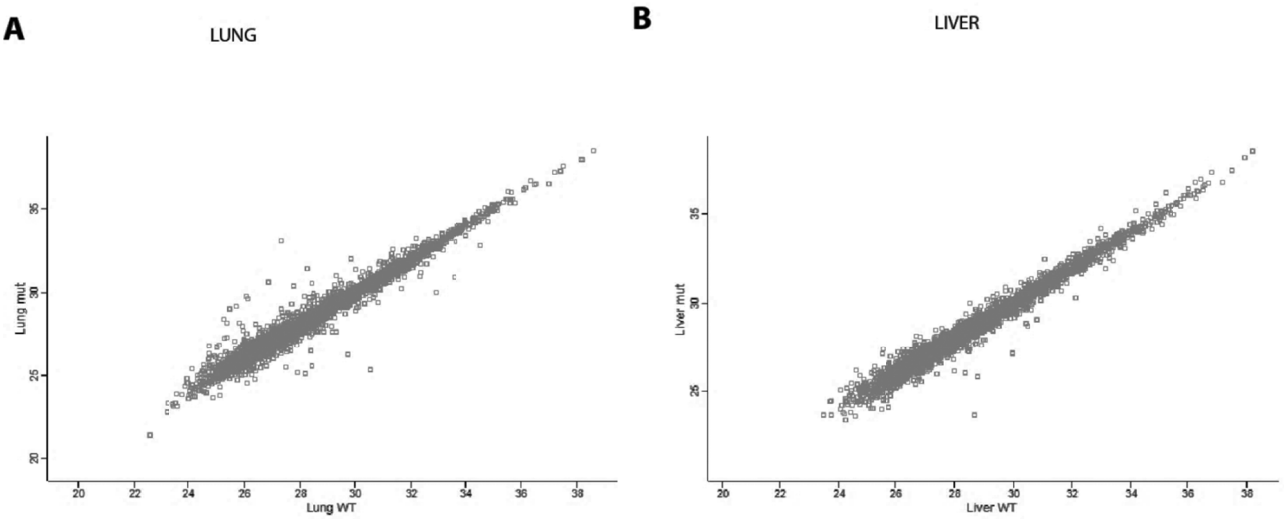

Fig. 38: **Scatter plot of protein expression intensities, E18.5 WT tissue against KO tissue.** A) lung and B) liver analysis. Note the more obvious expression changes in lung compared to liver as more data points differ from the diagonal.

Spots differing from the diagonal, thus representing protein expression differences when comparing GSKIP KO and WT situation, were screened and listed in Suppl. Tab. 6. Statistical significances could not be determined as the sample size was too low. Thus it was necessary to screen the results according to some criteria: Only proteins were included for which intensity values were available from at least two samples per genotype (two WT and two KO). In addition, only proteins were scored whose identity was determined by at least two unique peptides per sample; otherwise the result was classified as “not valid”. In order to narrow down the amount of altered proteins, the ones up- or downregulated at least by a factor of 2 were considered for further validation. This list includes 42 upregulated and 35 downregulated proteins (Suppl. Tab. 6).

For initial analysis, mitochondrial proteins were scrutinized aiming to link the mitochondrial phenotype of GSKIP KO E18.5 lungs with changes on the proteome level. All 16 mitochondrial proteins listed in Tab. 29 were clustered using the functional STRING tool according to their protein-protein associations (Fig. 39) and candidates for upcoming validation steps chosen from the clusters. The more lines are connecting different proteins, the more evident their association is, based on both experimental data and their co-mentioning in literature as well as databases. Thus, Hexokinase 1, 2 (Hk-1, Hk-2) and Sorbitol dehydrogenase (Sord) from one cluster as well as Glutamate dehydrogenase (Glud1) and Delta-1-pyrroline-5-carboxylate dehydrogenase (Aldh4a1) from the second apparent protein association cluster were selected. Carbamoyl-phosphate synthase (Cps1) was included as it showed a 40-fold increase in protein expression upon GSKIP KO, the overall highest enrichment detected in this screen. For the same reason the mitochondrial ATPase inhibitor 1 (Atpif1) with the highest decrease upon GSKIP KO was further considered as well. Of note, Glud1 protein

expression alterations were also observed upon GSKIP knockdown in A549 cells by proteomics (PhD thesis E. Perets).

Tab. 29: **Proteomics in E18.5 lung tissue detected expression changes for 16 proteins localizing to mitochondria in the absence of GSKIP**. n ≥ 2. Red: upregulated. Blue: downregulated. Purple: Overlapping protein comparing GSKIP KO in E18.5 lungs and GSKIP knockdown in A549 cells. GO: gene ontology prediction. HPA: human protein atlas.

Protein names	Gene names	Fold-change KO vs. WT	Intracellular localisation	Evidence for expression in lung
Carbamoyl-phosphate synthase [ammonia], mitochondrial	**Cps1**	**40.85**	**Mitochondrial inner membrane, nucleolus**	**Not expressed (HPA and others)**
Hydroxymethylglutaryl-CoA synthase, mitochondrial	Hmgcs2	11,52	Mitochondrial inner membrane	HPA: Expressed low
Cytosolic 10-formyltetrahydrofolate dehydrogenase	Aldh1l1	4.93	Cytoplasm; GO: mitochondrium	HPA: Expressed
Long-chain-fatty-acid--CoA ligase 1	Acsl1	2.62	Mitochondrial outer membrane, peroxisome membrane, microsome membrane, ER membrane	HPA: Expressed
Glycerol kinase	Gyk	2.37	Cytoplasm, mitochondrial outer membrane	HPA: Expressed low
Sorbitol dehydrogenase	**Sord**	**2.25**	**Mitochondrial membrane; Cilium, flagellum**	**HPA: Expressed**
Clusterin;Clusterin beta chain; Clusterin alpha chain	Clu	2.11	Secreted, cytoplasm, nucleus, mito membrane (upon apoptosis induction)	HPA: Not expressed
Glutamate dehydrogenase 1, mitochondrial	**Glud1**	**2.07**	**Mitochondrial matrix**	**HPA: Expressed high**
2-amino-3-ketobutyrate coenzyme A ligase, mitochondrial	Gcat	2.04	Mitochondrium, nucleus	HPA: Expressed
Delta-1-pyrroline-5-carboxylate dehydrogenase, mitochondrial	**Aldh4a1**	**2.03**	**Mitochondrial matrix**	**HPA: Expressed**
ATPase inhibitor, mitochondrial	**Atpif1**	**0.41**	**Mitochondrium**	**HPA: Ubiquitous; Expressed in lung**
Protein NipSnap homolog 2	Gbas	0.48	GO: mitochondrium	HPA: Expressed
Carnitine O-acetyltransferase	Crat	0.58	ER, mitochondrial inner membrane, peroxisome	HPA: Expressed
GTP:AMP phosphotransferase AK4, mitochondrial	Ak4	0.60	Mitochondrial matrix	HPA: Not expressed
Hexokinase-2 (HK-2)	**Hk2**	**0.60**	**Cytosol, membrane, mitochondrial outer membrane**	**HPA: Expressed**
Hexokinase-1 (HK-1)	**Hk1**	**0.62**	**Iso HK1: outer mitochondrial membrane;**	**HPA: Expressed**

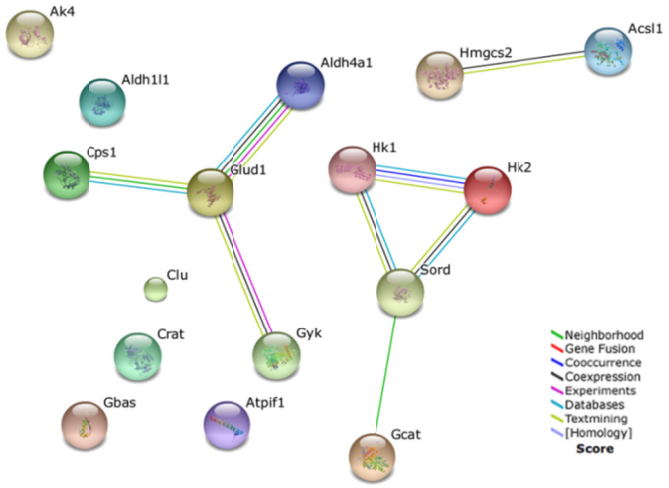

Fig. 39: **STRING protein association network of mitochondrial protein changes upon GSKIP KO in E 18.5 lungs.** (2015.05.18) Evidence view. Different line colours represent the types of evidence for the association. Interactions include direct (physical) and indirect (functional) associations; they are derived from four sources: high-throughput experiments, genomic context, previous knowledge and co-expression. For abbreviations, refer to Tab. 29.

From the list of proteins not having a mitochondrial localization (Suppl. Tab. 6), Talin-2 (focal adhesion protein linking integrins with actin cytoskeleton), Enolase 3 (striated muscle protein), Phospholipase C β3

(mediating second messenger DAG and IP3 production) and desmin (intermediate filament protein) were selected for validation *via* Western blot.

Additionally, proteomics results were reviewed for proteins which have already been shown to be altered in GSKIP-deficient tissue by previous experiments (microarray, Western Blotting and metabolomics) (Suppl. Tab. 7). GSKIP has not been identified in E18.5 lung and liver samples, neither in WT, nor in KO samples. GSK3β was only determined in lung where a 25 % reduction was observed upon GSKIP KO, in line with Fig. 32. PKA-C (α and β) subunits were downregulated by approx. 25 % (in contrast to Western blot observations, data presented in Fig. 32) while PKA-RII (α and β) subunits were unaltered upon GSKIP KO in lung. RGS1 and FRAT2 were not among the detected proteins. Glucose-6-phosphate isomerase (GPI) was determined to be unchanged upon GSKIP KO in E18.5 tissue (1.16-fold increase in lung; 1.02 in liver). Similar for Glucose-6-phosphate dehydrogenase (G6PD): the enzyme displayed a minor fold-change of 1.07 in lung and 0.89 in liver. Components of the PDH complex as well as SDHA subunits a, b and c did not change upon GSKIP KO. The surfactant proteins SP-A, SP-B and SP-C were identified *via* proteomics and only moderately changed: SP-B was slightly downregulated (0.91-fold) while SP-C was upregulated by a fold-change of 1.4. Hence, the observations for SP-B and SP-C were both in line with previous gene expression analysis *via* RTqPCR (Fig. 23). However, the pulmonary surfactant associated protein SP-A, binding to surfactant phospholipids and contributing to lower the surface tension at the air-liquid interface in the alveoli of the mammalian lung, was downregulated by 36 % (0.64-fold) in proteomics. Whether this is a primary or secondary effect due to failed respiratory activation and sequential absence of surfactant secretion, is unclear.

Validation of protein candidates discussed above (Tab. 29; Fig. 39) *via* Western blot confirmed changes on protein level only for the intermediate filament protein desmin (Fig. 40): upon GSKIP deficiency E18.5 lungs express 40 % less desmin compared to WT controls. Talin-2, Eno3, Atpif1, hexokinase pan (recognizing isoforms 1,2 and 3 around 100 kDa), hexokinase-2, PLCβ3, Aldh4a1 and Sord were unaltered upon GSKIP deficiency in E18.5 mouse lungs (Fig. 40 A). Cps1 was not detectable at all in E18.5 lung tissue.

The evaluation of GLUD1 caused difficulties, as the antibody recognized multiple bands in lung lysates (as well as in cells, data not shown). Likely the lower band represents GLUD1 while the upper one might rather be a post-translationally modified (e.g. poly-ubiquitinylated) variant of GLUD1, as there is only one isoform known in mice and not all tested lysates showed the upper band on a blot.

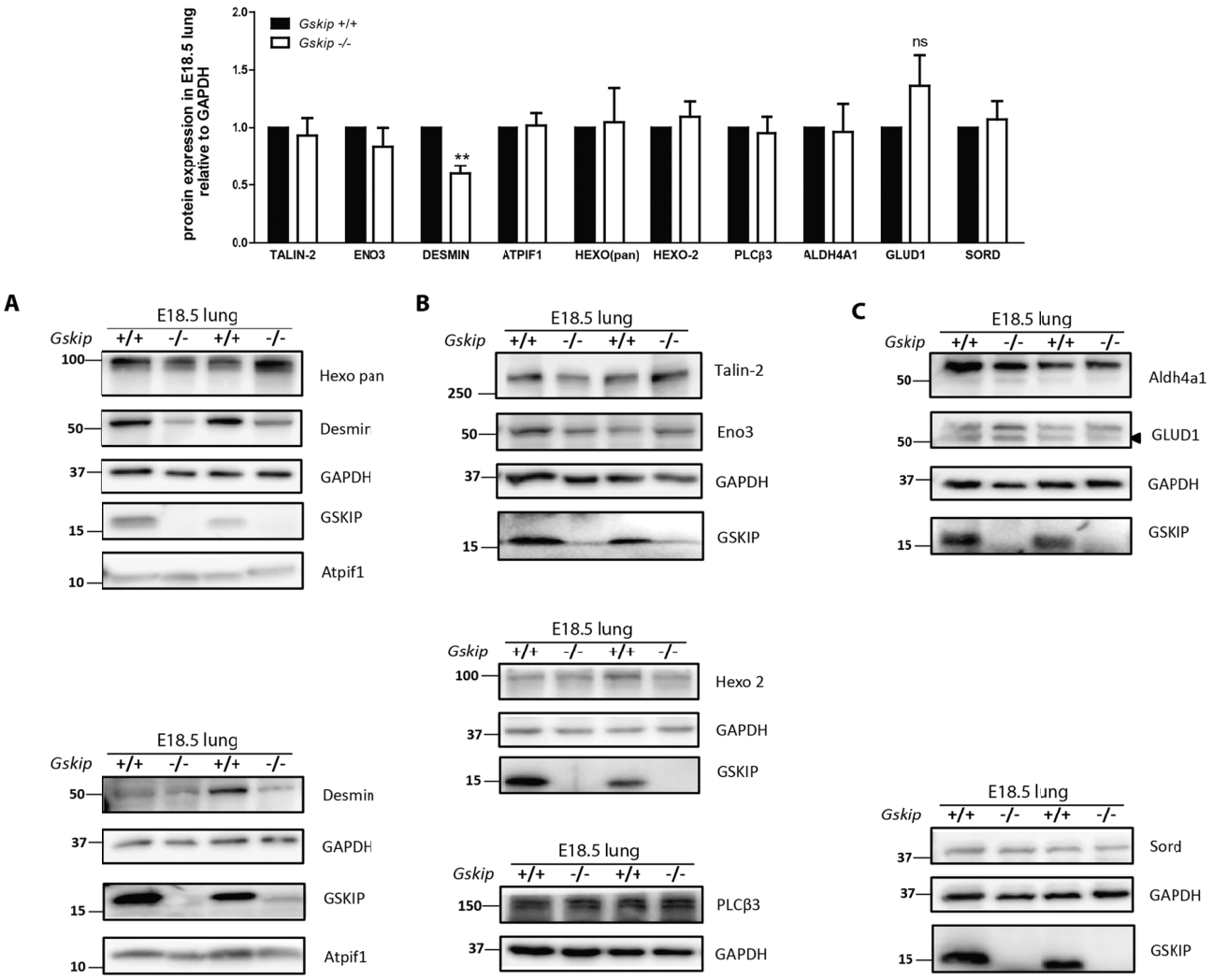

Fig. 40: **Validation of proteomics hits using Western blot.** Analysis of E18.5 lung lysates from WT (*Gskip*$^{+/+}$) and KO (*Gskip*$^{-/-}$) mice. Equal amount of proteins were loaded and lysates separated by 12 % SDS-PAGE (or 15 % for Atpif1 and Desmin). GAPDH was used as a loading control. Densitometric evaluation of signal intensities, relative to GAPDH. GSKIP KO was normalized to WT. n ≥ 6. Mean ± SEM; paired Student´s t-test. *p ≤ 0,05. ns: not significant.A) B) C) Representative blots are shown using antibodies targeting the depicted proteins. CPS1 was not detected at all in lung tissues at E18.5.

Desmin is a type III intermediate filament (IF) present in all kinds of muscle, but the major IF in both striated and smooth muscle cells, and an essential component of extra-sarcomeric cytoskeleton. A significant downregulation of desmin was detected upon GSKIP KO in lungs first by proteomics and successfully validated by Western blotting, implying a connection between GSKIP, desmin, muscle function and potentially also linked to mitochondria. Desmin can be dysregulated in disease, causing severe aggregation of proteins, mitochondrial abnormalities, cytoplasmic bodies and autophagic vacuoles. The alignment of myofibrils and positioning of organelles and cellular signalling events is dependent on filamentous frameworks involving desmin (Clemen *et al.* 2013). Notably, desmin mutations are involved in numerous myopathies. They were only occasionally studied in relation to pulmonary deficiencies, but are mainly related to cardiac and neuronal pathologies. Desmin KO mice are viable and fertile but develop a multisystem disorder involving cardiac, skeletal and smooth muscle development (Li *et al.* 1996; Milner *et al.* 1996).

The association between desmin and GSKIP-dependent changes in mouse E18.5 lungs remains to be determined.

5.9.3 Mouse embryonic fibroblasts serve as a primary system to study GSKIP knockout in cells

To avoid the excessive use of animals, the need for a primary GSKIP-deficient cell system emerged during this PhD project. In order to establish a GSKIP-deficient primary cell system for further analysis an isolation protocol was set up for the generation of primary mouse embryonic fibroblasts (MEFs) out of WT and GSKIP KO E12.5 embryos (4.2.7). Phenotypic differences were not observed under the microscope when comparing GSKIP WT and GSKIP KO MEFs. Cells were lysed and protein expression studied. Similar to early-stage whole embryos, the inhibitory phosphorylation of GSK3β at Ser9 is diminished in GSKIP KO MEFs, whereas none of the other tested proteins (β-catenin, CyclinD1, PKA subunits) showed any alterations in comparison with MEFs generated from WT embryos (Fig. 41). RGS1 protein expression is as well unaffected upon depletion of GSKIP in MEFs (Fig. 41 A); most likely RGS1 plays a role later in development.

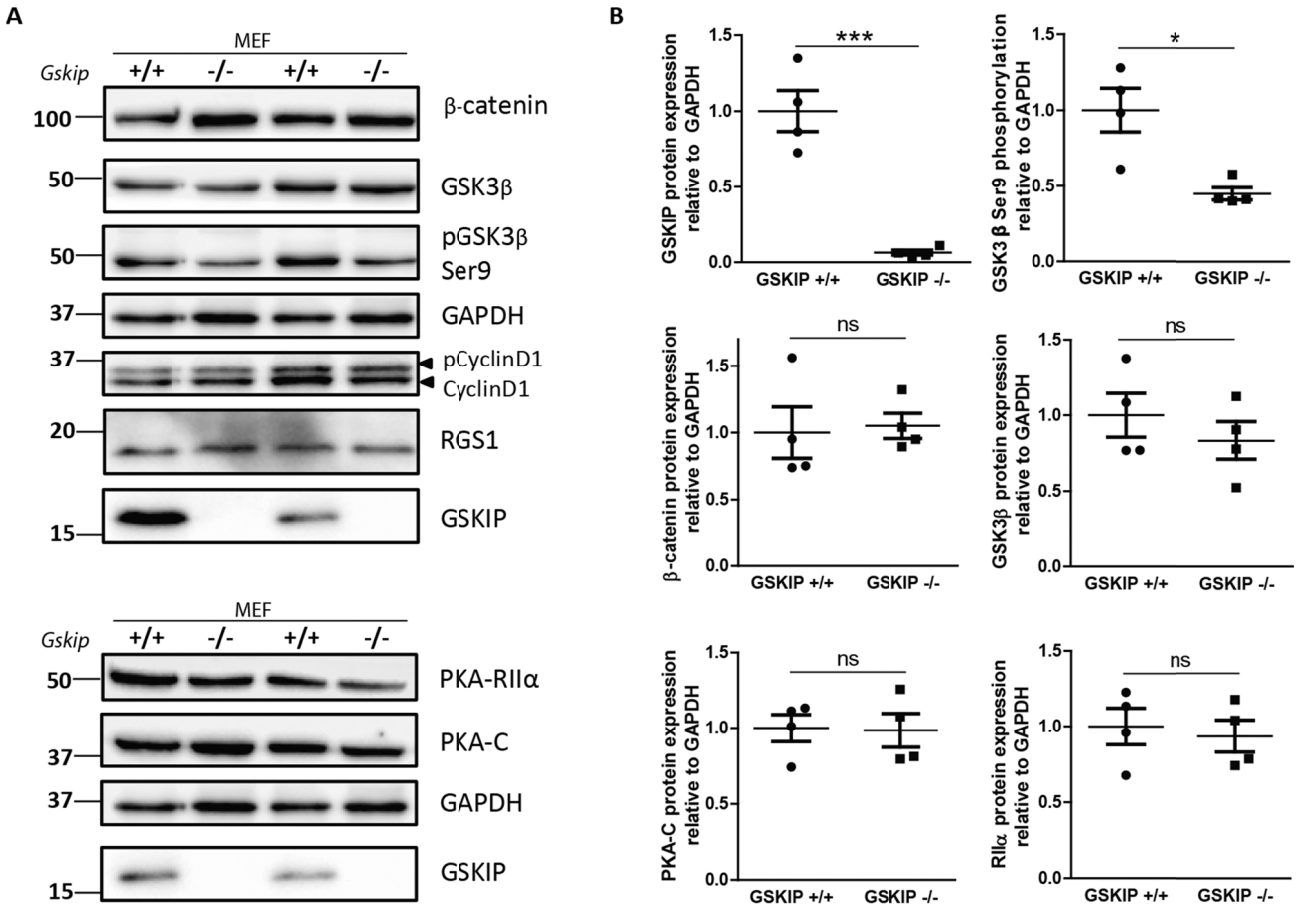

Fig. 41: **Protein expression studies in primary MEFs confirm reduced GSK3β Ser9 phosphorylation upon GSKIP KO.** Western blot analysis of MEF lysates generated from WT (*Gskip*$^{+/+}$) and KO (*Gskip*$^{-/-}$) E12.5 mouse embryos. 15 µg proteins were loaded and lysates separated by 12 % SDS-PAGE. GAPDH was used as a loading control. A) Representative Western blots are shown for GSKIP, (p)GSK3β, (p)CyclinD1, β-catenin, RGS1, PKA-RIIα and -C subunits as well as for GAPDH. B) Densitometric evaluation of signal intensities, relative to GAPDH. GSKIP KO was normalized to WT. n = 4. Mean ± SEM; unpaired Student´s t-test; *p ≤ 0,05. ns: not significant.

Even though the protein expression of PKA subunits was unaffected by GSKIP KO in MEFs, phosphorylated PKA substrates in unstimulated MEFs were analysed using Western blot (Fig. 42 A): the phosphorylation pattern of PKA substrates, however, was not altered upon GSKIP KO in primary MEFs. Nonetheless, PKA activity was tested with a PepTaq PKA kinase assay (Promega, 4.2.4.4) in order to define whether GSKIP's absence impairs PKA function under resting or forskolin (FSK)-stimulated conditions (Fig. 42 B). Forskolin is a potent stimulator of adenylyl cyclase. Noteworthy, the phospho-PKA substrate Western blot reflects the unstimulated condition and is not undoubtedly in line with the PKA assay result for the same condition: an almost 40 % increase in PKA activity upon GSKIP KO was detected in MEFs under resting conditions. FSK increased PKA activity in WT as well as KO MEFs, but the intergroup difference

was lost, meaning the response of PKA to FSK stimulation is not GSKIP-dependent. For unknown reasons, H89 incubation prior to FSK stimulation indeed inhibited PKA substrate phosphorylation (as shown by a representative Western blot in Fig. 42 B *lower panel*), but the inhibition was not recognized by the PepTaq assay. However, data is preliminary (n = 2) and the detection of PKA enzyme activity should be regarded critically.

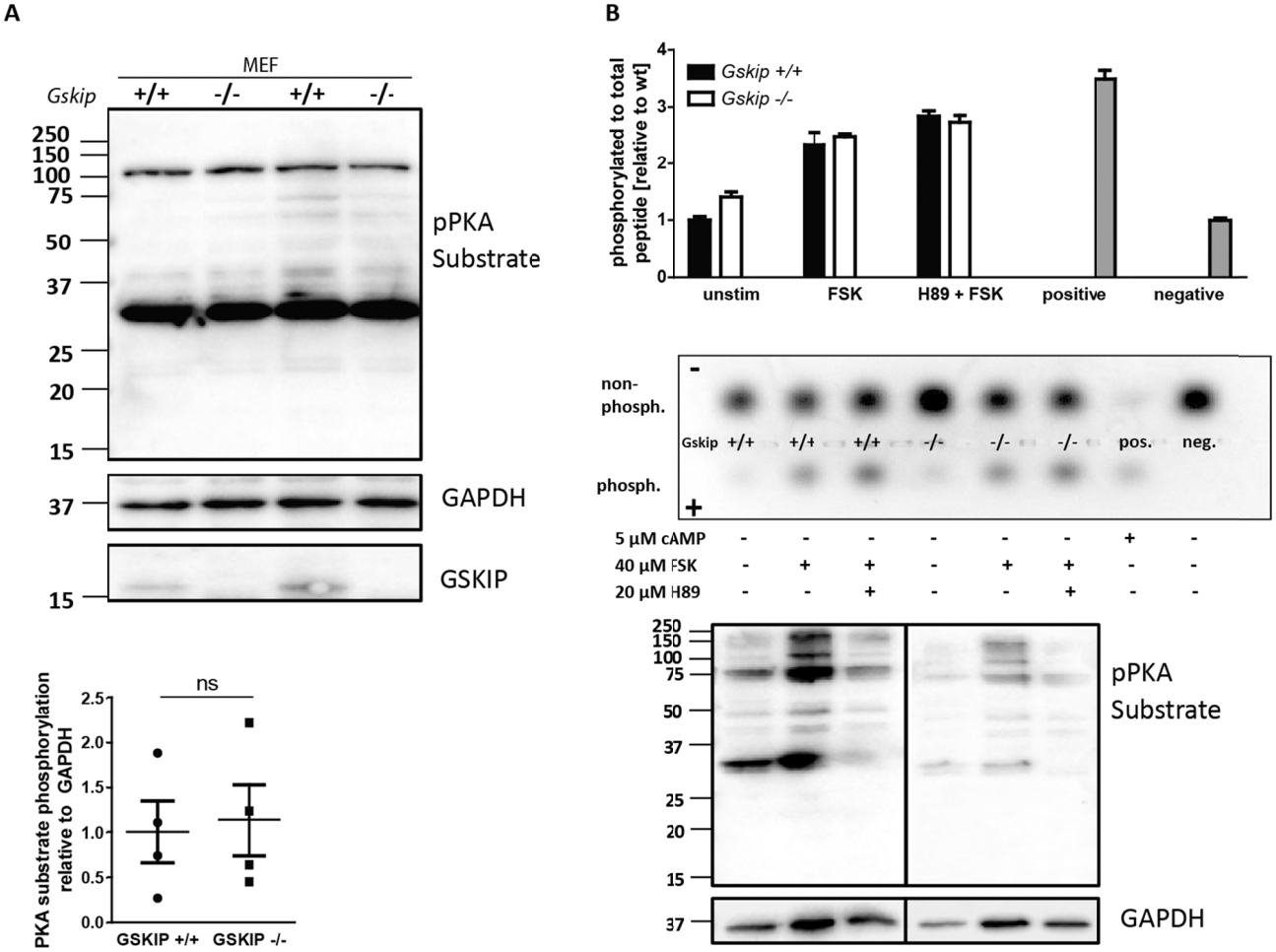

Fig. 42: **Protein analysis of MEFs isolated from wild type GSKIP and knockout GSKIP E12.5 embryos do not point towards GSKIP-dependent influences on PKA activity.** A) A representative Western blot is shown for phosphorylated PKA substrates using a Phospho-(Ser/Thr) PKA substrate antibody detecting peptides and proteins containing a phospho-serine/threonine residue with arginine at the -3 position (CS, #9621). Lysates with 15 µg of proteins were separated by 12 % SDS-PAGE. GAPDH was used as a loading control. Densitometric analysis of signal intensities, relative to GAPDH. GSKIP KO was normalized to WT. n = 4. Mean ± SEM; unpaired Student´s t-test. B) PepTaq PKA assay on unstimulated, forskolin (FSK; 40 µM for 30 min)- or FSK plus H89 (20 µM 30 min prior to FSK)-treated MEFs. n = 2. Non-phosphorylated peptide (PKA inactive) possesses a positive charge and hence migrates to the minus pole while PepTaq peptide phosphorylated by PKA, indicative for PKA activity, is negatively charged and moves towards the plus pole. Positive control: cAMP (5 µM) added to untreated WT lysate. Negative control: buffer only. ns: not significant.

The effects of GSKIP in MEFs were carefully assessed by Western blot determining expression levels of Wnt signalling proteins and GSK3β targets (Suppl. Fig. 10), but changes were not detected comparing WT- and GSKIP KO cells. In addition, SMYD2 was also not influenced by GSKIP absence on protein level (Suppl. Fig. 11 B). The intermediate filament desmin was not detected at protein level in MEFs.

Despite it is not known whether GSKIP-deficient MEFs possess a mitochondrial phenotype comparable to that of GSKIP-deficient lung tissue, mitochondrial proteins were studied (Suppl. Fig. 11 C). EMT transition and metabolic enzyme expression were assayed as well for protein expression changes, but did not reveal any involvement of GSKIP on their regulation (Suppl. Fig. 11 A, D).

GSKIP deficiency did not markedly influence MEF proliferation. Cytochrome C release (as determined in lysates containing mainly cytosolic fractions) was not impaired in GSKIP KO MEFs (Fig. 43 A, D). The same was true for autophagy: accompanied by the conversion of LC3A/B-I (16 kDa) into LC3A/B-II (14 kDa) autophagy was not affected by GSKIP deficiency (Fig. 43 B, D). Moreover, mTOR functions in autophagy as a kinase balancing the availability of cellular amino acids and ATP (Jung *et al.* 2010). However, mTOR did not show changes upon GSKIP KO in MEFs (Fig. 43 C, D). Though, GSKIP was ruled out to be implicated in MEF apoptosis or autophagy.

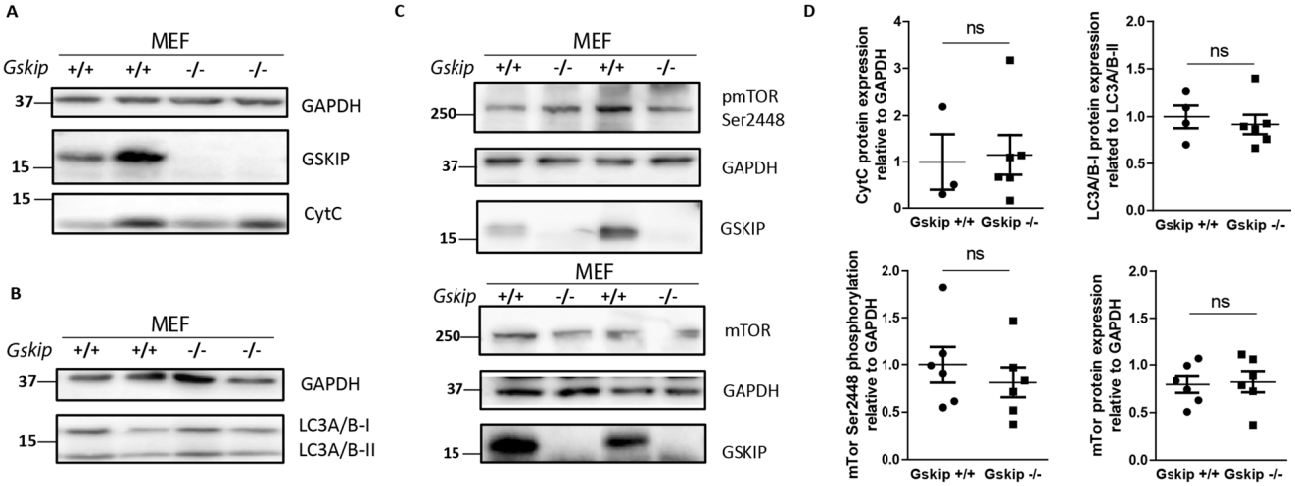

Fig. 43: **Elucidation of potential GSKIP-dependent effects on MEF apoptosis and autophagy.** Representative Western blots are shown. Equal amounts of protein were loaded and separated by 12 % SDS-PAGE. Cytochrome C (A) as an apoptotic factor, LC3A/B conversion (B) indicating autophagy as well as mTOR expression and phosphorylation (C) were studied. GAPDH was used as a loading control. D) Densitometric evaluation of signal intensities, relative to GAPDH. GSKIP KO was normalized to WT. The conversion of LC3A/B-I into -II is expressed as a ratio. n = 4. Mean ± SEM; unpaired Student´s t-test.

Recapitulating MEF experiments, an isolation protocol was successfully established and the aforementioned effect of GSKIP on GSK3β Ser9 phosphorylation once more confirmed. At the current state of this project, these cells have a limited applicability as they do not reflect a physiological condition relevant for a whole organism. However, for initial studies on GSKIP-deficient cells, e.g. narrowing down Shh- and non-canonical TGFβ signalling involved in cleft palate development, MEFs might serve as a starting point. Or, in case general questions have to be answered concerning the crosstalk of signalling pathways, MEFs should be included, as a primary cell system bridging siRNA studies in permanent cells with *in vivo* mouse analysis, prior to going directly into animal experiments.

6. Discussion

The perinatal lethality of conditional GSKIP KO mice at E18.5 points out an essential role for GSKIP in development. Upon KO of GSKIP, mice display a secondary cleft palate and delayed ossification of palatal bones. GSKIP-deficient animals suffering from respiratory distress at birth possess damaged mitochondria and show severely altered metabolite profiles (both in lung and liver) compared to WT controls, likely accounting for their death. A large-scale microarray and its subsequent validation defined GSKIP-dependent gene expression changes: *Frat2*, *Rgs1* and *Klf2* could be validated as misregulated upon GSKIP KO. Downregulation of GSK3β Ser9 phosphorylation upon GSKIP KO was observed in mice early in development, in whole embryos, primary MEFs and also in late stage E18.5 organs. A GSKIP-dependent impairment of PKA expression or activity was not detected. Proteomics revealed the muscle-specific intermediate filament protein desmin to be at least 50 % downregulated in GSKIP-deficient lungs at E18.5, potentially connecting the mitochondrial phenotype (present amongst others in airway smooth muscle cells) with respiratory inability ultimately accounting for the perinatal lethality of GSKIP KO mice.

In the following section, several aspects will be discussed, starting with the cleft palate, followed by the observed lung and metabolic phenotype. The general question of how GSKIP might impair the adaptation of an embryo to extrauterine life will be considered. On the molecular level, mitochondrial processes potentially involving GSKIP will be in the focus.

6.1 Secondary cleft palate and its consequences

The inability of GSKIP-deficient mice to initiate breathing appropriately is accompanied by the absence of correct palatal fusion. The inhaled air is not properly directed to the lower airways, but leaks (at least in part) through the palatal cleft into the nasal cavity. The anatomical defect of a craniofacial cleft palate is in general regarded as indicator for developmental delay (Turgeon & Meloche 2009). As described earlier, several Wnt signalling protein KOs as well as GSK3β KO mice display a cleft palate, and GSK3β's involvement in both palatal bone ossification and palatal bone fusion have been elucidated (Fig. 17; Fig. 18). Hence GSKIP´s function in palatal fusion is likely mediated (at least partially) by GSK3β, involving Shh, Wnt, BMP and FGF signalling. Of note, biochemical regulation of embryonic lung growth also involves those pathways (Warburton *et al.* 2010), possibly linking GSKIP deficiency-induced abnormalities in lung (potential AEC1 immaturity) with those affecting cleft palate development.

In consequence of an open connection between nasal and oral cavity, both resonant control and intraoral pressure are compromised and make screaming/yelling and suckling impossible, explaining that newborn GSKIP KO mice do not emit sounds upon soft pressure of their tail while GSKIP WT mice do. This is disadvantageous for the extrauterine development of a newborn. However, due to the early perinatal death of GSKIP KO mice before initiation of food intake the suckling and vocalization inability (ultimately resulting in death of starvation) is most likely not of relevance. In humans the anatomical dysfunction caused by a secondary cleft palate is known as velopharyngeal insufficiency and involves problems with breathing, eating, hearing and speech; treatment comprises speech therapy and surgery (Capra & Brigger 2012; Steinberg *et al.* 2012; Shetty *et al.* 2014).
The cleft palate alone likely does not account for the perinatal death within the rather short time window of less than 30 min. Even if air leaks, the lung should still be inflated in part and mitochondrial damage would not be expected so early; with a reduced breathing efficiency mice would survive longer even if they struggle and are exhausted. The cause of death of GSKIP KO mice is more due to the impairment of more than one physiological process, as various pathways are affected by GSKIP, summing up to an ultimate lethal threat.

Delayed ossification was not assayed in the entire body. However, bone mineralization and ossification might be compromised also outside the upper jaw. Rib cage movements, the presence of a diaphragm and a visual respiratory effort did not point towards an overt bone defect of the ribs and also excluded neuronal innervation defects and muscular dysfunction.

6.2 Lung development and adaptation to extrauterine life

At birth, the mouse foetus is exposed to an approximately sevenfold increased oxygen concentration compared to the hypoxic environment in the placenta (3 % O_2 in contrast to extrauterine 21 % O_2), considered as dramatic oxidative stress for the newborn (Vogel *et al.* 2015). In addition, the lung is subject to intense environmental changes in oxygen tension when lung liquid is rapidly replaced by air. Separation of the newborn from the umbilical cord induces catecholamine-mediated elimination of chloride secretion and stimulates Na^+/K^+-ATPase, followed by liquid absorption into the lung interstitium (Warburton *et al.* 2010). A large amount of free oxygen radicals becomes available within minutes and can elicit cytotoxic effects up to hyperoxic tissue damage (Rickett & Kelly 1990). Antioxidant genes induced in the fetal lung at late gestation encoding, amongst others, antioxidant enzymes protect against the dramatic change of oxygen tension at birth (Frank *et al.* 1996). However, the initiation of these events usually take some hours and might not be considered as the primary reason for the observed lung phenotype in GSKIP-deficient E18.5 mice as they die within a few minutes rather than within hours.

From the developmental point of view, neither lung architecture, nor functional surfactant protein expression are altered upon GSKIP KO. Gas exchange relies on the secretion of surfactant which was sporadically seen in TEM experiments even in GSKIP-deficient lungs (Fig. 26; in line with breathing efforts observed), but does not answer the question whether the secreted surfactant, a lipid-protein mixture, is functional or not in absence of GSKIP. Whether surfactant phospholipids are modified in absence of GSKIP was not analyzed. The main surfactant phospholipids are represented by phosphatidylcholine (PC), phosphatidylglycerol (PG) and phosphatidylinositol (PI). PC is the most abundant one, and its biosynthesis is of importance as AEC2 cells synthesize large quantities of disaturated PC, the surface-active agent of pulmonary surfactant, particularly at late gestation when the lung prepares for postnatal air breathing (Goss *et al.* 2013; Lopez-Rodriguez & Perez-Gil 2014). The phospholipids of surfactant are synthesized mainly from glycogen pools present in the cytosol and the presence of these glycogen pools was observable in the TEM experiments, still not excluding abnormalities. A detailed lipid analysis would be necessary to study phospholipids, hypothetically interesting also in the context of mitochondrial membranes (see 7.3). Morphological studies suggest GSKIP-dependent alterations affecting AEC1 cells, not surfactant-producing AEC2. Cells with damaged mitochondria do not proliferate and would not allow tissue development at all; hence cells must experience a sudden threat causing a fast reaction of their mitochondria to the stress they encounter. In addition, the observed mitochondrial damage potentially rather points to a rapid reaction in the lung upon air exposure explaining mouse lethality instead of a developmental process accounting for the perinatal death.

On the gene level, different studies have elucidated the consequences of air exposure at birth on a large scale; e.g. the transcription factor *Klf4*, induced in the lung by oxygen at birth, regulates perinatal fibroblast and myoblast differentiation (Jean *et al.* 2013). One might speculate that GSKIP-dependent gene expression changes, linked amongst others to the observed *Klf2* and *Pdpn* gene reduction, potentially impair lung cell development and differentiation. Both smooth muscle fibroblasts and/or alveolar epithelial type 1 cells might be affected by these changes within the GSKIP-deficient lung, resulting in cell immaturity and ultimately dysfunction of respiration. So far it remains unanswered whether myocytes or AEC1 cells or the combination of different lung cell types account for the fatal respiratory failure in GSKIP KO mice.

6.3 Metabolic transition at birth: link to metabolic profiling of GSKIP KO mice

At birth, a newborn mouse undergoes a profound metabolic transition and strongly relies on postnatal oxidative metabolism. The pulmonary circulation is replacing the placental one and the heart begins its aerobic metabolism (Pei *et al.* 2011; Hillman *et al.* 2012). The newborn must also quickly control its energy metabolism, from the secured continuous transplacental glucose supply to a variable fat-based energy source coordinated by hormonal changes (Ward Platt & Deshpande 2005). The metabolic switch represents a hallmark of the fetal to newborn transition. With delivery, plasma glucose as well as free fatty acid levels fall over the next hours after birth, accompanied by a reduction in insulin, the release of catecholamines and an increase in cortisol (Hillman *et al.* 2012). Glycogen deposits as well as fat stores serve as energy sources during the transition process and their availability challenges the adaptation of a newborn. The molecular details of these transitions have not been unraveled.

On gene level, the microarray analysis conducted by Jean *et al.* two hours after birth revealed gene categories being overrepresented upon oxygen exposure at birth, namely genes involved in transcriptional regulation, apoptosis and antioxidant activity (Jean *et al.* 2013). The presence of transient oxidative stress in mouse lungs two hours after birth suggests a response to a change in the local metabolism state of the lungs as the oxygen tension is altered. GSKIP-deficient mice obviously lack the ability to compensate for this oxidative stress.

Upon GSKIP deficiency, E18.5 mice accumulate glucose-6-phosphate as well as the branched chain amino acids (BCAAs) leucine and valine (Fig. 28). Glucose-6-phosphate, an allosteric activator of Glycogen Synthase (GS), could not be detected to be GSKIP-dependently phosphorylated by GSK3β (Fig. 33); however, other posttranslational modifications of GS were not studied. The molecular mechanism underlying the enrichment of glucose-6-phosphate in GSKIP-deficient tissue is not known. An overall impairment of mitochondrial function explains the observed disturbances, but the reason for the specific accumulation of some metabolites while others remain unchanged is unclear. Enzyme activities were not tested (except for specific enzyme phosphorylations), only enzyme expression levels were assessed during this thesis. Moreover, the question remains to be answered how the accumulated BCAAs are metabolized. BCAAs are generally incorporated into proteins; the increased availability of BCAAs might thus either arise from an increased protein catabolism yielding high amounts of BCAA or a decreased incorporation of BCAA into proteins.

Concluding from the phenotype of GSKIP KO mice (based on the results of this PhD thesis), GSKIP seems to play a pivotal role in diverse physiological processes: bone development, energy homoeostasis, lung mitochondrial stability and the initiation of respiration after birth. In addition, mitochondrial damage was detected in lungs.

Albeit an early brain phenotype was excluded, the experimental approach does not allow a general assumption concerning a potential brain phenotype, especially regarding the hindbrain which harbours the respiratory center and hence may show GSKIP-dependent defects. The majority of unique gene expression changes on the microarray were detected in the lung and in the brain, suggesting a brain-specific response in parallel to a lung-specific reaction to GSKIP deficiency in mice at birth.

6.4 Molecular aspects involving GSKIP

6.4.1 The PKA/GSKIP/GSK3β/Drp1 complex

Mitochondrial fission, a process of mitochondrial division involved e.g. in apoptosis, cell growth and development is regulated by Dynamin-related protein 1 (Drp1), a GTPase involved in controlling mitochondrial size, shape, remodelling and maintenance (Capetanaki *et al.* 2015). Phosphorylation of Drp1 can stimulate or inhibit mitochondrial fission: phosphorylation of Drp1 Ser637 is mediated by PKA and inhibits fission, while Cdk1-/CyclinB-mediated phosphorylation of Drp1 at Ser616 stimulates the process (Shardonofsky *et al.* 2006; Mohamed *et al.* 2011). GSK3β phosphorylates Drp1 at Ser693 and, most important under oxidative stress, induces mitochondrial elongation *via* downregulation of apoptosis (Panagopoulou *et al.* 2008). Mitochondria adopt different shapes and sizes in order to accommodate their different roles in energy production, metabolism and cell death (Li *et al.* 1996; Milner *et al.* 1996). Mitochondria undergo constant fusion and fission under steady-state conditions, but also in response to different stimuli. They become fragmented during apoptosis, allowing the release of pro-apoptotic CytC, such as in neurodegenerative disorders. Fusion and hyper-fusion (resulting in elongation) are mechanisms by which mitochondria escape from degradation by autophagy; elongated mitochondria maintain high levels of ATP production and hence support the survival of the cell, e.g. in response to starvation (Winter *et al.* 2014).

Recently, Loh *et al.* suggested the existence of a complex comprising PKA/GSKIP/GSK3β/Drp1 (Loh *et al.* 2015). The overexpression of GSKIP (but not of its PKA-RII or GSK3β binding-deficient mutants) increased PKA-mediated Drp1 Ser637 phosphorylation in HEK293 cells, supporting a Drp1-associated protective role of the PKA-RII/GSK3β/GSKIP complex. In addition, the overexpression of kinase-dead GSK3β still binding GSKIP induced the same PKA-mediated Drp1 phosphorylation, while the ablation of both GSK3β kinase activity and GSK3β-GSKIP binding did not. Forskolin was used in this study to analyse PKA-mediated Drp1 signaling. The involvement of both GSKIP and GSK3β in the regulation of forskolin-induced Drp1 phosphorylation has been demonstrated additionally by knockdown experiments. Upon H_2O_2 treatment inducing apoptosis the expression of WT GSKIP seemed to be protective both in HEK293 and SH-SY5Y neuroblastoma cells in contrast to GSKIP variants deficient for either PKA or GSK3β binding. The modulation of mitochondrial morphology by the novel GSKIP-involving complex was however not clear. Moreover, the study by Loh *et al.* was based on GSKIP mutational variants which were barely expressed in the cell systems used. Thus, an unequivocal conclusion cannot be drawn from this study.

This newly proposed complex linking the mitochondrial phenotype and GSKIP suggested the analysis of both Drp1 and pDrp1 Ser637 levels in E18.5 lungs of GSKIP KO mice. No differences were observed for Drp1 protein levels (Fig. 44). As Drp1 recruitment to mitochondria is controlled by post-translational modifications such as PKA-dependent Ser637 phosphorylation, one might have expected a GSKIP-dependent alteration in GSKIP KO tissue. The effects of a modification may differ depending on the cellular context in which it occurs; even though Loh *et al.* described a GSKIP-dependent morphological change connected to phospho-Drp1 Ser637 in HEK293 cell mitochondria upon oxidative stress (Loh *et al.* 2015), this does not occur in E18.5 lungs (Fig. 44).

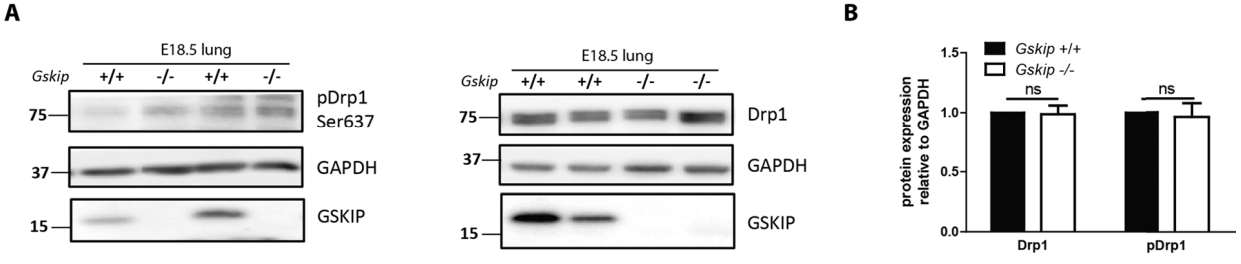

Fig. 44: **Drp1 protein expression and Drp1 Ser637 phosphorylation in E18.5 lung tissue is not altered upon GSKIP KO.** Western blot analysis of E18.5 lung lysates from WT (*Gskip*$^{+/+}$) and KO (*Gskip*$^{-/-}$) mice. 20 µg of protein were separated by 12 % SDS-PAGE. GAPDH was included as a loading control. A) Representative blots are shown. B) Semi-quantitative evaluation of signal intensities, relative to GAPDH. GSKIP KO was normalized to WT. n ≥ 6. Mean ± SEM; paired Student´s t-test. ns: not significant.

The elucidation of mitochondrial structure-function relationships is a relatively new field. The key proteins of mitochondrial dynamics mitofusin 1, 2 and optic atropy 1 (OPA1) favour mitochondrial fusion while Drp1 and fission 1 are pro-fission regulators. Mitochondrial fission, supported by Drp1, is characterized by increased mitochondrial membrane permeability, elevated ROS production, reduced oxidative capacity and induction of both mitophagy and apoptosis (Slats *et al.* 2008). Taking the proposed GSKIP-involving PKA/GSK3β/Drp1 complex one would expect upon respiratory distress, e.g. exposure to air upon birth, a drastic change of mitochondria involving increased apoptosis and mitophagy in GSKIP-deficient cells and tissue compared to controls. The evaluation of mitophagy- or apoptosis-related proteins upon GSKIP KO did not support this hypothesis: the assessment of mitophagy and apoptosis markers *via* Western Blot did not reveal differences upon GSKIP deficiency in E18.5 lungs (Fig. 35). In addition, on a large scale (microarray and proteomics) neither mitochondrial fission or fusion regulators, nor autophagy-related genes (or the proteins they encode) were detected as GSKIP-dependently altered.

6.4.2 GSK3β and VDAC in mitochondria

GSK3β regulates, amongst others, the opening of the mitochondrial permeability transition pore and translocates from the cytosol to mitochondria upon oxidative stress (Jung *et al.* 2010). This translocation depends on the interaction of GSK3β with VDAC as well as on the kinase activity of GSK3β. H_2O_2 treatment of H9C2 cardiac myoblasts overexpressing GSK3β (WT), a mutant GSK3β insensitive to Ser9 phosphorylation and a kinase-dead GSK3β induced a translocation of GSK3β to mitochondria: in the WT and phosphorylation-insensitive GSK3β situation the translocation was much faster compared to the kinase-dead GSK3β variant.
Juhaszova *et al.* previously demonstrated the contribution of GSK3β to mitochondrial permeability transition pore regulation: the knockdown of GSK3β elevated the threshold for pore opening (Juhaszova *et al.* 2004). In addition, the inactivation of mitochondrial GSK3β is associated with suppressed pore opening (Miki *et al.* 2009). Noteworthy, these studies consider increased GSK3β phosphorylation as well as the increased abundance of GSK3β in mitochondria as an anti-cardioprotective mechanism in the heart, but no studies aimed at elucidating mitochondrial GSK3β in lung or muscle.
Even though GSKIP cannot be detected in lung mitochondria, it might still be involved in the facilitation of GSK3β´s translocation by interacting on the cytosolic site with GSK3β through the PKA-anchored GSKIP-GSK3β complex. VDAC expression changes, however, were not detected in GSKIP-deficient lungs at E18.5. Whether GSKIP-deficient lung mitochondria have an altered GSK3β phosphorylation pattern compared to controls was not determined.

Increased oxidative demand and mitochondrial energy deficiency trigger for example the compensatory induction of mitochondrial proliferation. However, data resulting from mitochondrial analyses of GSKIP KO mice rather allow to conclude that the mitochondrial protein content within the cell is not changed in GSKIP-deficient lungs (all mitochondrial proteins showed no change in abundance; Fig. 35). It is more likely the distribution and shape of mitochondria within the tissue that is altered.

6.4.3 Desmin and mitochondria

Desmin is a muscle-specific type III intermediate filament (IF) linking the Z-disc (or intercalated disc) to the nucleus, the subsarcolemmal cytoskeleton, the plasma membrane and other membraneous structures such as mitochondria (Fig. 45). Hence, desmin is connecting the contractile unit with membranes, thereby maintaining cellular integrity during contraction and supporting force transmission (Paulin & Li 2004; Goldfarb & Dalakas 2009).

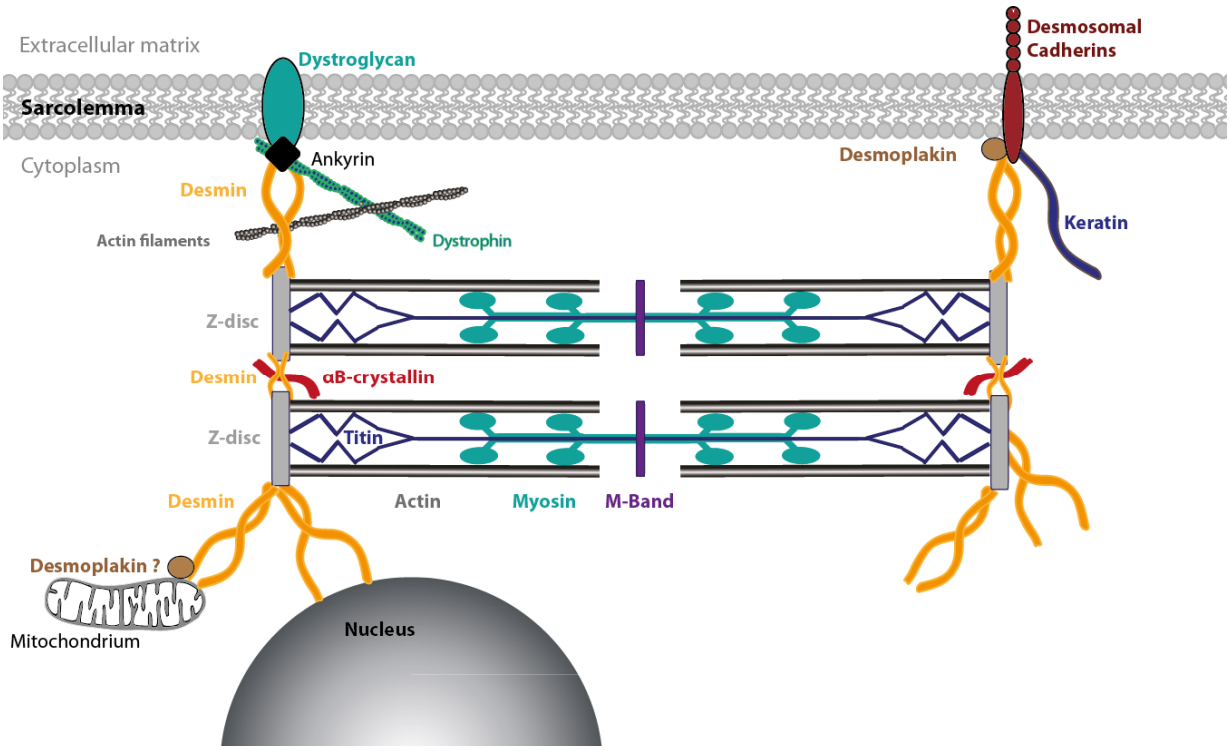

Fig. 45: **Desmin is the main muscle intermediate filament (IF) protein.** It forms a continuous cytoskeletal IF network and connects the contractile apparatus with membraneous structures within the cell, e.g. with the nucleus, the mitochondria, the sarcolemma (cell membrane of the myocyte) and further cytoskeletal proteins such as dystrophin and actin. Moreover, desmin connects the sarcomeric cytoskeleton with the extracellular matrix, ankyrins serve as linkers between desmins and integral membrane proteins, for example dystroglycans (Bennett & Healy 2009). αB-crystallin is a desmin chaperone, while desmoplakin is an adaptor protein linking the IFs desmin and keratin to desmosomal Cadherins as part of desmosomes, cell–cell adhesive junctions in tissues that undergo mechanical stress such as the heart (Kimura *et al.* 2007; Goldfarb & Dalakas 2009). The muscle unit between two neighbouring Z-discs is called sarcomere and is build up by thin actin filaments, thick myosins (cross-linked in the middle by the M band) and a giant titin band that connects the two Z-discs.

Desmin-related myopathies, also called desminopathies, are caused by a dysfunctional desmin network due to desmin gene mutations or altered post-translational modifications. To date, nearly 70 human desmin mutations associated with desminopathy are known, having a wide range of clinical manifestation. The majority of mutations induce a cardiac phenotype, and less frequently skeletal muscle is affected as well. On the molecular level, desmin cleavage leads to aggregate formation, mitochondrial abnormalities, intercalated disc destabilization and cell death (Capetanaki *et al.* 2015). Novel insights were provided by studying the mechanism of desmin cleavage: TNF-α signalling induces caspase-6-mediated proteolytic cleavage of desmin followed by heart failure (Panagopoulou *et al.* 2008). A further pathophysiological mechanism including the impairment of desmin turnover leading to desmin accumulation was reported in patients with dilated cardiomyopathy (Heling *et al.* 2000). Hence, the loss of normal desmin function as well as the toxic effects of aggregated desmin is linked to muscle pathophysiology. Desmin is the target for a variety of post-translational modifications, including phosphorylation, ADP-ribosylation, ubiquitination (associated with TRIM32), oxidation and nitration, most of them causing the disassembly of the desmin network (excluding ubiquitination inducing desmin degradation) (Winter *et al.* 2014).

Early TEM analyses of desmin-deficient cardiac muscle demonstrated swollen and degenerated mitochondria detectable very early before other structural defects became apparent (Milner *et al.* 2000). These observations resemble the GSKIP-deficient mitochondrial phenotype observed in lungs, even though in this thesis mainly non-muscle cells were in the focus of TEM analysis (Fig. 26). The mitochondrial phenotype of lung fibroblasts is currently studied (TEM core facility, MDC).
Milner *et al.* noticed an age-related phenomenon of mitochondrial proliferation within the muscle: the older desmin-deficient mice, the more mitochondrial proliferation was apparent upon pressure overload in the heart (Milner *et al.* 2000). In addition, their studies revealed a decreased maximal respiration *in vivo* for desmin-deficient mitochondria in both cardiac and soleus muscles.

Physiological studies of desmin KO mice mainly focused on cardiac, visceral and skeletal muscle, even though desmin is expressed in the smooth muscle of both conducting airways and alveolar ducts. However, Shardonovsky *et al.* showed that desmin influences lung compliance and airway contractile responsiveness by stiffening the airways and consequently the lung (Shardonofsky *et al.* 2006). Hence, desmin is not only involved in controlling macromechanical transduction and elasticity in the heart and cardiac muscle but is also important for the transmission of mechanical stresses in the lung. Also in the diaphragm desmin increases the transverse stiffness of muscle fibers (Boriek *et al.* 2001). Moreover, both in desmin KO mice as well as in desmin-deficient human airway smooth muscle cells (ASMCs) desmin was shown to have an anti-hypertrophic role necessary for ASMC homoeostasis; this was also confirmed *in vivo* in mice. The Erk1/2/Egr-1/microRNA-26a (miR-26a)/GSK3β pathway has been revealed to be induced upon desmin KO in which miR-26a targets the GSK3β gene (Mohamed *et al.* 2011). Upon depletion of desmin, miR-26a is upregulated, inhibits protein expression of GSK3β followed by an increase of global cellular protein synthesis. As a result, hypertrophic marker proteins (α-actin, smooth muscle myosin heavy chain, transgelin SM22) are upregulated, initiating ASMC hypertrophy. In a follow-up study, the ankyrin repeat protein 1 (Ankrd1) directly binding desmin has been identified as upregulated in human ASMCs upon siRNA-mediated knockdown of desmin, involving the Akt/NFκB pathway (Mohamed & Boriek 2012).

Asthma is a chronic lung disease characterized by abnormal ASMCs leading to defects in the airway smooth muscle contraction and in airway remodelling, inflammation and hyperresponsiveness (Sferrazza Papa *et al.* 2014). Bronchial biopsies of asthmatic patients show a negative correlation between desmin expression and airway hyperresponsiveness, further supporting the indispensable role of desmin in airway smooth muscle (Slats *et al.* 2008).
The most prominent pathologic change in the airways of asthma patients is an increased smooth muscle mass. GSK3β has been clearly implicated in airway smooth muscle hypertrophy also in a desmin-unrelated manner (Deng *et al.* 2008). The inhibition of anti-hypertrophic GSK3β-mediated eukaryotic translation initiation factor 2Bε (eIF2Bε) phosphorylation contributes to airway smooth muscle hypertrophy.

To date, the physical association of mitochondria with IFs has not been completely unraveled, but is thought to be indirect involving desmoplakin (Fig. 45). Desmoplakin is an adaptor protein linking keratin and desmin IFs to the plasma membrane-associated desmosomal plaque on the intracellular site of a desmosome. The assembly of desmosomes is GSK3β-dependent and coimmunoprecipitation indeed proved a direct interaction between desmoplakin and GSK3β, further supported by colocalisation (Albrecht *et al.* 2015). Ser2849 of desmoplakin is phosphorylated by GSK3β, while the same site was previously demonstrated to be essential for desmoplakin-IF interaction. Based on the link between GSK3β, desmin and desmoplakin, and all three proteins being down-regulated upon GSKIP depletion in lungs GSKIP may be involved in the interplay of mitochondria and IFs.

Desminopathy-related desmin mutations reduce GSK3-mediated phosphorylation of the autophagy receptor NBR1 (acting as receptor for autophagosomal degradation of ubiquitinated targets) at Thr586, a phosphorylation event which reduces desmin-dependent protein aggregation (due to inhibition of aggregate formation) and stabilizes ubiquitinated proteins. In a physiological context, this study uncovered a strong decrease of GSK3-dependent NBR1 phosphorylation correlating with the severity of protein aggregation in muscles of patients suffering from muscle proteinopathy (Nicot *et al.* 2014).

In order to analyse whether desmin and PKA- or GSK3-dependent pathways and/or mitochondrial proteins are connected, a predictive online tool was used called STRING (Search Tool for the Retrieval of interacting Genes/Proteins). Known interaction partners of desmin, visualized by STRING, are presented in Fig. 46. Desmin interacts with different myosin and troponin isoforms, tropomyosin 1α, titin as well as actinin 2α, key regulator proteins in muscle structure and contraction. Hence, upon loss of GSKIP muscle defects are

potentially observable, may have a physiological relevance and should be considered in future studies. However, mitochondrial proteins or key proteins of PKA- and/or GSK3-mediated signalling cascades were not present in the *Mus musculus* desmin interactome (Fig. 46).

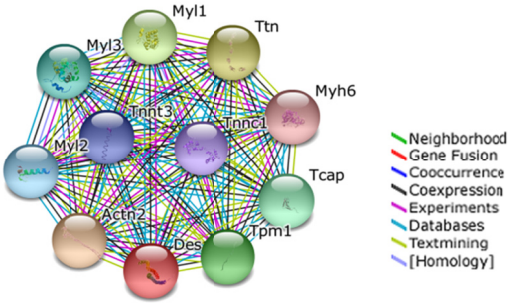

Fig. 46: **STRING protein association network of mouse DESMIN** (2015.06.29). Evidence view: Different line colours represent the types of evidence for the association. Interactions include direct (physical) and indirect (functional) associations; they are derived from four sources: high-throughput experiments, genomic context, previous knowledge and co-expression. Myl 1, 2, 3: myosin light polypeptide 1, 2, 3; Myh6: Myosin heavy polypeptide 6; Des: Desmin; Ttn: Titin; Tcap: Titin-cap assembly protein; Tpm: Tropomyosin; Actn2: Actinin alpha 2; Tnnc1/Tnnt3: Troponin C, Troponin T3.

6.5 GSKIP protein association networks and their evaluation by omics approaches

Using prediction tools, known and potential association networks of protein-protein-interactions can be predicted and databases searched for new connections. The STRING tool was used in order to screen literature for GSKIP-related interactions and relate them to results obtained during this thesis work. The database uses different experimental as well as literature-based information to predict functional networks and interaction partners. The *Mus musculus* GSKIP search yielded direct and indirect interaction partners, listed in Tab. 30 and illustrated in Fig. 47.

In a next step, microarray data and proteomics results were searched for evidence to confirm any of the displayed connections and to study potential GSKIP-dependent effects. However, during this PhD thesis only GSKIP/GSK3β associations were confirmed.

Neither Cadherin-2 (N-Cadherin), nor Cadherin-4 were accurately detected in proteomics (of note, Cadherin-1 (E-Cadherin) was detected to be unchanged in E18.5 lungs upon GSKIP KO). Protein phosphatase 1 regulatory subunit 1l (Ppp1r1l), yrdC domain containing (YrdC) protein, Phf1, Mbd3l1, and Zfp710 were also not identified in proteomics. Bag1 protein abundance was reduced by 10 % in GSKIP KO lungs compared to controls (Suppl. Tab. 7). The measurement of GSK3α was invalid and GSK3β showed a (0.75-fold) reduced protein abundance in GSKIP-deficient lungs (by proteomics as well as Western blot).

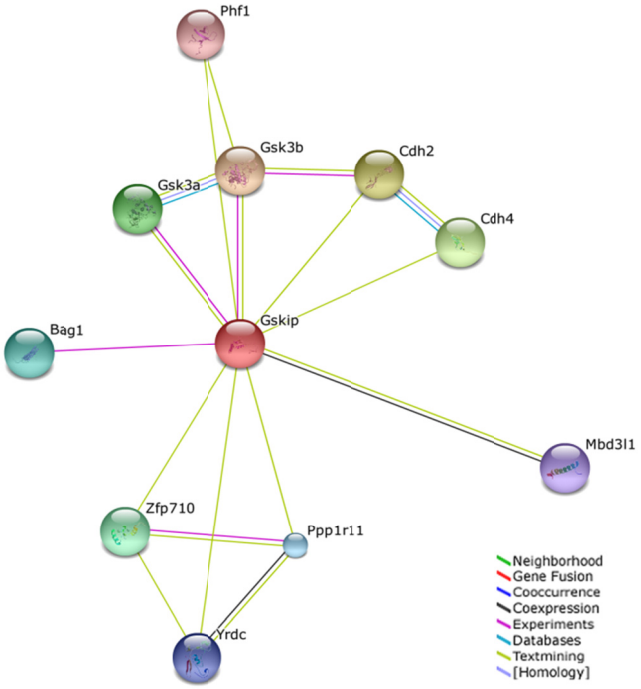

Fig. 47: **Direct (physical) and indirect (functional) association network of predicted interaction partners for mouse GSKIP.** RIKEN cDNA 4933433P14 gene was screened for known and predicted protein-protein-interactions and yielded, according to STRING database, a network comprising 10 proteins. Predicted functional partners are shown as listed in Tab. 30. The database integrates interaction data from previous publications, high-throughput experiments, co-expression studies and from genomic content (2015.06.29, Evidence view). For abbreviations, see Tab. 30.

Tab. 30: **Predictive STRING tool results regarding protein-protein interactions and indirect associations for mouse GSKIP.**

	Predicted Functional Partners (STRING) of mouse GSKIP
Gsk3b	Glycogen synthase kinase 3 beta; Constitutively active protein kinase
Cdh2	Cadherin 2
Cdh4	Cadherin 4
Gsk3a	Glycogen synthase kinase 3 alpha
Zfp710	Zinc finger protein 710
Bag1	BCL2-associated athanogene 1
Ppp1r11	Protein phosphatase 1, regulatory (inhibitor) subunit 11; Inhibitor of protein phosphatase 1
Yrdc	YrdC domain containing (E.coli)
Mbd3l1	Methyl-CpG binding domain protein 3-like 1; Transcriptional repressor
Phf1	PHD finger protein 1; Polycomb group (PcG) that specifically binds histone H3

In addition, none of the genes coding for the above listed proteins (Tab. 30) showed GSKIP-dependent alterations on the genome-wide expression array.

Noteworthy, the value of omics approaches using entire tissues, comprised of several different cell types, is rather limited and causes difficulties as the detection of cell type-specific changes which do not affect all cells within an organ are possibly overlooked. Hence, for future experiments the focus on one specific cell type may be more appropriate, especially when aiming to elucidate molecular pathways. For example, one of the large-scale approaches could be repeated with isolated cell populations derived from GSKIP-deficient and GSKIP WT lung tissue to narrow down the effects of GSKIP depletion to smooth muscle fibroblasts or type 1 and 2 AECs.

7. Outlook

The conducted analyses proved that *in vivo* in mice the expression levels of several proteins targeted either by GSK3β- and/or PKA are not altered upon the loss of GSKIP. Hence, one would expect changes regarding activities and/or subcellular distribution, which do not influence protein abundance.
Even though progress has been made towards defining GSKIP´s function in a physiological context, many questions remained unanswered. Some aspects, pathways and techniques to consider in future projects are described in the following section.

7.1 GSKIP´s role in the miR-26a/GSK3β pathway

As discussed in 6.4.3, airway smooth muscle hypertrophy involves desmin and is regulated by the Erk1/2/Egr-1/miR-26a/GSK3β signalling cascade. Hypertrophic markers were shown to be upregulated when desmin is depleted in ASMCs. By later studies, the involvement of the Akt/NFκB pathway in ASMC hypertrophy was additionally determined.
In this thesis, a major 22-fold increase of *Nppa* gene expression was identified in the large-scale microarray (but not reproducibly detected by RTqPCR). Akt phosphorylation was not observed to be GSKIP-dependently altered in mice (Fig. 33). Proteins of the NFκB pathway were not assessed during the PhD thesis. Taken together own observations and the current literature, it might be worth studying the role of GSKIP in GSK3β-dependent hypertrophic signalling, for example in GSKIP KO MEFs or siRNA-treated human ASMCs. In addition, a potential ASMC hypertrophy induced upon the deletion of GSKIP in mouse lung should be addressed.

7.2 GSKIP´s involvement in interferon signalling

Interferon (IFN) binding to its receptor activates the Janus kinase (JAK)/ Signal transducer and activator of transcription (STAT) pathway leading to an increased transcription of IFN-responsive genes such as IRF7 upon binding of phospho-STAT proteins to the corresponding gene promoters in the nucleus (Ivashkiv & Donlin 2014). The IFN response has an activating function in the adaptive immune system, promoting the development of T and B cell responses. In addition, Wang *et al.* discovered in dendritic cells that upon IFN-β the PI3K/Akt pathway is activated, resulting in the Akt1-mediated suppression of GSK3β (Wang *et al.* 2011). GSK3β in turn is linked to IRF7 *via* cAMP responsive element binding (CREB): GSK3β mediates the Ser133 phosphorylation of CREB.

IFN response genes (amongst others *Irf7*) showed alterations upon GSKIP KO in E18.5 mouse tissues on the large-scale microarray. Initial experiments showed decreased IRF7 protein expression in the absence of GSKIP upon IFN stimulation in several cell lines (HEK293, Jurkat, MEF), but not under resting conditions (PhD project A. Dema). However, IRF7 levels in the unstimulated condition in cells might be comparable to those in E18.5 mouse tissues; *Irf7* gene expression was downregulated on the microarray in GSKIP KO tissue, but was not apparently altered on protein level. In all above-mentioned cells, IRF7 protein expression changes were exclusively detected upon IFN stimulation switching on the type 1 IFN response, pointing out that the IFN signalling cascade might only be GSKIP-dependently regulated upon its prior activation; the effect of GSKIP is only profound if IFN response is turned on.

Of note, CREB serves as a substrate for PKA and CREB1 KO die immediately after birth from respiratory distress (a phenotype resembling the GSKIP KO phenotype characterized during this PhD project), additionally displaying impaired fetal T cell development (Rudolph *et al.* 1998). Hence, GSKIP might be a potential player in IFN signalling. T cell function upon GSKIP KO should be addressed in future studies, including primary immune cells generated from GSKIP KO mice. IFN signalling is also involved both in

COPD and asthma (Caramori *et al.* 2014; Dima *et al.* 2015), possibly connecting the observed cytoskeletal changes in GSKIP-deficient lung smooth muscle with altered IFN responses.

7.3 Lipid profiling of GSKIP-deficient membranes in lung cells

Profound mitochondrial damage, in line with robust metabolic alterations and specific protein expression changes related to mitochondrial as well as cytosolic proteins, was observed in GSKIP-deficient lungs after exposure to air at E18.5. In addition, membrane disorganization such as cristae staple disarrangements within the mitochondria and mitochondrial outer membrane disturbances were visible, potentially responsible for the swollen, roundish shape and ultimate burst of mitochondria upon the respiratory distress GSKIP-deficient mice suffered from. Whether this occurs as a primary or secondary effect is unclear. Mitochondrial membranes differ from other cellular membranes as they contain cardiolipin (CL) (Li *et al.* 2015) which is involved in mitochondrial bioenergetics as well as in mitochondrial fission. It is responsible for stabilizing and adhering to respiratory chain proteins, including the complexes I, III and IV and the ATP synthase (Paradies *et al.* 2004; Camberg *et al.* 2007; Petrosillo *et al.* 2013). Moreover, CL is obligatory for anchoring the oxidative phosphorylation proteins (Haines & Dencher 2002). CL and some mitochondrial lipids are assembled within the mitochondrium while others are imported from the cytosol (assembled in the endoplasmic reticulum). CL can either be remodeled or *de novo* synthesized originating from phosphatidic acid (Hatch 1998; Schlame *et al.* 2000). The enzymes involved were not identified in the proteomics measurement conducted during this thesis work; nonetheless enzyme expressions and/or activities may be changed upon GSKIP depletion in E18.5 lungs. Overall, fatty acid, lipid and phospholipid composition of membranes might be affected by GSKIP deficiency. Thus lipid / phospholipid profiling of GSKIP-deficient mitochondria might shed light into GSKIP-related mitochondrial lipid changes underlying the observed mitochondrial defect, as to date GSKIP-dependent protein changes do not entirely allow for an adequate explanation of the lung phenotype.

7.4 Generation of adult inducible GSKIP knockout mice

In order to overcome the observed perinatal lethality of the conditional GSKIP KO, two adult inducible GSKIP KO mice were established (during this PhD project) as tools for future investigations regarding GSKIP´s function in an adult organism independent of its function in development.
For this, two different inducible Cre recombinases were integrated into the genome of $GSKIP^{flx/flx}$ animals to generate on the one hand cardiomyocyte-specific GSKIP KO animals (α-MHC-MerCreMer GSKIP mice) and on the other hand tissue-unrestricted GSKIP KO animals (UBC-CreERT2 GSKIP mice) (Fig. 48). As inducible systems, both KO models are activated by intraperitoneal injection of tamoxifen which binds cytosolic UBC Cre or MerCreMer respectively, thus inducing Cre translocation to the nucleus followed by homologous recombination leading to the depletion of Exon 2 of GSKIP within 4-8 weeks. Hence, the KO of GSKIP can be induced in adult individuals upon i.p. injection at the desired age. For details, see Methods 4.2.1.2.2.

These adult inducible GSKIP KO systems can be used to distinguish the role of GSKIP in development from those in an adult organism. Inducible adult KO models have not been published so far for PKA or GSK3; however, the heart-specific KO of PKA RIα subunit (α-MHC-PKARIα-KO) exhibits marked thinning of ventricular walls, reduced cardiomyocyte proliferation and die at E11.5 due to poor cardiac contraction and heart failure (Yin *et al.* 2008a); a heart-specific KO of PKA RIIα/β subunit has not been reported yet. Additionally, α-MHC-PKAC transgenic mice with constitutively active PKA C subunits develop dilated cardiomyopathy with reduced cardiac contractility, arrhythmias, and susceptibility to sudden death (Antos *et al.* 2001). As the dysregulation of PKA has an obvious effect in cardiac tissue, it is likely that the heart-

specific α-MHC-MerCreMer-GSKIP KO model (Fig. 48 B) might exhibit a similar cardiac phenotype if GSKIP´s function as an AKAP indeed dominates over GSKIP´s other, AKAP-unrelated functions in a physiological context. However, the above-mentioned mouse models (α-MHC-PKAC KO; α-MHC-PKARIα-KO) rather relate to the proteins function in development as they are based on mouse models with an early onset of the KO already at zygote stage, in contrast to the generated inducible heart-specific models were the gene KO is initiated in adult age when development is completed. Thus, the predictive value of the above-discussed PKA subunit KO mice is very limited for a hypothetical function of GSKIP in adults. In addition, GSK3 heart-specific KO animals have not been studied at all so far.

In the generated inducible, tissue-unrestricted UBC-CreERT2-GSKIP KO mouse, neither PKA, nor GSK3β can be tethered by GSKIP after efficient gene KO is achieved. However, due to the ubiquitous expression of GSKIP, knocking out GSKIP in adult mice in all organs (Fig. 48 A) may be lethal.

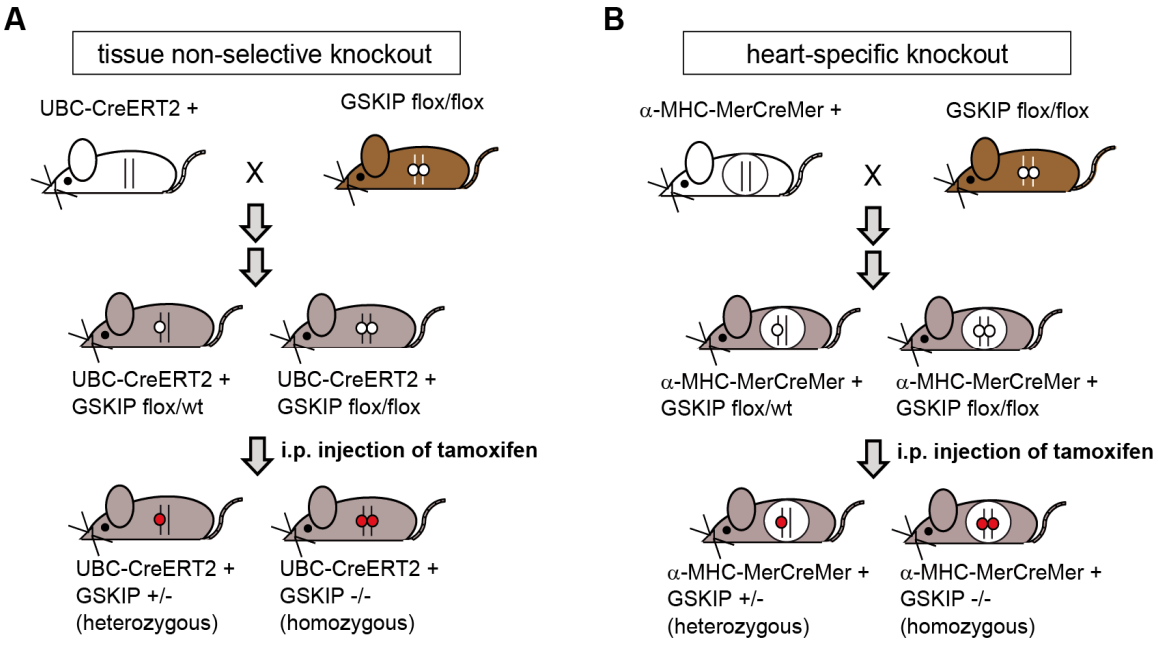

Fig. 48: **Inducible adult GSKIP KO mouse models generated for future evaluation of GSKIP´s physiological role independent of development.** The Cre/loxP system and tissue-specific, tamoxifen-inducible Cre-ERT2 constructs were utilized. For details, see text and Methods 4.2.1.2.2. Breeding schemes for A) ubiquitous adult inducible GSKIP KO mice, and B) adult inducible cardiac muscle-specific GSKIP KO mice are shown. UBC-CreERT2: ubiquitous tamoxifen-inducible Cre recombinase. α-MHC-MerCreMer: tamoxifen-inducible Cre recombinase restricted to cardiac muscle.

Adult heterozygous GSKIP KO mice, the model studied in the beginning of this thesis, may possibly serve as a help when narrowing down the physiological function of GSKIP in mitochondrial stability. Albeit heterozygous adult GSKIP KO animals lack an apparent phenotype and compensate for the heterozygous loss of GSKIP on protein level, they might be of value for mitochondrial analysis. As mitochondria are inherited by the mother, female heterozygous GSKIP KO animals may display (or acquire during their life) compromised mitochondrial function which they pass on to the next generation.

7.5 *In Situ* Hybridization as a promising tool to define the expression of GSKIP during development, cleft palate formation and bone ossification

Digoxigenin-labeled *in situ* hybridization (ISH) probes have been designed and amplified (targeted against GSKIP, FRAT2 and RGS1 mRNA) and should enable first ISH experiments to define the specific expression of GSKIP within the embryo at different embryonic stages as well as within entire tissues. Antibodies

recognizing GSKIP repeatedly failed to yield specific signals in immunofluorescence studies, both in mouse tissue and cells. Hence, detection of GSKIP mRNA *via* ISH will help to determine GSKIP´s expression profile in specific cell populations within tissues. The establishment of GSKIP expression patterns at different developmental stages will help to define expression hot spots as well as overlaps with GSK3β and PKA mRNA expression patterns along development.

Moreover, molecular pathways underlying both secondary palate development and ossification are studied extensively by ISH, a popular tool in embryology. As palatal bone development is impaired upon GSKIP deficiency in conditional KO mice, using ISH will help to directly correlate newly obtained results with published data from literature and to pinpoint relevant pathways to have a deeper look at. Whole embryo sections and coronal sections of the skull and/or jaw would be suitable to detect GSKIP e.g. along the midepithelial seam between the two lateral secondary palates that fail to fuse and show an ossification delay upon GSKIP KO at E18.5. The molecular processes underlying secondary palate development and fusion are well-established: GSK3β and Sonic/ Indian hedgehog (Shh/ Ihh) are involved (discussed in 6.1) and might thus be linked to GSKIP using ISH probes to define the function of the GSK3/Shh/GSKIP interplay for embryonic palate development and ossification.

7.6 Value of primary MEFs for elucidation of GSKIP´s role in cell proliferation and mitochondrial morphology and function

The generation of a primary GSKIP-depleted cell system has been established and serves as a tool to study *in vivo* the consequences of GSKIP KO, e.g. to analyze molecular mechanisms of cell differentiation and mitochondrial fusion/ fission processes. Recent work identified the ability of MEFs to differentiate into three different mesenchymal lineages, namely into adipogenic, chondrogenic and osteogenic lineages expressing typical differentiation markers (Dastagir *et al.* 2014). These findings suggest the future use of MEFs for studying signal transduction underlying ossification and cleft palate formation representing processes impaired upon GSKIP KO.

8. References

Adamson, I.Y. & Bowden, D.H. (1975). Derivation of type 1 epithelium from type 2 cells in the developing rat lung. *Laboratory investigation; a journal of technical methods and pathology*, 32, 736-745.

Ahmad, F., Lal, H., Zhou, J., Vagnozzi, R.J., Yu, J.E., Shang, X. *et al.* (2014). Cardiomyocyte-specific deletion of Gsk3alpha mitigates post-myocardial infarction remodeling, contractile dysfunction, and heart failure. *Journal of the American College of Cardiology*, 64, 696-706.

Akella, A. & Deshpande, S.B. (2013). Pulmonary surfactants and their role in pathophysiology of lung disorders. *Indian journal of experimental biology*, 51, 5-22.

Akinbi, H.T., Breslin, J.S., Ikegami, M., Iwamoto, H.S., Clark, J.C., Whitsett, J.A. *et al.* (1997). Rescue of SP-B knockout mice with a truncated SP-B proprotein. Function of the C-terminal propeptide. *The Journal of biological chemistry*, 272, 9640-9647.

Albrecht, L.V., Zhang, L., Shabanowitz, J., Purevjav, E., Towbin, J.A., Hunt, D.F. *et al.* (2015). GSK3- and PRMT-1-dependent modifications of desmoplakin control desmoplakin-cytoskeleton dynamics. *The Journal of cell biology*, 208, 597-612.

Alto, N.M., Soderling, J. & Scott, J.D. (2002). Rab32 is an A-kinase anchoring protein and participates in mitochondrial dynamics. *J Cell Biol*, 158, 659-668.

Amieux, P.S., Howe, D.G., Knickerbocker, H., Lee, D.C., Su, T., Laszlo, G.S. *et al.* (2002). Increased basal cAMP-dependent protein kinase activity inhibits the formation of mesoderm-derived structures in the developing mouse embryo. *The Journal of biological chemistry*, 277, 27294-27304.

Andreeva, A.V., Kutuzov, M.A. & Voyno-Yasenetskaya, T.A. (2007). Regulation of surfactant secretion in alveolar type II cells. *American journal of physiology. Lung cellular and molecular physiology*, 293, L259-271.

Antos, C.L., Frey, N., Marx, S.O., Reiken, S., Gaburjakova, M., Richardson, J.A. *et al.* (2001). Dilated cardiomyopathy and sudden death resulting from constitutive activation of protein kinase a. *Circ Res*, 89, 997-1004.

Appert-Collin, A., Baisamy, L. & Diviani, D. (2006). Regulation of g protein-coupled receptor signaling by a-kinase anchoring proteins. *Journal of receptor and signal transduction research*, 26, 631-646.

Aven, L. & Ai, X. (2013). Mechanisms of respiratory innervation during embryonic development. *Organogenesis*, 9, 194-198.

Baillie, G.S. (2009). Compartmentalized signalling: spatial regulation of cAMP by the action of compartmentalized phosphodiesterases. *The FEBS journal*, 276, 1790-1799.

Bauler, T.J., Kamiya, N., Lapinski, P.E., Langewisch, E., Mishina, Y., Wilkinson, J.E. *et al.* (2011). Development of severe skeletal defects in induced SHP-2-deficient adult mice: a model of skeletal malformation in humans with SHP-2 mutations. *Dis Model Mech*, 4, 228-239.

Beaulieu, J.M., Sotnikova, T.D., Yao, W.D., Kockeritz, L., Woodgett, J.R., Gainetdinov, R.R. *et al.* (2004). Lithium antagonizes dopamine-dependent behaviors mediated by an AKT/glycogen synthase kinase 3 signaling cascade. *Proceedings of the National Academy of Sciences of the United States of America*, 101, 5099-5104.

Beaulieu, J.M., Zhang, X., Rodriguiz, R.M., Sotnikova, T.D., Cools, M.J., Wetsel, W.C. *et al.* (2008). Role of GSK3 beta in behavioral abnormalities induced by serotonin deficiency. *Proceedings of the National Academy of Sciences of the United States of America*, 105, 1333-1338.

Bennett, V. & Healy, J. (2009). Membrane domains based on ankyrin and spectrin associated with cell-cell interactions. *Cold Spring Harbor perspectives in biology*, 1, a003012.

Bersudsky, Y., Shaldubina, A., Kozlovsky, N., Woodgett, J.R., Agam, G. & Belmaker, R.H. (2008). Glycogen synthase kinase-3beta heterozygote knockout mice as a model of findings in postmortem schizophrenia brain or as a model of behaviors mimicking lithium action: negative results. *Behavioural pharmacology*, 19, 217-224.

Beurel, E., Grieco, S.F. & Jope, R.S. (2014). Glycogen synthase kinase-3 (GSK3): Regulation, actions, and diseases. *Pharmacology & therapeutics*. Epub ahead of print.

Bhattacharjee, R., Goswami, S., Dudiki, T., Popkie, A.P., Phiel, C.J., Kline, D. *et al.* (2015). Targeted Disruption of Glycogen Synthase Kinase 3a (Gsk3a) Affects Sperm Motility Resulting in Male Infertility. *Biology of reproduction*. Epub ahead of print.

Biel, M. & Michalakis, S. (2009). Cyclic nucleotide-gated channels. *Handbook of experimental pharmacology*, 111-136.

Bijur, G.N. & Jope, R.S. (2003). Glycogen synthase kinase-3 beta is highly activated in nuclei and mitochondria. *Neuroreport*, 14, 2415-2419.

Boriek, A.M., Capetanaki, Y., Hwang, W., Officer, T., Badshah, M., Rodarte, J. *et al.* (2001). Desmin integrates the three-dimensional mechanical properties of muscles. *American journal of physiology. Cell physiology*, 280, C46-52.

Brandon, E.P., Logue, S.F., Adams, M.R., Qi, M., Sullivan, S.P., Matsumoto, A.M. *et al.* (1998). Defective motor behavior and neural gene expression in RIIbeta-protein kinase A mutant mice. *The Journal of neuroscience : the official journal of the Society for Neuroscience*, 18, 3639-3649.

Brandon, E.P., Zhuo, M., Huang, Y.Y., Qi, M., Gerhold, K.A., Burton, K.A. *et al.* (1995). Hippocampal long-term depression and depotentiation are defective in mice carrying a targeted disruption of the gene encoding the RI

beta subunit of cAMP-dependent protein kinase. *Proceedings of the National Academy of Sciences of the United States of America*, 92, 8851-8855.

Brownlees, J., Irving, N.G., Brion, J.P., Gibb, B.J., Wagner, U., Woodgett, J. *et al.* (1997). Tau phosphorylation in transgenic mice expressing glycogen synthase kinase-3beta transgenes. *Neuroreport*, 8, 3251-3255.

Bruystens, J.G., Wu, J., Fortezzo, A., Kornev, A.P., Blumenthal, D.K. & Taylor, S.S. (2014). PKA RIalpha homodimer structure reveals an intermolecular interface with implications for cooperative cAMP binding and Carney complex disease. *Structure*, 22, 59-69.

Burgers, P.P., van der Heyden, M.A., Kok, B., Heck, A.J. & Scholten, A. (2014). A Systematic Evaluation of Protein Kinase A - A-kinase Anchoring Protein Interaction Motifs. *Biochemistry*. Epub ahead of print.

Burnette, W.N. (1981). "Western blotting": electrophoretic transfer of proteins from sodium dodecyl sulfate--polyacrylamide gels to unmodified nitrocellulose and radiographic detection with antibody and radioiodinated protein A. *Analytical biochemistry*, 112, 195-203.

Burton, K.A., Johnson, B.D., Hausken, Z.E., Westenbroek, R.E., Idzerda, R.L., Scheuer, T. *et al.* (1997). Type II regulatory subunits are not required for the anchoring-dependent modulation of Ca2+ channel activity by cAMP-dependent protein kinase. *Proceedings of the National Academy of Sciences of the United States of America*, 94, 11067-11072.

Camberg, J.L., Johnson, T.L., Patrick, M., Abendroth, J., Hol, W.G. & Sandkvist, M. (2007). Synergistic stimulation of EpsE ATP hydrolysis by EpsL and acidic phospholipids. *The EMBO journal*, 26, 19-27.

Canning, B.J. (2006). Reflex regulation of airway smooth muscle tone. *Journal of applied physiology*, 101, 971-985.

Capetanaki, Y., Papathanasiou, S., Diokmetzidou, A., Vatsellas, G. & Tsikitis, M. (2015). Desmin related disease: a matter of cell survival failure. *Current opinion in cell biology*, 32, 113-120.

Capra, G. & Brigger, M.T. (2012). Surgery for velopharyngeal insufficiency. *Advances in oto-rhino-laryngology*, 73, 137-144.

Caramori, G., Adcock, I.M., Di Stefano, A. & Chung, K.F. (2014). Cytokine inhibition in the treatment of COPD. *International journal of chronic obstructive pulmonary disease*, 9, 397-412.

Carnegie, G.K., Soughayer, J., Smith, F.D., Pedroja, B.S., Zhang, F., Diviani, D. *et al.* (2008). AKAP-Lbc mobilizes a cardiac hypertrophy signaling pathway. *Mol Cell*, 32, 169-179.

Carr, D.W. & Newell, A.E. (2007). The role of A-kinase anchoring proteins (AKaps) in regulating sperm function. *Society of Reproduction and Fertility supplement*, 63, 135-141.

Carr, D.W., Stofko-Hahn, R.E., Fraser, I.D., Bishop, S.M., Acott, T.S., Brennan, R.G. *et al.* (1991). Interaction of the regulatory subunit (RII) of cAMP-dependent protein kinase with RII-anchoring proteins occurs through an amphipathic helix binding motif. *The Journal of biological chemistry*, 266, 14188-14192.

Carr, M.J. & Undem, B.J. (2003). Bronchopulmonary afferent nerves. *Respirology*, 8, 291-301.

Chagoyen, M. & Pazos, F. (2013). Tools for the functional interpretation of metabolomic experiments. *Briefings in bioinformatics*, 14, 737-744.

Chandel, N.S. (2014). Mitochondria as signaling organelles. *BMC biology*, 12, 34.

Chen, H., Wild, C., Zhou, X., Ye, N., Cheng, X. & Zhou, J. (2014). Recent advances in the discovery of small molecules targeting exchange proteins directly activated by cAMP (EPAC). *Journal of medicinal chemistry*, 57, 3651-3665.

Chou, H.Y., Howng, S.L., Cheng, T.S., Hsiao, Y.L., Lieu, A.S., Loh, J.K. *et al.* (2006). GSKIP is homologous to the Axin GSK3beta interaction domain and functions as a negative regulator of GSK3beta. *Biochemistry*, 45, 11379-11389.

Chuang, D.T., Ku, L.S. & Cox, R.P. (1982). Biochemical basis of thiamin-responsive maple syrup urine disease. *Transactions of the Association of American Physicians*, 95, 196-204.

Clemen, C.S., Herrmann, H., Strelkov, S.V. & Schroder, R. (2013). Desminopathies: pathology and mechanisms. *Acta neuropathologica*, 125, 47-75.

Clevers, H. & Nusse, R. (2012). Wnt/beta-catenin signaling and disease. *Cell*, 149, 1192-1205.

Conti, M. & Beavo, J. (2007). Biochemistry and physiology of cyclic nucleotide phosphodiesterases: essential components in cyclic nucleotide signaling. *Annual review of biochemistry*, 76, 481-511.

Cooper, D.M. & Tabbasum, V.G. (2014). Adenylate cyclase-centred microdomains. *The Biochemical journal*, 462, 199-213.

Corbin, J.D., Soderling, T.R. & Park, C.R. (1973). Regulation of adenosine 3',5'-monophosphate-dependent protein kinase. I. Preliminary characterization of the adipose tissue enzyme in crude extracts. *The Journal of biological chemistry*, 248, 1813-1821.

Cordes, S.P. (2001). Molecular genetics of cranial nerve development in mouse. *Nature reviews. Neuroscience*, 2, 611-623.

Crapo, J.D., Barry, B.E., Gehr, P., Bachofen, M. & Weibel, E.R. (1982). Cell number and cell characteristics of the normal human lung. *The American review of respiratory disease*, 126, 332-337.

Cruciat, C.M. (2014). Casein kinase 1 and Wnt/beta-catenin signaling. *Current opinion in cell biology*, 31C, 46-55.

Cummings, D.E., Brandon, E.P., Planas, J.V., Motamed, K., Idzerda, R.L. & McKnight, G.S. (1996). Genetically lean mice result from targeted disruption of the RII beta subunit of protein kinase A. *Nature*, 382, 622-626.

Czyzyk, T.A., Sikorski, M.A., Yang, L. & McKnight, G.S. (2008). Disruption of the RIIbeta subunit of PKA reverses the obesity syndrome of Agouti lethal yellow mice. *Proceedings of the National Academy of Sciences of the United States of America*, 105, 276-281.

Da Cruz, S., Parone, P.A., Gonzalo, P., Bienvenut, W.V., Tondera, D., Jourdain, A. *et al.* (2008). SLP-2 interacts with prohibitins in the mitochondrial inner membrane and contributes to their stability. *Biochimica et biophysica acta*, 1783, 904-911.

Dajani, R., Fraser, E., Roe, S.M., Yeo, M., Good, V.M., Thompson, V. *et al.* (2003). Structural basis for recruitment of glycogen synthase kinase 3beta to the axin-APC scaffold complex. *EMBO J*, 22, 494-501.

Dajani, R., Fraser, E., Roe, S.M., Young, N., Good, V., Dale, T.C. *et al.* (2001). Crystal structure of glycogen synthase kinase 3 beta: structural basis for phosphate-primed substrate specificity and autoinhibition. *Cell*, 105, 721-732.

Dastagir, K., Reimers, K., Lazaridis, A., Jahn, S., Maurer, V., Strauss, S. *et al.* (2014). Murine embryonic fibroblast cell lines differentiate into three mesenchymal lineages to different extents: new models to investigate differentiation processes. *Cellular reprogramming*, 16, 241-252.

de Rooij, J., Boenink, N.M., van Triest, M., Cool, R.H., Wittinghofer, A. & Bos, J.L. (1999). PDZ-GEF1, a guanine nucleotide exchange factor specific for Rap1 and Rap2. *The Journal of biological chemistry*, 274, 38125-38130.

de Rooij, J., Rehmann, H., van Triest, M., Cool, R.H., Wittinghofer, A. & Bos, J.L. (2000). Mechanism of regulation of the Epac family of cAMP-dependent RapGEFs. *The Journal of biological chemistry*, 275, 20829-20836.

Deak, V.A. & Klussmann, E. (2015). Pharmacological interference with protein-protein interactions of A-kinase anchoring proteins as a strategy for the treatment of disease. *Current drug targets*. Epub ahead of print.

Deng, H., Dokshin, G.A., Lei, J., Goldsmith, A.M., Bitar, K.N., Fingar, D.C. *et al.* (2008). Inhibition of glycogen synthase kinase-3beta is sufficient for airway smooth muscle hypertrophy. *The Journal of biological chemistry*, 283, 10198-10207.

Desai, T.J., Brownfield, D.G. & Krasnow, M.A. (2014). Alveolar progenitor and stem cells in lung development, renewal and cancer. *Nature*, 507, 190-194.

Dessauer, C.W. (2009). Adenylyl cyclase--A-kinase anchoring protein complexes: the next dimension in cAMP signaling. *Molecular pharmacology*, 76, 935-941.

Di, R.M., Feng, Q.T., Chang, Z., Luan, Q., Zhang, Y.Y., Huang, J. *et al.* (2010). PDK1 plays a critical role in regulating cardiac function in mice and human. *Chin Med J (Engl)*, 123, 2358-2363.

Dima, E., Koltsida, O., Katsaounou, P., Vakali, S., Koutsoukou, A., Koulouris, N.G. *et al.* (2015). Implication of Interleukin (IL)-18 in the pathogenesis of chronic obstructive pulmonary disease (COPD). *Cytokine*, 74, 313-317.

Diodato, D., Ghezzi, D. & Tiranti, V. (2014). The Mitochondrial Aminoacyl tRNA Synthetases: Genes and Syndromes. *International journal of cell biology*, 2014, 787956.

Diviani, D., Maric, D., Perez Lopez, I., Cavin, S. & Del Vescovo, C.D. (2013). A-kinase anchoring proteins: molecular regulators of the cardiac stress response. *Biochimica et biophysica acta*, 1833, 901-908.

Diviani, D., Soderling, J. & Scott, J.D. (2001). AKAP-Lbc anchors protein kinase A and nucleates Galpha 12-selective Rho-mediated stress fiber formation. *The Journal of biological chemistry*, 276, 44247-44257.

Dobbs, L.G., Gonzalez, R., Matthay, M.A., Carter, E.P., Allen, L. & Verkman, A.S. (1998). Highly water-permeable type I alveolar epithelial cells confer high water permeability between the airspace and vasculature in rat lung. *Proceedings of the National Academy of Sciences of the United States of America*, 95, 2991-2996.

Dominguez, I., Itoh, K. & Sokol, S.Y. (1995). Role of glycogen synthase kinase 3 beta as a negative regulator of dorsoventral axis formation in Xenopus embryos. *Proceedings of the National Academy of Sciences of the United States of America*, 92, 8498-8502.

Eom, T.Y. & Jope, R.S. (2009). Blocked inhibitory serine-phosphorylation of glycogen synthase kinase-3alpha/beta impairs in vivo neural precursor cell proliferation. *Biological psychiatry*, 66, 494-502.

Erdogan, D.K.D.P.T. (1995). Visualisation of fetal skeletal system by double staining with Alizarin Red and Alcian Blue. *Gazi Medical Journal*, 55-58.

Ewing, R.M., Chu, P., Elisma, F., Li, H., Taylor, P., Climie, S. *et al.* (2007). Large-scale mapping of human protein-protein interactions by mass spectrometry. *Molecular systems biology*, 3, 89.

Ferguson, M.W. (1988). Palate development. *Development*, 103 Suppl, 41-60.

Flynn, M.P., Maizels, E.T., Karlsson, A.B., McAvoy, T., Ahn, J.H., Nairn, A.C. *et al.* (2008). Luteinizing hormone receptor activation in ovarian granulosa cells promotes protein kinase A-dependent dephosphorylation of microtubule-associated protein 2D. *Molecular endocrinology*, 22, 1695-1710.

Francis, S.H., Blount, M.A. & Corbin, J.D. (2011). Mammalian cyclic nucleotide phosphodiesterases: molecular mechanisms and physiological functions. *Physiological reviews*, 91, 651-690.

Frank, L., Price, L.T. & Whitney, P.L. (1996). Possible mechanism for late gestational development of the antioxidant enzymes in the fetal rat lung. *Biology of the neonate*, 70, 116-127.

Friedel, R.H., Wurst, W., Wefers, B. & Kuhn, R. (2011). Generating conditional knockout mice. *Methods in molecular biology*, 693, 205-231.

Fujino, T., Asaba, H., Kang, M.J., Ikeda, Y., Sone, H., Takada, S. *et al.* (2003). Low-density lipoprotein receptor-related protein 5 (LRP5) is essential for normal cholesterol metabolism and glucose-induced insulin secretion. *Proceedings of the National Academy of Sciences of the United States of America*, 100, 229-234.

Ge, Y., Si, J., Tian, L., Zhuang, S., Dworkin, L.D. & Gong, R. (2011). Conditional ablation of glycogen synthase kinase 3beta in postnatal mouse kidney. *Lab Invest*, 91, 85-96.

Gehlenborg, N., O'Donoghue, S.I., Baliga, N.S., Goesmann, A., Hibbs, M.A., Kitano, H. *et al.* (2010). Visualization of omics data for systems biology. *Nature methods*, 7, S56-68.

Gelman, I.H. (2002). The role of SSeCKS/gravin/AKAP12 scaffolding proteins in the spaciotemporal control of signaling pathways in oncogenesis and development. *Frontiers in bioscience : a journal and virtual library*, 7, d1782-1797.

Gill, G.N. & Garren, L.D. (1970). A cyclic-3',5'-adenosine monophosphate dependent protein kinase from the adrenal cortex: comparison with a cyclic AMP binding protein. *Biochemical and biophysical research communications*, 39, 335-343.

Glasser, S.W., Detmer, E.A., Ikegami, M., Na, C.L., Stahlman, M.T. & Whitsett, J.A. (2003). Pneumonitis and emphysema in sp-C gene targeted mice. *The Journal of biological chemistry*, 278, 14291-14298.

Goerke, J. (1998). Pulmonary surfactant: functions and molecular composition. *Biochimica et biophysica acta*, 1408, 79-89.

Gold, M.G., Lygren, B., Dokurno, P., Hoshi, N., McConnachie, G., Tasken, K. *et al.* (2006). Molecular basis of AKAP specificity for PKA regulatory subunits. *Mol Cell*, 24, 383-395.

Goldfarb, L.G. & Dalakas, M.C. (2009). Tragedy in a heartbeat: malfunctioning desmin causes skeletal and cardiac muscle disease. *The Journal of clinical investigation*, 119, 1806-1813.

Gomez-Sintes, R., Hernandez, F., Bortolozzi, A., Artigas, F., Avila, J., Zaratin, P. *et al.* (2007). Neuronal apoptosis and reversible motor deficit in dominant-negative GSK-3 conditional transgenic mice. *The EMBO journal*, 26, 2743-2754.

Gong, Y., Slee, R.B., Fukai, N., Rawadi, G., Roman-Roman, S., Reginato, A.M. *et al.* (2001). LDL receptor-related protein 5 (LRP5) affects bone accrual and eye development. *Cell*, 107, 513-523.

Goss, V., Hunt, A.N. & Postle, A.D. (2013). Regulation of lung surfactant phospholipid synthesis and metabolism. *Biochimica et biophysica acta*, 1831, 448-458.

Gruber, M., Mathew, L.K., Runge, A.C., Garcia, J.A. & Simon, M.C. (2010). EPAS1 Is Required for Spermatogenesis in the Postnatal Mouse Testis. *Biol Reprod*, 82, 1227-1236.

Guyenet, P.G., Stornetta, R.L., Abbott, S.B., Depuy, S.D. & Kanbar, R. (2012). The retrotrapezoid nucleus and breathing. *Advances in experimental medicine and biology*, 758, 115-122.

Haines, T.H. & Dencher, N.A. (2002). Cardiolipin: a proton trap for oxidative phosphorylation. *FEBS letters*, 528, 35-39.

Hall, M.E., Smith, G., Hall, J.E. & Stec, D.E. (2011). Systolic dysfunction in cardiac-specific ligand-inducible MerCreMer transgenic mice. *Am J Physiol Heart Circ Physiol*, 301, H253-260.

Hatch, G.M. (1998). Cardiolipin: biosynthesis, remodeling and trafficking in the heart and mammalian cells (Review). *International journal of molecular medicine*, 1, 33-41.

He, F., Popkie, A.P., Xiong, W., Li, L., Wang, Y., Phiel, C.J. *et al.* (2010). Gsk3beta is required in the epithelium for palatal elevation in mice. *Developmental dynamics : an official publication of the American Association of Anatomists*, 239, 3235-3246.

He, F., Xiong, W., Yu, X., Espinoza-Lewis, R., Liu, C., Gu, S. *et al.* (2008). Wnt5a regulates directional cell migration and cell proliferation via Ror2-mediated noncanonical pathway in mammalian palate development. *Development*, 135, 3871-3879.

Heling, A., Zimmermann, R., Kostin, S., Maeno, Y., Hein, S., Devaux, B. *et al.* (2000). Increased expression of cytoskeletal, linkage, and extracellular proteins in failing human myocardium. *Circulation research*, 86, 846-853.

Henn, V., Edemir, B., Stefan, E., Wiesner, B., Lorenz, D., Theilig, F. *et al.* (2004). Identification of a novel A-kinase anchoring protein 18 isoform and evidence for its role in the vasopressin-induced aquaporin-2 shuttle in renal principal cells. *The Journal of biological chemistry*, 279, 26654-26665.

Herschman, H.R. (1991). Primary response genes induced by growth factors and tumor promoters. *Annual review of biochemistry*, 60, 281-319.

Hillman, N.H., Kallapur, S.G. & Jobe, A.H. (2012). Physiology of transition from intrauterine to extrauterine life. *Clinics in perinatology*, 39, 769-783.

Hino, S., Tanji, C., Nakayama, K.I. & Kikuchi, A. (2005). Phosphorylation of beta-catenin by cyclic AMP-dependent protein kinase stabilizes beta-catenin through inhibition of its ubiquitination. *Molecular and cellular biology*, 25, 9063-9072.

Hoeflich, K.P., Luo, J., Rubie, E.A., Tsao, M.S., Jin, O. & Woodgett, J.R. (2000). Requirement for glycogen synthase kinase-3beta in cell survival and NF-kappaB activation. *Nature*, 406, 86-90.

Hollenhorst, M.I., Richter, K. & Fronius, M. (2011). Ion transport by pulmonary epithelia. *Journal of biomedicine & biotechnology*, 2011, 174306.

Hooper, C., Markevich, V., Plattner, F., Killick, R., Schofield, E., Engel, T. *et al.* (2007). Glycogen synthase kinase-3 inhibition is integral to long-term potentiation. *The European journal of neuroscience*, 25, 81-86.

Houslay, M.D. (2010). Underpinning compartmentalised cAMP signalling through targeted cAMP breakdown. *Trends in biochemical sciences*, 35, 91-100.

Howe, D.G., Wiley, J.C. & McKnight, G.S. (2002). Molecular and behavioral effects of a null mutation in all PKA C beta isoforms. *Molecular and cellular neurosciences*, 20, 515-524.

Huang da, W., Sherman, B.T. & Lempicki, R.A. (2009). Systematic and integrative analysis of large gene lists using DAVID bioinformatics resources. *Nature protocols*, 4, 44-57.

Huang, Y., Roelink, H. & McKnight, G.S. (2002). Protein kinase A deficiency causes axially localized neural tube defects in mice. *The Journal of biological chemistry*, 277, 19889-19896.

Hundsrucker, C. & Klussmann, E. (2008). Direct AKAP-mediated protein-protein interactions as potential drug targets. *Handb Exp Pharmacol*, 483-503.

Hundsrucker, C., Krause, G., Beyermann, M., Prinz, A., Zimmermann, B., Diekmann, O. *et al.* (2006). High-affinity AKAP7delta-protein kinase A interaction yields novel protein kinase A-anchoring disruptor peptides. *Biochem J*, 396, 297-306.

Hundsrucker, C., Skroblin, P., Christian, F., Zenn, H.M., Popara, V., Joshi, M. *et al.* (2010). Glycogen synthase kinase 3beta interaction protein functions as an A-kinase anchoring protein. *The Journal of biological chemistry*, 285, 5507-5521.

Hurley, J.H. (1999). Structure, mechanism, and regulation of mammalian adenylyl cyclase. *The Journal of biological chemistry*, 274, 7599-7602.

Hurst, J.H. & Hooks, S.B. (2009). Regulator of G-protein signaling (RGS) proteins in cancer biology. *Biochem Pharmacol*, 78, 1289-1297.

Imbeaud, S., Graudens, E., Boulanger, V., Barlet, X., Zaborski, P., Eveno, E. *et al.* (2005). Towards standardization of RNA quality assessment using user-independent classifiers of microcapillary electrophoresis traces. *Nucleic acids research*, 33, e56.

Ivashkiv, L.B. & Donlin, L.T. (2014). Regulation of type I interferon responses. *Nature reviews. Immunology*, 14, 36-49.

Jang, H.D., Shin, J.H., Park, D.R., Hong, J.H., Yoon, K., Ko, R. *et al.* (2011). Inactivation of glycogen synthase kinase-3beta is required for osteoclast differentiation. *The Journal of biological chemistry*, 286, 39043-39050.

Jarnaess, E., Ruppelt, A., Stokka, A.J., Lygren, B., Scott, J.D. & Tasken, K. (2008). Dual specificity A-kinase anchoring proteins (AKAPs) contain an additional binding region that enhances targeting of protein kinase A type I. *The Journal of biological chemistry*, 283, 33708-33718.

Jean, J.C., George, E., Kaestner, K.H., Brown, L.A., Spira, A. & Joyce-Brady, M. (2013). Transcription factor Klf4, induced in the lung by oxygen at birth, regulates perinatal fibroblast and myofibroblast differentiation. *PloS one*, 8, e54806.

Jeffery, I.B., Higgins, D.G. & Culhane, A.C. (2006). Comparison and evaluation of methods for generating differentially expressed gene lists from microarray data. *BMC bioinformatics*, 7, 359.

Jones, G.N., Tep, C., Towns, W.H., 2nd, Mihai, G., Tonks, I.D., Kay, G.F. *et al.* (2008). Tissue-specific ablation of Prkar1a causes schwannomas by suppressing neurofibromatosis protein production. *Neoplasia*, 10, 1213-1221.

Jope, R.S. & Johnson, G.V. (2004). The glamour and gloom of glycogen synthase kinase-3. *Trends in biochemical sciences*, 29, 95-102.

Jozefczuk, J., Drews, K. & Adjaye, J. (2012). Preparation of mouse embryonic fibroblast cells suitable for culturing human embryonic and induced pluripotent stem cells. *Journal of visualized experiments : JoVE*.

Juhaszova, M., Zorov, D.B., Kim, S.H., Pepe, S., Fu, Q., Fishbein, K.W. *et al.* (2004). Glycogen synthase kinase-3beta mediates convergence of protection signaling to inhibit the mitochondrial permeability transition pore. *The Journal of clinical investigation*, 113, 1535-1549.

Jung, C.H., Ro, S.H., Cao, J., Otto, N.M. & Kim, D.H. (2010). mTOR regulation of autophagy. *FEBS letters*, 584, 1287-1295.

Juriloff, D.M., Harris, M.J. & Brown, C.J. (2001). Unravelling the complex genetics of cleft lip in the mouse model. *Mammalian genome : official journal of the International Mammalian Genome Society*, 12, 426-435.

Juriloff, D.M., Harris, M.J., Dewell, S.L., Brown, C.J., Mager, D.L., Gagnier, L. *et al.* (2005). Investigations of the genomic region that contains the clf1 mutation, a causal gene in multifactorial cleft lip and palate in mice. *Birth defects research. Part A, Clinical and molecular teratology*, 73, 103-113.

Juriloff, D.M., Harris, M.J. & Mah, D.G. (1996). The clf1 gene maps to a 2- to 3-cM region of distal mouse chromosome 11. *Mammalian genome : official journal of the International Mammalian Genome Society*, 7, 789.

Juriloff, D.M., Harris, M.J., McMahon, A.P., Carroll, T.J. & Lidral, A.C. (2006). Wnt9b is the mutated gene involved in multifactorial nonsyndromic cleft lip with or without cleft palate in A/WySn mice, as confirmed by a genetic complementation test. *Birth defects research. Part A, Clinical and molecular teratology*, 76, 574-579.

Kaidanovich-Beilin, O., Lipina, T.V., Takao, K., van Eede, M., Hattori, S., Laliberte, C. *et al.* (2009). Abnormalities in brain structure and behavior in GSK-3alpha mutant mice. *Molecular brain*, 2, 35.

Kaidanovich-Beilin, O. & Woodgett, J.R. (2011). GSK-3: Functional Insights from Cell Biology and Animal Models. *Front Mol Neurosci*, 4, 40.

Kawasaki, H., Springett, G.M., Mochizuki, N., Toki, S., Nakaya, M., Matsuda, M. *et al.* (1998). A family of cAMP-binding proteins that directly activate Rap1. *Science*, 282, 2275-2279.

Kerkela, R., Kockeritz, L., Macaulay, K., Zhou, J., Doble, B.W., Beahm, C. *et al.* (2008). Deletion of GSK-3beta in mice leads to hypertrophic cardiomyopathy secondary to cardiomyoblast hyperproliferation. *The Journal of clinical investigation*, 118, 3609-3618.

Kim, C., Cheng, C.Y., Saldanha, S.A. & Taylor, S.S. (2007). PKA-I holoenzyme structure reveals a mechanism for cAMP-dependent activation. *Cell*, 130, 1032-1043.

Kim, W., Kim, M. & Jho, E.H. (2013). Wnt/beta-catenin signalling: from plasma membrane to nucleus. *The Biochemical journal*, 450, 9-21.

Kim, W.Y., Wang, X., Wu, Y., Doble, B.W., Patel, S., Woodgett, J.R. *et al.* (2009). GSK-3 is a master regulator of neural progenitor homeostasis. *Nature neuroscience*, 12, 1390-1397.

Kimura, T.E., Merritt, A.J. & Garrod, D.R. (2007). Calcium-independent desmosomes of keratinocytes are hyper-adhesive. *The Journal of investigative dermatology*, 127, 775-781.

Kinderman, F.S., Kim, C., von Daake, S., Ma, Y., Pham, B.Q., Spraggon, G. *et al.* (2006). A dynamic mechanism for AKAP binding to RII isoforms of cAMP-dependent protein kinase. *Mol Cell*, 24, 397-408.

Kirschner, L.S. (2010). PRKAR1A and the evolution of pituitary tumors. *Molecular and cellular endocrinology*, 326, 3-7.

Kirschner, L.S., Kusewitt, D.F., Matyakhina, L., Towns, W.H., 2nd, Carney, J.A., Westphal, H. *et al.* (2005). A mouse model for the Carney complex tumor syndrome develops neoplasia in cyclic AMP-responsive tissues. *Cancer research*, 65, 4506-4514.

Kirschner, L.S., Yin, Z., Jones, G.N. & Mahoney, E. (2009). Mouse models of altered protein kinase A signaling. *Endocr Relat Cancer*, 16, 773-793.

Kockeritz, L., Doble, B., Patel, S. & Woodgett, J.R. (2006). Glycogen synthase kinase-3--an overview of an over-achieving protein kinase. *Current drug targets*, 7, 1377-1388.

Kraemer, A., Rehmann, H.R., Cool, R.H., Theiss, C., de Rooij, J., Bos, J.L. *et al.* (2001). Dynamic interaction of cAMP with the Rap guanine-nucleotide exchange factor Epac1. *Journal of molecular biology*, 306, 1167-1177.

Lal, H., Zhou, J., Ahmad, F., Zaka, R., Vagnozzi, R.J., Decaul, M. *et al.* (2012). Glycogen synthase kinase-3alpha limits ischemic injury, cardiac rupture, post-myocardial infarction remodeling and death. *Circulation*, 125, 65-75.

Latapy, C., Rioux, V., Guitton, M.J. & Beaulieu, J.M. (2012). Selective deletion of forebrain glycogen synthase kinase 3beta reveals a central role in serotonin-sensitive anxiety and social behaviour. *Philosophical transactions of the Royal Society of London. Series B, Biological sciences*, 367, 2460-2474.

Lester, L.B., Langeberg, L.K. & Scott, J.D. (1997). Anchoring of protein kinase A facilitates hormone-mediated insulin secretion. *Proceedings of the National Academy of Sciences of the United States of America*, 94, 14942-14947.

Levi, B., Brugman, S., Wong, V.W., Grova, M., Longaker, M.T. & Wan, D.C. (2011). Palatogenesis: engineering, pathways and pathologies. *Organogenesis*, 7, 242-254.

Li, D.W., Liu, Z.Q., Chen, W., Yao, M. & Li, G.R. (2014). Association of glycogen synthase kinase-3beta with Parkinson's disease (review). *Molecular medicine reports*, 9, 2043-2050.

Li, L., Yuan, H., Weaver, C.D., Mao, J., Farr, G.H., 3rd, Sussman, D.J. *et al.* (1999). Axin and Frat1 interact with dvl and GSK, bridging Dvl to GSK in Wnt-mediated regulation of LEF-1. *EMBO J*, 18, 4233-4240.

Li, X.X., Tsoi, B., Li, Y.F., Kurihara, H. & He, R.R. (2015). Cardiolipin and its different properties in mitophagy and apoptosis. *The journal of histochemistry and cytochemistry : official journal of the Histochemistry Society*, 63, 301-311.

Li, Z., Colucci-Guyon, E., Pincon-Raymond, M., Mericskay, M., Pournin, S., Paulin, D. *et al.* (1996). Cardiovascular lesions and skeletal myopathy in mice lacking desmin. *Developmental biology*, 175, 362-366.

Lin, C.C., Chou, C.H., Howng, S.L., Hsu, C.Y., Hwang, C.C., Wang, C. *et al.* (2009). GSKIP, an inhibitor of GSK3beta, mediates the N-cadherin/beta-catenin pool in the differentiation of SH-SY5Y cells. *Journal of cellular biochemistry*, 108, 1325-1336.

Lisewski, U., Shi, Y., Wrackmeyer, U., Fischer, R., Chen, C., Schirdewan, A. *et al.* (2008). The tight junction protein CAR regulates cardiac conduction and cell-cell communication. *J Exp Med*, 205, 2369-2379.

Liu, K.J., Arron, J.R., Stankunas, K., Crabtree, G.R. & Longaker, M.T. (2007). Chemical rescue of cleft palate and midline defects in conditional GSK-3beta mice. *Nature*, 446, 79-82.

Livak, K.J. & Schmittgen, T.D. (2001). Analysis of relative gene expression data using real-time quantitative PCR and the 2(-Delta Delta C(T)) Method. *Methods*, 25, 402-408.

Loh, J.K., Lin, C.C., Yang, M.C., Chou, C.H., Chen, W.S., Hong, M.C. *et al.* (2015). GSKIP- and GSK3-mediated anchoring strengthens cAMP/PKA/Drp1 axis signaling in the regulation of mitochondrial elongation. *Biochimica et biophysica acta*, 1850, 1796-1807.

Lopez-Rodriguez, E. & Perez-Gil, J. (2014). Structure-function relationships in pulmonary surfactant membranes: from biophysics to therapy. *Biochimica et biophysica acta*, 1838, 1568-1585.

Lucas, J.J., Hernandez, F., Gomez-Ramos, P., Moran, M.A., Hen, R. & Avila, J. (2001). Decreased nuclear beta-catenin, tau hyperphosphorylation and neurodegeneration in GSK-3beta conditional transgenic mice. *The EMBO journal*, 20, 27-39.

Luconi, M., Cantini, G., Baldi, E. & Forti, G. (2011). Role of a-kinase anchoring proteins (AKAPs) in reproduction. *Frontiers in bioscience*, 16, 1315-1330.

Luzzatto, L. & Seneca, E. (2014). G6PD deficiency: a classic example of pharmacogenetics with on-going clinical implications. *British journal of haematology*, 164, 469-480.

Ma, T., Fukuda, N., Song, Y., Matthay, M.A. & Verkman, A.S. (2000). Lung fluid transport in aquaporin-5 knockout mice. *The Journal of clinical investigation*, 105, 93-100.

MacAulay, K., Doble, B.W., Patel, S., Hansotia, T., Sinclair, E.M., Drucker, D.J. *et al.* (2007). Glycogen synthase kinase 3alpha-specific regulation of murine hepatic glycogen metabolism. *Cell metabolism*, 6, 329-337.

Maina, J.N. (2000). Comparative respiratory morphology: themes and principles in the design and construction of the gas exchangers. *The Anatomical record*, 261, 25-44.

Maniscalco, W.M., Wilson, C.M., Gross, I., Gobran, L., Rooney, S.A. & Warshaw, J.B. (1978). Development of glycogen and phospholipid metabolism in fetal and newborn rat lung. *Biochimica et biophysica acta*, 530, 333-346.

Martinez, A., Castro, A., Dorronsoro, I. & Alonso, M. (2002). Glycogen synthase kinase 3 (GSK-3) inhibitors as new promising drugs for diabetes, neurodegeneration, cancer, and inflammation. *Med Res Rev*, 22, 373-384.

Matsuda, T., Zhai, P., Maejima, Y., Hong, C., Gao, S., Tian, B. *et al.* (2008). Distinct roles of GSK-3alpha and GSK-3beta phosphorylation in the heart under pressure overload. *Proceedings of the National Academy of Sciences of the United States of America*, 105, 20900-20905.

Mauban, J.R., O'Donnell, M., Warrier, S., Manni, S. & Bond, M. (2009). AKAP-scaffolding proteins and regulation of cardiac physiology. *Physiology (Bethesda)*, 24, 78-87.

Maurice, D.H., Ke, H., Ahmad, F., Wang, Y., Chung, J. & Manganiello, V.C. (2014). Advances in targeting cyclic nucleotide phosphodiesterases. *Nature reviews. Drug discovery*, 13, 290-314.

Maurin, H., Lechat, B., Dewachter, I., Ris, L., Louis, J.V., Borghgraef, P. *et al.* (2013). Neurological characterization of mice deficient in GSK3alpha highlight pleiotropic physiological functions in cognition and pathological activity as Tau kinase. *Molecular brain*, 6, 27.

McCarthy, D.J. & Smyth, G.K. (2009). Testing significance relative to a fold-change threshold is a TREAT. *Bioinformatics*, 25, 765-771.

McCormick, K. & Baillie, G.S. (2014). Compartmentalisation of second messenger signalling pathways. *Current opinion in genetics & development*, 27, 20-25.

McManus, E.J., Sakamoto, K., Armit, L.J., Ronaldson, L., Shpiro, N., Marquez, R. *et al.* (2005). Role that phosphorylation of GSK3 plays in insulin and Wnt signalling defined by knockin analysis. *The EMBO journal*, 24, 1571-1583.

Miki, K. & Eddy, E.M. (1999). Single amino acids determine specificity of binding of protein kinase A regulatory subunits by protein kinase A anchoring proteins. *J Biol Chem*, 274, 29057-29062.

Miki, T., Miura, T., Hotta, H., Tanno, M., Yano, T., Sato, T. *et al.* (2009). Endoplasmic reticulum stress in diabetic hearts abolishes erythropoietin-induced myocardial protection by impairment of phospho-glycogen synthase kinase-3beta-mediated suppression of mitochondrial permeability transition. *Diabetes*, 58, 2863-2872.

Milner, D.J., Mavroidis, M., Weisleder, N. & Capetanaki, Y. (2000). Desmin cytoskeleton linked to muscle mitochondrial distribution and respiratory function. *The Journal of cell biology*, 150, 1283-1298.

Milner, D.J., Weitzer, G., Tran, D., Bradley, A. & Capetanaki, Y. (1996). Disruption of muscle architecture and myocardial degeneration in mice lacking desmin. *The Journal of cell biology*, 134, 1255-1270.

Miura, T. & Tanno, M. (2012). The mPTP and its regulatory proteins: final common targets of signalling pathways for protection against necrosis. *Cardiovascular research*, 94, 181-189.

Mohamed, J.S. & Boriek, A.M. (2012). Loss of desmin triggers mechanosensitivity and up-regulation of Ankrd1 expression through Akt-NF-kappaB signaling pathway in smooth muscle cells. *FASEB journal : official publication of the Federation of American Societies for Experimental Biology*, 26, 757-765.

Mohamed, J.S., Hajira, A., Li, Z., Paulin, D. & Boriek, A.M. (2011). Desmin regulates airway smooth muscle hypertrophy through early growth-responsive protein-1 and microRNA-26a. *The Journal of biological chemistry*, 286, 43394-43404.

Moratz, C., Hayman, J.R., Gu, H. & Kehrl, J.H. (2004). Abnormal B-cell responses to chemokines, disturbed plasma cell localization, and distorted immune tissue architecture in Rgs1-/- mice. *Mol Cell Biol*, 24, 5767-5775.

Morita, M., Gravel, S.P., Hulea, L., Larsson, O., Pollak, M., St-Pierre, J. *et al.* (2015). mTOR coordinates protein synthesis, mitochondrial activity and proliferation. *Cell cycle*, 14, 473-480.

Myers, A.C. (2007). Electrophysiology of airway nerves. *Current protocols in pharmacology / editorial board, S.J. Enna*, Chapter 11, Unit11 10.

Nelson, E.R., Levi, B., Sorkin, M., James, A.W., Liu, K.J., Quarto, N. *et al.* (2011). Role of GSK-3beta in the osteogenic differentiation of palatal mesenchyme. *PloS one*, 6, e25847.

Newhall, K.J., Cummings, D.E., Nolan, M.A. & McKnight, G.S. (2005). Deletion of the RIIbeta-subunit of protein kinase A decreases body weight and increases energy expenditure in the obese, leptin-deficient ob/ob mouse. *Molecular endocrinology*, 19, 982-991.

Newlon, M.G., Roy, M., Morikis, D., Carr, D.W., Westphal, R., Scott, J.D. *et al.* (2001). A novel mechanism of PKA anchoring revealed by solution structures of anchoring complexes. *The EMBO journal*, 20, 1651-1662.

Newlon, M.G., Roy, M., Morikis, D., Hausken, Z.E., Coghlan, V., Scott, J.D. *et al.* (1999). The molecular basis for protein kinase A anchoring revealed by solution NMR. *Nature structural biology*, 6, 222-227.

Nicot, A.S., Lo Verso, F., Ratti, F., Pilot-Storck, F., Streichenberger, N., Sandri, M. *et al.* (2014). Phosphorylation of NBR1 by GSK3 modulates protein aggregation. *Autophagy*, 10, 1036-1053.

Niehrs, C. (2012). The complex world of WNT receptor signalling. *Nature reviews. Molecular cell biology*, 13, 767-779.

Niinaka, Y., Paku, S., Haga, A., Watanabe, H. & Raz, A. (1998). Expression and secretion of neuroleukin/phosphohexose isomerase/maturation factor as autocrine motility factor by tumor cells. *Cancer research*, 58, 2667-2674.

Nijholt, I.M., Dolga, A.M., Ostroveanu, A., Luiten, P.G., Schmidt, M. & Eisel, U.L. (2008). Neuronal AKAP150 coordinates PKA and Epac-mediated PKB/Akt phosphorylation. *Cellular signalling*, 20, 1715-1724.

Nolan, M.A., Sikorski, M.A. & McKnight, G.S. (2004). The role of uncoupling protein 1 in the metabolism and adiposity of RII beta-protein kinase A-deficient mice. *Molecular endocrinology*, 18, 2302-2311.

O'Brien, W.T., Harper, A.D., Jove, F., Woodgett, J.R., Maretto, S., Piccolo, S. *et al.* (2004). Glycogen synthase kinase-3beta haploinsufficiency mimics the behavioral and molecular effects of lithium. *The Journal of neuroscience : the official journal of the Society for Neuroscience*, 24, 6791-6798.

O'Hare K, H. & Braunschweig, R.J. (1975). The effects of various fixative-buffer combinations on lung fine structure. *The Anatomical record*, 181, 545-559.

O'Hare, K.H. & Sheridan, M.N. (1970). Electron microscopic observations on the morphogenesis of the albino rat lung, with special reference to pulmonary epithelial cells. *The American journal of anatomy*, 127, 181-205.

Oksvold, M.P., Funderud, A., Kvissel, A.K., Skarpen, E., Henanger, H., Huitfeldt, H.S. *et al.* (2008). Epidermal growth factor receptor levels are reduced in mice with targeted disruption of the protein kinase A catalytic subunit. *BMC cell biology*, 9, 16.

Oliveria, S.F., Dell'Acqua, M.L. & Sather, W.A. (2007). AKAP79/150 anchoring of calcineurin controls neuronal L-type Ca2+ channel activity and nuclear signaling. *Neuron*, 55, 261-275.

Omata, N., Chiu, C.T., Moya, P.R., Leng, Y., Wang, Z., Hunsberger, J.G. *et al.* (2011). Lentivirally mediated GSK-3beta silencing in the hippocampal dentate gyrus induces antidepressant-like effects in stressed mice. *The international journal of neuropsychopharmacology / official scientific journal of the Collegium Internationale Neuropsychopharmacologicum*, 14, 711-717.

Osman, C., Merkwirth, C. & Langer, T. (2009). Prohibitins and the functional compartmentalization of mitochondrial membranes. *Journal of cell science*, 122, 3823-3830.

Panagopoulou, P., Davos, C.H., Milner, D.J., Varela, E., Cameron, J., Mann, D.L. *et al.* (2008). Desmin mediates TNF-alpha-induced aggregate formation and intercalated disk reorganization in heart failure. *The Journal of cell biology*, 181, 761-775.

Pansters, N.A., Schols, A.M., Verhees, K.J., de Theije, C.C., Snepvangers, F.J., Kelders, M.C. *et al.* (2015). Muscle-specific GSK-3beta ablation accelerates regeneration of disuse-atrophied skeletal muscle. *Biochimica et biophysica acta*, 1852, 490-506.

Paradies, G., Petrosillo, G., Pistolese, M., Di Venosa, N., Federici, A. & Ruggiero, F.M. (2004). Decrease in mitochondrial complex I activity in ischemic/reperfused rat heart: involvement of reactive oxygen species and cardiolipin. *Circulation research*, 94, 53-59.

Park, S.G., Schimmel, P. & Kim, S. (2008). Aminoacyl tRNA synthetases and their connections to disease. *Proceedings of the National Academy of Sciences of the United States of America*, 105, 11043-11049.

Paulin, D. & Li, Z. (2004). Desmin: a major intermediate filament protein essential for the structural integrity and function of muscle. *Experimental cell research*, 301, 1-7.

Pei, L., Leblanc, M., Barish, G., Atkins, A., Nofsinger, R., Whyte, J. *et al.* (2011). Thyroid hormone receptor repression is linked to type I pneumocyte-associated respiratory distress syndrome. *Nature medicine*, 17, 1466-1472.

Perez Lopez, I., Cariolato, L., Maric, D., Gillet, L., Abriel, H. & Diviani, D. (2013). A-kinase anchoring protein Lbc coordinates a p38 activating signaling complex controlling compensatory cardiac hypertrophy. *Mol Cell Biol*, 33, 2903-2917.

Petrosillo, G., De Benedictis, V., Ruggiero, F.M. & Paradies, G. (2013). Decline in cytochrome c oxidase activity in rat-brain mitochondria with aging. Role of peroxidized cardiolipin and beneficial effect of melatonin. *Journal of bioenergetics and biomembranes*, 45, 431-440.

Pinson, K.I., Brennan, J., Monkley, S., Avery, B.J. & Skarnes, W.C. (2000). An LDL-receptor-related protein mediates Wnt signalling in mice. *Nature*, 407, 535-538.

Podda, M.V. & Grassi, C. (2014). New perspectives in cyclic nucleotide-mediated functions in the CNS: the emerging role of cyclic nucleotide-gated (CNG) channels. *Pflugers Archiv : European journal of physiology*, 466, 1241-1257.

Polter, A., Beurel, E., Yang, S., Garner, R., Song, L., Miller, C.A. *et al.* (2010). Deficiency in the inhibitory serine-phosphorylation of glycogen synthase kinase-3 increases sensitivity to mood disturbances. *Neuropsychopharmacology : official publication of the American College of Neuropsychopharmacology*, 35, 1761-1774.

Ponten, F., Jirstrom, K. & Uhlen, M. (2008). The Human Protein Atlas--a tool for pathology. *The Journal of pathology*, 216, 387-393.

Prickaerts, J., Moechars, D., Cryns, K., Lenaerts, I., van Craenendonck, H., Goris, I. *et al.* (2006). Transgenic mice overexpressing glycogen synthase kinase 3beta: a putative model of hyperactivity and mania. *The Journal of neuroscience : the official journal of the Society for Neuroscience*, 26, 9022-9029.

Qi, M., Zhuo, M., Skalhegg, B.S., Brandon, E.P., Kandel, E.R., McKnight, G.S. *et al.* (1996). Impaired hippocampal plasticity in mice lacking the Cbeta1 catalytic subunit of cAMP-dependent protein kinase. *Proceedings of the National Academy of Sciences of the United States of America*, 93, 1571-1576.

Rajewsky, K., Gu, H., Kuhn, R., Betz, U.A., Muller, W., Roes, J. *et al.* (1996). Conditional gene targeting. *The Journal of clinical investigation*, 98, 600-603.

Rall, T.W. & Sutherland, E.W. (1958). Formation of a cyclic adenine ribonucleotide by tissue particles. *The Journal of biological chemistry*, 232, 1065-1076.

Rao, Y., Fischer, Q.S., Yang, Y., McKnight, G.S., LaRue, A. & Daw, N.W. (2004). Reduced ocular dominance plasticity and long-term potentiation in the developing visual cortex of protein kinase A RII alpha mutant mice. *The European journal of neuroscience*, 20, 837-842.

Rehmann, H., Das, J., Knipscheer, P., Wittinghofer, A. & Bos, J.L. (2006). Structure of the cyclic-AMP-responsive exchange factor Epac2 in its auto-inhibited state. *Nature*, 439, 625-628.

Richardson, M.W., Jadlowsky, J., Didigu, C.A., Doms, R.W. & Riley, J.L. (2012). Kruppel-like factor 2 modulates CCR5 expression and susceptibility to HIV-1 infection. *Journal of immunology*, 189, 3815-3821.

Rickett, G.M. & Kelly, F.J. (1990). Developmental expression of antioxidant enzymes in guinea pig lung and liver. *Development*, 108, 331-336.

Ridge, K.M., Olivera, W.G., Saldias, F., Azzam, Z., Horowitz, S., Rutschman, D.H. *et al.* (2003). Alveolar type 1 cells express the alpha2 Na,K-ATPase, which contributes to lung liquid clearance. *Circulation research*, 92, 453-460.

Ridsdale, R. & Post, M. (2004). Surfactant lipid synthesis and lamellar body formation in glycogen-laden type II cells. *American journal of physiology. Lung cellular and molecular physiology*, 287, L743-751.

Roberts, O.L. & Dart, C. (2014). cAMP signalling in the vasculature: the role of Epac (exchange protein directly activated by cAMP). *Biochemical Society transactions*, 42, 89-97.

Rogner, U.C. & Avner, P. (2003). Congenic mice: cutting tools for complex immune disorders. *Nature reviews. Immunology*, 3, 243-252.

Rudolph, D., Tafuri, A., Gass, P., Hammerling, G.J., Arnold, B. & Schutz, G. (1998). Impaired fetal T cell development and perinatal lethality in mice lacking the cAMP response element binding protein. *Proceedings of the National Academy of Sciences of the United States of America*, 95, 4481-4486.

Ruzankina, Y., Pinzon-Guzman, C., Asare, A., Ong, T., Pontano, L., Cotsarelis, G. *et al.* (2007). Deletion of the developmentally essential gene ATR in adult mice leads to age-related phenotypes and stem cell loss. *Cell Stem Cell*, 1, 113-126.

Salvador, L.M., Flynn, M.P., Avila, J., Reierstad, S., Maizels, E.T., Alam, H. *et al.* (2004). Neuronal microtubule-associated protein 2D is a dual a-kinase anchoring protein expressed in rat ovarian granulosa cells. *The Journal of biological chemistry*, 279, 27621-27632.

Sarbassov, D.D., Guertin, D.A., Ali, S.M. & Sabatini, D.M. (2005). Phosphorylation and regulation of Akt/PKB by the rictor-mTOR complex. *Science*, 307, 1098-1101.

Sarma, G.N., Kinderman, F.S., Kim, C., von Daake, S., Chen, L., Wang, B.C. *et al.* (2010). Structure of D-AKAP2:PKA RI complex: insights into AKAP specificity and selectivity. *Structure*, 18, 155-166.

Schafer, G., Milic, J., Eldahshan, A., Gotz, F., Zuhlke, K., Schillinger, C. *et al.* (2013). Highly functionalized terpyridines as competitive inhibitors of AKAP-PKA interactions. *Angew Chem Int Ed Engl*, 52, 12187-12191.

Schillace, R.V., Voltz, J.W., Sim, A.T., Shenolikar, S. & Scott, J.D. (2001). Multiple interactions within the AKAP220 signaling complex contribute to protein phosphatase 1 regulation. *The Journal of biological chemistry*, 276, 12128-12134.

Schlame, M., Rua, D. & Greenberg, M.L. (2000). The biosynthesis and functional role of cardiolipin. *Progress in lipid research*, 39, 257-288.

Schroeder, A., Mueller, O., Stocker, S., Salowsky, R., Leiber, M., Gassmann, M. *et al.* (2006). The RIN: an RNA integrity number for assigning integrity values to RNA measurements. *BMC molecular biology*, 7, 3.

Scott, J.D., Dessauer, C.W. & Tasken, K. (2013). Creating order from chaos: cellular regulation by kinase anchoring. *Annual review of pharmacology and toxicology*, 53, 187-210.

Sferrazza Papa, G.F., Pellegrino, G.M. & Pellegrino, R. (2014). Asthma and respiratory physiology: putting lung function into perspective. *Respirology*, 19, 960-969.

Shardonofsky, F.R., Capetanaki, Y. & Boriek, A.M. (2006). Desmin modulates lung elastic recoil and airway responsiveness. *American journal of physiology. Lung cellular and molecular physiology*, 290, L890-896.

Sherwood, V. (2015). WNT signaling: an emerging mediator of cancer cell metabolism? *Molecular and cellular biology*, 35, 2-10.

Shetty, N.B., Shetty, S., E, N., D'Souza, R. & Shetty, O. (2014). Management of velopharyngeal defects: a review. *Journal of clinical and diagnostic research : JCDR*, 8, 283-287.

Skalhegg, B.S., Huang, Y., Su, T., Idzerda, R.L., McKnight, G.S. & Burton, K.A. (2002). Mutation of the Calpha subunit of PKA leads to growth retardation and sperm dysfunction. *Molecular endocrinology*, 16, 630-639.

Skroblin, P., Grossmann, S., Schafer, G., Rosenthal, W. & Klussmann, E. (2010). Mechanisms of protein kinase A anchoring. *International review of cell and molecular biology*, 283, 235-330.

Skurat, A.V. & Roach, P.J. (1995). Phosphorylation of sites 3a and 3b (Ser640 and Ser644) in the control of rabbit muscle glycogen synthase. *The Journal of biological chemistry*, 270, 12491-12497.

Slats, A.M., Janssen, K., van Schadewijk, A., van der Plas, D.T., Schot, R., van den Aardweg, J.G. *et al.* (2008). Expression of smooth muscle and extracellular matrix proteins in relation to airway function in asthma. *The Journal of allergy and clinical immunology*, 121, 1196-1202.

Sohal, D.S., Nghiem, M., Crackower, M.A., Witt, S.A., Kimball, T.R., Tymitz, K.M. *et al.* (2001). Temporally regulated and tissue-specific gene manipulations in the adult and embryonic heart using a tamoxifen-inducible Cre protein. *Circ Res*, 89, 20-25.

Song, L., Li, Y., Wang, K., Wang, Y.Z., Molotkov, A., Gao, L. *et al.* (2009). Lrp6-mediated canonical Wnt signaling is required for lip formation and fusion. *Development*, 136, 3161-3171.

Soni, S., Scholten, A., Vos, M.A. & van Veen, T.A. (2014). Anchored protein kinase A signalling in cardiac cellular electrophysiology. *J Cell Mol Med*. Epub ahead of print.

Spittaels, K., Van den Haute, C., Van Dorpe, J., Terwel, D., Vandezande, K., Lasrado, R. *et al.* (2002). Neonatal neuronal overexpression of glycogen synthase kinase-3 beta reduces brain size in transgenic mice. *Neuroscience*, 113, 797-808.

Steinberg, B., Caccamese, J., Jr. & Padwa, B.L. (2012). Cleft and craniofacial surgery. *Journal of oral and maxillofacial surgery : official journal of the American Association of Oral and Maxillofacial Surgeons*, 70, e137-161.

Tanji, C., Yamamoto, H., Yorioka, N., Kohno, N., Kikuchi, K. & Kikuchi, A. (2002). A-kinase anchoring protein AKAP220 binds to glycogen synthase kinase-3beta (GSK-3beta) and mediates protein kinase A-dependent inhibition of GSK-3beta. *The Journal of biological chemistry*, 277, 36955-36961.

Tanno, M., Kuno, A., Ishikawa, S., Miki, T., Kouzu, H., Yano, T. *et al.* (2014). Translocation of glycogen synthase kinase-3beta (GSK-3beta), a trigger of permeability transition, is kinase activity-dependent and mediated by interaction with voltage-dependent anion channel 2 (VDAC2). *The Journal of biological chemistry*, 289, 29285-29296.

Tao, M., Salas, M.L. & Lipmann, F. (1970). Mechanism of activation by adenosine 3':5'-cyclic monophosphate of a protein phosphokinase from rabbit reticulocytes. *Proceedings of the National Academy of Sciences of the United States of America*, 67, 408-414.

Taylor, S.S., Ilouz, R., Zhang, P. & Kornev, A.P. (2012). Assembly of allosteric macromolecular switches: lessons from PKA. *Nature reviews. Molecular cell biology*, 13, 646-658.

Taylor, S.S., Kim, C., Cheng, C.Y., Brown, S.H., Wu, J. & Kannan, N. (2008). Signaling through cAMP and cAMP-dependent protein kinase: diverse strategies for drug design. *Biochimica et biophysica acta*, 1784, 16-26.

Taylor, S.S., Zhang, P., Steichen, J.M., Keshwani, M.M. & Kornev, A.P. (2013). PKA: lessons learned after twenty years. *Biochimica et biophysica acta*, 1834, 1271-1278.

Tokieda, K., Whitsett, J.A., Clark, J.C., Weaver, T.E., Ikeda, K., McConnell, K.B. *et al.* (1997). Pulmonary dysfunction in neonatal SP-B-deficient mice. *The American journal of physiology*, 273, L875-882.

Torgersen, K.M., Aandahl, E.M. & Tasken, K. (2008). Molecular architecture of signal complexes regulating immune cell function. *Handb Exp Pharmacol*, 327-363.

Tran, T., Paz, P., Velichko, S., Cifrese, J., Belur, P., Yamaguchi, K.D. *et al.* (2010). Interferonbeta-1b Induces the Expression of RGS1 a Negative Regulator of G-Protein Signaling. *Int J Cell Biol*, 2010, 529376.

Troger, J., Moutty, M.C., Skroblin, P. & Klussmann, E. (2012). A-kinase anchoring proteins as potential drug targets. *British journal of pharmacology*, 166, 420-433.

Turgeon, B. & Meloche, S. (2009). Interpreting neonatal lethal phenotypes in mouse mutants: insights into gene function and human diseases. *Physiological reviews*, 89, 1-26.

Uhlen, M., Fagerberg, L., Hallstrom, B.M., Lindskog, C., Oksvold, P., Mardinoglu, A. *et al.* (2015). Proteomics. Tissue-based map of the human proteome. *Science*, 347, 1260419.

Urs, N.M., Daigle, T.L. & Caron, M.G. (2011). A dopamine D1 receptor-dependent beta-arrestin signaling complex potentially regulates morphine-induced psychomotor activation but not reward in mice. *Neuropsychopharmacology : official publication of the American College of Neuropsychopharmacology*, 36, 551-558.

van Amerongen, R., Nawijn, M., Franca-Koh, J., Zevenhoven, J., van der Gulden, H., Jonkers, J. *et al.* (2005). Frat is dispensable for canonical Wnt signaling in mammals. *Genes Dev*, 19, 425-430.

van Amerongen, R., Nawijn, M.C., Lambooij, J.P., Proost, N., Jonkers, J. & Berns, A. (2010). Frat oncoproteins act at the crossroad of canonical and noncanonical Wnt-signaling pathways. *Oncogene*, 29, 93-104.

van Amerongen, R., van der Gulden, H., Bleeker, F., Jonkers, J. & Berns, A. (2004). Characterization and functional analysis of the murine Frat2 gene. *J Biol Chem*, 279, 26967-26974.

Venner, T.J., Singh, B. & Gupta, R.S. (1990). Nucleotide sequences and novel structural features of human and Chinese hamster hsp60 (chaperonin) gene families. *DNA and cell biology*, 9, 545-552.

Veugelers, M., Wilkes, D., Burton, K., McDermott, D.A., Song, Y., Goldstein, M.M. *et al.* (2004). Comparative PRKAR1A genotype-phenotype analyses in humans with Carney complex and prkar1a haploinsufficient mice. *Proceedings of the National Academy of Sciences of the United States of America*, 101, 14222-14227.

Vijayaraghavan, S., Goueli, S.A., Davey, M.P. & Carr, D.W. (1997). Protein kinase A-anchoring inhibitor peptides arrest mammalian sperm motility. *The Journal of biological chemistry*, 272, 4747-4752.

Vijayaraghavan, S., Liberty, G.A., Mohan, J., Winfrey, V.P., Olson, G.E. & Carr, D.W. (1999). Isolation and molecular characterization of AKAP110, a novel, sperm-specific protein kinase A-anchoring protein. *Molecular endocrinology*, 13, 705-717.

Vogel, E.R., Britt, R.D., Jr., Trinidad, M.C., Faksh, A., Martin, R.J., MacFarlane, P.M. *et al.* (2015). Perinatal oxygen in the developing lung. *Canadian journal of physiology and pharmacology*, 93, 119-127.

Walsh, D.A., Perkins, J.P. & Krebs, E.G. (1968). An adenosine 3',5'-monophosphate-dependant protein kinase from rabbit skeletal muscle. *The Journal of biological chemistry*, 243, 3763-3765.

Wang, H., Brown, J., Garcia, C.A., Tang, Y., Benakanakere, M.R., Greenway, T. *et al.* (2011). The role of glycogen synthase kinase 3 in regulating IFN-beta-mediated IL-10 production. *Journal of immunology*, 186, 675-684.

Wani, M.A., Conkright, M.D., Jeffries, S., Hughes, M.J. & Lingrel, J.B. (1999a). cDNA isolation, genomic structure, regulation, and chromosomal localization of human lung Kruppel-like factor. *Genomics*, 60, 78-86.

Wani, M.A., Wert, S.E. & Lingrel, J.B. (1999b). Lung Kruppel-like factor, a zinc finger transcription factor, is essential for normal lung development. *The Journal of biological chemistry*, 274, 21180-21185.

Warburton, D., El-Hashash, A., Carraro, G., Tiozzo, C., Sala, F., Rogers, O. *et al.* (2010). Lung organogenesis. *Current topics in developmental biology*, 90, 73-158.

Warburton, D., Schwarz, M., Tefft, D., Flores-Delgado, G., Anderson, K.D. & Cardoso, W.V. (2000). The molecular basis of lung morphogenesis. *Mechanisms of development*, 92, 55-81.

Ward Platt, M. & Deshpande, S. (2005). Metabolic adaptation at birth. *Seminars in fetal & neonatal medicine*, 10, 341-350.

Whitelaw, A.G., Rogers, P.A., Hopkinson, D.A., Gordon, H., Emerson, P.M., Darley, J.H. *et al.* (1979). Congenital haemolytic anaemia resulting from glucose phosphate isomerase deficiency: genetics, clinical picture, and prenatal diagnosis. *Journal of medical genetics*, 16, 189-196.

Winter, D.L., Paulin, D., Mericskay, M. & Li, Z. (2014). Posttranslational modifications of desmin and their implication in biological processes and pathologies. *Histochemistry and cell biology*, 141, 1-16.

Wong, W. & Scott, J.D. (2004). AKAP signalling complexes: focal points in space and time. *Nature reviews. Molecular cell biology*, 5, 959-970.

Wu, J., Brown, S.H., von Daake, S. & Taylor, S.S. (2007). PKA type IIalpha holoenzyme reveals a combinatorial strategy for isoform diversity. *Science*, 318, 274-279.

Xia, J., Psychogios, N., Young, N. & Wishart, D.S. (2009). MetaboAnalyst: a web server for metabolomic data analysis and interpretation. *Nucleic acids research*, 37, W652-660.

Xia, J., Sinelnikov, I.V., Han, B. & Wishart, D.S. (2015). MetaboAnalyst 3.0-making metabolomics more meaningful. *Nucleic acids research*. Epub ahead of print.

Yao, P. & Fox, P.L. (2013). Aminoacyl-tRNA synthetases in medicine and disease. *EMBO molecular medicine*, 5, 332-343.

Yee, M., Buczynski, B.W. & O'Reilly, M.A. (2014). Neonatal hyperoxia stimulates the expansion of alveolar epithelial type II cells. *American journal of respiratory cell and molecular biology*, 50, 757-766.

Yin, Z., Jones, G.N., Towns, W.H., 2nd, Zhang, X., Abel, E.D., Binkley, P.F. *et al.* (2008a). Heart-specific ablation of Prkar1a causes failure of heart development and myxomagenesis. *Circulation*, 117, 1414-1422.

Yin, Z., Williams-Simons, L., Parlow, A.F., Asa, S. & Kirschner, L.S. (2008b). Pituitary-specific knockout of the Carney complex gene Prkar1a leads to pituitary tumorigenesis. *Molecular endocrinology*, 22, 380-387.

Zaccolo, M., Di Benedetto, G., Lissandron, V., Mancuso, L., Terrin, A. & Zamparo, I. (2006). Restricted diffusion of a freely diffusible second messenger: mechanisms underlying compartmentalized cAMP signalling. *Biochemical Society transactions*, 34, 495-497.

Zheng, Q. & Wang, X.J. (2008). GOEAST: a web-based software toolkit for Gene Ontology enrichment analysis. *Nucleic acids research*, 36, W358-363.

Zhou, J., Freeman, T.A., Ahmad, F., Shang, X., Mangano, E., Gao, E. *et al.* (2013). GSK-3alpha is a central regulator of age-related pathologies in mice. *The Journal of clinical investigation*, 123, 1821-1832.

Zhou, J., Lal, H., Chen, X., Shang, X., Song, J., Li, Y. *et al.* (2010). GSK-3alpha directly regulates beta-adrenergic signaling and the response of the heart to hemodynamic stress in mice. *The Journal of clinical investigation*, 120, 2280-2291.

Zhou, T.B. & Qin, Y.H. (2013). Signaling pathways of prohibitin and its role in diseases. *Journal of receptor and signal transduction research*, 33, 28-36.

9. Publication list

Articles

Deák, V.A. & Klussmann, E. (2015). Pharmacological interference with protein-protein interactions of A-kinase anchoring proteins as a strategy for the treatment of disease. *Current drug targets*. Epub ahead of print.

Deák, V.A., Skroblin P., Dittmayer C. , Knobeloch K.P., Bachmann S. & Klussmann, E. (2015). The A-kinase anchoring protein GSKIP regukates GSK3β activity and controls palatal shelf fusion in mice. *Journal of Biological Chemistry*. 2015 Nov 18. doi: 10.1074/jbc.M115.701177.

Dema, A., Perets, E., Schulz, M.S., **Deák, V.A.** and Klussmann, E. (2015). Pharmacological targeting of AKAP-directed compartmentalized cAMP signalling. *Cellular Signalling*. Accepted.

Schröter, M.F., Dema, A., Perets, E., Skroblin, P., Moutty, M.C., **Deák, V.A.**, Birchmeier, W. and Klussmann, E. (2015). The AKAPs GSKIP and AKAP220 regulate distinct pools of GSK3β with different outcomes on Wnt signaling. In Revision.

Oral presentations

Heringsdorf Group Retreat, *June 30-July 2, 2014*
Schmilka Group Retreat, *September 1-4, 2013*
Wendelstorf Group Retreat, *June 10-12, 2013*
Schmilka Group Retreat, *September 2-5, 2012*

Poster presentations

Transcard Joint CMD PhD Retreat 2014, November 26-28, 2014
V. Deák, P. Skroblin, M. Schröter, H. Schulz, N. Hübner, S. Kempa, W. Rosenthal, E. Klussmann.
Determining physiological functions of the A-kinase anchoring protein GSKIP in conditional knockout mice

DZHK (German Centre for Cardiovascular Research) Symposium "Receptors, G proteins and Ca^{2+} signalling in the cardiovascular system", Berlin, Germany, November 20-21, 2014
V. Deák, P. Skroblin, M. Schröter, H. Schulz, N. Hübner, W. Rosenthal, E. Klussmann.
Elucidating physiological functions of the A-kinase anchoring protein GSKIP using conditional knockout mice

"Sciensation" 2013 MDC/FMP joint PhD Retreat, Kremmen, Germany, August 29-31, 2013
V. Deák, P. Skroblin, M. Schröter, E. Perets, W. Rosenthal and E. Klussmann.
Elucidating the physiological function of the A-kinase anchoring protein GSKIP in conditional knockout mice

EMBO/FEBS Summer School "Protein interactions, assemblies and disease", Spetses, Greece, September 16-26, 2013
V. Deák, P. Skroblin, M. Schröter, H. Schulz, N. Hübner, W. Rosenthal, E. Klussmann.
Determining physiological functions of the AKAP GSKIP using *in vivo* mouse models

DGPT 2013, Annual Meeting of the German Society for Pharmacology and Toxicology, Halle, Germany, March 4-7, 2013
V. Deák, P. Skroblin, W. Rosenthal and E. Klussmann.
Defining the physiological function of the A-kinase anchoring protein GSKIP using different GSKIP knockout mouse models

"Sciensation" 2012 MDC/FMP joint PhD Retreat, Liebenwalde, Germany, August 30-September 1, 2012
V. Deák, P. Skroblin, W. Rosenthal, E. Klussmann.
Defining the physiological functions of the A-kinase anchoring protein GSKIP using knockout mice

10. Appendix

10.1 Statistics

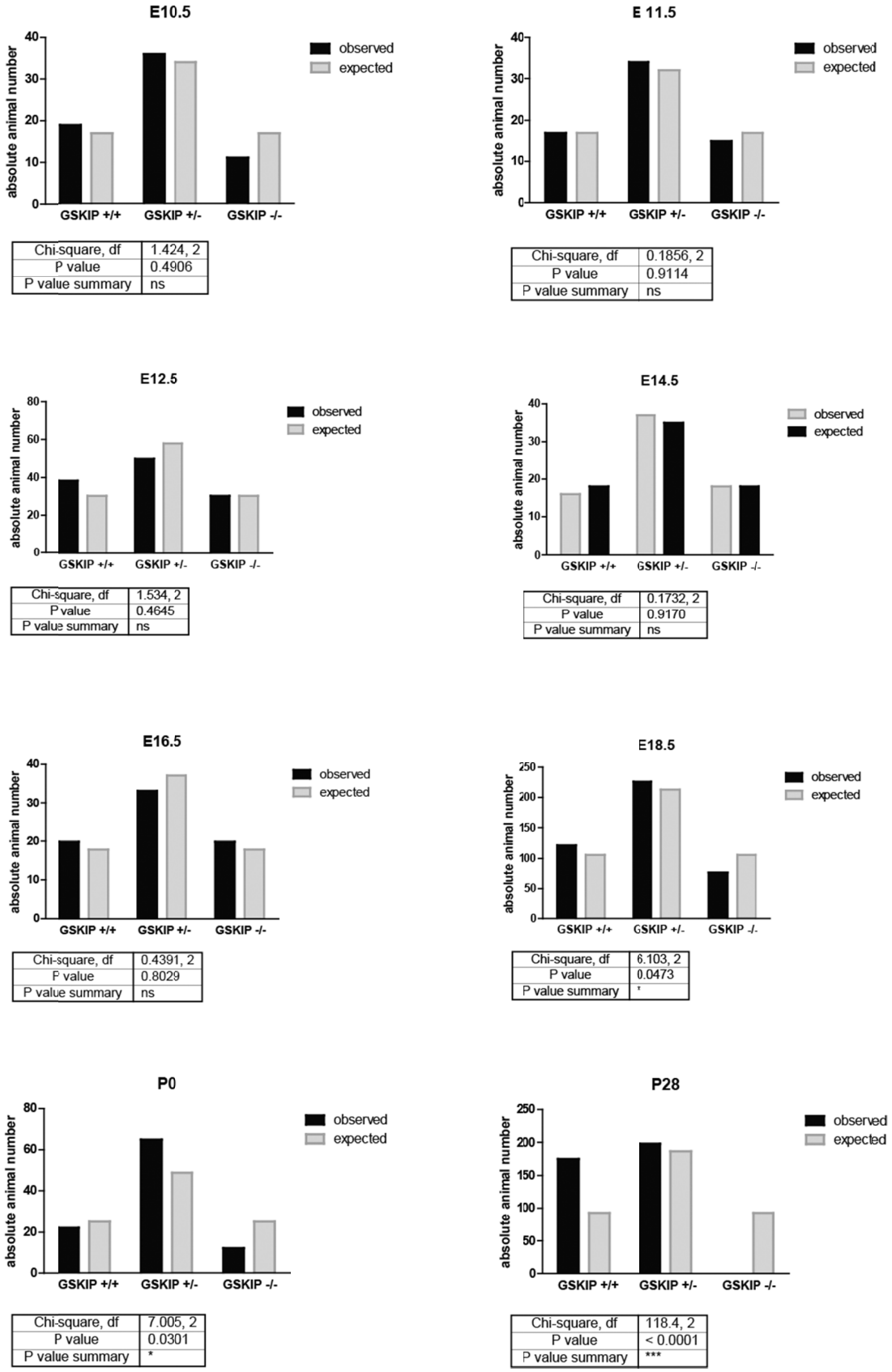

Suppl. Fig. 1: **Offspring genotype distributions of GSKIP$^{+/-}$ intercrosses: Chi square test.** For details refer to embryo analysis (Methods 4.2.1.4; 4.2.1.3 and 5.4).

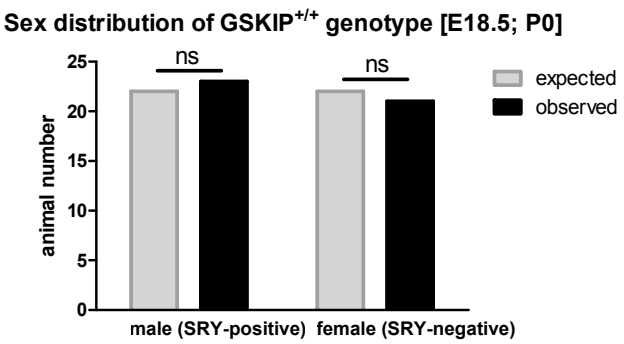

Fisher´s exact test; two-sided

P value	1.0000
P value summary	ns
One- or two-sided	Two-sided

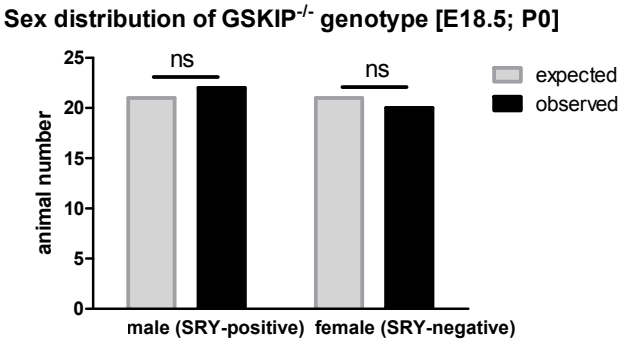

Fisher´s exact test; two-sided

P value	1.0000
P value summary	ns
One- or two-sided	Two-sided

Suppl. Fig. 2: **Sex determination of GSKIP WT and KO E 18.5 and P0 offspring: Fisher´s exact test.** For details, refer to Methods 4.2.1.3 and 5.4.

10.2 Illumina Microarray

10.2.1 Interpretation of microarray statistical evaluation

Statistical evaluation was done in collaboration with H. Schulz. Principal component (PC) #1 illustrates the outstanding expression differences between brain and other internal organs (Suppl. Fig. 3 A; 31% of dataset variance). PC #2 on the other hand describes differences between heart and the other organs of the experiment (Suppl. Fig. 3 A; 16.9% of dataset variance). In PC #3 is driven by lung and liver specific components (Suppl. Fig. 3 B; 13.6% of dataset variance), in PC #4 is driven by the outlier-effect (Suppl. Fig. 3 B; 8.16% of dataset variance), PCs #5 and #6 partially by batch effects (Suppl. Fig. 3 D; 5.7% of dataset variance). As the first 3 PCs suggested the most prominent factor in the ANOVA model is the tissue (Suppl. Fig. 3 E). Nevertheless 498 probes were detected having either a significant knock out or interaction effect. After clustering of tissue effect residuals each time three clusters of general KO up (1, 4, 7) and down (3, 5, 6) regulated probes could be identified (Suppl. Fig. 3 H right). In contrast to cluster 7 which is quite equal expressed in the four tissues other clusters represent probes with different expression differences between tissues (Suppl. Fig. 3 H left): Cluster 1 upregulated in kidney, cluster 2 upregulated in brain, cluster 3 upregulated in heart, cluster 4 down-regulated in brain, cluster 5 upregulated in heart and lung, cluster 6 upregulated in lung. The expression profile of tissue residuals is quite heterogeneous in cluster 2. Accordingly we sub-clustered cluster 2 probes which resulted in a heterogeneous set of tissue effect and KO effect combinations (Suppl. Fig. 3 I).

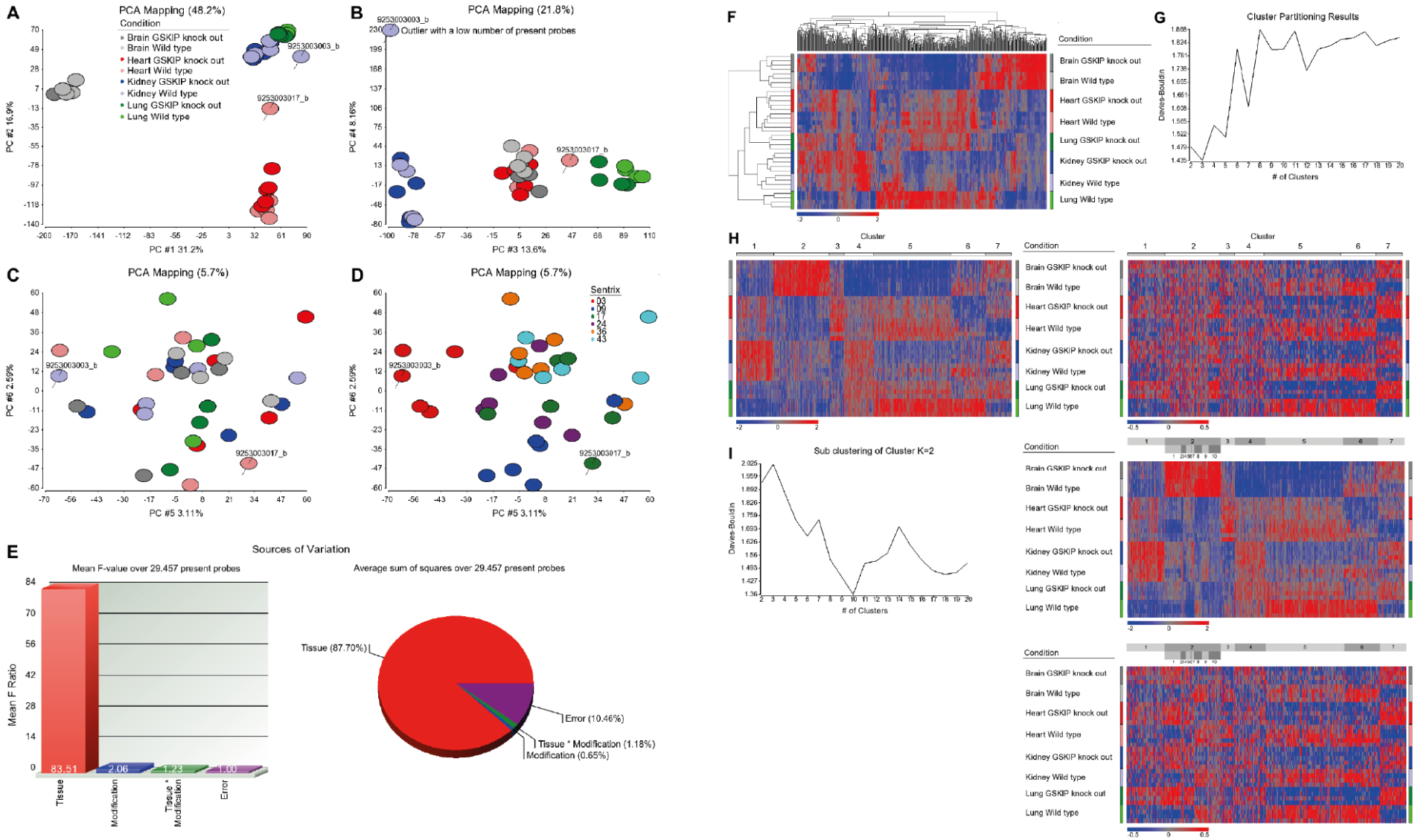

Suppl. Fig. 3: **Statistical evaluation of Illumina Microarray Data** in collaboration with H. Schulz. See text for details.

10.2.2 Raw Data Gene lists for lung tissue

Suppl. Tab. 1: **Complete list of significantly altered genes of the lung before setting threshold and their fold-change compared to WT lung.** n=4. Grey: significant downregulation; Red: significant upregulation. n.d.: not determined.

Symbol (RefSeq)	Fold-change compared to WT	Definition (Ensembl)
Fosb	-6.30119	FBJ osteosarcoma oncogene B (Fosb)
Atf3	-5.22085	activating transcription factor 3 (Atf3)
Fos	-4.40688	FBJ osteosarcoma oncogene (Fos)
Egr1	-3.77137	early growth response 1 (Egr1)
Cyr61	-3.29577	cysteine rich protein 61 (Cyr61)
Axud1	-2.76368	AXIN1 up-regulated 1 (Axud1)
Apold1	-2.67621	PREDICTED: apolipoprotein L domain containing 1 (Apold1)
Car4	-2.65521	carbonic anhydrase 4 (Car4)
Cyr61	-2.62133	cysteine rich protein 61 (Cyr61)
4933433P14Rik	-2.60787	Gsk3b interacting protein (Gskip)
Junb	-2.47836	Jun-B oncogene (Junb)
Myd116	-2.29983	myeloid differentiation primary response gene 116 (Myd116)
LOC100038882	-2.27786	PREDICTED: hypothetical protein LOC100038882 (LOC100038882)
8430403J19Rik	-2.21972	RIKEN cDNA 8430403J19 gene; n.d.
Klf4	-2.20217	Kruppel-like factor 4 (gut) (Klf4)
Tmem49	-2.19802	transmembrane protein 49 (Tmem49)
Dusp1	-2.19385	dual specificity phosphatase 1 (Dusp1)
Sgk1	-2.1353	serum/glucocorticoid regulated kinase 1 (Sgk1)
Rgs1	-2.09591	regulator of G-protein signalling 1 (Rgs1)
Igf2bp3	-2.05146	insulin-like growth factor 2 mRNA binding protein 3
Hist1h1c	-1.98321	histone cluster 1. H1c (Hist1h1c)
2810454F19Rik	-1.92958	RIKEN cDNA 2810454F19 gene; n.d.
Chst1	-1.89155	carbohydrate (keratan sulfate Gal-6) sulfotransferase 1 (Chst1)
4732473B16Rik	-1.87711	RIKEN cDNA 4732473B16 gene (4732473B16Rik)
Ifit3	-1.86564	interferon-induced protein with tetratricopeptide repeats 3 (Ifit3)
Idb2	-1.85529	n.d.
Ifi27	-1.84072	interferon. alpha-inducible protein 27 (Ifi27)
1500001E21Rik	-1.82555	Calmodulin 1/2/3
Tmem100	-1.82497	transmembrane protein 100 (Tmem100)
Klf2	-1.8245	Kruppel-like factor 2 (lung) (Klf2)
Jun	-1.80554	Jun oncogene (Jun)
Cirbp	-1.79042	cold inducible RNA binding protein (Cirbp)
Wfdc1	-1.7672	WAP four-disulfide core domain 1
LOC380706	-1.76573	n.d.
Scel	-1.74476	sciellin (Scel)
9430049I24Rik	-1.74473	RIKEN cDNA 9430049I24 gene; n.d.
Lims2	-1.74321	LIM and senescent cell antigen like domains 2 (Lims2)
8430438E03Rik	-1.74299	RIKEN cDNA 8430438E03 gene; n.d.
Sfrs5	-1.72376	splicing factor. arginine/serine-rich 5 (SRp40. HRS) (Sfrs5). transcript variant 2
Frat2	-1.72276	frequently rearranged in advanced T-cell lymphomas 2 (Frat2)
A130095K04Rik	-1.71319	RIKEN cDNA A130095K04 gene; n.d.
Klf6	-1.69563	Kruppel-like factor 6 (Klf6)
Ccl4	-1.68336	chemokine (C-C motif) ligand 4 (Ccl4)
Gbp3	-1.67891	guanylate nucleotide binding protein 3 (Gbp3)
Trim30	-1.67885	tripartite motif-containing 30 (Trim30)
Per	-1.66273	Period circadian clock (Per)
1500041J02Rik	-1.65933	Coenzyme Q10 homolog B (S. cerevisiae)
Zfp36	-1.64072	zinc finger protein 36 (Zfp36)
Usp18	-1.63689	ubiquitin specific peptidase 18 (Usp18)
LOC100047427	-1.62778	PREDICTED: similar to thyroid hormone receptor (LOC100047427)
H2-Q5	-1.62274	histocompatibility 2. Q region locus 5 (H2-Q5)
Dtna	-1.60172	Dystrobrevin alpha
Lgals3bp	-1.60096	lectin. galactoside-binding. soluble. 3 binding protein (Lgals3bp)
Lamc2	-1.59561	Laminin. gamma 2
Slamf9	-1.58379	SLAM family member 9 (Slamf9)
Gpr146	-1.58029	G protein-coupled receptor 146
LOC638301	-1.57131	PREDICTED: similar to interferon activated gene 204 (LOC638301)
Ldlr	-1.56461	Low density lipoprotein receptor
Ctgf	-1.56215	Connective tissue growth factor
Gbp3	-1.55475	guanylate binding protein 3 (Gbp3)
Irf7	-1.55195	interferon regulatory factor 7 (Irf7)
Sh3rf2	-1.54512	SH3 domain containing ring finger 2 (Sh3rf2)
Spink2	-1.54213	serine peptidase inhibitor. Kazal type 2 (Spink2)
9530077A17Rik	-1.53979	RIKEN cDNA 9530077A17 gene; n.d.
Ifi35	-1.52938	interferon-induced protein 35 (Ifi35)
Amhr2	-1.52235	anti-Mullerian hormone type 2 receptor (Amhr2)
Gpr146	-1.51091	G protein-coupled receptor 146 (Gpr146). transcript variant 2
Sfrs5	-1.50699	splicing factor. arginine/serine-rich 5 (SRp40. HRS) (Sfrs5). transcript variant 1

D14Ertd668e	-1.50449	DNA segment. Chr 14. ERATO Doi 668. expressed (D14Ertd668e)
Ctgf	-1.49627	connective tissue growth factor (Ctgf)
Slco3a1	-1.49575	solute carrier organic anion transporter family. member 3a1 (Slco3a1). transcript variant 1
D14Ertd668e	-1.49519	DNA segment. Chr 14. ERATO Doi 668. expressed (D14Ertd668e)
Frap1	-1.49118	n.d.
2200002D01Rik	-1.48515	RIKEN cDNA 2200002D01 gene; n.d.
Klf9	-1.48114	Kruppel-like factor 9 (Klf9)
Gvin1	-1.47347	GTPase. very large interferon inducible 1 (Gvin1). transcript variant B
Tnfrsf6	-1.47018	n.d.
Hist2h2aa1	-1.46906	histone cluster 2. H2aa1
E130118D18Rik	-1.46098	n.d.
Sp100	-1.45697	Nuclear antigen Sp100
Oas1g	-1.44947	2'-5' oligoadenylate synthetase 1G (Oas1g)
Prdm16	-1.44918	PR domain containing 16 (Prdm16)
Traf6	-1.44759	Tnf receptor-associated factor 6 (Traf6)
Rgs1	-1.4471	regulator of G-protein signalling 1 (Rgs1)
2310051E17Rik	-1.44646	PREDICTED: RIKEN cDNA 2310051E17 gene (2310051E17Rik)
Gna13	-1.44496	Guanine nucleotide binding protein. alpha 13
Trim27	-1.4359	Tripartite motif-containing 27
A530021P12Rik	-1.42823	n.d.
Zfp26	-1.42005	zinc finger protein 26 (Zfp26) XM_974728 XM_977451 XM_977486
Sema3b	-1.41467	Sema domain. immunoglobulin domain (Ig). short basic domain. secreted. (semaphorin) 3B
4732469G06Rik	-1.41201	n.d.
Tinagl1	-1.4082	tubulointerstitial nephritis antigen-like 1 (Tinagl1)
9030607L17Rik	-1.4065	RIKEN cDNA 9030607L17 gene (9030607L17Rik)
2310047C04Rik	-1.40433	n.d.
Chic2	-1.40216	Cysteine-rich hydrophobic domain 2
Tmem49	-1.39486	transmembrane protein 49 (Tmem49)
Klhl15	-1.39471	kelch-like 15 (Drosophila) (Klhl15). transcript variant 3
5730543M03Rik	-1.39205	n.d.
Ly6a	-1.38398	lymphocyte antigen 6 complex. locus A (Ly6a)
Rap1gap	-1.38043	Rap1 GTPase-activating protein (Rap1gap)
Gpm6b	-1.37611	Glycoprotein m6b
Rnf208	-1.37498	ring finger protein 208 (Rnf208)
LOC623121	-1.37493	PREDICTED: similar to Interferon-activatable protein 203 (Ifi-203) (Interferon-inducible protein p203) (LOC623121)
4732458O05Rik	-1.36805	n.d.
4933433P14Rik	-1.36668	RIKEN cDNA 4933433P14 gene (4933433P14Rik)
LOC100044430	-1.36624	PREDICTED: similar to Interferon activated gene 205 (LOC100044430)
Rsdr1-pending	-1.36308	Rsdr1-pending
Cxcl14	-1.35917	Chemokine (C-X-C motif) ligand 14
St6galnac5	-1.35486	ST6 (alpha-N-acetyl-neuraminyl-2.3-beta-galactosyl-1. 3)-N-acetylgalactosaminide alpha-2.6-sialyltransferase 5 (St6galnac5)
Aqp1	-1.35412	aquaporin 1 (Aqp1)
Grpel1	-1.35236	GrpE-like 1. mitochondrial (Grpel1). nuclear gene encoding mitochondrial protein
Mybpc2	-1.34845	myosin binding protein C. fast-type (Mybpc2)
Ptpn14	-1.34359	Protein tyrosine phosphatase. non-receptor type 14
Hspa1a	-1.33862	heat shock protein 1A (Hspa1a)
1810011O10Rik	-1.33822	RIKEN cDNA 1810011O10 gene (1810011O10Rik)
Haghl	-1.33428	hydroxyacylglutathione hydrolase-like (Haghl)
Fdps	-1.33335	farnesyl diphosphate synthetase (Fdps)
Aqp4	-1.33306	aquaporin 4 (Aqp4)
Stat1	-1.33135	signal transducer and activator of transcription 1 (Stat1)
Ank	-1.32962	progressive ankylosis (Ank)
9930016I07Rik	-1.32955	n.d.
Stim2	-1.32941	stromal interaction molecule 2 (Stim2)
Ube1l	-1.31105	ubiquitin-activating enzyme E1-like (Ube1l)
Igf2bp2	-1.3093	insulin-like growth factor 2 mRNA binding protein 2 (Igf2bp2)
Chmp2a	-1.30796	chromatin modifying protein 2A (Chmp2a)
Slc1a1	-1.30289	solute carrier family 1 (neuronal/epithelial high affinity glutamate transporter. system Xag). member 1 (Slc1a1) XM_001002173 XM_001002184 XM_001002198 XM_001002207
Slc25a35	-1.30288	solute carrier family 25. member 35 (Slc25a35)
4930546H06Rik	-1.3025	RIKEN cDNA 4930546H06 gene (4930546H06Rik)
C230084O18Rik	-1.29886	n.d.
Cenpb	-1.29815	centromere protein B (Cenpb)
Pnpla2	-1.2963	patatin-like phospholipase domain containing 2 (Pnpla2)
Fbxo6	-1.29577	F-box protein 6 (Fbxo6)
Vstm2b	-1.29443	V-set and transmembrane domain containing 2B (Vstm2b)
E230024B12Rik	-1.29377	n.d.
Vti1a	-1.29021	Vesicle transport through interaction with t-SNAREs 1A
Fstl3	-1.28506	follistatin-like 3 (Fstl3)
Fbn1	-1.28421	Fibrillin 1
Pla2g12a	-1.28396	Phospholipase A2. group XIIA
Mtf1	-1.28174	Metal response element binding transcription factor 1
1600023H17Rik	-1.27712	n.d.

6430573D20Rik	-1.27709	n.d.
9030607L17Rik	-1.27549	n.d.
Pps	-1.27495	n.d.
Slc23a3	-1.27432	solute carrier family 23 (nucleobase transporters). member 3 (Slc23a3)
Il20rb	-1.27201	interleukin 20 receptor beta (Il20rb). transcript variant 2
Klhl15	-1.27141	kelch-like 15 (Drosophila) (Klhl15). transcript variant 4
Acot10	-1.27014	acyl-CoA thioesterase 10 (Acot10)
Cryab	-1.27009	crystallin. alpha B (Cryab)
Wars	-1.26934	tryptophanyl-tRNA synthetase (Wars)
C230043E16Rik	-1.26914	Lysine (K)-specific demethylase 3A
Adamtsl5	-1.26872	ADAMTS-like 5 (Adamtsl5). transcript variant 2
C330013J21Rik	-1.26717	RIKEN cDNA C330013J21 gene
Zbtb46	-1.26207	zinc finger and BTB domain containing 46 (Zbtb46)
Hist2h2aa1	-1.2615	histone cluster 2. H2aa1 (Hist2h2aa1)
Myo5b	-1.25572	myosin Vb (Myo5b)
Parp12	-1.25213	poly (ADP-ribose) polymerase family. member 12 (Parp12)
C920006O11Rik	-1.25174	PREDICTED: RIKEN cDNA C920006O11 gene (C920006O11Rik)
Bckdha	-1.24515	branched chain ketoacid dehydrogenase E1. alpha polypeptide (Bckdha)
4632427N05Rik	-1.24236	n.d.
Siah1a	-1.24223	seven in absentia 1A (Siah1a)
E230014G11Rik	-1.23995	n.d.
Gbp6	-1.2398	guanylate binding protein 6 (Gbp6)
Syne1	-1.23836	synaptic nuclear envelope 1 (Syne1). transcript variant 1
D7Ertd413e	-1.23675	n.d.
Nrip3	-1.23635	nuclear receptor interacting protein 3 (Nrip3)
LOC100040462	-1.23189	PREDICTED: similar to interferon-activatable protein (LOC100040462)
Wdr23	-1.23119	WD repeat domain 23 (Wdr23)
B430216N15Rik	-1.23113	n.d.
Dnajc16	-1.22444	DnaJ (Hsp40) homolog. subfamily C. member 16 (Dnajc16)
1810062G17Rik	-1.22432	PREDICTED: RIKEN cDNA 1810062G17 gene (1810062G17Rik)
E130302P19Rik	-1.22041	n.d.
LOC674611	-1.21863	PREDICTED: similar to Su48. transcript variant 3 (LOC674611)
Asb13	-1.21795	ankyrin repeat and SOCS box-containing 13 (Asb13)
Slc6a6	-1.2169	Solute carrier family 6 (neurotransmitter transporter. taurine). member 6
Sema3b	-1.21495	sema domain. immunoglobulin domain (Ig). short basic domain. secreted. (semaphorin) 3B (Sema3b). transcript variant 1
Akirin1	-1.20941	akirin 1 (Akirin1)
Rpo2tc1	-1.20622	n.d.
Frat1	-1.19828	frequently rearranged in advanced T-cell lymphomas (Frat1)
Rbbp4	-1.19728	retinoblastoma binding protein 4 (Rbbp4)
1700010A01Rik	-1.19508	n.d.
Fhit	-1.19373	fragile histidine triad gene (Fhit)
Cib1	-1.1896	calcium and integrin binding 1 (calmyrin) (Cib1)
Pnkp	-1.18522	polynucleotide kinase 3'- phosphatase (Pnkp)
Cul2	-1.1834	cullin 2 (Cul2)
Tdrd7	-1.18273	tudor domain containing 7 (Tdrd7)
Mvk	-1.18043	Mevalonate kinase
Baiap2l1	-1.17947	BAI1-associated protein 2-like 1 (Baiap2l1)
Hipk2	-1.17615	Homeodomain interacting protein kinase 2
1700019E19Rik	-1.17595	RIKEN cDNA 1700019E19 gene (1700019E19Rik)
A930026H04Rik	-1.17277	n.d.
Prr7	-1.17227	proline rich 7 (synaptic) (Prr7)
Bsdc1	-1.17097	BSD domain containing 1 (Bsdc1)
D9Ertd392e	-1.16372	n.d.
Yaf2	-1.15841	YY1 associated factor 2 (Yaf2)
Dhrs3	-1.1518	dehydrogenase/reductase (SDR family) member 3 (Dhrs3)
A530023B05Rik	-1.15159	n.d.
1500005N04Rik	-1.14407	n.d.
Mras	-1.14235	muscle and microspikes RAS (Mras)
Nkd2	-1.14149	naked cuticle 2 homolog (Drosophila) (Nkd2)
Tprgl	-1.13517	transformation related protein 63 regulated like (Tprgl)
Chrnb1	-1.13502	cholinergic receptor. nicotinic. beta polypeptide 1 (muscle) (Chrnb1)
Kctd6	-1.12857	potassium channel tetramerisation domain containing 6 (Kctd6)
Edil3	-1.11599	EGF-like repeats and discoidin I-like domains 3
Zfp50	1.11311	n.d.
Tmem98	1.13611	transmembrane protein 98 (Tmem98)
Eif3eip	1.13615	eukaryotic translation initiation factor 3. subunit E interacting protein (Eif3eip)
Vezf1	1.13858	vascular endothelial zinc finger 1 (Vezf1)
Zfp78	1.14758	zinc finger protein 78 (Zfp78). transcript variant 2
Hist1h2bb	1.14842	histone cluster 1. H2bb (Hist1h2bb)
Eftud2	1.15284	elongation factor Tu GTP binding domain containing 2 (Eftud2)
Fcer1a	1.156	Fc receptor. IgE. high affinity I. alpha polypeptide (Fcer1a)
Slc30a5	1.1575	solute carrier family 30 (zinc transporter). member 5 (Slc30a5)
LOC234915	1.16135	n.d.
1700001J11Rik	1.16271	PREDICTED: RIKEN cDNA 1700001J11 gene (1700001J11Rik). misc RNA.

Dguok	1.16301	Deoxyguanosine kinase
F8	1.16393	coagulation factor VIII (F8)
Usp21	1.16407	ubiquitin specific peptidase 21 (Usp21)
Brca2	1.16428	breast cancer 2 (Brca2). transcript variant 2
Nup50	1.16591	nucleoporin 50 (Nup50)
Zfp791	1.17109	zinc finger protein 791 (Zfp791)
Zfp526	1.17187	zinc finger protein 526 (Zfp526)
Ppil1	1.17533	peptidylprolyl isomerase (cyclophilin)-like 1 (Ppil1)
4632419I22Rik	1.17622	BRCA1 interacting protein C-terminal helicase 1. opposite strand
Dcun1d3	1.17825	DCN1. defective in cullin neddylation 1. domain containing 3 (S. cerevisiae) (Dcun1d3)
2810432D09Rik	1.18185	RIKEN cDNA 2810432D09 gene (2810432D09Rik)
Rsbn1	1.18268	rosbin. round spermatid basic protein 1 (Rsbn1)
Pds5a	1.18683	PDS5. regulator of cohesion maintenance. homolog A (S. cerevisiae) (Pds5a)
2010007H12Rik	1.18723	RIKEN cDNA 2010007H12 gene (2010007H12Rik)
Ddx31	1.18794	DEAD/H (Asp-Glu-Ala-Asp/His) box polypeptide 31 (Ddx31)
LOC380888	1.1893	n.d.
Nup155	1.19031	nucleoporin 155 (Nup155)
B930007L02Rik	1.19188	n.d.
Shprh	1.19602	SNF2 histone linker PHD RING helicase (Shprh). transcript variant 1
Zdhhc6	1.19679	zinc finger. DHHC domain containing 6 (Zdhhc6). transcript variant 2
Mycbp	1.19781	C-myc binding protein
Pabpc4	1.19998	poly A binding protein. cytoplasmic 4 (Pabpc4). transcript variant 1
Zfp583	1.2001	zinc finger protein 583 (Zfp583)
Ctdspl2	1.20459	CTD (carboxy-terminal domain. RNA polymerase II. polypeptide A) small phosphatase like 2 (Ctdspl2)
Rgs3	1.20581	regulator of G-protein signalling 3 (Rgs3). transcript variant 2
Ubr5	1.20815	ubiquitin protein ligase E3 component n-recognin 5 (Ubr5)
Bcor	1.21106	BCL6 interacting corepressor (Bcor). transcript variant c
9830167H18Rik	1.21236	PREDICTED: RIKEN cDNA 9830167H18 gene. transcript variant 1 (9830167H18Rik)
Polr1a	1.21615	polymerase (RNA) I polypeptide A (Polr1a)
Mybbp1a	1.21669	MYB binding protein (P160) 1a (Mybbp1a)
Zfp128	1.21747	zinc finger protein 128 (Zfp128)
Polr1a	1.2204	polymerase (RNA) I polypeptide A (Polr1a)
2410017P07Rik	1.22095	RIKEN cDNA 2410017P07 gene (2410017P07Rik)
Zfp418	1.22177	zinc finger protein 418 (Zfp418)
Rad51ap1	1.2225	RAD51 associated protein 1
LOC100044829	1.22265	PREDICTED: similar to Fibrillarin. transcript variant 1 (LOC100044829)
C130027E04Rik	1.22822	n.d.
Suhw2	1.23063	suppressor of hairy wing homolog 2 (Drosophila) (Suhw2)
L3mbtl3	1.23159	l(3)mbt-like 3 (Drosophila) (L3mbtl3)
2010003J03Rik	1.23301	RIKEN cDNA 2010003J03 gene (2010003J03Rik)
Ssrp1	1.23418	structure specific recognition protein 1 (Ssrp1)
Hnrnph1	1.23565	heterogeneous nuclear ribonucleoprotein H1 (Hnrnph1)
2310005L22Rik	1.23573	n.d.
Zfp560	1.23737	zinc finger protein 560 (Zfp560)
Pwp2	1.23813	PWP2 periodic tryptophan protein homolog (yeast) (Pwp2)
Sf3b3	1.23852	splicing factor 3b. subunit 3 (Sf3b3)
Senp8	1.23913	SUMO/sentrin specific peptidase 8 (Senp8)
4732486I23Rik	1.24067	n.d.
Tead2	1.24292	TEA domain family member 2 (Tead2)
A630072M18Rik	1.24601	RIKEN cDNA A630072M18 gene
Fam13b	1.2483	family with sequence similarity 13. member B (Fam13b)
Cdk4	1.24861	cyclin-dependent kinase 4 (Cdk4)
Epha7	1.24967	Eph receptor A7 (Epha7)
Zfp316	1.25448	zinc finger protein 316 (Zfp316)
Pcdhb3	1.25498	protocadherin beta 3 (Pcdhb3)
Zfp202	1.2556	zinc finger protein 202 (Zfp202)
Zfp213	1.25918	zinc finger protein 213 (Zfp213)
Zfp260	1.25939	zinc finger protein 260 (Zfp260)
4933424B01Rik	1.26118	RIKEN cDNA 4933424B01 gene (4933424B01Rik)
Ddx51	1.26193	DEAD (Asp-Glu-Ala-Asp) box polypeptide 51 (Ddx51)
Zfp157	1.26452	zinc finger protein 157 (Zfp157)
Cops2	1.2651	COP9 (constitutive photomorphogenic) homolog. subunit 2 (Arabidopsis thaliana) (Cops2)
Taf3	1.2658	TAF3 RNA polymerase II. TATA box binding protein (TBP)-associated factor
Nid2	1.26626	nidogen 2 (Nid2)
Hnrpll	1.26782	heterogeneous nuclear ribonucleoprotein L-like (Hnrpll)
E430018J23Rik	1.268	RIKEN cDNA E430018J23 gene (E430018J23Rik)
Pitrm1	1.26806	pitrilysin metallepetidase 1 (Pitrm1)
scl0002064.1_2	1.27184	n.d.
Gprasp1	1.27574	G protein-coupled receptor associated sorting protein 1 (Gprasp1). transcript variant 1
Alkbh4	1.28356	alkB. alkylation repair homolog 4 (E. coli) (Alkbh4)
Zfp27	1.28476	zinc finger protein 27 (Zfp27). transcript variant 1
1700123A16Rik	1.2881	PREDICTED: RIKEN cDNA 1700123A16 gene (1700123A16Rik)
Rbm15	1.28995	RNA binding motif protein 15 (Rbm15)
Lyl1	1.29004	lymphoblastomic leukemia 1 (Lyl1)

9330175B01Rik	1.29193	n.d.
Rabggtb	1.29269	RAB geranylgeranyl transferase. b subunit (Rabggtb)
A130042E20Rik	1.29277	RIKEN cDNA A130042E20 gene (A130042E20Rik)
Zfp655	1.29944	zinc finger protein 655 (Zfp655). transcript variant 1
Igfbp2	1.29969	insulin-like growth factor binding protein 2 (Igfbp2)
Cirh1a	1.30581	cirrhosis. autosomal recessive 1A (human) (Cirh1a)
Pigc	1.30706	phosphatidylinositol glycan anchor biosynthesis. class C (Pigc). transcript variant 1
Fem1b	1.30738	feminization 1 homolog b (C. elegans) (Fem1b)
Tbl2	1.31255	Transducin (beta)-like 2
Coil	1.31483	coilin (Coil)
Kbtbd8	1.3162	kelch repeat and BTB (POZ) domain containing 8 (Kbtbd8)
Nup43	1.32139	nucleoporin 43 (Nup43)
Fubp1	1.3217	Far upstream element (FUSE) binding protein 1
Zscan20	1.32472	zinc finger and SCAN domains 20 (Zscan20)
4631422C13Rik	1.32589	PREDICTED: RIKEN cDNA 4631422C13 gene (4631422C13Rik)
Ifnar2	1.32721	interferon (alpha and beta) receptor 2 (Ifnar2)
Zmym1	1.32838	zinc finger. MYM domain containing 1 (Zmym1)
Prpf3	1.33179	PRP3 pre-mRNA processing factor 3 homolog (yeast) (Prpf3)
4930553M18Rik	1.34432	TATA box binding protein (Tbp)-associated factor. RNA polymerase I. D
Trim32	1.34546	tripartite motif-containing 32 (Trim32)
5730403M16Rik	1.34675	RIKEN cDNA 5730403M16 gene (5730403M16Rik)
Zfp235	1.34752	zinc finger protein 235 (Zfp235)
4933421E11Rik	1.34932	RIKEN cDNA 4933421E11 gene (4933421E11Rik). transcript variant 2
Bbs10	1.34992	PREDICTED: Bardet-Biedl syndrome 10 (human). transcript variant 1 (Bbs10)
Rbm4	1.357	RNA binding motif protein 4 (Rbm4)
Rreb1	1.35707	ras responsive element binding protein 1 (Rreb1). transcript variant 1
Ppp1r3b	1.35753	Protein phosphatase 1. regulatory (inhibitor) subunit 3B
1810026B05Rik	1.36132	RIKEN cDNA 1810026B05 gene
BC025546	1.36258	cDNA sequence BC025546 (BC025546)
Snx16	1.3647	sorting nexin 16 (Snx16)
Vcan	1.36996	versican (Vcan). transcript variant 1
Mtbp	1.37108	Mdm2. transformed 3T3 cell double minute p53 binding protein (Mtbp)
Trrp2	1.37181	n.d.
2010305A19Rik	1.37412	RIKEN cDNA 2010305A19 gene (2010305A19Rik)
Rbbp5	1.37631	retinoblastoma binding protein 5 (Rbbp5)
1110038B12Rik	1.37686	PREDICTED: RIKEN cDNA 1110038B12 gene. transcript variant 6 (1110038B12Rik)
Zfp770	1.3797	zinc finger protein 770 (Zfp770)
Rbak	1.38223	RB-associated KRAB repressor (Rbak). transcript variant 1
LOC100048384	1.38455	PREDICTED: similar to programmed cell death protein 7 (LOC100048384). misc RNA.
Tmem185b	1.39574	transmembrane protein 185B (Tmem185b)
Zfp87	1.3994	zinc finger protein 87 (Zfp87)
Spata5l1	1.40128	PREDICTED: spermatogenesis associated 5-like 1 (Spata5l1)
Zfp82	1.4014	zinc finger protein 82 (Zfp82)
Zfp101	1.40373	zinc finger protein 101 (Zfp101)
Zfp119	1.41268	zinc finger protein 119 (Zfp119)
1190005F20Rik	1.42217	RIKEN cDNA 1190005F20 gene (1190005F20Rik)
5430433E21Rik	1.42247	PREDICTED: RIKEN cDNA 5430433E21 gene (5430433E21Rik)
Nme4	1.42284	non-metastatic cells 4. protein expressed in (Nme4). nuclear gene encoding mitochondrial protein
Mex3a	1.42365	mex3 homolog A (C. elegans) (Mex3a)
Zfp623	1.42372	zinc finger protein 623 (Zfp623)
Aplnr	1.42411	apelin receptor (Aplnr)
OTTMUSG00000000421	1.425	predicted gene. OTTMUSG00000000421 (OTTMUSG00000000421)
Sfrs7	1.42799	splicing factor. arginine/serine-rich 7 (Sfrs7)
Zfp30	1.4404	zinc finger protein 30 (Zfp30)
Zfp790	1.44073	zinc finger protein 790 (Zfp790)
Igfbp4	1.44117	insulin-like growth factor binding protein 4 (Igfbp4)
Zxdc	1.45039	ZXD family zinc finger C (Zxdc). transcript variant 1
LOC100048280	1.45577	PREDICTED: similar to crooked legs CG14938-PB. transcript variant 1 (LOC100048280)
Epc1	1.45822	enhancer of polycomb homolog 1 (Drosophila) (Epc1). transcript variant 1
Zbtb45	1.45857	zinc finger and BTB domain containing 45 (Zbtb45)
Zfp597	1.46176	zinc finger protein 597 (Zfp597)
A430106B04Rik	1.46555	n.d.
BC043301	1.49175	cDNA sequence BC043301 (BC043301)
Dctd	1.49635	dCMP deaminase (Dctd)
Cdc2a	1.4986	cell division cycle 2 homolog A (S. pombe) (Cdc2a)
LOC100041797	1.5084	PREDICTED: hypothetical protein LOC100041797 (LOC100041797)
Vcam1	1.51758	vascular cell adhesion molecule 1 (Vcam1)
Snora65	1.52399	small nucleolar RNA. H/ACA box 65 (Snora65) on chromosome 2.
2610037P13Rik	1.53724	RIKEN cDNA 2610037P13 gene; n.d.
Rbm3	1.56655	RNA binding motif protein 3 (Rbm3)
Slc40a1	1.57312	solute carrier family 40 (iron-regulated transporter). member 1 (Slc40a1)
Hbb-y	1.59181	hemoglobin Y. beta-like embryonic chain (Hbb-y)
Ppp1r3c	1.59444	protein phosphatase 1. regulatory (inhibitor) subunit 3C (Ppp1r3c)
scl00238693.1_37	1.60096	n.d.

Zfp748	1.60276	zinc finger protein 748 (Zfp748). transcript variant 1
Igsf10	1.60402	Immunoglobulin superfamily. member 10
Zfp60	1.65004	zinc finger protein 60 (Zfp60). transcript variant 2
Cpa3	1.6503	carboxypeptidase A3. mast cell (Cpa3)
H13	1.67454	n.d.
6720463L11Rik	1.675	RIKEN cDNA 6720463L11 gene; n.d.
2610019E17Rik	1.67543	Novel gene associated with 75614
Skp2	1.82766	S-phase kinase-associated protein 2 (p45) (Skp2). transcript variant 2
1110001A07Rik	1.8308	RIKEN cDNA 1110001A07 gene (1110001A07Rik); n.d.
Fbxo30	2.15396	F-box protein 30
Lrrc29	2.20159	leucine rich repeat containing 29 (Lrrc29)
Angptl4	2.38172	angiopoietin-like 4 (Angptl4)
Nppa	22.297	natriuretic peptide precursor type A (Nppa)

10.2.3 Gene ontology enrichment analysis

10.2.3.1 GOE on lung results above 50 % cut-off using GOEAST (2015.05.07)

GOIDs and their hierarchical relationships in "biological process", "cellular component" or "molecular function" GO categories are displayed in the following as graphs. Boxes represent Gene Ontology terms, labeled by its GOID, p value and detailed information. Significantly enriched GO terms are marked in yellow, non-significant ones are white. The degree of color saturation of each node is positively correlated with the significance of enrichment of the corresponding GO term. Non-significant GO terms within the hierarchical tree are either shown as white boxes or drawn as points. Branches of the GO hierarchical tree without significant enriched GO terms are not shown. Red edges stand for relationship between two enriched GO terms, black solid edges stand for relationship between enriched and unenriched terms, black dashed edges stand for relationship between two unenriched GO terms. The detail information labeled in the enriched GO nodes are organized as “count of genes associated with the listed GOID in the entered dataset/ total number of genes in the entered dataset | count of genes associated with the listed GOID on the Illumina platform/ total number of genes on the Illumina platform (p value)”. Explanations taken from Zheng *et al.,* 2008 (Zheng & Wang 2008).

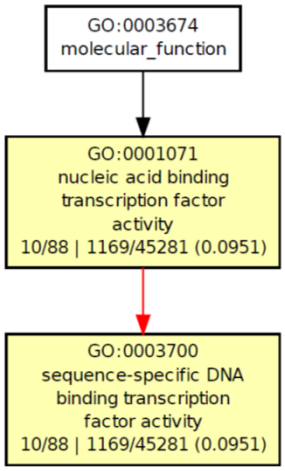

Suppl. Fig. 4: **Microarray data for lung - Gene ontology (GO) enrichment analysis on genes after setting 50% threshold**. GO for molecular function. Both GO for molecular component and GO for biological process did not yield any results. Note that the result is not significant.
Institute of Genetics and Developmental Biology, Chinese Academy of Sciences ©Version 1.30 Copy Right 2007-2013 GOEAST org. Beijing

Suppl. Tab. 2: **Genes of the microarray enriched in "nucleic acid binding transcription factor activity" as well as "sequence-specific DNA binding transcription factor activity" upon GSKIP KO.**

probe_ID	Definition	Gene Symbol
ILMN_2619408	Mus musculus activating transcription factor 3 (Atf3), mRNA.	Atf3
ILMN_2636403	Mus musculus AXIN1 up-regulated 1 (Axud1), mRNA.	Axud1
ILMN_2662926	Mus musculus early growth response 1 (Egr1), mRNA.	Egr1
ILMN_2750515	Mus musculus FBJ osteosarcoma oncogene (Fos), mRNA.	Fos
ILMN_2778279	Mus musculus FBJ osteosarcoma oncogene B (Fosb), mRNA.	Fosb
ILMN_1227573	Mus musculus interferon regulatory factor 7 (Irf7), mRNA.	Irf7
ILMN_2646625	Mus musculus Jun oncogene (Jun), mRNA.	Jun
ILMN_1220034	Mus musculus Jun-B oncogene (Junb), mRNA.	Junb
ILMN_2604029	Mus musculus Kruppel-like factor 2 (lung) (Klf2), mRNA.	Klf2
ILMN_1221264	Mus musculus Kruppel-like factor 4 (gut) (Klf4), mRNA.	Klf4

10.2.3.2 GOE on lung hit gene list without setting a threshold using GOEAST (2015.05.07)

Analogous to 10.2.3.1, outcomes of gene ontology enrichment analysis are displayed as graphs. In contrast to 10.2.3.1, all three analyzed categories showed results, represented in Suppl. Fig. 5, Suppl. Fig. 6 and Suppl. Fig. 7.

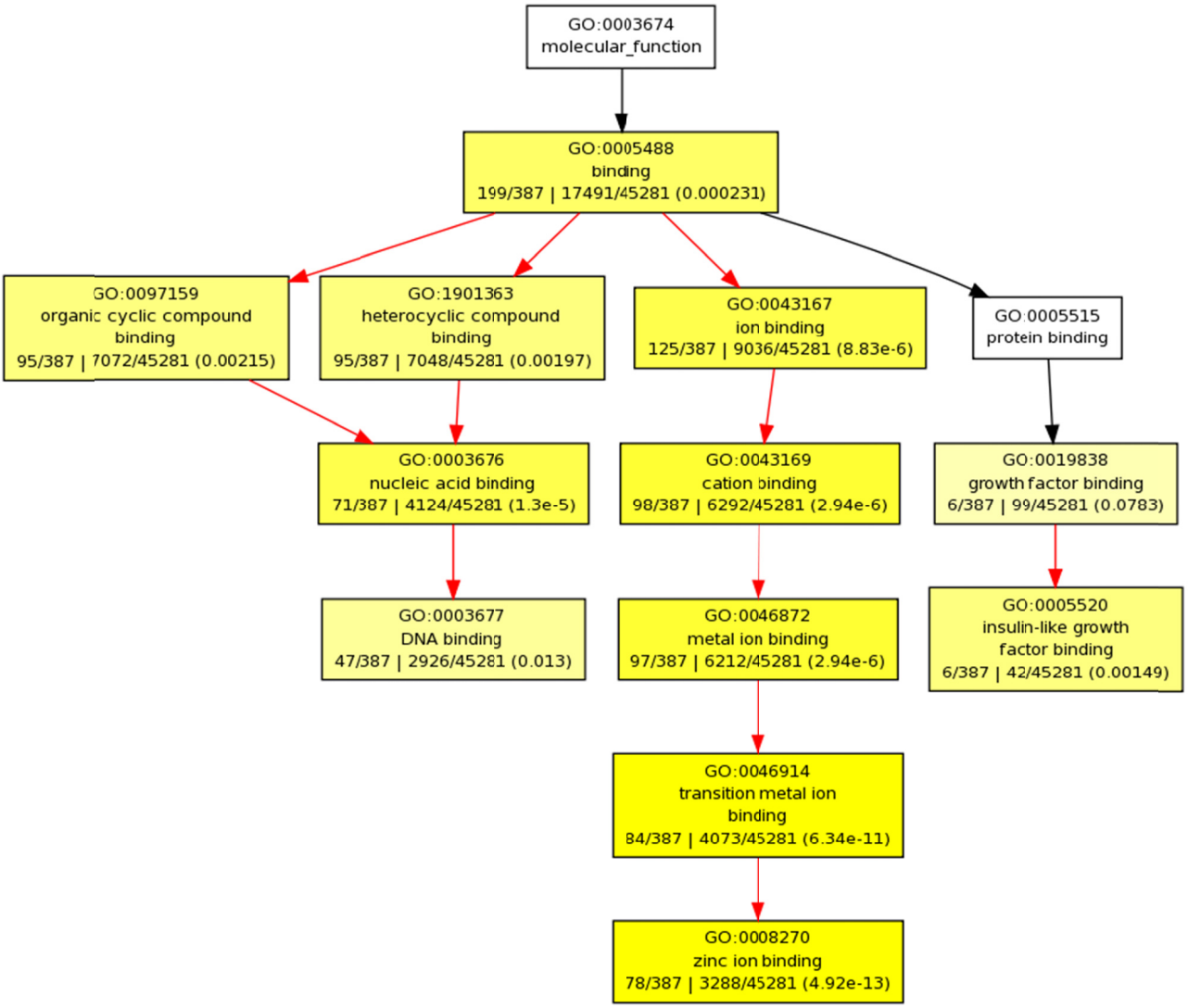

Suppl. Fig. 5: **Microarray data for E18.5 lung - Gene ontology (GO) enrichment analysis for molecular function of all significantly changed genes upon GSKIP KO using GOEAST** (2015.05.07). 387 valid IDs were entered and accepted as valid and included in the analysis. Numbers in brackets represent p values. Institute of Genetics and Developmental Biology, Chinese Academy of Sciences ©Version 1.30 Copy Right 2007-2013 GOEAST org. Beijing.

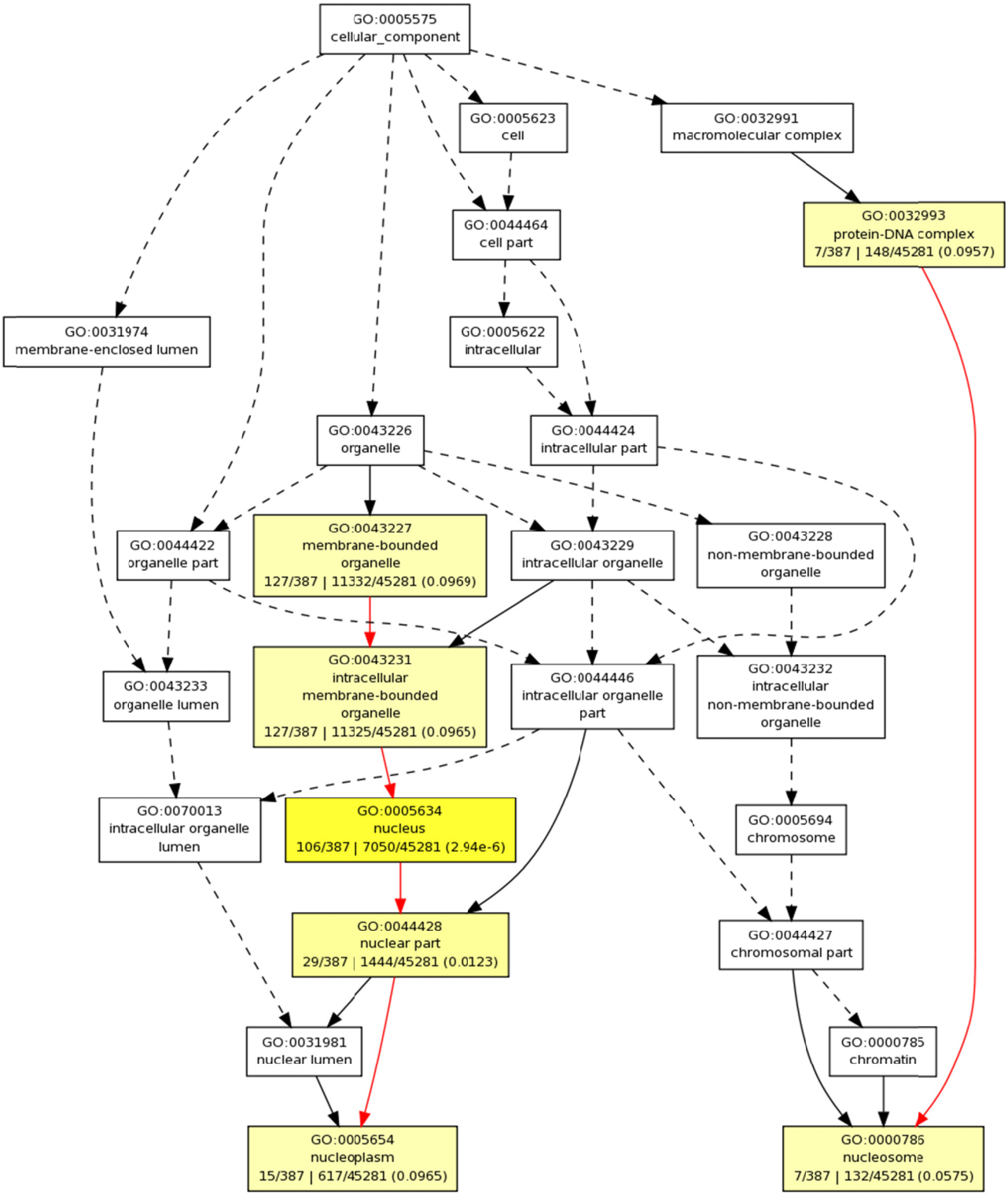

Suppl. Fig. 6: **Microarray data for E18.5 lung - Gene ontology (GO) enrichment analysis for cellular component of all significantly changed genes upon GSKIP KO using GOEAST** (2015.05.07). 387 valid IDs were entered and accepted as valid and included in the analysis. Numbers in brackets represent p values. Institute of Genetics and Developmental Biology, Chinese Academy of Sciences ©Version 1.30 Copy Right 2007-2013 GOEAST org. Beijing.

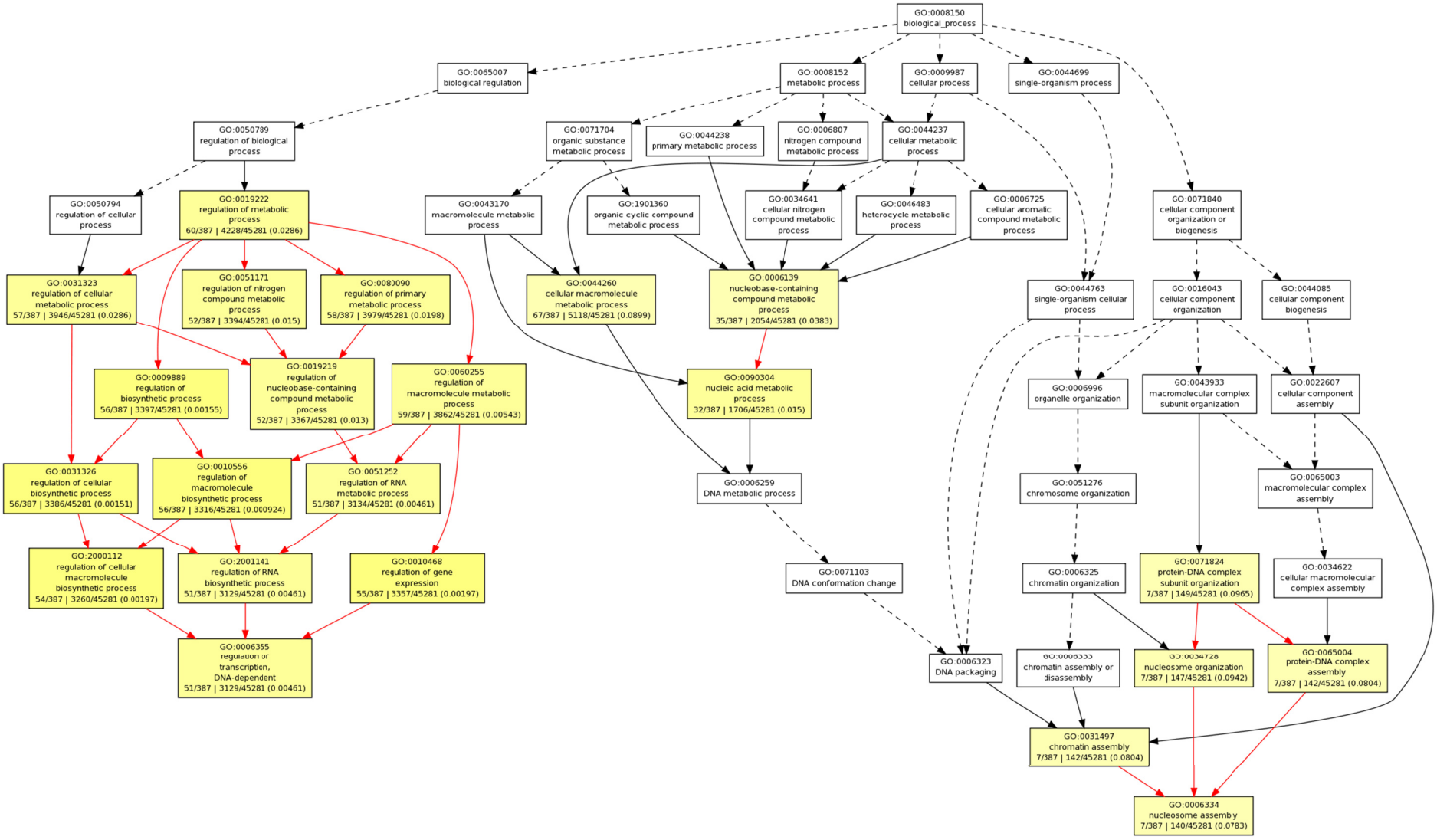

Suppl. Fig. 7: **Microarray data for E18.5 lung - Gene ontology (GO) enrichment analysis for biological process of all significantly changed genes upon GSKIP KO using GOEAST** (2015.05.07). 387 valid IDs were entered and accepted as valid and included in the analysis. Numbers in brackets represent p values. Institute of Genetics and Developmental Biology, Chinese Academy of Sciences ©Version 1.30 Copy Right 2007-2013 GOEAST org. Beijing.

10.2.4 Microarray validation *via* Western blot and RTqPCR

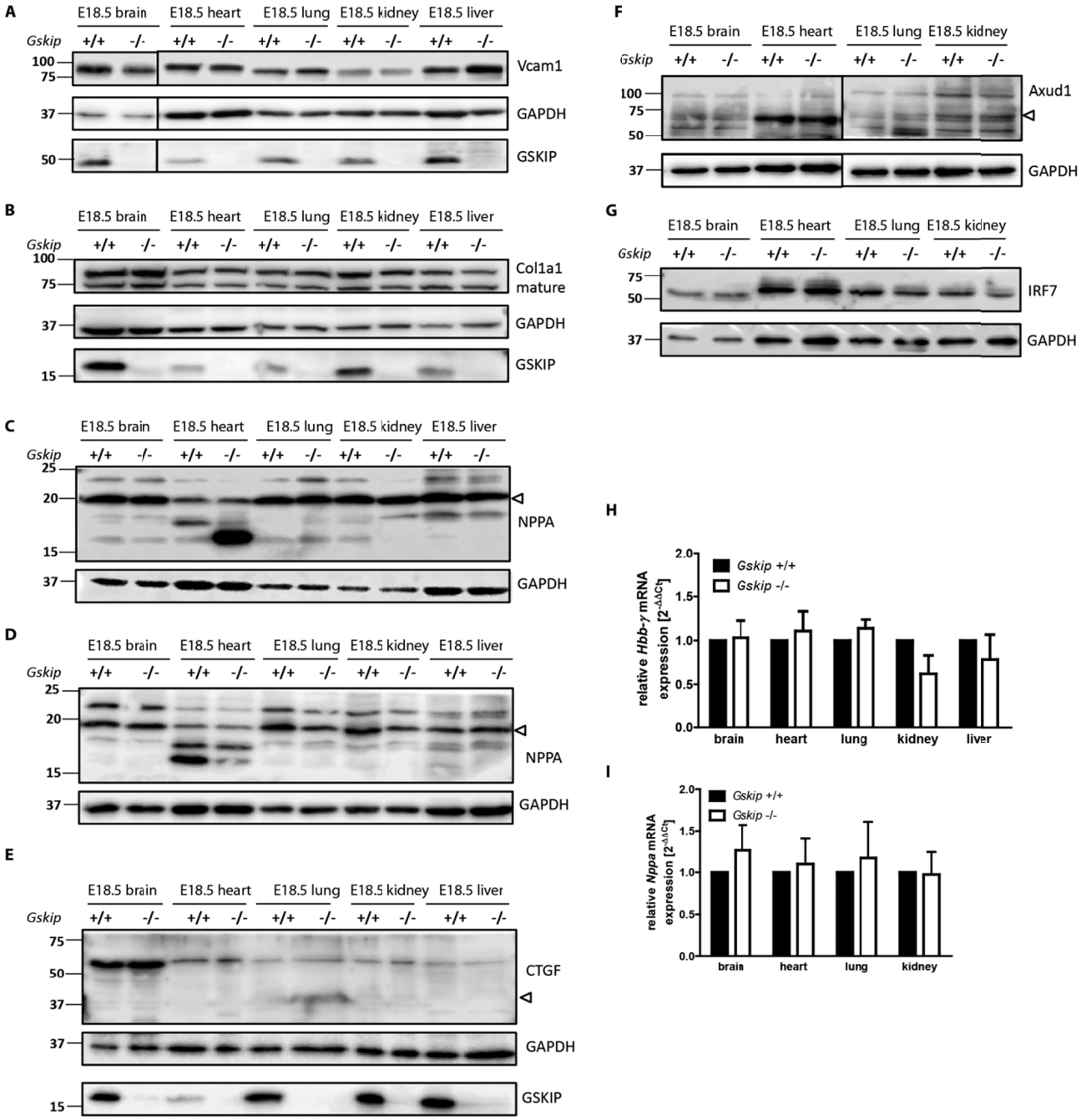

Suppl. Fig. 8: **Validation of gene expression microarray data on protein level did not confirm GSKIP KO-related changes.**
Western blots (A-G) and RTqPCR studies (H, I) showing no change upon GSKIP KO for Vcam 1 (A), Col1a1 (B), NPPA (C, D), CTGF (D), Axud1 (E) or IRF7 (F) protein expression in E18.5 tissues. Representative blots are shown for heart, lung, liver, brain and kidney lysates separated by SDS-PAGE. Embryonic haemoglobin *Hbb-y* and *Nppa* mRNA expression levels did not differ in absence of GSKIP compared to WT situation. $n \geq 4$.

10.3 Metabolomics

10.3.1 Metabolomics Raw Data

Suppl. Tab. 3: **Metabolite list showing fold-changes of KO tissue in comparison to WT and p values calculated from student´s t test** (Raw data table, analysis conducted by S. Kempa). Bold: significant changes. Red: significant p values.

Metabolite	Fold-change (KO vs. WT)			p value [t Test]		
	Blood	Liver	Lung	Blood	Liver	Lung
Succinic acid	1.51	**1.93**	**2.20**	0.15	0.00	0.00
Lactic acid	0.99	1.08	1.05	0.79	0.28	0.44
Glucose-6-phosphate	1.48	**2.73**	**2.25**	0.12	0.00	0.00
Pyruvic acid	**0.44**	**0.17**	**0.12**	0.00	0.02	0.00
Citric acid	0.94	0.59	**0.34**	0.81	0.29	0.00
Glucose-6-phosphate	1.40	**2.25**	**2.09**	0.13	0.01	0.00
Glutaric acid, 2-oxo	0.85	0.44	**0.16**	0.18	0.21	0.00
Glycolic acid	0.97	1.01	**0.85**	0.79	0.88	0.00
Phosphoric acid	**1.37**	0.95	**1.28**	0.03	0.42	0.00
Fumaric acid	**0.65**	1.17	**0.74**	0.01	0.16	0.01
Ethanolamine	0.76	0.94	0.57	0.13	0.64	0.00
Glucose	1.86	0.71	1.39	0.08	0.50	0.20
Glutamic acid	0.84	1.23	**1.59**	0.47	0.25	0.00
Glutaric acid, 2-hydroxy	**0.58**	1.21	**0.86**	0.00	0.09	0.00
Threonic acid	0.58	1.25	**0.64**	0.12	0.08	0.01
Valine	**1.31**	**1.44**	**2.01**	0.01	0.00	0.00
Valine	1.32	**1.42**	**1.40**	0.10	0.00	0.00
Siloxane	0.86	0.92	0.79	0.55	0.83	0.53
Erythritol	1.04	1.22	0.83	0.79	0.28	0.11
Galactose	1.82	0.72	1.49	0.08	0.46	0.15
Aspartic acid	0.75	0.95	0.92	0.13	0.82	0.59
Glutamic acid	0.98	0.98	1.06	0.92	0.88	0.56
Serine	1.09	**1.28**	**1.77**	0.59	0.03	0.00
Glycine	0.96	1.03	0.89	0.91	0.83	0.40
Threonine	1.19	1.03	1.34	0.08	0.90	0.06
Alanine	1.03	0.87	0.75	0.83	0.31	0.07
Inositol, myo-	0.93	**1.21**	**0.84**	0.67	0.00	0.03
Guanosine-5-monophosphate	0.82	1.39	1.07	0.67	0.23	0.74
Phenylalanine	1.05	**1.45**	**1.39**	0.70	0.00	0.00
Serine	1.09	1.31	**1.45**	0.79	0.08	0.02
Xylose	1.05	1.29	**0.76**	0.72	0.08	0.02
Aspartic acid	0.78	0.92	**0.64**	0.15	0.66	0.00
Ribitol	0.95	1.22	0.86	0.74	0.14	0.06
Glycerol-3-phosphate	1.52	**1.63**	1.22	0.06	0.02	0.08
Lactose	1.69	**2.38**	**1.58**	0.19	0.01	0.02
Creatinine	1.02	0.86	**1.27**	0.87	0.09	0.01
Putrescine	0.95	1.03	**0.48**	0.73	0.80	0.00
Alanine	1.25	1.04	0.92	0.27	0.85	0.71
Ethanolaminephosphate	0.89	1.03	0.85	0.52	0.83	0.02
Malic acid	**0.73**	1.11	0.80	0.03	0.41	0.08
Proline, 4-hydroxy-, trans-	0.92	0.90	0.94	0.74	0.64	0.46
Glutaric acid	1.02	0.37	0.88	0.94	0.16	0.15
Methionine	1.19	**1.26**	**1.21**	0.30	0.01	0.01
Butanoic acid, 2-amino	1.29	1.06	1.06	0.14	0.64	0.30
Lysine	0.92	1.12	1.01	0.57	0.74	0.97
Uracil	1.04	0.91	0.84	0.85	0.67	0.55
Pantothenic acid	**1.27**	**1.32**	**1.47**	0.03	0.00	0.01
Sucrose	**0.68**	1.00	**0.75**	0.02	0.98	0.00
Gluconic acid	1.16	**0.72**	**0.84**	0.27	0.00	0.03
Lysine, L-	0.51	**0.24**	**0.50**	0.35	0.03	0.00
Alanine, beta-	0.93	0.73	0.97	0.74	0.19	0.69
Siloxane	0.72	0.67	0.39	0.20	failed	0.41
Tyrosine	1.17	1.09	0.90	0.55	0.85	0.82
Hypotaurine	0.90	**0.40**	1.06	0.58	0.03	0.69
Ascorbic acid	2.49	1.00	**1.85**	failed	0.99	0.01
Gluconic acid	1.21	0.94	**0.73**	0.23	0.66	0.01
Decane, n-	1.03	0.97	0.95	0.90	0.71	0.40
Ribose-5-phosphate	0.39	1.00	0.86	failed	1.00	0.19
Siloxane	0.81	1.47	0.88	0.50	0.58	0.67
Proline	1.02	1.14	0.80	0.91	0.35	0.10
Asparagine	1.12	0.84	1.30	0.71	0.23	0.12
Isoleucine	**1.94**	1.19	1.17	0.00	0.09	0.17

Tricosane, n-	1.00	1.02	0.95	0.99	0.81	0.39
Alanine	1.12	0.74	0.92	0.72	0.10	0.29
Heptadecane, n-	1.01	1.00	0.98	0.95	0.97	0.81
Proline	0.90	0.89	**1.17**	0.28	0.63	0.02
Threonine, allo-	1.09	1.14	1.12	0.71	0.26	0.26
Glucopyranose	1.01	**1.57**	0.93	0.93	0.00	0.68
Tryptophan	0.97	**1.29**	1.22	0.78	0.05	0.12
Butanoic acid, 3-hydroxy-	**1.71**	0.72	0.80	0.02	0.15	0.29
Proline	0.88	0.70	**0.66**	0.63	0.20	0.02
Hexadecane, n-	1.03	1.01	0.98	0.91	0.90	0.70
Hypoxanthine	2.15	1.39	**1.84**	0.09	0.06	0.03
Uridine 5'-monophosphate	0.27	1.11	0.80	0.28	0.48	0.12
Cysteine	0.75	1.15	1.13	0.30	0.47	0.47
Inositol, myo-	1.09	0.93	0.73	0.64	0.83	0.28
Glycine	0.47	0.83	0.90	0.15	0.29	0.25
Nicotinamide	0.72	0.84	0.93	0.08	0.38	0.37
Glycerophosphoglycerol	0.91	1.17	0.86	0.65	0.35	0.05
Glycine, N.N-dimethyl-	0.97	0.88	0.90	0.84	0.83	0.21
Octadecanoic acid	0.95	1.01	0.91	0.80	0.90	0.17
Cinnamic acid. trans-	1.00	0.94	0.89	0.99	0.45	0.17
Hexadecanoic acid	0.95	1.01	0.96	0.78	0.91	0.50
Siloxane	0.86	1.45	0.93	0.27	0.09	0.62
alpha-D-Galactopyranosyl-(1,4)-D-galactopyranoside	1.37	**2.12**	1.14	0.36	0.00	0.50
Proline, 4-hydroxy-. cis-	1.05	0.81	1.24	0.41	0.62	0.36
Maltotriose	**2.19**	**2.27**	1.04	0.04	0.00	0.89
Glucose-6-phosphate	0.87	1.10	1.68	0.51	0.80	0.09
Hydrogen sulfide	failed	1.40	1.15	failed	0.32	0.11
Siloxane	0.57	1.05	0.79	0.21	0.93	0.65
Leucine	**1.71**	**1.39**	**1.40**	0.00	0.04	0.04
Tritriacontane, n-	1.03	1.01	0.92	0.91	0.88	0.20
Pyridine, 2-hydroxy-	1.10	0.95	0.92	0.31	0.46	0.63
Siloxane	0.80	1.06	1.50	0.40	0.91	0.28
Urea	0.88	1.05	0.93	0.44	0.38	0.60
Glyceric acid	0.63	1.06	0.80	0.27	0.60	0.20
Dehydroascorbic acid dimer	1.95	0.95	1.00	0.08	0.61	0.99
Oxalic acid	**1.09**	1.78	0.62	0.02	0.55	0.32
Siloxane	0.95	2.50	0.56	0.87	failed	0.33
Fructose	**0.61**	1.15	1.05	0.00	0.45	0.72
Hydroxylamine	1.17	1.09	0.88	0.60	0.37	0.08
Siloxane	0.65	2.05	1.20	0.22	0.35	0.55
Dihydroxyacetone phosphate	1.15	failed	1.32	0.27	failed	0.20
Galacturonic acid	1.69	0.90	**0.60**	0.16	0.55	0.02
Indole-3-lactic acid	1.11	1.03	0.87	0.64	0.80	0.22
Alanyl-alanine	0.56	1.00	0.75	0.23	0.99	0.10
Siloxane	0.44	failed	1.51	failed	failed	failed
Tridecane, n-	0.89	0.61	0.87	0.54	0.25	0.14
Siloxane	0.92	1.35	1.45	0.83	0.68	0.13
Methionine	1.14	0.99	1.20	0.12	0.93	0.32
Phosphoenolpyruvic acid	0.92	0.83	0.86	0.89	0.48	0.36
Adenosine (3TMS)	1.00	1.03	1.05	0.98	0.62	0.51
Siloxane	0.74	1.21	0.77	0.34	0.38	0.29
Urea (2TMS)	0.82	1.18	0.74	0.34	0.13	0.06
Analyte 239	1.05	0.91	0.95	0.73	0.44	0.60
Threonic acid	0.89	1.07	**0.63**	0.77	0.60	0.00
Pyroglutamic acid	0.73	1.14	1.20	0.57	0.84	0.59
Propionic acid. 3-ureido-	1.01	0.86	0.90	0.98	0.33	0.58
Diethanolamine	0.83	1.05	0.95	0.69	0.77	0.61
Glucose-6-phosphate	1.50	**2.38**	**2.64**	0.06	0.00	0.00
Lactic acid, 3-(4-hydroxyphenyl)-	1.24	**1.20**	0.77	0.41	0.02	0.07

10.3.2 Liver metabolite enrichment analysis using MetaboAnalyst 3.0

Suppl. Tab. 4: **GSKIP KO accounts for relevant changes in liver metabolism.** Pathway analysis module results for GSKIP KO liver metabolites by MetaboAnalyst 3.0. Red: significantly enriched pathways (with highest p and highest pathway impact values). Total: total number of metabolites within the pathway. Hits: altered metabolites submitted to the analysis within all metabolites of a metabolic process. FDR: False Discovery Rate-adjusted p value. Algorithms used for analysis: Hypergeometric test for overrepresentation analysis, relative-betweenness centrality for pathway topology analysis.

Pathway Name	Total	Hits	p	-log(p)	FDR	Impact
Aminoacyl-tRNA biosynthesis	69	6	8.6864E-5	9.3512	0.0071229	0.12903
Valine, leucine and isoleucine biosynthesis	11	3	2.2338E-4	8.4066	0.0091588	0.66666
Cysteine and methionine metabolism	27	3	0.0035145	5.6509	0.096062	0.1351
Pantothenate and CoA biosynthesis	15	2	0.012983	4.3441	0.26615	0.02041
Citrate cycle (TCA cycle)	20	2	0.022679	3.7863	0.2976	0.0975
Butanoate metabolism	22	2	0.027187	3.605	0.2976	0.0
Pyruvate metabolism	23	2	0.029568	3.5211	0.2976	0.18375
Alanine, aspartate and glutamate metabolism	24	2	0.03203	3.4411	0.2976	0.0
Galactose metabolism	26	2	0.03719	3.2917	0.2976	0.0161
Glycolysis or Gluconeogenesis	26	2	0.03719	3.2917	0.2976	0.09891
Inositol phosphate metabolism	28	2	0.042651	3.1547	0.2976	0.11163
Lysine biosynthesis	4	1	0.047181	3.0538	0.2976	0.0
Phenylalanine, tyrosine and tryptophan biosynthesis	4	1	0.047181	3.0538	0.2976	0.5
Glycine, serine and threonine metabolism	31	2	0.051375	2.9686	0.30091	0.23848
Biotin metabolism	5	1	0.058645	2.8363	0.32059	0.0
Cyanoamino acid metabolism	6	1	0.069978	2.6596	0.35673	0.0
Valine, leucine and isoleucine degradation	38	2	0.073956	2.6043	0.35673	0.0
Taurine and hypotaurine metabolism	8	1	0.092261	2.3831	0.4203	0.28571
Ascorbate and aldarate metabolism	9	1	0.10321	2.271	0.42317	0.0
Methane metabolism	9	1	0.10321	2.271	0.42317	0.4
Phenylalanine metabolism	11	1	0.12475	2.0815	0.4871	0.40741
Propanoate metabolism	20	1	0.21576	1.5336	0.80325	0.0
Sphingolipid metabolism	21	1	0.2253	1.4903	0.80325	0.0
Lysine degradation	23	1	0.24406	1.4103	0.83388	0.0

10.3.3 Blood metabolite enrichment analysis using MetaboAnalyst 3.0

Suppl. Tab. 5: **GSKIP KO accounts for relevant changes in blood metabolism.** Pathway analysis module results for GSKIP KO blood metabolites by MetaboAnalyst 3.0.
Red: significantly enriched pathways (with highest p and highest pathway impact values). Total: total number of metabolites within the pathway. Hits: altered metabolites submitted to the analysis within all metabolites of a metabolic process. FDR: False Discovery Rate-adjusted p value. Algorithms used for analysis: Hypergeometric test for overrepresentation analysis, relative-betweenness centrality for pathway topology analysis.

Pathway Name	Total	Hits	p	-log(p)	FDR	Impact
Valine, leucine and isoleucine biosynthesis	11	3	9.557E-5	9.2557	0.0078367	0.66666
Pantothenate and CoA biosynthesis	15	2	0.007630	4.8756	0.26163	0.02041
Starch and sucrose metabolism	19	2	0.012172	4.4086	0.26163	0.00233
Citrate cycle (TCA cycle)	20	2	0.013455	4.3084	0.26163	0.09872
Butanoate metabolism	22	2	0.016189	4.1234	0.26163	0.0
Alanine, aspartate and glutamate metabolism	24	2	0.019144	3.9558	0.26163	0.00316
Valine, leucine and isoleucine degradation	38	2	0.045354	3.0933	0.53128	0.0
Aminoacyl-tRNA biosynthesis	69	2	0.12901	2.0478	1.0	0.0
Pyruvate metabolism	23	1	0.19237	1.6483	1.0	0.18375
Galactose metabolism	26	1	0.21477	1.5382	1.0	0.04068
Glycolysis or Gluconeogenesis	26	1	0.21477	1.5382	1.0	0.09891
Cysteine and methionine metabolism	27	1	0.22211	1.5046	1.0	0.02292
Glycine, serine and threonine metabolism	31	1	0.25084	1.383	1.0	0.0
Amino sugar and nucleotide sugar metabolism	37	1	0.29209	1.2307	1.0	0.0
Arginine and proline metabolism	44	1	0.33757	1.086	1.0	0.0
Tyrosine metabolism	44	1	0.33757	1.086	1.0	0.0

10.4 Biochemical analysis of GSKIP KO

10.4.1 E18.5 tissues

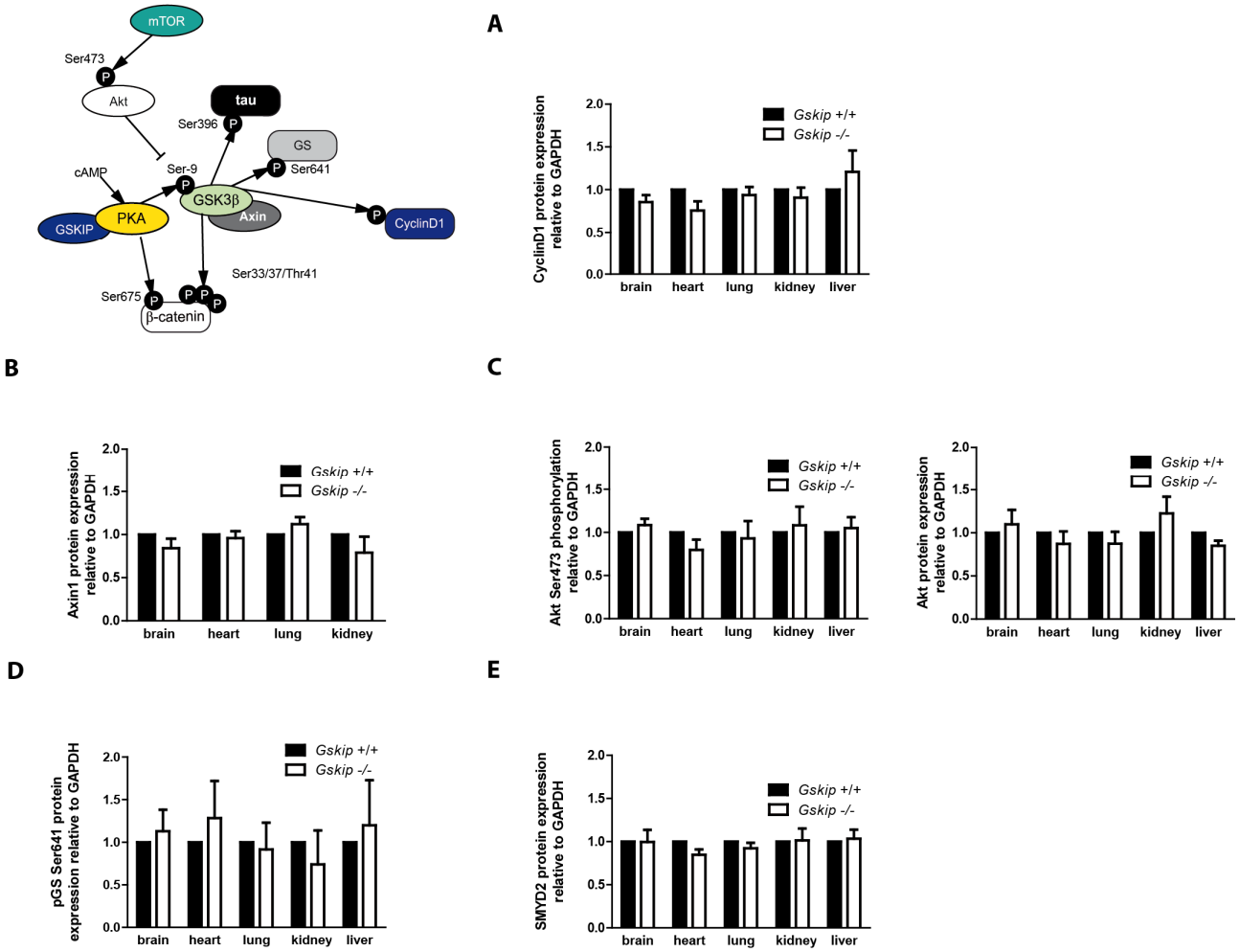

Suppl. Fig. 9: **Semiquantitative analysis of Western blot signal intensities revealed no significant GSKIP-dependent protein expression alterations.** Bar graphs are displaying Axin1 (A), phospho-GS (B), CyclinD1 (C), (phospho-)Akt (D) and SMYD2 (E) expression relative to GAPDH in various mouse tissues at E18.5. n = 4-6. Mean ± SEM.

10.4.2 Primary MEFs

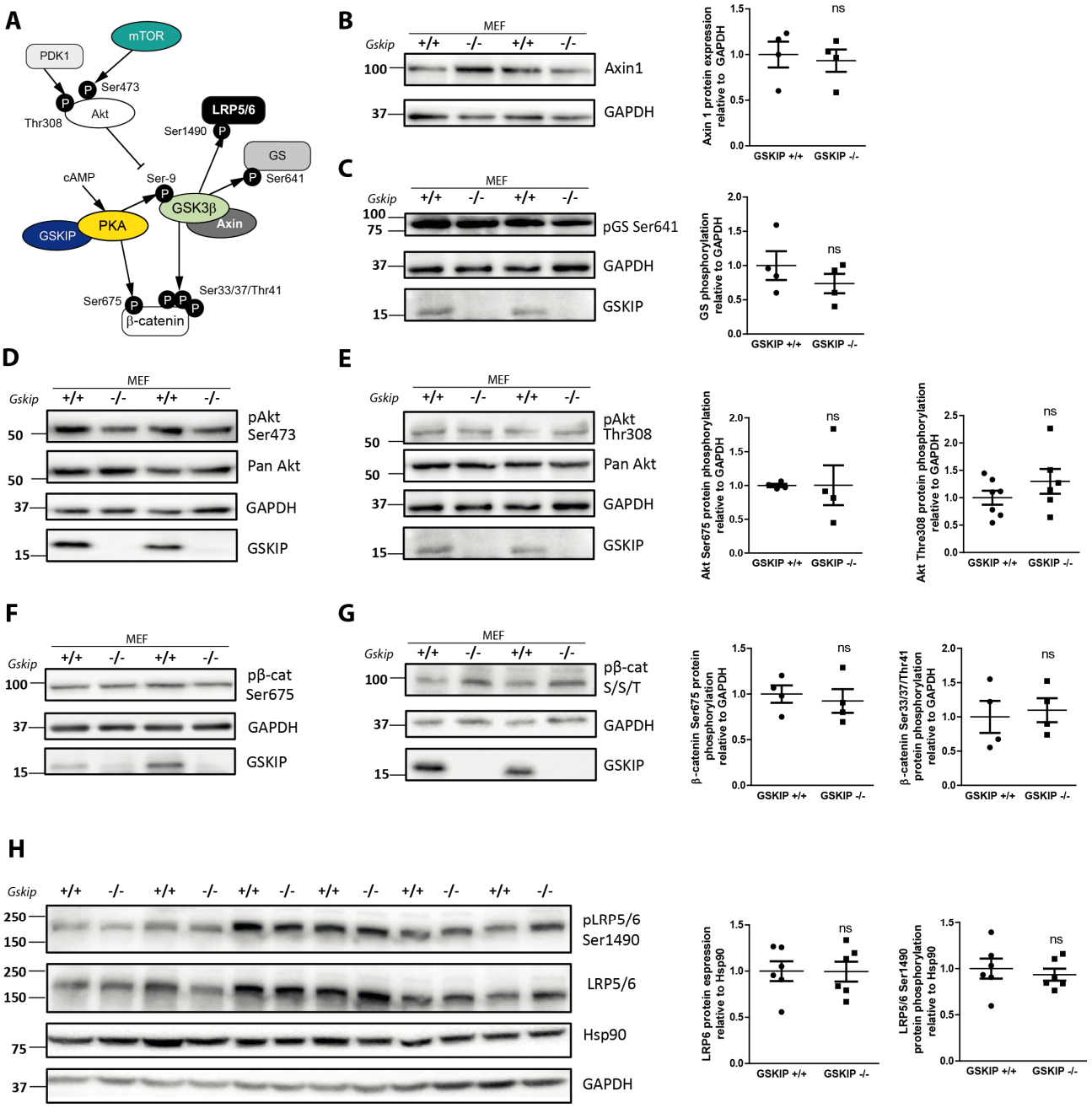

Suppl. Fig. 10: **Protein expression of PKA- and GSK3β-dependent targets did not define changes comparing WT and GSKIP-deficient primary MEFs.** A) Illustration depicting a protein network regulating GSK3β-dependent processes with a possible relevance for GSKIP in different signalling pathways. B) -H) *left:* Western blot analysis of MEFs generated from E12.5 WT ($GSKIP^{+/+}$) and KO ($GSKIP^{-/-}$) embryos. 15 µg of proteins were loaded and lysates separated by 12 % SDS-PAGE (or in H) 8 %). GAPDH (or in case of LRP5/6 Hsp90) was used as a loading control. *right:* Densitometric evaluation of signal intensities, relative to GAPDH [in case of (p)LRP5/6 to Hsp90]. GSKIP KO was normalized to WT. n = 4-6. Mean ± SEM; unpaired Student´s t-test.

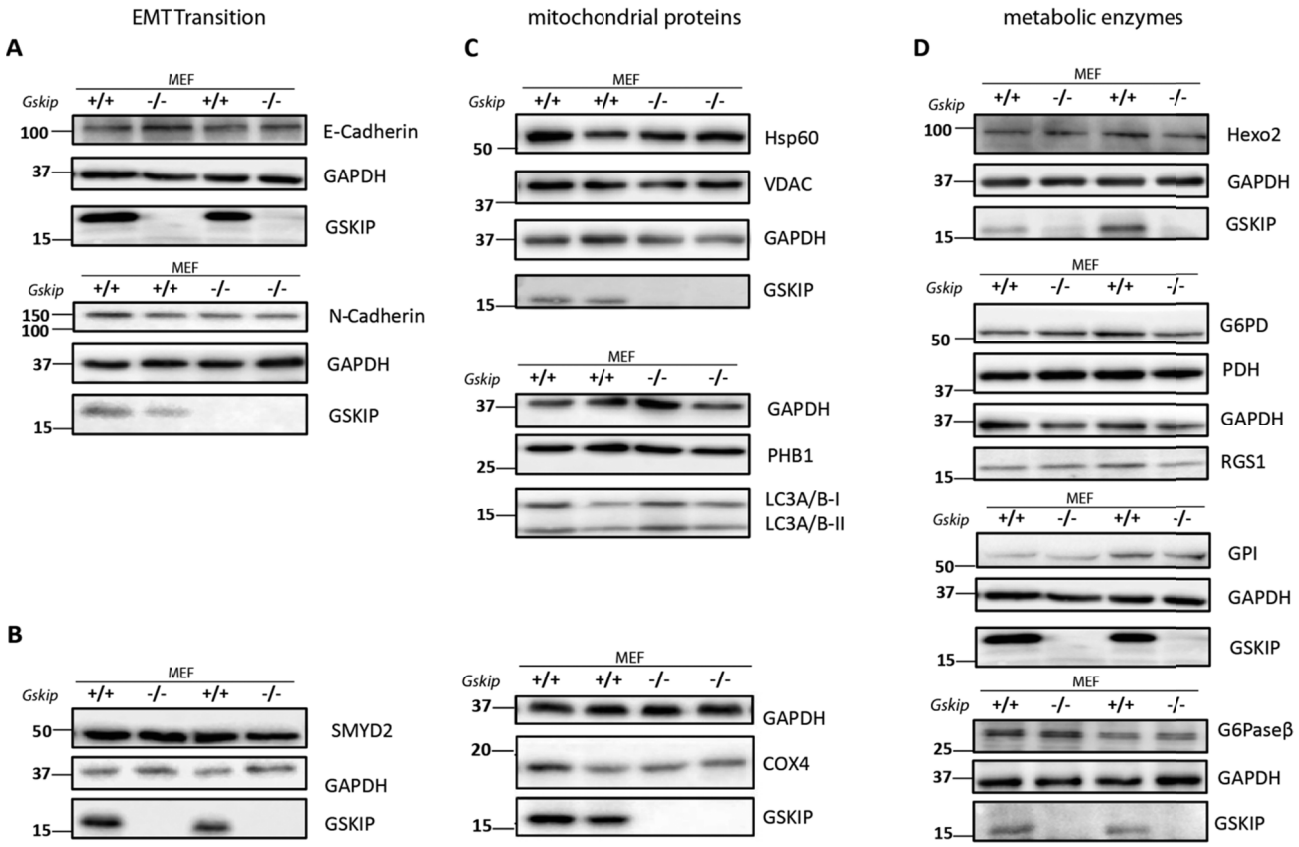

Suppl. Fig. 11: **Western blot analysis of potential GSKIP-dependent proteins in primary MEFs did not point out differences on protein level.** Representative Western blots of WT (GSKIP$^{+/+}$) and KO (GSKIP$^{-/-}$) MEFs are shown, generated from E12.5 embryos. Equal amounts of protein were loaded and lysates separated by 12 % SDS-PAGE. GAPDH was included as a loading control. $n \geq 6$.

10.5 Proteomics

10.5.1 Raw Data

Suppl. Tab. 6: **42 upregulated and 35 downregulated proteins including mitochondrial proteins from Tab. 29.** Bold: preselection of proteins for further validation.

Protein names	Gene names	Fold-change KO vs. WT	Intracellular localisation
Carbamoyl-phosphate synthase [ammonia], mitochondrial	**Cps1**	**40.8450498**	**Mito inner membrane, nucleolus**
Bifunctional ATP-dependent dihydroxyacetone kinase/FAD-AMP lyase (cyclizing); ATP-dependent dihydroxyacetone kinase;FAD-AMP lyase (cyclizing)	Dak	18.4373669	Extracellular peroxisomal exosome, nucleus
Hydroxymethylglutaryl-CoA synthase, mitochondrial	Hmgcs2	11.5225249	Mitochondrial inner membrane
Betaine--homocysteine S-methyltransferase 1	Bhmt	11.3772701	Cytoplasm
Microsomal triglyceride transfer protein large subunit	Mttp	10.1299824	Iso 1: ER; Iso2: ER, Golgi
Fructose-1,6-bisphosphatase 1	Fbp1	9.20347588	Extracellular peroxisomal exosome, cytoplasm
Fatty acid-binding protein. liver	Fabp1	6.37865392	Cytoplasm
Chitinase-3-like protein 3	Chi3l3	6.22780191	Cytoplasm, rough ER lumen, extracellular
Regucalcin	Rgn	5.22821645	Cytoplasm, nucleus, nucleoplasm
Cytosolic 10-formyltetrahydrofolate dehydrogenase	Aldh1l1	4.93042302	Cytoplasm; GO annotation also in mitochondria
Parathymosin	Ptms	4.70425925	
Receptor expression-enhancing protein 6	Reep6	3.44242415	ER membrane
Gamma-tubulin complex component 3; GCP3	Tubgcp3	3.42068048	Cytoplasm, centrosome
Alpha-hemoglobin-stabilizing protein	Ahsp	3.37133353	Cytoplasm
Myeloperoxidase;Myeloperoxidase light chain;Myeloperoxidase heavy chain	Mpo	3.34909217	Lysosome
Neutrophilic granule protein; Bectenecin	Ngp	3.17125423	Secreted, cytoplasmic granules/vesicles
Fructose-bisphosphate aldolase B	Aldob	2.78593442	Cytoplasm, centrioles
Lactotransferrin	Ltf	2.65827156	Secreted, cytoplasmic granules
Long-chain-fatty-acid--CoA ligase 1	Acsl1	2.61816928	Mito outer membrane, peroxisome membrane, microsome membrane, ER membrane
Glutathione S-transferase theta-1	Gstt1	2.53431767	Cytosol, nucleus
Pyrroline-5-carboxylate reductase 3	Pycrl	2.51913537	
Cell growth-regulating nucleolar protein	Lyar	2.47648815	Nucleus, nucleolus
Rapamycin-insensitive companion of mTOR	Rictor	2.3935261	
Complement factor B;Complement factor B Ba fragment;Complement factor B Bb fragment	Cfb	2.38858868	Secreted, extracellular space
Glycerol kinase	Gyk	2.37320581	Cytoplasm, mitochondrial outer membrane
Dihydropyrimidine dehydrogenase [NADP(+)]	Dpyd	2.32661381	Cytoplasm
Peptidylprolyl isomerase domain and WD repeat-containing protein 1	Ppwd1	2.27981196	Nucleus
Sorbitol dehydrogenase	**Sord**	**2.25105699**	**Mitochondrial membrane; Cilium, flagellum**
Glycerol-3-phosphate dehydrogenase [NAD(+)], cytoplasmic	Gpd1	2.23692972	Cytoplasm
Antithrombin-III	Serpinc1	2.23047721	Secreted, extracellular space
High mobility group protein HMGI-C	Hmga2	2.16380615	Nucleus
Prostaglandin reductase 2	Ptgr2	2.1303292	Cytoplasm
Clusterin;Clusterin beta chain;Clusterin alpha chain	Clu	2.11874781	Secreted, cytoplasm,

			nucleus, mitochondrial membrane
Glutamate dehydrogenase 1, mitochondrial	**Glud1**	**2.06884668**	**Mito matrix**
KH domain-containing. RNA-binding, signal transduction-associated protein 1	Khdrbs1	2.06772836	Nucleus, membrane
Nipped-B-like protein	Nipbl	2.06607975	Nucleus
Protein pelota homolog	Pelo	2.05778095	Nucleus, cytoplasm
2-amino-3-ketobutyrate coenzyme A ligase, mitochondrial	Gcat	2.04225901	Mitochondrium, nucleus
Delta-1-pyrroline-5-carboxylate dehydrogenase, mitochondrial	**Aldh4a1**	**2.0349982**	**Mito matrix**
Neutrophil cytosol factor 1	Ncf1	2.00116515	Cytoplasm, membrane
Maleylacetoacetate isomerase	Gstz1	1.99897065	Cytosol
Fumarylacetoacetase	Fah	1.98870579	Extracellular vesicular exosome
Talin-2	**Tln2**	**0.16611387**	**Cell junction, focal adhesion, cell membrane, cytoplasm, cytoskeleton**
Arf-GAP with GTPase. ANK repeat and PH domain-containing protein 3	Agap3	0.16649417	Cytoplasm, PML nuclear bodies
Fatty acid-binding protein, adipocyte	Fabp4	0.21386202	Cytoplasm, nucleus
Antigen KI-67; Ki-67 or *MKI67*	Mki67	0.23532476	
pre-mRNA 3 end processing protein WDR33	Wdr33	0.24443199	Nucleus
Decorin	Dcn	0.25586634	Secreted, extracellular space
Ig gamma-3 chain C region		0.36404437	Iso 1: cell membrane, Iso2: secreted
Filamin-C	Flnc	0.36694954	Cytoplasm, cytoskeleton, myofibril (Z line)
Creatine kinase M-type	Ckm	0.3836454	Cytoplasm
ATPase inhibitor, mitochondrial	**Atpif1**	**0.41802062**	**Mitochondrium**
Beta-enolase	**Eno3**	**0.42369557**	**Cytoplasm, Z line, M-band**
Desmin	**Des**	**0.42418628**	**Cytoplasm, cell membrane (sarcolemma)**
Desmoplakin	Dsp	0.46618779	Cell junction desmosome, Cytoplasm. cytoskeleton
Acetolactate synthase-like protein	Ilvbl	0.47471218	Membrane
Protein NipSnap homolog 2	Gbas	0.48194737	GO: mitochondrium
Proteasome maturation protein	Pomp	0.50387218	Cytoplasm, Nucleus, microsome membrane
Protein S100-A11	S100a11	0.50741225	Cytoplasm, nucleus
BAG family molecular chaperone regulator 3	Bag3	0.51265729	Cytoplasm. plasma membrane
GMP reductase 1	Gmpr	0.51896188	
Tropomodulin-1	Tmod1	0.52109131	Cytoskeleton, sarcomeric structure
Coronin-1A;Coronin	Coro1a	0.55057231	Cytoplasm, cell cortex, cytoskeleton
	Reep5	0.55632594	Membrane
Laminin subunit alpha-2	Lama2	0.55845417	Extracellular matrix
Alpha-ketoglutarate-dependent dioxygenase FTO	Fto	0.56006868	Nucleus. nucleus speckles
Protein Dr1	Dr1	0.5615577	Nucleus
Cullin-4B	Cul4b	0.57390963	
Periaxin	Prx	0.57742012	Iso1: cell membrane; Iso2: cytoplasm
Carnitine O-acetyltransferase	Crat	0.58235977	ER, mito inner membrane, peroxisome
Phosphoglycerate mutase 2	Pgam2	0.58550253	Cytosol, nucleus, extracellular vesicular exosomes
Pumilio homolog 1	Pum1	0.58658749	Cytoplasm
1-phosphatidylinositol 4.5-bisphosphate phosphodiesterase beta-3; PLCβ3	**Plcβ3**	**0.58722547**	**Nucleus**

GTP:AMP phosphotransferase AK4, mitochondrial	Ak4	0.60007217	Mito matrix
Hexokinase-2; HK-2	**Hk2**	**0.60059577**	**Cytosol, membrane, mito outer membrane**
Guanine nucleotide-binding protein subunit alpha-13	Gna13	0.60551541	Membrane, cytoplasm, nucleus
Hexokinase-1; HK-1	**Hk1**	**0.62**	**Iso HK1: outer mito membrane; Iso HK1-SC: membrane**

10.5.2 STRING protein association networks for listed proteins

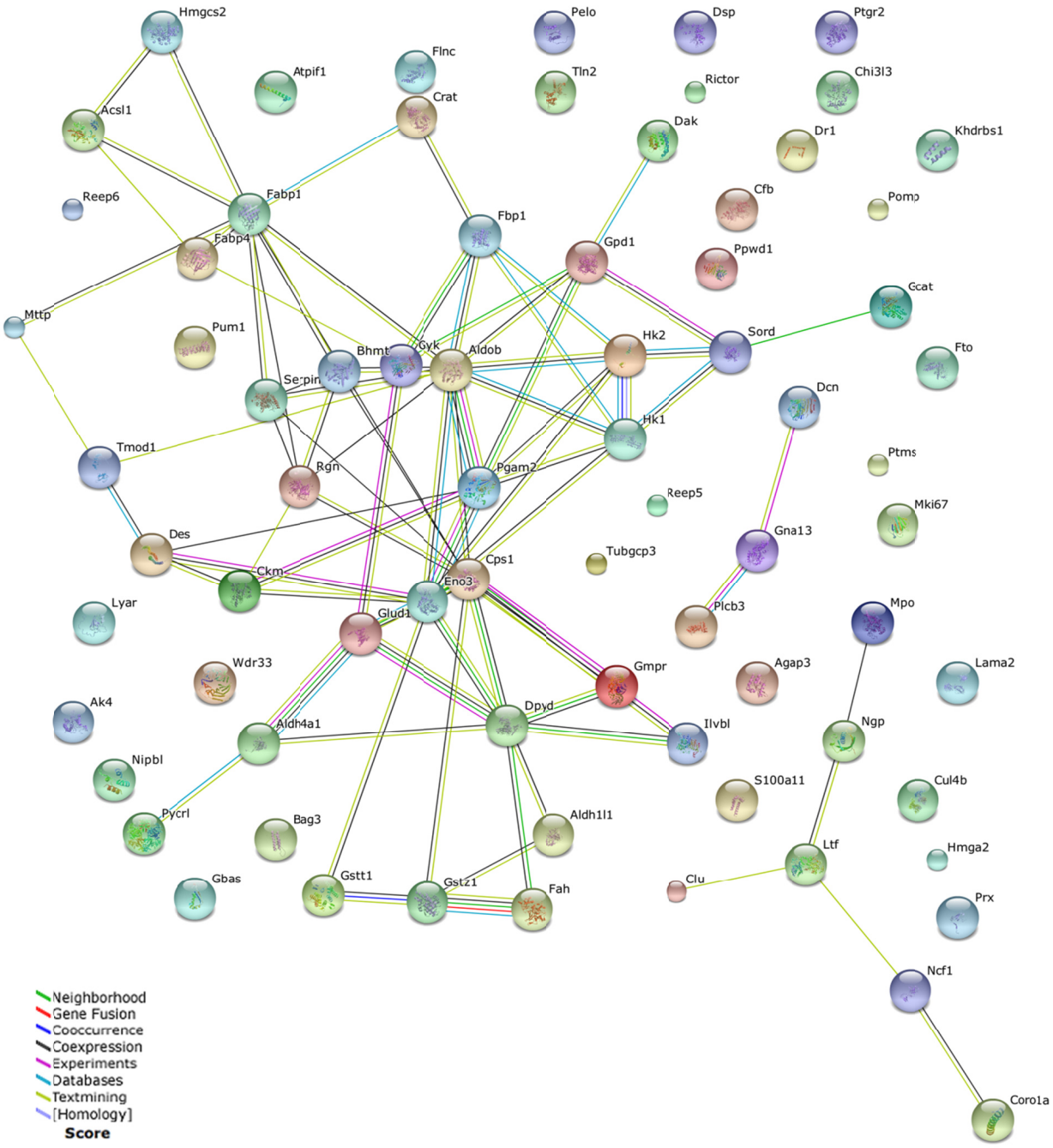

Suppl. Fig. 12: **String network of all changed proteins listed in Suppl. Tab. 6.** (2015.05.18; Evidence view. Different line colours represent the types of evidence for the association). Interactions include direct (physical) and indirect (functional) associations; they are derived from four sources: high-throughput experiments, genomic context, previous knowledge and coexpression. For abbreviations, refer to Suppl. Tab. 6.

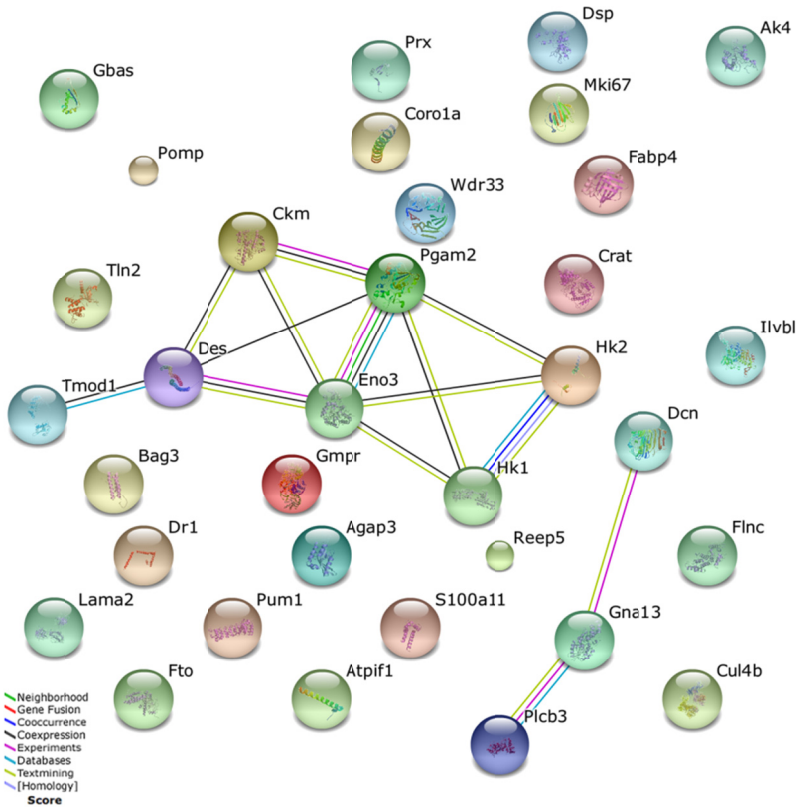

Suppl. Fig. 13: **String network of downregulated proteins.** (2015.05.18; Evidence view. Different line colours represent the types of evidence for the association). Interactions include direct (physical) and indirect (functional) associations; they are derived from four sources: high-throughput experiments, genomic context, previous knowledge and coexpression. For abbreviations, refer to Suppl. Tab. 6.

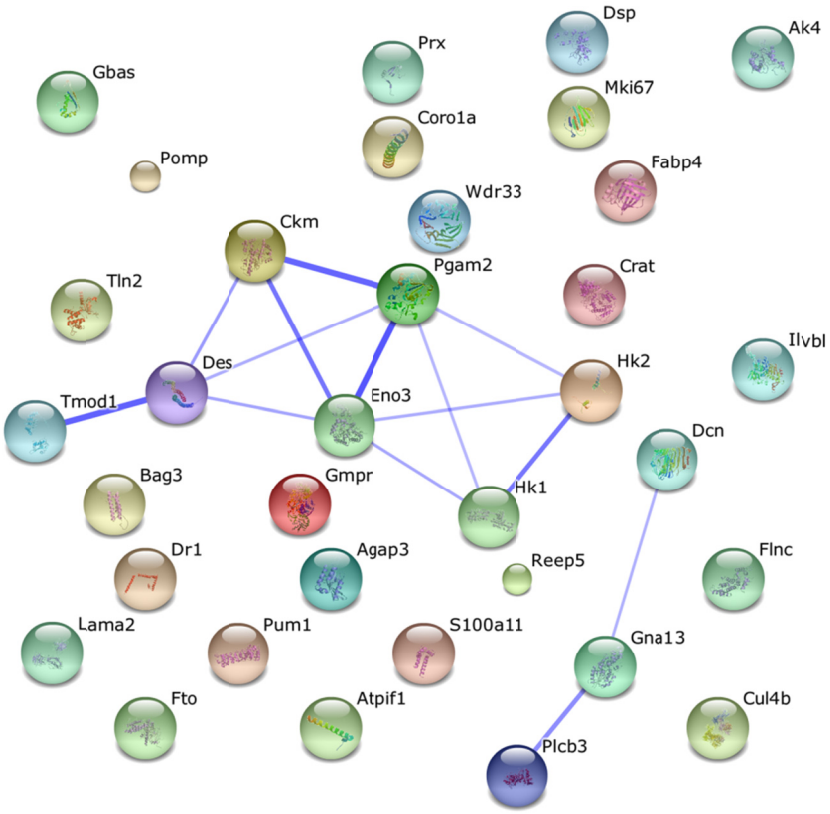

Suppl. Fig. 14: **Confidence view of downregulated proteins upon GSKIP KO in E18.5 lung.** (2015.05.18; Confidence view. Stronger associations are represented by thicker lines). Interactions include direct (physical) and indirect (functional) associations; they are derived from four sources: high-throughput experiments, genomic context, previous knowledge and coexpression. For abbreviations, refer to Suppl. Tab. 6.

10.5.3 **Selection of additional proteins identified *via* proteomics and their expression levels** (mentioned and discussed in thesis work)

Suppl. Tab. 7: **Additional selection of identified proteins from proteomics screen conducted on GSKIP-deficient E18.5 lung and liver.** Out of in total 6598 proteins detected in proteomics, only examplaric ones are shown discussed in PhD thesis.
n.v.: not valid (unique proteins determined unsatisfying (≤ 2)). n.d.; not determined (protein not identified).

Protein names	Gene names	Fold-change KO vs. WT lung	Fold-change KO vs. WT liver
Adenomatous polyposis coli protein	Apc	n.v.	n.v.
A-kinase anchor protein 1, mitochondrial	Akap1	n.v.	0.837524
A-kinase anchor protein 11 (AKAP220)	Akap11	n.v.	n.d.
A-kinase anchor protein 13	Akap13	1.039763	n.v.
A-kinase anchor protein 5 (AKAP79)	Akap5	0.812738	n.v.
Axin	Axin	n.d.	n.d.
BAG family molecular chaperone regulator 1	Bag1	0.902566	n.v.
BAG family molecular chaperone regulator 2	Bag2	n.v.	1.39461
BAG family molecular chaperone regulator 5	Bag5	1.131829	n.v.
Cadherin-1; E-Cadherin; CTF1	Cdh1	1.067086	0.979122
Cadherin-11	Cdh11	n.v.	n.v.
Cadherin-16	Cdh16	n.v.	n.v.
Cadherin-2; N-Cadherin	Cdh2	n.v.	n.v.
Cadherin-5	Cdh5	1.379552	n.v.
cAMP-dependent protein kinase catalytic subunit alpha	Prkaca	0.774697	n.v.
cAMP-dependent protein kinase catalytic subunit beta	Prkacb	0.751318	0.873426
cAMP-dependent protein kinase type I-alpha regulatory subunit	Prkar1a	1.119524	0.849568
cAMP-dependent protein kinase type II-alpha regulatory subunit	Prkar2a	0.999609	0.791495
cAMP-dependent protein kinase type II-beta regulatory subunit	Prkar2b	0.9728	0.768741
Casein kinase I isoform alpha	Csnk1a1	1.037074	0.823543
Casein kinase I isoform delta	Csnk1d	n.v.	n.v.
Casein kinase I isoform gamma-3;Casein kinase I isoform gamma-2	Csnk1g3; Csnk1g2	n.v.	n.v.
Casein kinase II subunit alpha	Csnk2a2	1.039845	0.635993
Casein kinase II subunit alpha	Csnk2a1	1.14922	1.170722
Casein kinase II subunit beta	Csnk2b	0.961556	1.404462
Catenin alpha-1	Ctnna1	0.925732	0.926911
Catenin beta-1	Ctnnb1	0.915924	0.985053
Catenin delta-1; delta-2; alpha-2	Ctnnd1	n.v.	n.v.
Frequently rearranged in T-cell lymphoma	Frat2	n.d.	n.d.
Frizzled-1; Frizzled-2; Frizzled-7	Fzd1; Fzd2; Fzd7	n.v.	n.v.
Glucose-6-phosphatase	G6pc	n.v.	n.v.
Glucose-6-phosphate 1-dehydrogenase X	G6pdx	1.073733	0.894503
Glucose-6-phosphate isomerase	Gpi	1.161727	1.017045
Glyceraldehyde-3-phosphate dehydrogenase	Gapdh	1.199181	1.129784
Glycogen [starch] synthase, liver	Gys2	n.v.	0.853057
Glycogen [starch] synthase, muscle	Gys1	0.644082	n.v.
Glycogen synthase kinase-3 alpha	Gsk3a	n.v.	n.v.

Glycogen synthase kinase-3 beta	Gsk3b	0.755337	n.v.
Glycogen synthase kinase-3 interaction protein	**Gskip**	**n.d.**	**n.d.**
Large proline-rich protein BAG6	Bag6	0.741413	1.012531
Low-density lipoprotein receptor-related protein 1	Lrp1	1.033517	0.880987
Low-density lipoprotein receptor-related protein 4	Lrp4	0.980888	n.d.
N-lysine methyltransferase SMYD2	Smyd2	n.v.	n.d.
PHD finger protein 1	Phf1	n.d.	n.d.
Protein phosphatase 1 regulatory subunit 11	Ppp1r11	n.v.	n.v.
Pyruvate dehydrogenase E1 component subunit alpha, somatic form. mitochondrial	Pdha1	0.870506	1.063531
Pyruvate dehydrogenase E1 component subunit beta, mitochondrial	Pdhb	1.010881	0.996424
Pyruvate dehydrogenase protein X component, mitochondrial	Pdhx	0.850581	1.079227
Regulator of G-protein signalling 1	Rgs1	n.d.	n.d.
Segment polarity protein dishevelled homolog DVL-2	Dvl2	n.v.	n.v.
Succinate dehydrogenase [ubiquinone] cytochrome b small subunit, mitochondrial	Sdhd	n.v.	n.v.
Succinate dehydrogenase [ubiquinone] flavoprotein subunit, mitochondrial	Sdha	0.935381	0.944783
Succinate dehydrogenase [ubiquinone] iron-sulfur subunit, mitochondrial	Sdhb	0.913673	0.842792
Succinate dehydrogenase cytochrome b560 subunit, mitochondrial	Sdhc	n.v.	0.909956
yrdC domain containing (E.coli)	Yrdc	n.d.	n.d.